Nonlinear static procedures for the seismic assessment of irregular URM buildings

Salvatore Marino

Nonlinear static procedures for the seismic assessment of irregular URM buildings

by

Salvatore Marino

Dissertation discussed in partial fulfillment of

the requirements for the Degree of

DOCTOR OF PHILOSOPHY
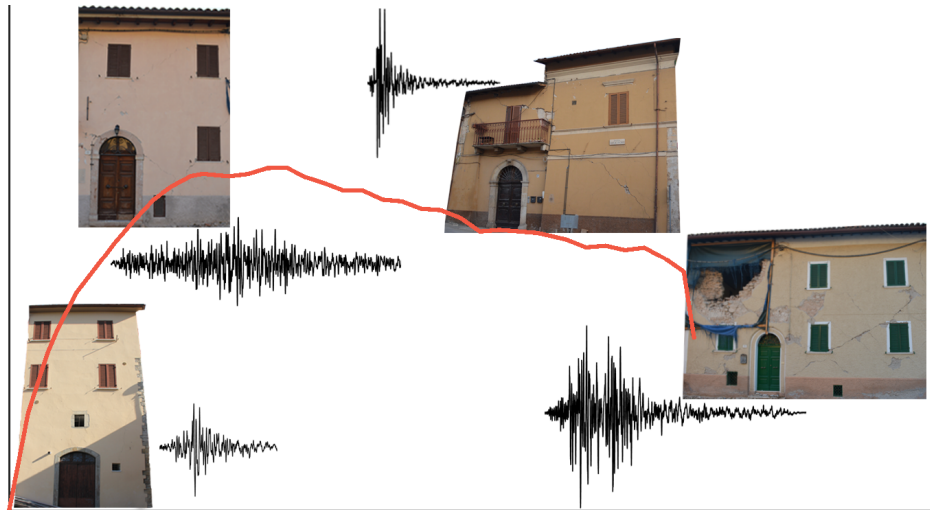
Civil, Chemical and Environmental Engineering
curriculum in Structural and Geotechnical Engineering, Mechanics and
Materials,

Department of Civil, Chemical and Environmental Engineering, University

of Genoa, Italy

March, 2018

Advisers:

Prof. Sergio Lagomarsino - Department of Civil, Chemical and Environmental Engineering, University of Genoa

Prof. Serena Cattari - Department of Civil, Chemical and Environmental Engineering, University of Genoa

External Reviewers:

Prof. Andreas Kappos - Department of Civil Engineering, City University of London

Prof. Stefano Pampanin - Department of Structural and Geotechnical Engineering, La Sapienza University of Rome

Examination Committee:

Prof. Antonio Brencich - Department of Civil, Chemical and Environmental Engineering, University of Genoa

Prof. Ivo Calió - Department of Civil Engineering and Architecture, University of Catania

Prof. Marco Paggi - IMT School for Advanced Studies Lucca

Prof. Riccardo Zandonini - Department of Civil, Environmental and Mechanical Engineering, University of Trento

Ad Enzo

"...finché non verrá il tempo
in faccia a tutto il mondo per rincontrarlo"

Abstract

Earthquakes are the main cause of damage for existing and ancient unreinforced (URM) masonry buildings, but the seismic assessment of the latter is a complex task. In fact, they were usually built without any engineered procedure; in addition, they often present features that distinguish them from new modern buildings such as structural irregularities and diaphragms not rigid in their plane. Then, the mechanical response of masonry further complicates a seismic analysis, in fact it shows a distinct nonlinear behavior already for low horizontal forces.

In order to guarantee their preservation it is necessary to possess reliable procedures to assess both their seismic capacity and demand. The nonlinear dynamic procedure (NDP) is considered as the most accurate between those currently allowed by codes. However, its complexity still precludes a wide application in the professional practice. Therefore, in the last decades, nonlinear static procedures (NSPs) have been conceived and developed with the aim to be more precise than the linear procedures and more practice-oriented than NDP. However, the NSPs present in currently adopted codes were conceived for the seismic analysis of reinforced concrete buildings and, as a consequence, do not take into account the particular features of URM.

The aim of this thesis is to contribute to the improvement of the nonlinear static procedure for the seismic assessment of existing URM buildings. In particular three steps of NSPs are analyzed and discussed in detail: 1) the load pattern(s) to apply to the building model, 2) the definition of the damage/performance levels on the pushover curve; 3) the evaluation of nonlinear displacement demand for each performance level and the corresponding intensity measure that causes its attainment.

The application of NSPs is tested on numerical MDOF models representative of URM buildings. From a base and "regular" model both in plan and elevation irregularities are introduced, then the effects derived due to the presence of not rigid diaphragms are studied. Finally, the effect of constructive details such as tie rods and ring beams effect is analyzed. Totally, 13 numerical models representative of 3 and 4 stories URM buildings are studied. The results derived by the application of NSPs are compared with the NDP, considered as the reference solution. Based on the findings of the present research, original contributions are provided to the three steps above outlined, with the aim to improve the seismic performance prediction of NSPs currently proposed in codes for this type of buildings.

Contents

Introduction

Earthquakes are the main cause of damage for ancient unreinforced masonry (URM) buildings. Therefore, in order to reduce their vulnerability with compatible and light interventions, it is necessary to have reliable, but not overly conservative, assessment procedures for their seismic assessment.

The practical objective of inelastic seismic assessment/design procedures is to predict the expected behavior of the structure in future earthquake shaking. This has become increasingly important with the emergence of performance-based earthquake engineering, PBEE, that characterizes performance primarily in terms of expected damage to structural components and contents. Since structural damage implies inelastic behavior, traditional design and analysis procedures that use linear elastic techniques can predict performance only implicitly [FEM05]. In fact, linear analyses need a behavior factor known to give rise to many problems and inconsistencies in the assessment of masonry buildings, possibly more than for other structural types [LBB$^+$17]. The reason is that to define the behavior factor an overstrength ratio should be accounted for that strongly depends on the structural layout of the building[1]. This issue is very relevant for the seismic assessment of existing buildings. In fact, an underestimation of their seismic capacity may lead to invasive and unnecessary interventions, whereas an overestimation is dangerous for the safety of occupants. Therefore, in last decades, several researchers have worked on the development of nonlinear procedures that in last years focused on the displacement-based approach (DBA). In fact, displacements and deformations can be directly

---

[1]In URM buildings "the strength of walls is essentially a result of the geometry, which is governed to a great extent by architectural needs, and of how the floor systems distribute the gravity loads to the walls. As a result, the overstrength ratio can vary widely from building to building (and even for the same building depending on the direction of seismic loading)" [LBB$^+$17].

related to damage limit states as a consequence, "an accurate prediction of the inelastic deformation demands assumes an essential role within a performance-based seismic design or assessment process" [GGPM17]. In particular, as discussed in [LC15b], the displacement-based approach (DBA) is the more appropriate for existing URM buildings[2], which crack even for low intensity earthquakes and can survive to severe ones only if they have a sufficient displacement capacity.

Two different nonlinear procedures are available: the nonlinear static (NSP) and nonlinear dynamic (NDP) procedure. Even though it is generally accepted that nonlinear dynamic procedure is the most accurate analysis technique, its use is still not common in the everyday engineering practice [MRPM14]. The main reasons of that are outlined in Chapter 1. On the contrary, nonlinear static procedures (NSPs) represent a widely used tool in the professional practice for the seismic assessment performance of existing buildings. However, it lacks in literature an extensive validation of NSPs adopted by current codes when applied to irregular URM buildings with not rigid diaphragms.

Therefore, the aims of the present research are: 1) to identify the main characteristics of currently adopted NSPs; 2) understand their limitations and whether they are suitable for the seismic assessment of existing URM buildings; 3) if not, propose refinements to overcome the main issues.

As pointed out in the draft of the new version of Eurocode 8 [EC817] the seismic design/assessment is clearly divided into three steps: *modeling*, *analysis* and *verification*. For the *analysis* and *verification* phases, a critical state of art review is presented in Chapters 3 and 4 respectively. In particular, in Chapter 3 issues outlined from codes and literature regarding the analysis methodology and the definition of the performance levels are discussed. Then Chapter 4 deals with issues related to the verification in terms of performance evaluation. A comparison between static and dynamic procedures was carried out in terms of intensity measure (IM). The IM is a

---

[2]The reasons to use a DBA are comprehensively detailed in [LC15b]: "the mechanical models widely used at present for the analysis of ancient masonry structures consider a verification approach in terms of forces; the consequence is that in the past strengthening techniques were aimed at increasing stiffness and strength. However, earthquake induces deformations and dynamic amplification; therefore, it is better to keep the original flexibility of the structures and improve the displacement capacity, in terms of ductility or rocking, in order to survive even to rare destructive earthquakes".

representation of the anticipated seismic ground motion [FEM05]. Different procedures to compute the IM with a static procedure are analyzed and discussed. Then the dynamic procedure adopted is outlined. For both chapters the starting point is a critical state of the art review, the main issues of each step are outlined and then completed with the original proposals for both analysis and verification. In fact, the outcome of the present research is to improve the different steps that form the NSP, therefore it seemed more effective not to write separately state of art and original proposals, but to compare them for each of the steps analyzed.

The issues related to the modeling phase are beyond the scope of this study. A modeling approach that is considered suitable for the seismic assessment of URM buildings is adopted: in Chapter 2 its main characteristics are described and the peculiarities of the case study buildings are presented. In particular, among the wide variety of historical masonry structures, buildings characterized by a box-type behavior are considered and studied in the present research. This type of buildings may be modeled using the equivalent frame (EF) approach, in which masonry walls are considered by the assembling of nonlinear piers and spandrels. Among the different modeling strategies proposed in the literature, the equivalent frame approach seems particularly attractive since it allows the analysis of complete 3D buildings with a reasonable computational effort, suitable also for practice engineering aims [LPGC13]. Moreover, it is also expressly recommended in several national and international codes.

The limitations of the present research are those intrinsic in the modeling technique itself, which, so far does not allow to study the out-of-plane behavior of URM walls. Therefore, the attention is focused only on the in-plane response of URM walls: that is assumed through proper connections that prevent the activation of local failures, hence the building presents a box-type behavior. For this type of buildings and in particular when they present a regular distribution of openings, the use of the equivalent frame approach is accepted in the literature [QMC17], and therefore the modeling issue is not studied in the present thesis. However, an out-of-plane assessment needs to be conducted separately when necessary (i.e. the activation of local mechanisms is possible).

The results derived from NSPs are successively compared with those obtained with an NDP considered as the "exact" reference solution. In this

research the *incremental dynamic analysis* was used to conduct the NDPs and it is discussed in Chapter 3. In the same Chapter the methodology for the performance levels definition is detailed, in fact in most of the currently adopted codes no specific provisions are provided. Then, in Chapter 4 the procedure to compute the IM using the NDP is discussed.

Finally, the structure of the thesis is outlined: in Chapter 1 a general overview of nonlinear analysis methods is provided; chapters from 2 to 4 detail the procedure adopted for both NSP and NDP; in Chapter 5 the main results are reported and compared; in Chapter 7 the conclusions and the outlooks for future researches are discussed.

Chapter 1

Nonlinear procedures: overview

Most buildings experience significant inelastic deformations when affected by strong earthquakes. Unreinforced masonry (URM) is a building material that shows a significant nonlinear behavior also for a low level of stress (due to its low tensile strength) and constitutes the majority of existing (often ancient) buildings in Italy and the rest of Europe. The aim of existing/historical buildings preservation may hinder the need to ensure the safety of occupants. Therefore it is necessary to possess reliable tools that allow, as much as possible, an accurate evaluation of both seismic capacity and demand that guarantees an "acceptable safety level" and, in the case of heritage buildings, making reference to the principle of "minimum intervention" [LC15b]. As a consequence, in last years, the effort of researchers was established in the improvement of nonlinear analyses, with the aim to calibrate procedures that can be both precise but practical for the engineering practice. The alternative consists in the linear analyses, however, as stated in [Faj17] "although the concept for taking into account the influence of inelastic behavior in linear analysis has served the profession well for several decades, a truly realistic assessment of structural behavior in the inelastic range can be made only by means of nonlinear analysis".

Two possible options are available for an engineer that wants to undertake a nonlinear analysis: the nonlinear static procedure (NSP) that need to conduct a so called "pushover analysis" or a nonlinear dynamic procedure (NDP) based on nonlinear response history analyses. The latter represents

the most advanced analysis method available today, and its use is allowed
in currently adopted codes for the seismic analysis of any type of structure,
however the procedure is still far from an extensive application in common
practice. This is not only because it is computationally demanding (this is
a problem whose importance has been gradually reduced), but principally
for a series of drawbacks listed herein and divided into three categories: 1)
modeling, 2) analysis, 3) verification.

1. There is limited availability of software that allows the performance
   of time history analysis, especially for the case of masonry struc-
   tures [MRPM14], in fact there are still "intrinsic uncertainties and
   complexities of defining *cyclic* constitutive models, assigning viscous
   damping models, knowing significant physical properties" [GGPM17],
   particularly at high ductilities.

2. Difficulties in selecting appropriate input ground motion records that
   allow obtaining results representative of the actual structural be-
   havior. In fact the results strongly depend on the input data. As a
   consequence, the variability of ground motion results in significant
   dispersion in engineering demand parameters[1], and note that "the
   dispersion increases with higher shaking intensity and with greater
   elasticity" [FEM05]. On the contrary, for NSPs currently adopted in
   codes, only an average spectrum is needed.

3. The use of the analysis results is not straightforward, in particular the
   difficulty in the "interpretation of the results of nonlinear dynamic
   analysis in terms of *performance limits*." [MRPM14]. Furthermore
   there is not sufficient information for undertaking NDPs in currently
   adopted codes: in [EC804] "is regulated very deficiently by only three
   clauses" [Faj17], and in some codes such as [ASC14] it is prescribed
   that "where the NDP procedure is used, the authority having juris-
   diction shall consider the requirement of review and approval by an
   independent third-party engineer with experience in seismic design
   and nonlinear procedures".

---

[1]Engineering demand parameters (EDPs) are typical structural response measures
that form the output from an analysis. Examples of EDP: the story drifts, the defor-
mations of the "deformation-controlled" components and the force demands in "force-
controlled" (i.e. brittle) components [Faj17].

An extensive comparison between pros and cons of nonlinear static and dynamic procedures is discussed in [LC15b]. The formulation of the nonlinear static analysis dates back to the 1970s but only recently has been included extensively in seismic code provisions, and this is also due to the fact that in recent years the availability of both general purpose and masonry dedicated software strongly increased, indeed the NSP is the most popular in the professional practice. However, "most of the methods subscribed by major seismic codes for seismic analysis of new or existing buildings have been originally defined for simple regular structures" [DSM15]. Currently adopted codes attempt to provide definitions of the concept of "regularity", giving prescriptions related to the distribution of mass, stiffness and strength in the building both in plan and in elevation [DSM15]. Therefore the concepts of in plan and elevation regularity are introduced. The first is usually related to the earthquake induced torsion, the latter to the importance in considering the higher modes in seismic analysis. However, old and/or ancient existing (URM) buildings rarely comply with regularity requirements, because most of them were built without any engineering design, therefore the validity of NSP for their seismic assessment is still debated. In addition to the frequent presence of in plan and elevation irregularities, this kind of buildings often present diaphragms that are not rigid in their own plane. In fact, it is not uncommon to find timber diaphragms or vaults.

The limits of the present research are now outlined. It is known that the seismic response of masonry buildings depends on the behavior of masonry walls, both in-plane and out-of-plane, on the connection between walls, and on the interaction with horizontal diaphragms. The present research was conducted under the hypothesis that the out-of-plane mechanisms are prevented. Therefore the seismic capacity of a masonry building was evaluated by considering the in-plane behavior of masonry walls only.

In the draft of the new version of Eurocode 8 [EC817] the seismic design/assessment is clearly divided into three steps: modeling, analysis and verification. In the next sections a general overview of these main steps is provided: the development of a model able to detect the main features of the building under analysis (Section 1.1); the procedure necessary to conduct the analysis (Section 1.2) and a proper evaluation of nonlinear

displacement demand and consequently the intensity measure (IM) that caused its attainment (Section 1.3).

Finally, it is worth reminding that in these sections only a general overview is given, with the aim to introduce the context of this research the state of art being critically discussed in Chapters 2 to 4.

1.1 Modeling

Due to the wide variety of materials, geometry, constructive details and preservation state of historic URM buildings, the choice of the most suitable modeling strategy represents a very complex task.

As clearly discussed in [CCLR10], the difficulty in modeling URM buildings depends mainly on three fundamental problems:

- the composite nature of masonry, made up of a system of units and joints inducing a strongly anisotropic response;

- the mechanical non-linearity of the material, also for low stress values;

- the geometric complexity of masonry structures, commonly requiring the adoption of complex 3D modeling approaches.

With reference to the mechanical non-linearity of the material, models should balance accuracy and efficiency. In fact, the performance-based approach that was in the recent years adopted in the seismic codes worldwide, requires tools capable to evaluate the evolution of the response in the nonlinear range, theoretically, up to collapse.

Different modeling approaches are found in the literature for URM walls. A recent review of the different modeling procedures is in [QMC17], and a more detailed, but older, is present in [CCLR10]. In the latter the Authors classified the modeling strategies following two criteria: scale of analysis (whether material or structural element one) and type of description of masonry continuum (whether continuous or discrete). Models developed at material scale are oriented to describe in an accurate way the complex behavior of masonry solids, and the continuous constitutive law model (CCLM) is considered as the most detailed approach. Within this framework, masonry is "usually considered as a fictitious homogeneous material while the structure is described by means of a continuous mesh of 2D or

3D Finite Elements" [QMC17]. However, although this method has the advantage of being quite general, without making any simplification on the localization of the masonry damage pattern and the structure's geometry, it presents a series of disadvantages: 1) it requires a high computational burden (especially for large structures and/or when nonlinear dynamic analyses are carried out); 2) it needs many input data, many mechanical parameters that are not easy to evaluate in practice, and may strongly affect the analysis results; 3) since in the CCLM the structure is modelled as a continuum, the elements on which the drift parameters generally related to the limit states are monitored should be identified after the analyses and this identification may be ambiguous [QMC17].

Discrete and/or rigid element approaches could be considered as a valid alternative to CCLM models. However, always in [QMC17] it is pointed out that even in this case a relevant size of buildings leads to a huge computational demand that can be reduced only with a coarser or unrealistic discretization.

Therefore, in order to perform global analyses with a reasonable computational effort and a small amount of mechanical parameters, in the last decades several Structural Element Models (SEM) have been developed. This approach aims at evaluating the overall response of masonry structures made up of walls with regular openings, describing with adequate accuracy the in-plane behavior of single structural elements. The technique is based on the identification of macroscopic structural elements (piers, spandrels and rigid nodes). In the SEM field, the so called *equivalent frame* (EF) models are the most widely used. They consider the walls as an idealized frame, in which the deformable elements (piers alone, or piers and spandrels) connect rigid nodes.

The reliability of this method depends on the consistency between the strongly simplified hypothesis on which it is based and the actual behavior of the building analyzed [QMC17]. In fact, the EF modelling approach for URM buildings, if compared with FEM, has the following limitations: 1) restriction of the number of degrees of freedom, 2) predefined idealization of URM walls into "equivalent frames", i.e. the geometry of piers and spandrels is defined *a priori* and 3) neglecting of out-of-plane wall response. As a result, "it is highlighted that the EFM can be reasonably used as a first conservative approach for the seismic assessment of existing

URM buildings with box behavior and quite regular opening patterns" [QMC17]. Under these hypotheses, in fact, the reliability of this approach for URM buildings was proven in experimental tests ([CCD+14], [BTPP15], [PSGM16]), simulations of existing damaged structures ([CL13a], [CNR14], [MCL+16]) and in comparison with more detailed finite element modeling procedures ([CCL09a], [RCL15]). However, it is worth underlining that in presence of irregular openings distributions, the applicability of the method and the rules to adopt for the definition of piers and spandrels are still debated as very recently discussed in [SSC+17] and [CCL18].

The EF method may be adopted to conduct both linear and nonlinear analyses. In the latter case, it is necessary to define proper nonlinear constitutive laws for the panels (i.e. piers and spandrels) that constitute the building under analysis. In particular, in order to carry out analysis under cyclic loading (i.e. nonlinear dynamic), it is necessary to define rules for the hysteretic response of the panels. This is discussed in Section 2.1.

Finally, there is the issue of diaphragm modeling. In fact, in existing URM buildings it is not uncommon to find timber diaphragms or vaults, that can not be considered as rigid in their plane. Very little information is present in literature to take into account the effect of not rigid diaphragms in the global seismic response of buildings [AKS15]. Furthermore, most of the commercial software available for the seismic assessment of URM buildings do not allow the presence of not rigid diaphragms.

1.2   Analysis

Having defined a proper numerical model of the building under analysis, the second step of a seismic assessment procedure is the analysis. For the reasons mentioned at the beginning of this chapter, in the present thesis only the nonlinear analyses were studied.

The nonlinear static procedure (NSP) was introduced already in the 1970s thanks to the study of Freeman and its collaborators. Then, in 1978, Tomaževič proposed a simple pushover approach, which could be applied at the story level and used for the seismic assessment of low-rise masonry buildings [Faj17]. The method, named as POR method, was developed assuming spandrels as infinitely stiff and strong portions, assuring a perfect coupling between piers. In particular, "the POR method considers a storey

failure mechanism, in which the global response of each storey in terms of base shear-storey displacement is computed as the sum of the individual response of each wall" [ML11]. The POR method incorporated the experience obtained with the Skopje earthquake in 1963 and it was the first seismic assessment method for masonry structures in Italy [ML11], being adopted in the Italian code in 1981 [Lag17]. However, URM buildings damaged by earthquakes showed also other possible mechanism, therefore in last decades a series of more refined analysis were proposed. A comprehensive summary of pushover analyses is provided in [AÖ10]. NSPs have a series of advantages, in fact, compared to traditional elastic analyses, provide a wealth of additional important information about the expected structural response, data on the strength and ductility of structures, as well as a helpful insight into the structural aspects which control performance during severe earthquakes [Faj17].

The main assumption in basic pushover-based methods is that the structure vibrates predominantly in a single mode (see Section 1.3). However, this assumption may not be valid, especially in high-rise buildings, where higher mode effects may be important along their height [Faj17]. This issue is well known in the literature and in the last years many researchers proposed refinements to NSPs to overcome it. URM buildings are usually low-rise buildings, therefore are exempt from this issue. However, also for this kind of building higher modes effect may be significant, but for different reasons: 1) they may present in-plan irregularities and therefore be sensitive to torsional effects; 2) they may have diaphragms not rigid in their plane therefore the first mode does not activate all the walls.

Some researchers thought to overcome the higher modes influence working on the load patters applied to the buildings. As outlined in [KS97], "the load patterns are intended to represent and bound the distribution of inertia forces in a design earthquake. It is clear that the distribution of inertia forces will vary with the severity of the earthquake and with time within an earthquake". Therefore, in most codes, it is proposed to apply at least two different load patterns to the building under analysis. However still there is not an agreement and the issues connected to the load patterns are discussed in Section 3.1.1.

In a performance-based framework, the load patterns "push" the structure up to displacements that are associated with specific performance

levels. These displacement are often called as *target displacements*. It is therefore necessary to have proper criteria able to detect the most significant performance objectives also for irregular URM buildings, that present a particular seismic response, different than RC structures. In fact, for RC buildings the structural elements usually are modeled without a post-peak strength degradation and the seismic assessment is conducted through local safety checks. This procedure is not suitable for URM buildings, in fact their structural elements often present a significant strength degradation that need an analysis that involves the building in its entirety. These issues are examined more in detail in Section 3.2.

For nonlinear dynamic procedures the uncertainties increase, as discussed at the beginning of this chapter. The procedure adopted in the present research is discussed in Section 3.3

1.3 Verification

The final aim of a seismic assessment procedure is the verification, and in the present research it was conducted studying the *intensity measure* (IM) that caused the attainment of the different performance levels under analyses. Then, the IMs computed with the NSPs were compared with the results derived from NDP.

The NSPs combine the pushover analysis with the response spectrum approach. In particular, the seismic demand can be determined for an equivalent single-degree-of-freedom (SDOF) system from a response spectrum that considers the effects due to inelasticity. In literature two are the main options to consider the effects due to inelasticity, through: 1) inelastic response spectra [NR80], [VFF94], [Faj99], or 2) using overdamped elastic response spectra [ATC96], [Fre04].

However, a transformation of the multi-degree-of-freedom (MDOF) system into an equivalent SDOF system is needed. This transformation, "which represents the main limitation of the applicability of pushover-based methods, would be exact only in the case that the analysed structure vibrated in a single mode with a deformation shape that did not change over time. This condition is, however, fulfilled only in the case of a linear elastic structure with the negligible influence of higher modes. Nevertheless, the assumption of a single time-invariant mode is used in pushover-based methods

for inelastic structures, as an approximation" [Faj17]. Always in [Faj17] it is stated that an important milestone was the paper [MPKF93], in which the acceleration-displacement response spectrum (ADRS) format was introduced, enabling visualization on the assessment procedure. Although the graphical displays of the procedure is not necessary, it is important to understand the relations between seismic demand and capacity. Therefore in Section 4.1.1 the AD space is introduced and in the sections afterwards is used.

In the previous section the concept of target displacement was introduced as an estimate of the global displacement the structure is expected to experience for a given performance level. In case of assessment of an existing building, it is then necessary to evaluate if the displacement capacity overcomes the displacement demand, that, as said, should consider the effect of inelasticity. In fact, masonry possesses a considerable reserve of non-linear capacity provided by inelastic deformations and high levels of energy dissipation [ML11].

As stated in [KS97], the equivalent SDOF curve is only the skeleton needed for the computation of nonlinear displacement demand. In fact, in literature are present several procedures that compute the nonlinear displacement demand that integrate the equivalent SDOF curve characteristics through the use of more or less explicit modification factors to consider: yield strength, stiffness degradation or pinching, strength deterioration, effective viscous damping. Finally, also structural irregularities (both in plan and elevation) and the presence of not rigid floor diaphragms are expected to affect the target displacement and the corresponding intensity measure.

Chapter 2

Procedure: modeling

The seismic assessment of masonry buildings requires reliable nonlinear models as effective tools for their evaluation. Among the possible modeling strategies proposed in literature and codes, the present research focused on the equivalent frame modeling strategy which is detailed in Section 2.1. In Section 2.2 the numerical case studies developed are described and the main dynamic properties derived from the modal analysis are discussed in Section 2.3.

2.1 Modeling technique and constitutive laws adopted

The present research focused on existing URM buildings characterized by a box-type behavior, i.e. assuming that proper connections prevent the activation of local failure modes mainly associated with the out-of-plane response of walls [LPGC13]. Within this context, the building seismic response is related to both "the in-plane capacity of walls and the connections and load transfer effects due to floor and roof diaphragms" [LPGC13]. Therefore, the use of three-dimensional models is suggested.

Among the possible modeling strategies proposed in literature and codes, the present research used the *equivalent frame* (EF) modeling strategy with a purposely developed software, TREMURI. This software, described in detail in [LPGC13], has been developed at University of Genoa since 2001 and then implemented in the commercial software 3muri [S.T16]. The
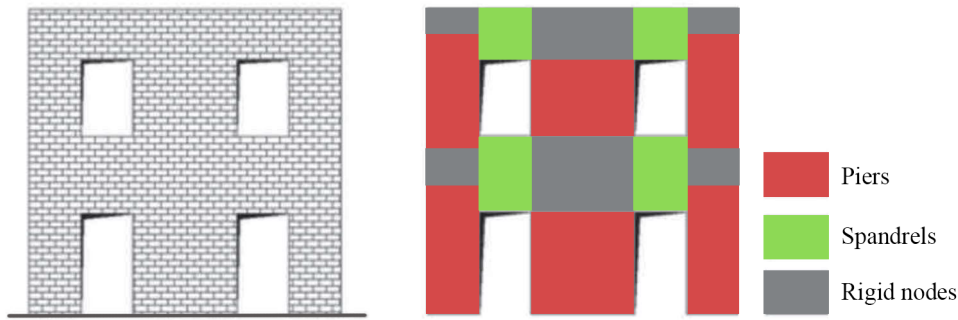
Figure 2.1: URM wall idealization using the EF modeling approach

software has been tested in previous researches that proved its reliability for standalone URM buildings [CCL09a], [CCD⁺14], [CNR14], [RCL15], [PSGM16]. This modeling strategy was chosen because it allows to conduct both nonlinear static and dynamic analyses of whole buildings with reasonable computational effort. The TREMURI software was chosen also because it allows the explicit modeling of flexible horizontal diaphragms, which are very common, particularly in ancient existing buildings [LPGC13]. In fact, in such context "the possibility of modeling flexible diaphragms (timber floors, masonry vaults), aimed to properly simulate the redistribution of seismic actions among walls, constitutes an essential requisite for a reliable assessment" [LC15b].

The EF modeling strategy is based on discretization of the walls into a set of masonry panels (piers and spandrels), wherein the nonlinear response is concentrated, connected by rigid areas called nodes. Fig. 2.1 shows an example of an URM wall idealization using the EF modeling approach.

Piers are vertical panels and the most important elements since they resist both gravity loads and seismic action; spandrels are the horizontal elements between two vertically-aligned openings and connect two piers, limiting their end rotations. Each element is described by nonlinear constitutive laws, in terms of generalized forces (axial force N, shear V and bending moment M) and corresponding movements (horizontal displacement u, vertical displacement v, and rotation φ), defined by proper failure criteria (e.g. as illustrated in [CCL09b], [BM13], for piers and spandrels respectively) and drift limits (e.g. as discussed in [PB14]) [LC15b]. Within the Europen research project PERPETUATE (www.perpetuate.eu,
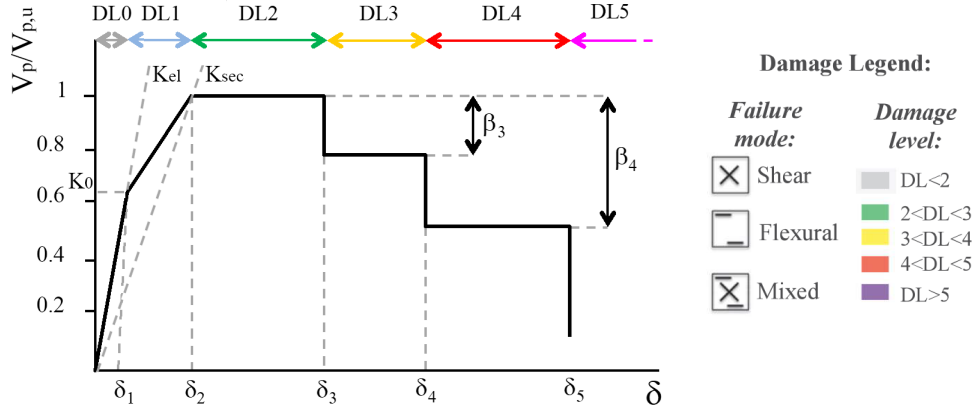
Figure 2.2: Backbone of a masonry panel based on a multilinear constitutive law and legend adopted to describe the damage, adapted from [LC15b].

[LMP$^+$10], [CCDA$^+$12]), for both piers and spandrels multilinear constitutive laws were introduced in TREMURI software. These constitutive laws are described in detail in [CL13b], from which the main features reported herein are taken. The constitutive laws are based on a phenomenological approach and allow to describe: the non linear response until very severe damage levels through progressing strength decay (β_i) in correspondence of assigned structural elements drift (δ_i), as shown in Fig. 2.2.

In accordance with beam theory, the elastic response phase of the masonry pier and spandrel panels is described by defining the initial Young's (E_m) and shear (G_m) moduli of masonry and then approximating progressive degradation using secant stiffness. The elastic values are defined by multiplying the secant stiffness by a coefficient, which in this case was equal to 2 (as suggested in [EC804]); the initial stiffness limit, K_0, was set equal to 0.7. For more information on the mechanical parameters adopted for the present research see Section 2.2.2.

The maximum shear strength is defined on the basis of common criteria proposed in the literature as a function of different failure modes examined (either flexural or shear). The drift limits are associated with the achievement of reference damage levels DLi (with i=1,5, where DL5 is associated with "collapse" of the panel, representing the state in which the panel loses the capacity to support horizontal loads). The limits adopted for the constitutive laws are summarized in Table 2.1; the values adopted

17

to describe a progressive nonlinear response are differentiated for spandrels and piers. Piers were also differentiated as a function of the two failure modes (shear or flexural). Despite this classification, as testified by the post-earthquake damage observation and experimental campaigns [VZPB17], it is evident that mixed modes are also possible and quite common. Therefore, mixed failure modes were considered within the modeling strategy by interpolating the values assigned for basic failure modes, where the two strength criteria associated with shear and flexural response provide similar predictions. Strength decay values for piers reflect those reported in experimental campaigns on piers characterized by brick and mortar masonry (e.g., [AMM94], [PB14]). For the flexural behavior of spandrels, an equivalent tensile strength contribution was considered, as proposed in [CL08] and [Bey12].

Table 2.1: Summary of the thresholds used for piers and spandrels, values in %.

Structural element	δ_3	δ_4	δ_5	β_3	β_4
Piers[*]	0.6 - 0.3	1.0 - 0.5	1.5 - 0.7	0 - 30	15 - 60
Spandrels	0.2	0.6	2.0	40	40

[*] The first value is assumed for prevailing flexural behavior, the second value for shear behavior.

In order to undertake cyclic analyses, it was necessary to define rules for the hysteretic response of the panels (i.e. piers and spandrels). To this aim the constitutive laws proposed in [CL13b] were adopted, and a sketch of the idealization of masonry panels response is depicted in Figure 2.3).

Where: α coefficients are aimed to define K_u, β coefficients define the strength reductions and γ are aimed to define the extension of unloading branch. All the coefficients are defined for the two failure modes (f, and s subscripts for flexural and shear failure modes respectively). For a detailed explanation of these coefficients refer to [CL13b]. This hysteretic response was adopted also in other studies such as [CCD+14] and [CCL+17]. The values adopted to model the case study buildings are listed in Table 2.2 and they are calibrated on the basis of experimental evidences [CL13a].

The final part of the modeling strategy was to account for diaphragms. They are modeled as finite horizontal orthotropic membrane elements. This part of modeling procedure is discussed in Section 2.2.1.
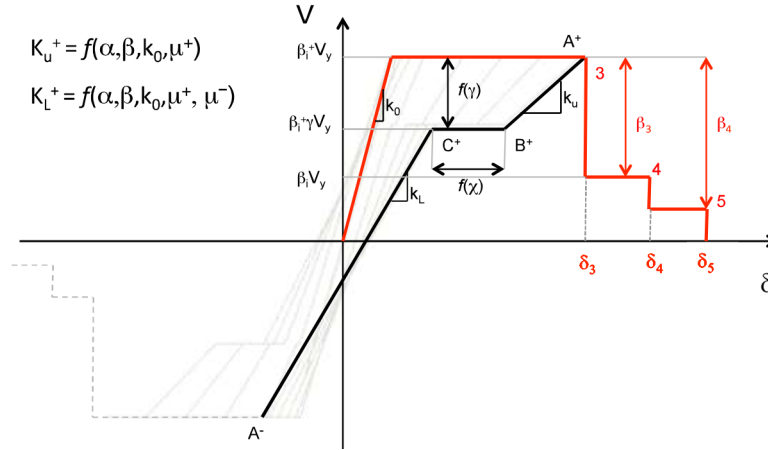
Figure 2.3: Sketch of the idealization of masonry panels cyclic response according to the multilinear constitutive laws implemented in TREMURI (adapted from [CL13b])

Table 2.2: Summary of parameters that define the hysteretic response adopted for the case-study buildings

Structural element	α_s	β_s	γ_s	α_f	β_f	γ_f
Piers	0.8	0.8	0	0.9	0.8	0.6
Spandrels	0.2	0	0.3	0.2	0	0.3

2.2 Case studies description

The intention in the definition of the prototype buildings was to consider rather simple structures but representative of the typical existing buildings present in Italy and, more generally, in European countries, although of course not exhaustive of all the possible architectural configurations. The base model, which has been defined starting from a building analyzed in [CL13b], is represented by a three-story full clay masonry building with lime mortar and steel tie rods at each level (Fig. 2.4). The thickness of the external walls is 48 cm at the ground floor and at the first floor, while it is 36 cm at the top level; the internal walls have a constant thickness for all the levels that is equal to 24 cm. For all the defined configurations the same type of masonry has been used, and its mechanical properties, are summarized in Section 2.2.2.

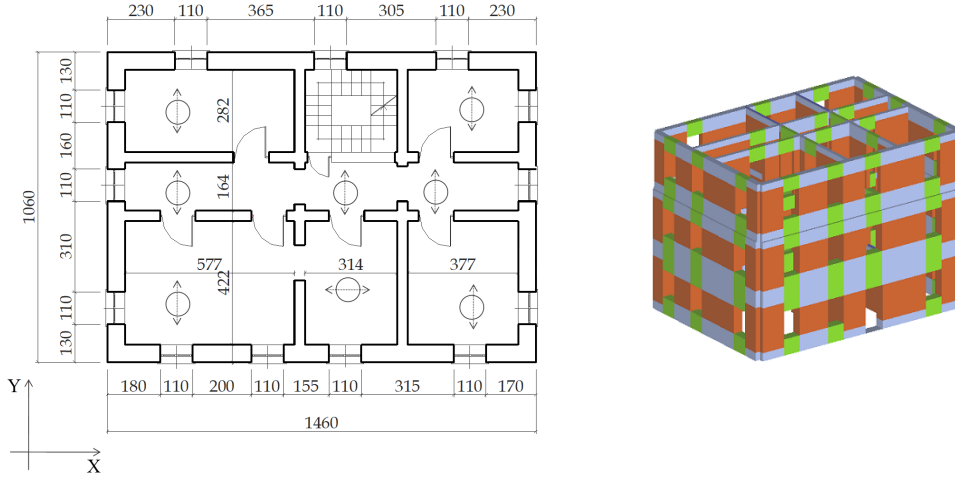It is worth highlighting that the equivalent frame idealization of 3D

19

Figure 2.4: Base configuration of the prototype buildings: plan view (measurements in centimeters) and 3D view showing the equivalent frame idealization (orange = piers; green = spandrels; blue = rigid nodes).

models has been generated by using the 3Muri software [S.T16], the commercial version of TREMURI research software. Then TREMURI has been used to carry out the nonlinear static and dynamic analyses by using the multilinear constitutive laws described in Section 2.1.

Figs. 2.5 and 2.6 show the URM walls geometry of the base model. Steel tie rods were inserted in the external walls (i.e. walls 1,2,3 and 4), 30 cm below each diaphragm, for a total of 12 tie rods. Each tie rod was subjected to a pre-tensioning of 20 kN. The insertion of tie rods justifies the hypothesis that the out-of-plane response is prevented and therefore a global response is expected.

Then, starting from this basic configuration, that has a regular openings distribution and is characterized by rigid diaphragms (RC slabs), different variations have been defined in order to examine the effects related to: 1) modifications in the structural details; 2) the introduction plan and elevation regularity; 3) the stiffness of diaphragms.

The structural details variation has been explored by replacing the tie rods with RC ring beams coupled with the spandrels at each level, thus leading to 2 different configurations: building A (with steel tie rods) and building B (with RC ring beams). The ring beams had rectangular cross-section 40

cm high and 25 cm wide with longitudinal reinforcement made by four 16 mm diameter bars both on top and bottom side and shear reinforcement consisted of 10 mm bars spaced 150 mm. This amount of reinforcement is more than the minimum required by [NTC08] for ring beams for the design of URM buildings.
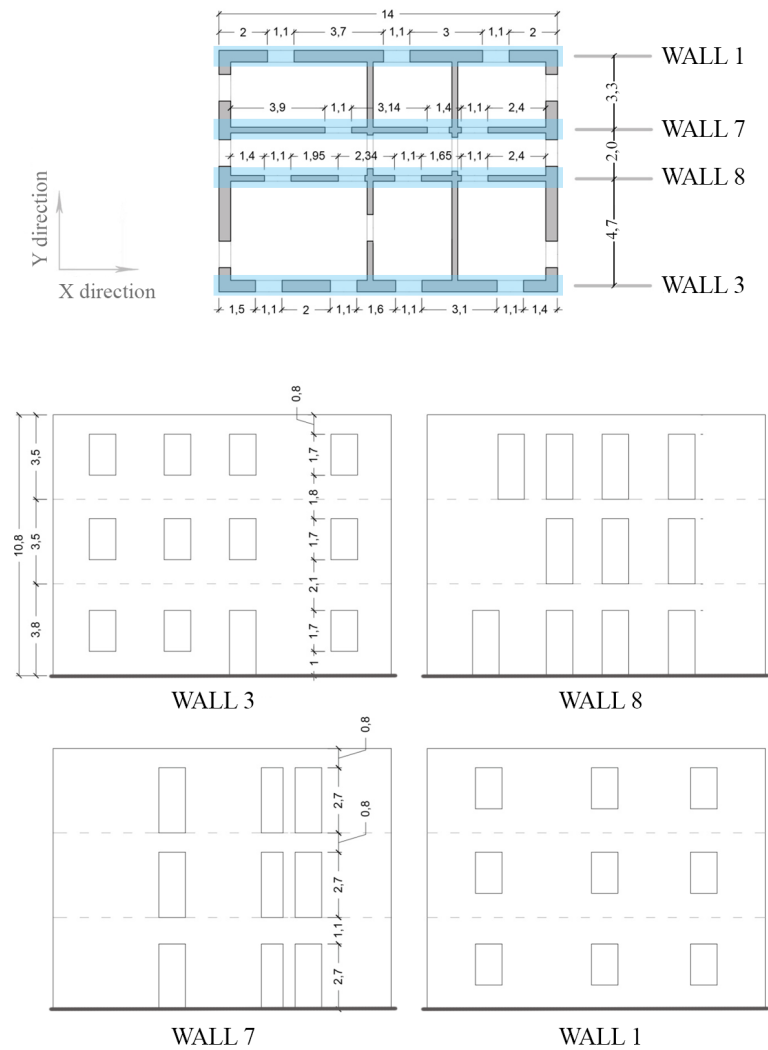

Figure 2.5: Base model, walls in X direction, measurements in meters.

In order to introduce plan irregularity, the stiffness of two outer walls has been changed by closing six of the nine openings of Wall 2 and enlarging the corresponding six windows in Wall 4 (see Fig. 2.7). In such a way it was possible to obtain a plan irregular configuration, that is characterized by a
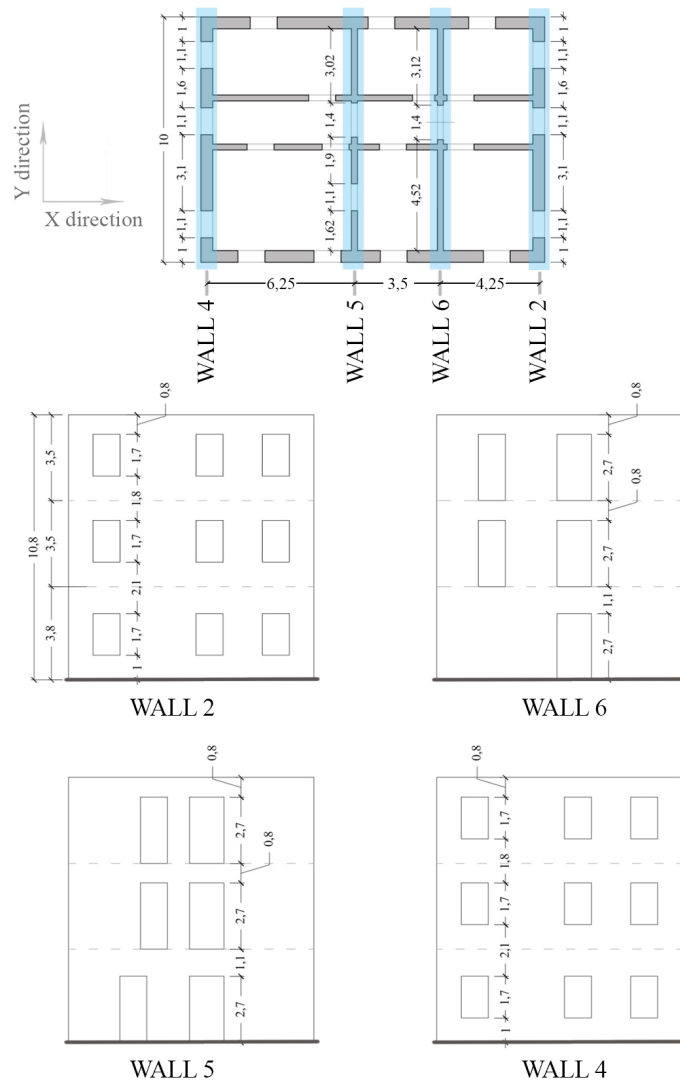
Figure 2.6: Base model, walls in Y direction, measurements in meters.

more significant distance between the mass center (CM) and the stiffness center (CS) than the base configuration (Fig. 2.8). Furthermore, since the openings in Wall 4 were enlarged by the same area of the openings that were closed in Wall 2, the total mass of the building did not change. In fact the aim was to study the effects caused by change of stiffness without introducing the further variability of a mass change.
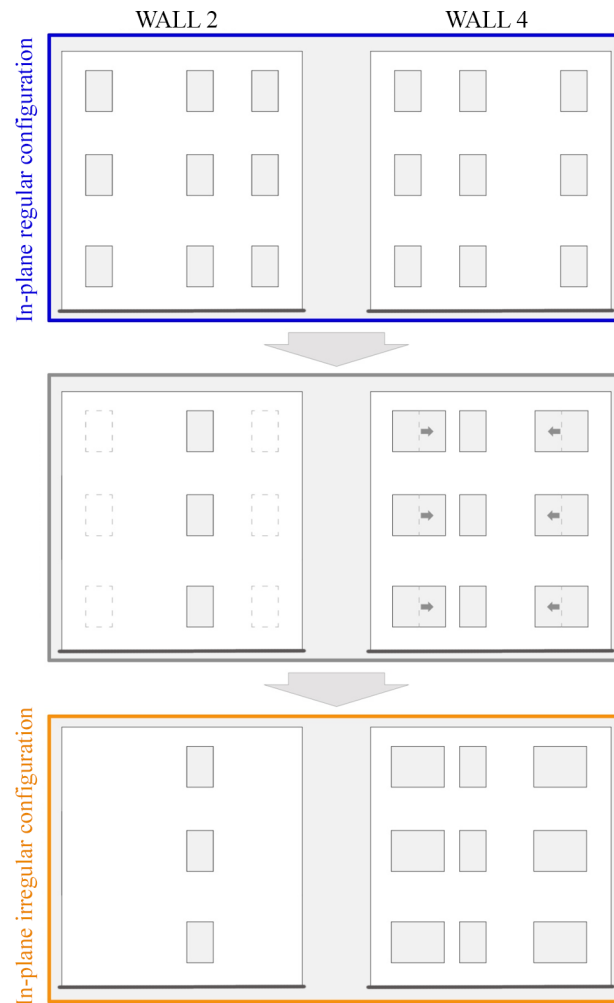

Figure 2.7: Transformations applied to walls 2 and 4 to develop an in plan irregular model.

The in plan irregular configuration presents a significant eccentricity between the CM and CS in X-direction. As a consequence the building shows also a torsional reaction for forces applied in the Y-direction. On the

contrary, for forces applied in X-direction the case study building is almost symmetric. Therefore, to reduce the number of analyses to be undertaken, both static and dynamic analyses were conducted applying only forces in the Y-direction, that, considering the building's geometry, it is also the weakest.
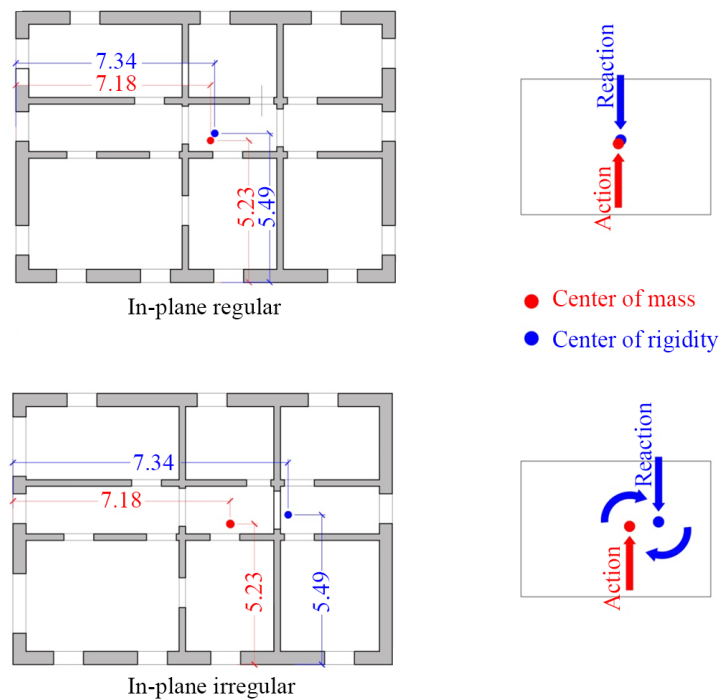

Figure 2.8: Center of mass and center of stiffness for the regular and irregular in plane configurations.

Then, only for in plan irregular models, a further configuration with an elevation irregularity was introduced, it was named with letter "C" and it is depicted in Fig. 2.9. This configuration is a common finding in the historical part of Italian and European cities. In fact, often partial extensions were built above existing buildings over time. As the other stories, the height of the extension is 3.5 meters.

2.2.1 Diaphragm stiffness

The stiffness and the strength of diaphragms play a central role in the seismic response of a building. In fact, diaphragms transfer the earthquake loads to shear walls.

In case of URM ancient and existing constructions, timber floors or vaults often constitute the diaphragms that are therefore far from rigid in their plane. In particular, in the case of timber floors the shear stiffness depends principally on: (i) the sheathing (single or double); (ii) the presence of steel dowels embedded in masonry walls; (iii) the quality of the connection provided by the joists. Reference values for the shear stiffness are provided in [BPP12]. Vaults represent a wide category as well, in this case the shear stiffness depends mainly on: (i) the thickness, (ii) the properties of the materials used and (iii) the shape and geometric proportions (i.e. the rise-to-span ratio, as discussed in [CRL08]).

As far as the floor stiffness is concerned, in [NZ217], when diaphragms are unable to transfer the earthquake loads to shear walls they are considered as *flexible*, on the contrary, when they are able to provide effective transfer of lateral loads to walls are considered *rigid*. These are limit cases and obviously existing diaphragms may show intermediate behavior. Effective stiffness values of a timber diaphragm are proposed in Table C8.8 present in [NZ217]. In that table the different values depend on the direction of loading, the joist continuity and the condition rating. Three condition ratings, based on qualitative observations on diaphragms state, are proposed.

In [ASC14] the diaphragms are classified differently, in particular three categories are proposed:

- *rigid* where the maximum lateral deformation of the diaphragm is less than half the average story drift of the vertical seismic-force-resisting elements of the story immediately below the diaphragm;

- *flexible* where the maximum horizontal deformation of the diaphragm along its length is more than twice the average story drift of the vertical seismic-force-resisting elements of the story immediately below the diaphragm;

- *stiff* when they are neither flexible nor rigid.

Therefore, to study the effect of different diaphragm stiffness on the global response of a multistory URM buildings, in the present research, two additional configurations have been defined, representative of a flexible and an intermediate condition, respectively. The diaphragm's shear stiffness for the three configurations is reported in Table 2.3. The values assigned to the *rigid* configurations are representative of a RC slab; the *flexible* condition is representative of a single straight sheathing, for timber floors, and barrel and cross vaults with a high rise-to-span ratio; finally the *intermediate* condition is representative of double straight sheathing with good connection provided by joists, for timber floors, and cloister vaults or barrel and cross vaults with a low rise-to-span ratio. For timber diaphragms, the values adopted for the *intermediate* and *flexible* configurations were derived from [CRL08], [BPP12] and are consistent with those proposed in [NZ217]. It should be noted that for the *intermediate* condition the *stiff* term was not adopted because to define the values corresponding to that configuration the procedure proposed in [ASC14] was not used.

In TREMURI, the diaphragms are identified by a principal direction (floor spanning orientation), with Young's modulus E_1 (direction of the joist in the case of a timber diaphragm) and E_2 (along the perpendicular direction), Poisson's ratio ν, and shear modulus G_{eq}. The moduli of elasticity E_1 and E_2 represent the normal stiffness of the membrane along the two perpendicular directions and account for the effect of the degree of connection between the walls and the horizontal diaphragm. The moduli provide a link between the in-plane horizontal displacement of the nodes belonging to the same wall-to-floor intersection and hence influence the axial force computed in the spandrels. The most important diaphragm parameter is G_{eq}, which influences the tangential stiffness of the diaphragm and the horizontal force transferred among the walls, in both linear and nonlinear phases [LPGC13]. In [NZ217] the diaphragm stiffness is indicated with G_d and has physical dimension of kN/m. In Table 2.3 G_d is reported as well, which is the product of the equivalent membrane shear modulus G_{eq} times its thickness t_d.

In the present research issues related to the strength of the diaphragms were not studied. Therefore they are modeled with an elastic behavior.
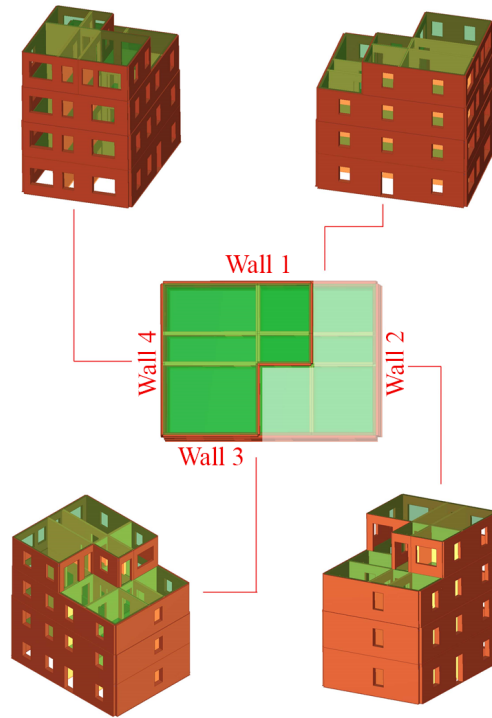
Figure 2.9: 3D view of the model with elevation irregularity, named "C" model.

Table 2.3: Main properties of the equivalent membrane used to simulate the diaphragms.

	Rigid	Intermediate	Flexible
E_1 [MPa]	58800	12000	12000
E_2 [MPa]	30000	1000	1000
G_{eq} [MPa]	12500	100	10
t_d [mm]	40	40	40
$G_d = G_{eq}t_d$ [kN/m]	500000	4000	400
ν [-]	0.2	0.2	0.2

2.2.2 Masonry mechanical properties and loads analysis

It was assumed that the case study buildings were made with full clay bricks and lime mortar. This a masonry typology very common in North Italy and in Table C8A.2.2 present in [Cir09] reference maxima and minima values of the mechanical parameters are present. In the present research the average values of the range proposed in [Cir09] were adopted and reported in Table 2.4, where f_m is the average compressive strength of masonry, τ_0 is the average shear resistance of masonry, E_m is the average value of the elastic modulus, G_m is the average value of the shear modulus and W_m is the average specific weight of the masonry. For f_m a smaller value than the average was assumed, however within the range proposed in [Cir09]. It should be noted that in Table 2.4 E_m and G_m are the secant modulus assumed as half the elastic ones, as proposed in both [EC804] and [NTC08].

Table 2.4: Main properties of masonry adopted for the case study buildings.

f_m [MPa]	τ_0[MPa]	E_m [MPa]	G_m [MPa]	W_m [kN/m^3]
2.80	0.076	750*	250*	18

* Secant stiffness values, assumed as the half of the elastic values reported in Table C8A.2.2 present in [Cir09].

As stated in [LPGC13], observation of seismic damage to complex masonry walls, as well as laboratory experimental tests, have shown that a masonry panel subjected to in-plane loading may show two typical types of behavior: *flexural* (associated to rocking or crushing) or *shear* (associated with diagonal cracking or shear sliding). In TREMURI both flexural and shear behavior are analyzed, but for each case only one failure mode is assumed. In particular the flexural behavior is associated to rocking whereas the shear to the diagonal cracking. For the latter the *Mann and Müller* criterion proposed in [MM80] was used. This choice derives by considerations on the type of masonry studied, characterized by a regular texture and it is assumed to have more resistant and stiff blocks than mortar joints. The *Mann and Müller* criterion is a Coulomb-type criterion based on equivalent cohesion $\tilde{c}$ and equivalent friction $\tilde{\mu}$ parameters, computed starting

Table 2.5: Original and *Mann and Müller* modified friction and cohesion parameters adopted for the masonry.

	Friction [-]	**Cohesion** [MPa]
Original	0.41	0.13
M & M modified	0.34	0.11

Table 2.6: Mechanical parameters of concrete and steel used in the numerical models.

	f_s [MPa]	E_s [MPa]	G_s [MPa]	W_s [kN/m^3]
steel (tie rods)	374	20600	78400	78.5
steel (reinforcements)	296	21000	80770	78.5
	f_c [MPa]	E_c [MPa]	G_c [MPa]	W_c [kN/m^3]
concrete	12.5	29000	12083	25

from those of mortar joints (μ, c) and including also the effect of masonry texture $\varphi = 2h_b/L_b$, where h_b and L_b are the height and the length of masonry units respectively. In the present research it was assumed $\varphi = 2$, and the original and modified values for friction and cohesion are reported in Table 2.5.

In Table 2.6 the material properties used for modeling the concrete of ring beams as well as the steel used for both tie-rods and the ring beams reinforcements are reported.

Loads on diaphragms

Regardless of the stiffness of the diaphragms adopted, the same loads acting on the diaphragms were assumed. The reason of this choice was not to introduce a further variability that may cause a more ambiguous interpretation of results. The loads were computed as the average loads that are expected when RC or wooden diaphragms are present. In particular, the permanent loads were assumed equal to 4.0 kN/m^2 for the roof and to 2.5 kN/m^2 for the other stories. For the roof a higher permanent load was applied because the presence of a crawl space was assumed. The imposed loads were assumed equal to 0.5 kN/m^2 for the roof and 2.0 kN/m^2 for the other stories. For the imposed load the combination coefficient for the

seismic analysis was assumed equal to 0.3, as suggested in [EC804] and [NTC08].

2.3   Modal analysis results

Prior to applying the nonlinear procedures, modal analysis was carried out to study the main dynamic features of the models developed. In fact, different sources of irregularity were inserted to the initial model that had rigid diaphragms and presented both in plan and elevation regularity. As already discussed, the in-plan irregularity was defined with the aim to induce a torsional response to the buildings when forces in Y-direction are applied. For this reason only the natural modes with a significant mass participation in Y-direction were studied and the main results are discussed herein. In Appendix A all the natural modes studied are reported.

For the buildings without elevation irregularity ("A" and "B" models) it was possible to observe that for the *first modes* the deformed shape was almost linear. In particular, in this thesis, the words *first modes* indicate the modes that in a given direction are characterized by a constant sign of displacements at different levels in each wall. In Fig. 2.10 an example of a *first* and a *second* mode is depicted. They refer to Wall 5 of $A_{r,int}$ model and, as it is expected the 1st mode corresponds to a constant sign of displacements at different levels, whereas the first *second mode* is the 8th one.
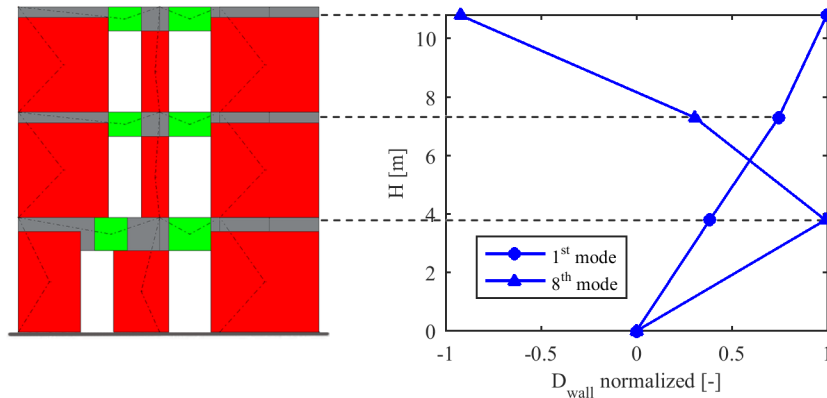
Figure 2.10: 1st and 8th modes deformed shape for Wall 5 of $A_{r,int}$ model. The 8th mode is the first *second mode* of a wall.

The linear deformed shape is typical for URM buildings, in fact in these buildings both stiffness and mass is distributed through the height of the walls. As a consequence it is expected that a triangular force distribution (see Section 3.1.1) may provide a good representation of the inertial forces that are activated by an earthquake. The in plan irregularity introduction caused a presence of a torsional response also in the translational modes. This aspect is shown in Fig. 2.11, where on the X-axis the modal displacement normalized to the maximum displacement of all walls and on the Y-axis the models' height are reported. In particular, 2.11a the 1st mode deformed shape for model $A_{r,rig}$ is depicted and it is possible to observe that all the walls show similar displacements. This is because it is a "pure" translational mode (see also the plan deformed shape in Fig. A.1), on the contrary the 1st mode deformed shape for model $A_{irr,rig}$ presents a torsion as shown in Fig. 2.11b and 2.12a).

(a) $A_{r,rig}$ model, 1st mode, elevation deformed shape

(b) $A_{irr,rig}$ model, 1st mode, elevation deformed shape
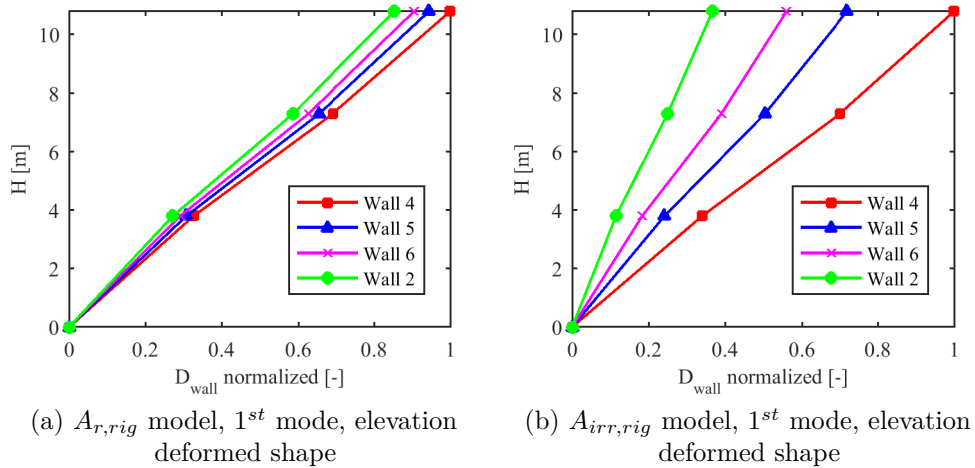
Figure 2.11: 1st mode elevation deformed shape for $A_{r,rig}$ and $A_{irr,rig}$ models.

Reducing the diaphragm stiffness, a single natural mode, usually, does not activate all the walls of the building. An example of that is shown in Fig. 2.12. In particular Fig. 2.12a shows the 1st mode plan deformed shape of $A_{irr,rig}$ model, and Figs. 2.12b, 2.12c, 2.12d the 1st, 2nd and 4th mode deformed shapes respectively of $A_{irr,flex}$ model. It is possible to observe that for $A_{irr,flex}$ model, the 1st mode is not representative of the whole

building's dynamic behavior, but of only a couple of walls (Wall 6 and in particular Wall 2 show almost zero displacements). The same observation is valid for the 2nd and 4th mode. It is therefore possible to say that, in presence of flexible diaphragms a single natural mode "activates" a single wall, rather than the whole building. Furthermore, although the building presents an in plan irregularity, reducing the diaphragm stiffness it is not possible to detect the torsional response anymore. This was noted already for the models with intermediate diaphragm stiffness; for a comparison, in Appendix A all the plan deformed shapes of the most relevant modes are depicted.

Further consequences of the introduction of an in plan irregularity are: 1) the period of the 1st mode increases; 2) the effective 1st mode mass decreases for the rigid and intermediate diaphragms stiffness and increases for the flexible case. The period increase is probably due to the displacement increase on one side of the building as a consequence of the torsional response present in the 1st mode. The variation in the effective mass when rigid diaphragms are present is attributed to the major importance assumed by the torsional mode. When the diaphragms assume the intermediate and the flexible stiffness values, the torsional response is negligible and therefore the effective mass varies according to the stiffness variation of the walls. In fact, for the intermediate case there is a small, less than 5%, reduction whereas in $A_{r,flex}$ the 1st mode effective mass is 36.4% and for $A_{irr,flex}$ is equal to 50.6%. For the flexible case each mode activates the response of single walls, in particular, the 1st mode activates mainly Wall 5 and partially wall 6 of $A_{r,flex}$ model (see Fig. A.29). This is because these are the most flexible walls (they are indeed the thinnest walls). Wall 4 is thicker, therefore more rigid and it is not activated for a period corresponding to the 1st mode. On the contrary, as said, to develop the in plan irregular model the openings present in Wall 4 were enlarged, as a consequence the stiffness of the wall reduced and its period is more similar to Wall 5 and 6. This could be observed in Fig. A.33. So, it is possible to say that when the diaphragms are not rigid, the 1st mode effective mass may be not small only if all the walls present a similar in-plane stiffness.

Similarly to the introduction of an in plan irregularity, the consequences of diaphragm stiffness decrease are that for the 1st mode: 1) the period increases; 2) the effective modal mass decreases. Indeed when the diaphragms

(a) $A_{irr,rig}$ model, 1st mode

(b) $A_{irr,flex}$ model, 1st mode

(c) $A_{irr,flex}$ model, 2nd mode

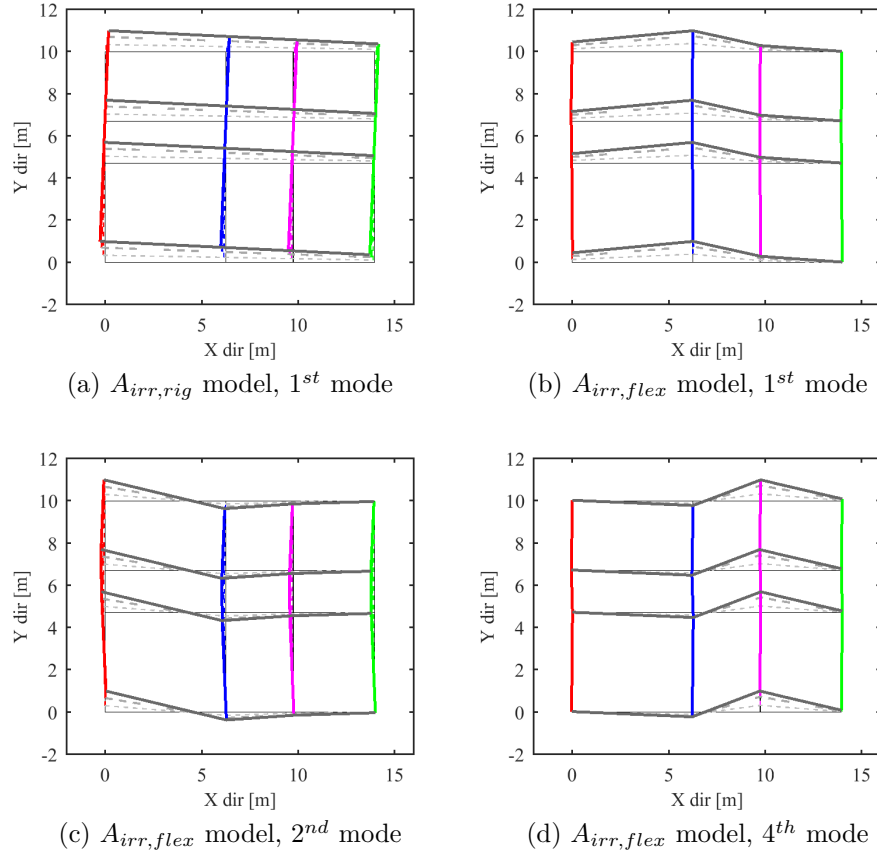(d) $A_{irr,flex}$ model, 4th mode

Figure 2.12: Plan deformed shape comparison between $A_{irr,rig}$ and $A_{irr,flex}$ models. Wall 4,5,6 and 2 colored in red, blue, magenta and green respectively.

are rigid all the wall are connected and therefore forced to move together; as a consequence, more mass is forced to move. It is also possible to observe that the 1st mode period of model $A_{r,rig}$ is equivalent to the average of the periods of the four modes that activate the four walls of model $A_{r,flex}$ (see Table 2.7). This observation is not valid for the model $A_{irr,rig}$ because for that model also the torsional mode activates a significant portion of the mass, whereas, as said, when the diaphragms are very flexible, as in model $A_{irr,flex}$ there is not any torsional effect anymore.

The introduction of ring beams did not cause evident variations in the modal response (see Table 2.7). The modal shapes are similar to the models with tie rods and also the most significant modes properties are the same

(see Appendix A). The most notable difference consists in a slight increase of the modal periods. Indeed, although the ring beams increase the stiffness of the spandrels, their weight increases the total mass as well. However, in the elastic field the increase of mass seemed more significant than the increase of stiffness, for this reason the periods slightly increased.

One of the reasons why models with an elevation irregularity were introduced was to have models with not linear modal deformed shape in elevation. This objective was reached only partially, in fact, as it is shown in Fig. 2.13, only Wall 6 presented a significant displacement increase at top floor. This is due to the fact that at top floor Wall 6 is not as long as the other walls (see Fig. 2.9), and it is therefore significantly less stiff.

(a) $C_{irr,int}$ model, 1st mode, elevation deformed shape

(b) $C_{irr,flex}$ model, 1st mode, elevation deformed shape
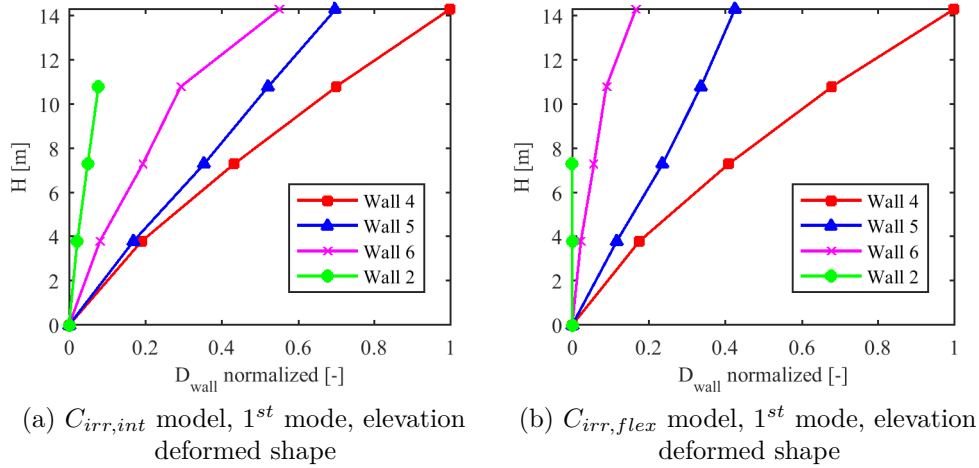
Figure 2.13: "C" models 1st mode deformed shape in elevation.

The main modal properties of the models analyzed are summarized in Table 2.7. It is noted that although the introduction of plane irregularity caused the presence of torsional effects, they were not so pronounced to need to consider the bidirectional effect of the ground motion. In fact, in [CNR14] it is suggested that the the contribution of the two excitation components should be considered when the ratio between the minimum and maximum participation factors is greater than 10%. This ratio is reported in the last column of Table 2.7 and it is possible to observe that for the 1st mode it is always smaller than 10%.

Table 2.7: *First modes* main properties

Model	Mode	T [s]	M_X [%]	M_Y [%]	Γ_X	Γ_Y	Γ_X/Γ_Y [%]
$A_{r,rig}$	1	0.30	0.00	82.8	0.01	1.46	**0.66**
$B_{r,rig}$	1	0.30	0.00	82.9	0.01	1.45	**0.51**
$A_{irr,rig}$	1	0.34	0.12	71.4	-0.07	1.71	**-4.14**
	3	0.21	3.39	11.1	-0.36	0.65	-55.3
$B_{irr,rig}$	1	0.34	0.12	71.4	-0.07	1.70	**-4.16**
	3	0.22	3.33	11.4	-0.36	0.66	54.0
$C_{irr,rig}$	1	0.42	0.04	62.1	-0.05	1.89	**2.56**
	3	0.23	0.77	15.0	-0.18	0.78	22.5
$A_{r,int}$	1	0.32	0.04	70.6	0.04	1.76	**2.41**
	4	0.22	0.00	11.9	0.01	0.70	1.47
$B_{r,int}$	1	0.33	0.03	70.6	0.04	1.76	**2.25**
	4	0.22	0.00	12.0	0.01	0.71	1.34
$A_{irr,int}$	1	0.36	0.03	66.1	-0.04	1.71	**-2.17**
	3	0.27	7.93	4.42	0.51	-0.38	-134
	4	0.21	0.00	8.81	-0.01	0.55	-1.93
	6	0.17	0.10	3.16	-0.07	0.40	-17.5
$B_{irr,int}$	1	0.36	0.03	66.1	-0.04	1.69	**-2.21**
	3	0.28	9.77	4.32	0.55	-0.36	-150
	4	0.21	0.00	9.04	-0.01	0.56	-2.13
	6	0.17	0.08	3.13	-0.06	0.39	-15.9
$C_{irr,int}$	1	0.46	0.03	58.2	-0.04	1.91	**-2.20**
	3	0.30	6.23	5.80	-0.58	0.56	104
$A_{r,flex}$	1	0.38	0.04	36.4	0.05	1.59	**3.15**
	3	0.30	0.01	10.4	-0.03	0.95	-2.66
	5	0.26	1.62	18.5	0.35	1.18	29.7
	6	0.24	1.18	17.4	-0.33	1.27	-26.0
$A_{irr,flex}$	1	0.38	0.01	50.6	-0.20	1.74	**-1.13**
	2	0.36	2.96	3.65	-0.45	0.50	-90.1
	4	0.30	0.00	11.7	0.00	1.02	0.22
	6	0.22	7.58	9.00	-0.59	0.65	-91.8
	7	0.20	13.3	7.21	0.76	0.56	73.5
$C_{irr,flex}$	1	0.49	0.15	43.9	-0.01	1.95	**-5.75**
	2	0.44	0.15	10.2	0.09	0.82	11.4
	4	0.33	0.28	7.83	-0.25	1.31	-18.8
	6	0.24	13.1	1.65	1.37	-0.49	-35.6

2.4   Summary

Starting from a three-story full clay masonry building with both in plan and elevation regularity, a total of 13 models were developed representative of typical residential existing buildings that it is possible to find in Italy and Europe. In order to define these numerical models the following issues were studied:

- structural details present (tie rods, ring beams);

- presence of in plan and/or elevation irregularity;

- shear stiffness of the diaphragms (three different values were adopted).

The procedure adopted to define the numerical models is summarized in Fig. 2.14.

The equivalent frame approach and the software TREMURI were adopted for the modeling and analysis.
The main dynamic characteristics derived by the modal analysis are listed herein:

- the introduction of an in-plan irregularity caused mixed translational-torsional modes;

- reducing the diaphragms shear stiffness:

  1. the fundamental natural mode activates a small amount of walls and therefore mass (often less than 80% of total dynamic mass, as reported in Table 3.1);

  2. the presence of an in plan irregularity does not imply a torsional response;

- the introduction of ring beams did not change the dynamic behavior of the models;

- due to the introduction of an elevation irregularity the mode shapes in elevation are not linear as for the other models;
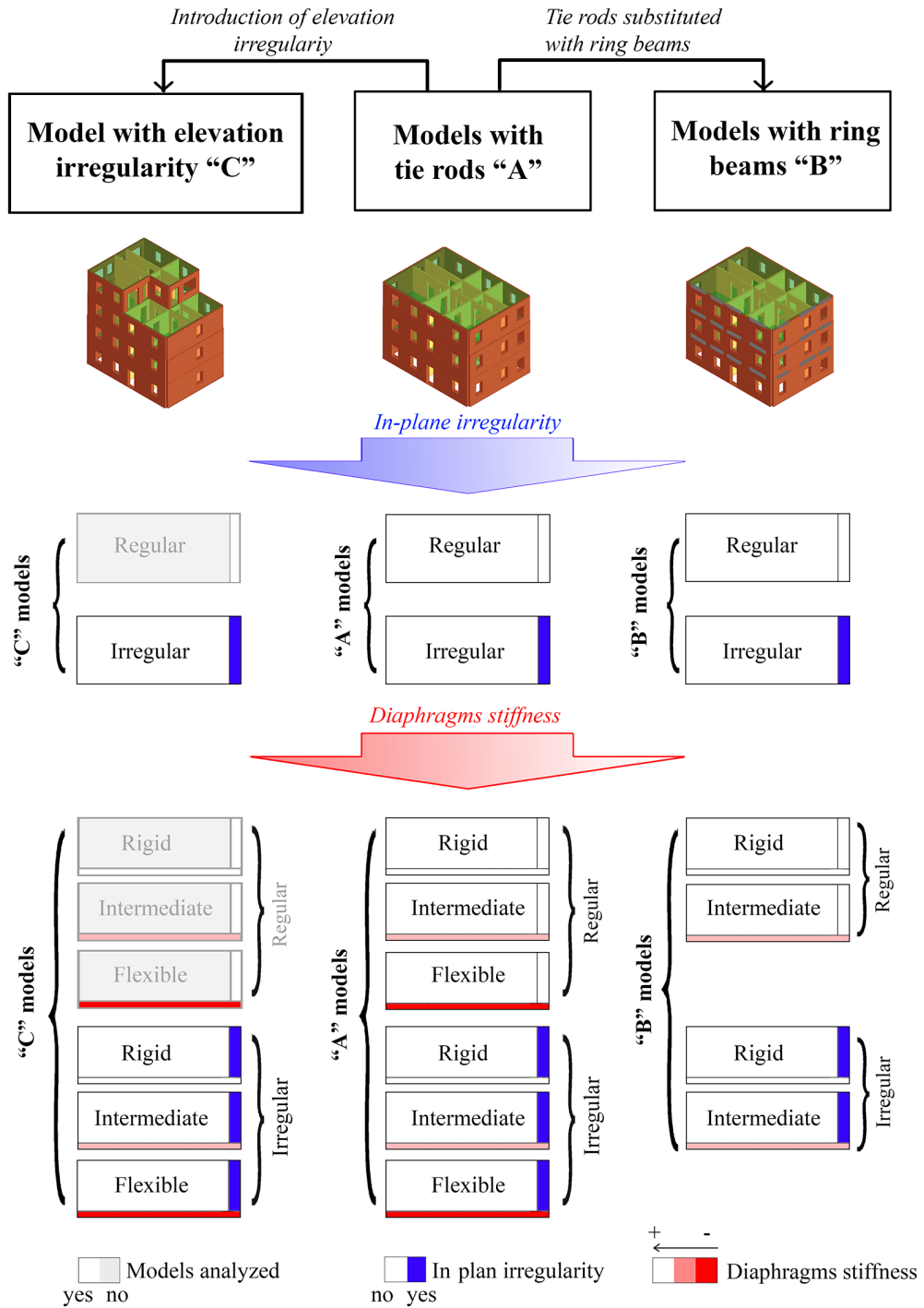
Figure 2.14: Summary of the models developed.

- the introduction of irregularities (in plan, in elevation and due to the diaphragm stiffness reduction) caused an increase of first mode period.

Chapter 3

Procedure: analysis and definition of the damage levels

A performance-based seismic assessment may be undertaken through static or dynamic analyses. In this thesis only nonlinear analyses were studied. The procedure in which the seismic forces are applied statically it is called *nonlinear static procedure* (NSP), whereas if the forces are applied dynamically is called *nonlinear dynamic procedure* (NDP). In both cases it is necessary: 1) for a NSP to define a proper load pattern (LP) to apply to the numerical model and for a NDP to select a number of time-history accelerograms; 2) evaluate the position of performance levels (PLs); 3) to compute the inelastic demand (in terms of displacements or accelerations) that causes the attainment of each PL. In this chapter issues 1) and 2) are discussed. In Section 3.1 the basic principles and the LPs applied for NSP are discussed, then the procedure used for the definition of PLs for the NSP is detailed in Section 3.2 and in Section 3.3 both arguments 1) and 2) are analyzed for NDPs. Issue 3) is discussed in Chapter 4.

3.1 NSP: general procedure in PBEE framework

The purpose of the performance-based seismic analysis is "to give a realistic assessment of how a structure will perform when subjected to either particular or generalized earthquake ground motion" [Fre04]. The two key
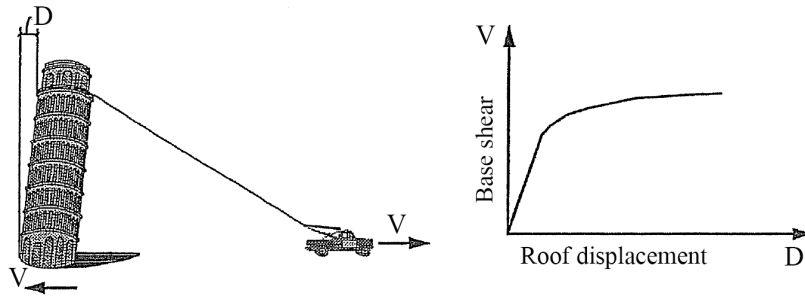
Figure 3.1: Example of a pushover curve (adapted from [ATC96]).

elements of a performance-based assessment procedure are capacity and demand [ATC96]. Demand is the representation of the earthquake ground motion, in this research is evaluated in terms of intensity measure (IM) and is discussed in Chapter 4; capacity is the representation of the structure's ability to resist the seismic demand. The comparison between demand and capacity provides indication of whether a defined level of performance is achieved or not. This section describes the procedures adopted to define the capacity using the nonlinear static procedures (NSPs). Within this procedure, capacity is represented by a pushover curve. Pushover curves are usually plotted by tracking the building base shear and a *control displacement*, usually a point of the roof (Fig. 3.1). This point may be a physical one (as a node of the structural model of the building under analysis) or not (as the weighted displacement of all the nodes at a level). If in case of regular buildings with rigid diaphragms the pushover curve is almost insensitive to the choice of the control displacement, in presence of irregularities and/or flexible diaphragms attention should be paid. In fact, the control displacement must be representative of the displacements of the buildings during an earthquake. For this reason, in this research the *average displacement of all nodes at top floor weighted by their masses* was used as control displacement. A similar criterion was already proposed in [CGLP06], but in that research the displacements of the nodes were not weighted by their masses. The choice of this control displacement derives from the observation that in presence of not rigid diaphragms and walls with different stiffness, the displacement of a single wall may be very different from the other walls' and therefore not representative of the whole building behavior.

Another important issue is the selection of the *master node*, that must

not be confused with the control displacement. In fact, pushover analyses are conducted for an increasing level of load monitoring the displacement of a node, the master node, that may be the same of the control displacement or not. Again, in case of rigid diaphragms this choice is not important, but in presence of flexible diaphragms the numerical results are more accurate if the master node "is selected in the wall that collapses as the first" [LC15a]. For this reason, in this research, for each model studied, the master node was located at the top level of the least stiff wall. The position at top level derives from the consideration that the master node must be above the level wherein collapse occurs [LC15a].

As said, pushover analyses are undertaken for increasing levels of load, and in the common case of multistory buildings the horizontal forces are not applied only at top story, but throughout the height of the building. Therefore the shape of the load patterns need to be defined and it is the topic of the next section.

3.1.1 Load patterns

The pushover curves are generated by subjecting the structural model of the building under analysis to one or more lateral load patterns. A load pattern is usually an approximate representation of the inertial forces that a building may be subjected to during an earthquake.

One of the primary assumptions of non-linear static analysis is that "the pushover curve is an envelope of the response of dynamic analyses; the accuracy of this assumption is strongly dependent on a correct choice of the initial force distribution" [GLP06]. During an earthquake, the distribution of forces on the structure changes continuously, this is due to both elastic and inelastic effects. As stated in [FEM05], in the elastic range "this is attributable to the fact that the response comprises contributions from multiple modes vibration; the actual distribution is difficult to assess since the dynamic characteristics of the ground motion itself are a major influence". Then, inelasticity further complicates the situation. In the early stages of damage (or in case of moderate seismic action), the response of a building is dominated by its modal characteristics that usually increases the action on higher stories. When the level of damage increases it is possible that intermediate levels cannot transfer more seismic actions from the base

of the building to its upper levels and the damage concentrates in the lower ones. This mechanism, more representative of a near collapse condition, is caught with a higher precision applying a load pattern proportional to the masses of the buildings.

For this reason, codes developed in Europe such as [NTC08] and [EC804] prescribe to conduct pushover analyses with at least two different load patterns that must be selected between two groups proposed. In [AÖ10] possible options for LPs are outlined. In the United States the philosophy about the load patterns to apply changed in the last years. In fact, older codes such as [FEM00] prescribed to apply at least two vertical distributions of lateral loads that shall be selected from two groups very similar to [NTC08] ones. On the contrary, in more recent codes such as [FEM05] and [ASC14] it is stated that "multiple force patterns do little to improve the accuracy of nonlinear static procedures and a single pattern based on the first mode shape is recommended". But, in the case of URM buildings with flexible diaphragms a load pattern based on the first mode shape is not reliable because it involves the local behavior of one (or few) wall(s), having therefore a low fraction of participating mass [LC15a]. However, to be exhaustive, also this load pattern was studied in the present research, and the results presented in Chapter 5 confirm its low reliability. Hence, in order to reach a significant total mass participation, an SRSS and a CQC rules based load patterns were defined. In literature, usually SRSS based load patterns foresee a combination of the effects (i.e. displacements, drifts and actions in the elements caused by the application of the forces) rather than the causes (i.e. the load patterns itself). An example of such a procedure is the so called *modal pushover analysis* (MPA), proposed in [CG02] and extended in [RC11] to combine, if necessary, the effect of both components of the seismic action. According to this procedure, separate pushover analyses are carried out each with a load pattern proportional to a modal shape, then the responses from each analysis are combined by appropriate modal combination rules (as the SRSS). A modified procedure of this approach is proposed in the document [CNR14]. In [Kun04] and [KK04] there are further proposals of lateral load distributions: separate analyses with LPs proportional to mode shapes and new LPs based on the combination of different mode shapes are proposed. In the present research, in order to consider the contribution of higher modes this last way

is followed, i.e. to conduct analyses applying LPs derived by the combination of LPs proportional to the more relevant mode shapes. To this aim the SRSS and CQC rules for the combination of the modes were used. For each model the modes that in a given direction were characterized by a constant sign of displacements at different levels in each wall (called in this thesis *first modes*) were used to compute the combined load pattern and they are summarized in Table 3.1. In fact in presence of not rigid diaphragms there is a certain number of modes that do not present change in signs of the displacements at different levels, see Section 2.3. Therefore, SRSS and CQC LPs were computed using the equations herein.

$$f_{SRSS,j} = \sqrt{\sum_{n=1}^{N_I} f_{n,j}^2} \qquad \text{SRSS LP} \qquad (3.1a)$$

$$f_{CQC,j} = \sqrt{\sum_{n=1}^{N_I} \sum_{m=1}^{N_I} \rho_{mn} f_{m,j} f_{n,j}} \qquad \text{CQC LP} \qquad (3.1b)$$

where $f_{m,j}$ and $f_{n,j}$ are the loads applied to node j of a MDOF system when a load pattern proportional to the m and n natural vibration modes respectively is applied, more information on their computation is present in Section C.2 of Appendix C; N_I is the number of first modes and ρ_{mn} is the correlation coefficient proposed in [NTC08] and already defined in [DK79] and computed as:

$$\rho_{mn} = \frac{8\xi_0^2 \beta_{mn}^{3/2}}{(1 + \beta_{mn})[(1 - \beta_{mn})^2 + 4\xi_0^2 \beta_{mn}]} \qquad (3.2)$$

where ξ is the elastic viscous damping (more information on it in Section 4.2.4) of modes m and n, β_{mn} is the inverse ratio of the periods of modes m and n, i.e. $\beta_{mn} = T_n/T_m$. The SRSS and CQC load patters were applied to all models with the exceptions of $A_{r,rig}$ and $B_{r,rig}$, because: 1) the first mode activated % of mass participation (e_1^*) higher than 80%; 2) the only other mode that was not a *second mode* was the torsional mode, but since the models are regular the mass participation is very small (smaller than 1%) and therefore those modes were neglected.

It should be noted that in the previous cited articles ([CG02], [RC11], [Kun04] and [KK04]) the research focused on medium-height or tall RC or steel buildings with rigid diaphragms that have a dynamic behavior very

Table 3.1: Modes combined to define SRSS and CQC load patterns

Diaph. stiffness	models	modes combined	e_1^*	Σe_n^*
Rigid	A_r	-	82.8%	-
	B_r	-	82.9%	-
	A_{irr}	1, 3	71.4%	82.5%
	B_{irr}	1, 3	71.4%	82.8%
	C_{irr}	1, 3	62.1%	77.1%
Intermediate	A_r	1, 4	70.6%	82.5%
	B_r	1, 4	70.6%	82.6%
	A_{irr}	1, 3, 4, 6	66.1%	82.5%
	B_{irr}	1, 3, 4, 6	66.1%	70.4%
	C_{irr}	1, 3	58.2%	64.0%
Flexible	A_r	1, 3, 5, 6	36.4%	82.6%
	A_{irr}	1, 2, 4, 6, 7	50.6%	82.2%
	C_{irr}	1, 2, 4, 6	43.9%	63.6%

different from that of existing URM buildings. In fact, for tall RC or steel buildings higher modes have different sign of displacements at different levels; furthermore, for this kind of buildings, the first modes are usually located in parts of the spectra where the acceleration is lower than the PGA. In case of URM instead, all the main modes are located in the acceleration spectrum plateau.

Finally, in the literature adaptive load patterns are proposed, [AP04a] and [AP04b], with few applications to URM buildings: [Gal06] and [GLP06]. Adaptive pushover however, "fails for systems exhibiting a negative tangent stiffness" [FEM05], such as URM buildings. In fact, as highlighted in [GLP06], adaptive pushover procedures when applied to URM buildings show contradictions that are less evident in RC structures. In fact, the presence of not rigid diaphragms reduces the possibility of redistribution of forces between walls, but "the adaptive algorithm causes redistribution of forces on the weakest wall even if this is not physically consistent" [GLP06]. For all the reasons above cited, adaptive pushover procedures were not adopted in this research.

It is important to underline that in the present research the LPs to conduct the pushover analyses were applied only in Y-direction (see Fig.2.4). In fact, as reported in Section 2.2, the numerical models present in plan

irregularity only for forces applied in Y-direction, on the contrary, for forces applied in X-direction the models are rather symmetric.

Computation of $SRSS^+$ load pattern

From the damage analysis of numerical models with elevation irregularity at the end of dynamic analysis it was observed that often the damage concentrated at the top level (i.e. at the level with a strong reduction in strength and stiffness), as shown in Fig. 3.2a. However, the most common LPs adopted, shown in Figs. 3.2b, 3.2c, 3.2d, at the level of the irregularity reduce the amount of forces applied. This is due to the following reasons: in case of uniform and triangular LPs the force intensity at each level is a function of the masses present at each level and since, due to the elevation irregularity, at top floor there are less masses, the forces are reduced. SRSS LP is computed by the combination of the *first modes*, but only in the *second modes* there is the major excitation at top floor.

Therefore the need to take into account also the second modes emerged. The first idea was to apply the MPA as proposed in [CG02], but this procedure was not pursued in this research because pushover analyses did not show satisfactory results, from a numerical point of view, when load patterns proportional to the *second modes* were applied. This choice is supported by a recent research [NDG$^+$17] in which the Authors state that the MPA is not suitable for URM buildings with flexible diaphragms because "the assumption of the independent 'modal' responses in the MPA, did not capture the cumulative nature of shear damage implemented in the numerical model".

For this reason it was thought to study a different LP, defined by summing the *second modes* contribution to the *first modes*, and in particular to SRSS combination (see Fig. 3.3). This further LP, called $SRSS^+$, was applied to the models with elevation irregularities. $SRSS^+$ LP was computed summing the LP proportional to the *second mode(s)* to the SRSS LP as shown in Fig. 3.3. The *second mode(s)* sign is chosen to increase the forces at the level of the elevation irregularity. The equation used to compute $SRSS^+$ LP is reported herein:

$$f_{SRSS^+,j} = f_{SRSS,j} \pm \sum_{n=1}^{N_{II}} f_{n,j} \qquad (3.3)$$

(a) Damage at the end of NLTH, See Fig. 2.2 for the meaning of colours

(b) Uniform LP

(c) Triangular LP
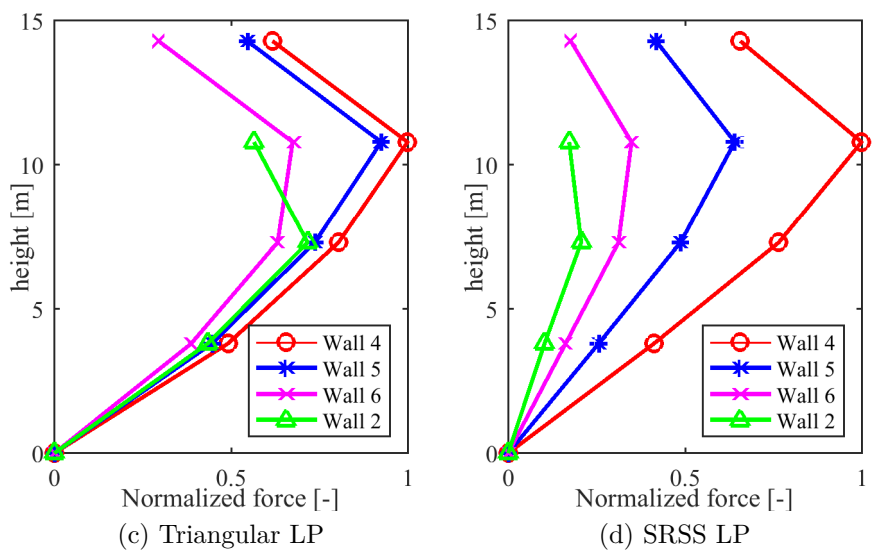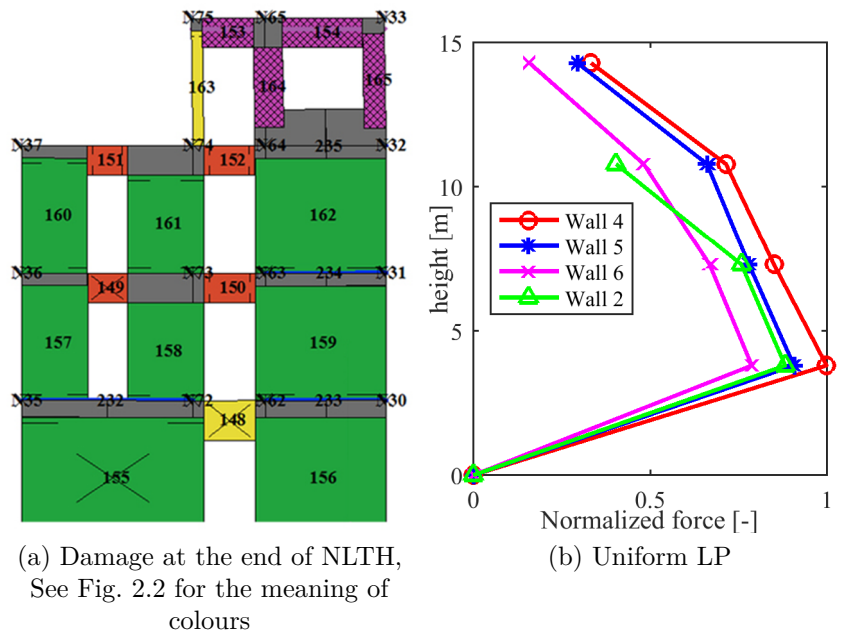
(d) SRSS LP

Figure 3.2: $C_{r,rig}$ model damage after the application of a NLTH and conventional load pattern shapes.

where N_{II} is the number of second modes that need to be considered.

(a) SRSS LP

(b) Proportional to second mode LP
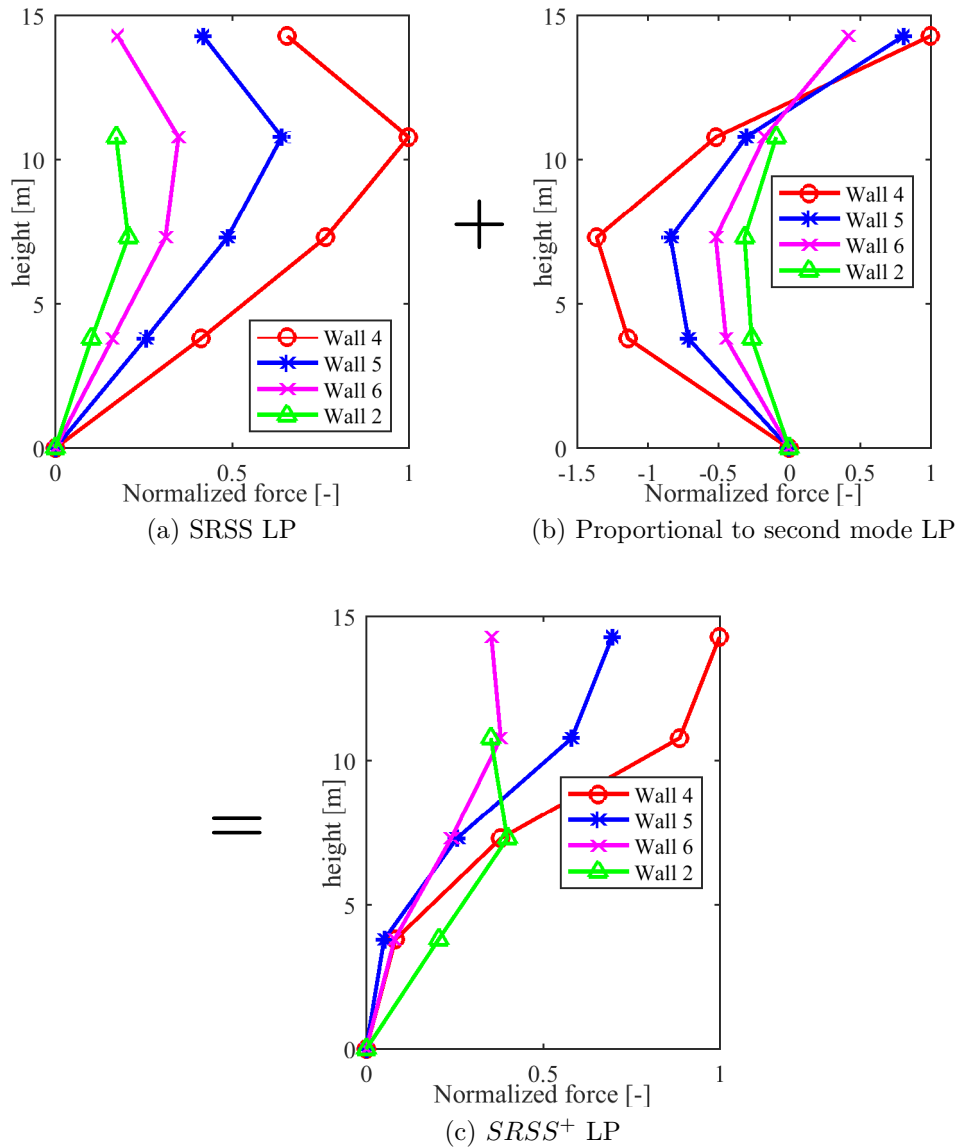
(c) $SRSS^+$ LP

Figure 3.3: Computation of $SRSS^+$ LP example.

3.2 NSP: performance levels evaluation

In order to be applicable, the PBSA requires the definition of *performance levels* (PLs), and in this thesis the *damage levels* (DLs) are the main variables introduced to check for the fulfillment of the corresponding PLs. To this end it is useful to make reference to the empirical definition adopted
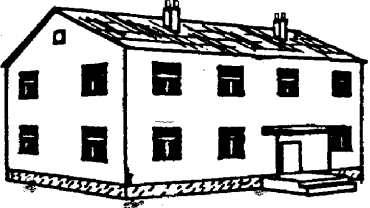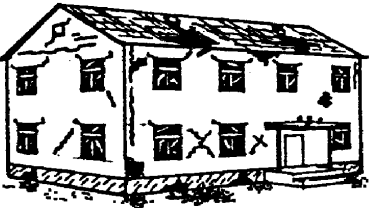
	Grade 1: Negligible to slight damage **(no structural damage,** **slight non-structural damage)** Hair-line cracks in very few walls. Fall of small pieces of plaster only. Fall of loose stones from upper parts of buildings in very few cases.
	Grade 2: Moderate damage **(slight structural damage, moderate** **non-structural damage)** Cracks in many walls. Fall of fairly large pieces of plaster. Partial collapse of chimneys.
	Grade 3: Substantial to heavy damage **(moderate structural damage,** **heavy non-structural damage)** Large and extensive cracks in most walls. Roof tiles detach. Chimneys fracture at the roof line; failure of individual non-structural elements (partitions, gable walls).
	Grade 4: Very heavy damage **(heavy structural damage,** **very heavy non-structural damage)** Serious failure of walls; partial structural failure of roofs and floors.
	Grade 5: Destruction **(very heavy structural damage)** Total or near total collapse.

Figure 3.4: Classification of damage to masonry buildings according to [Ge98].

in the macroseismic post-earthquake assessment [Ge98], of observational *damage states* (DS): 1) slight, 2) moderate, 3) heavy, 4) very heavy, 5) collapse. Fig. 3.4 shows examples of these DSs for an URM building.

These damage states are defined qualitatively, it is therefore impor-

tant to have quantitative methodologies to evaluate them into damage levels and then from the DLs get the PLs. A PL may be related to the use and safety of people but also to conservation requirements that may consider the architectural, and, if present, the artistic and cultural values of the building under seismic assessment. A comprehensive description of safety and conservation requirements, also in presence of artistic assets is presented in [LC15a]. In this thesis the artistic preservation issue is not studied, therefore the PLs were defined in terms of *use and human life* and *building conservation*. In the present research the collapse condition was not analyzed both because it indicates a condition of the building that must be avoided and because it is very hard to insert this condition in a numerically stable software routine. Therefore from the first four damage states (and consequently DLs) four PLs were defined and the connection between PLs and DLs is depicted in Fig. 3.5. The four PLs studied within this research are listed herein (in italic the conditions related to the use and human life) and

- DL1 → PL1: no damage / *fully operational*

- DL2 → PL2: damage limitation / *immediate occupancy*

- DL3 → PL3: significant damage / *life safety*

- DL4 → PL4: near collapse

There is a general agreement in literature that displacements and deformations are better indicators of damage than forces, [PCK07], therefore, the DLs (and consequently the PLs) are evaluated in terms of displacement values through the tracking of suitable quantities called *engineering demand parameters* (EDPs)[1]. For the choice of proper EDPs, as stated in [CLD+12]: "the interstory drift and some limit conditions in terms of base shear reached on the pushover curve (e.g. the maximum base shear or a fixed value of base shear decay) constitute some quite common assumptions as proposed in both codes ([NTC08], [EC804]) and literature ([Cal99]". Through properly defined thresholds of the EDP it is possible to identify

---

[1]The engineering demand parameters normally comprise global displacements (e.g., roof or other reference point), story drifts, story forces, component distortions, and component forces [FEM05].
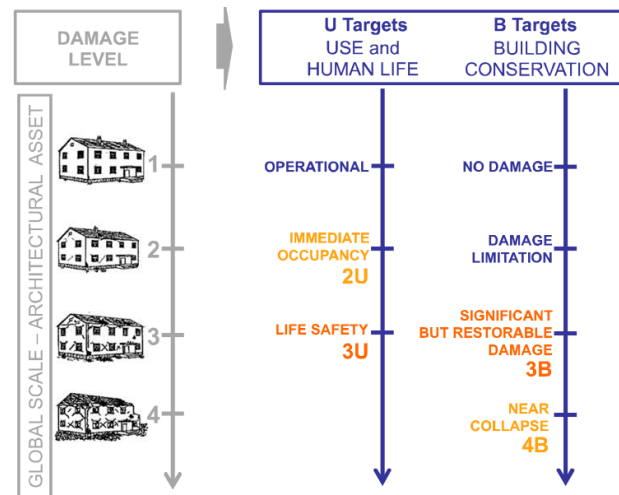
Figure 3.5: Damage levels (DLs) and corresponding performance levels
(PLs), adapted from [LC15a].

the DLs on the pushover curve (in the case of NSP). With the acronym
DLk (k=1,4) is indicated the point after which the building experiences a
DSk, the latter indicates a condition, and therefore the region between two
DLk. From a probabilistic point of view, the attainment of the threshold
that corresponds to DLk means the probability of being in a DS greater or
equal to k is 50%. The procedure currently adopted in codes and guideline
documents may be divided in two main categories [LC15a]:

- *structural element approach*: it assumes that the attainment of a
  certain DL corresponds to the step of the analysis in which the *first*
  structural element reaches the same DL;

- *heuristic approach*: DLs are directly defined on the pushover curve
  on the basis of conventional limits, usually expressed in terms of
  interstorey drift and decay rate of the overall base shear.

The structural element approach is the procedure currently adopted in
[ASC14] and it is commonly used when the constitutive law of the elements
present in the numerical model of the building under analysis does not
present a strength degradation, as for the nonlinear models used for RC
columns and beams that are usually elasto-plastic. As a consequence, the
pushover curve that is obtained does not present any strength degradation

and the verification of PLs is made at the level of single elements [LC15b]. On the contrary, in the case of masonry buildings the nonlinear constitutive laws for piers and spandrels should take into account the strength degradation and this allows to obtain a pushover curve that shows both stiffness and strength degradation. For this reason in the current codes such as [EC804] and [NTC08], that adopts the heuristic approach, the PLs are defined directly on the pushover curve and they require a verification directly in terms of the displacement demand and capacity of the whole building, monitoring a representative displacement (as the *control displacement* introduced in Section 3.1). According to the above cited codes ([EC804], [NTC08]) an *a posteriori* verification of each masonry element is not required.

The criteria currently proposed in the codes may be reclassified following a different philosophy, i.e. analyzing the scale they monitor. It is evident that the structural element approach evaluates the damage evolution of piers (but in literature there are proposals to track the damage in the spandrel as well as in [LC15a]), hence it focuses on a so called "local scale" if compared to checks based on the pushover curve evolution, that refers to the whole building. Therefore, quantities that are related to the whole building behavior refer to a "global scale". In-between a further scale may be considered, the "macroelement scale". The use of the term "macroelement" is clearly defined [CLD+12]: it "refers to portions of an architectonic asset for which, as testified by the earthquake damage survey, it is possible to recognize recurring seismic behaviors". A macroelement may include a set of structural elements (as in the case of a wall, in which piers and spandrels are included) or, in some cases, may coincide with the structure itself. Therefore the response of the building may be evaluated at three scales as shown in Fig. 3.6 and listed herein.

- *global scale*: checks on the pushover curve (Section 3.2.1).

- *architectural elements scale*: damage in macroelements (Section 3.2.2);

- *structural element scale*: local damage to a single pier or spandrel (Section 3.2.3);

The procedures currently proposed in codes are detailed from Section 3.2.1 to 3.2.3 according to the scale they focus. However, as it is shown by the results reported in Chapter 5, to focus only to one scale to check

Structural element / Local scale	Architectural asset / Macroelement scale	Whole asset / Global scale
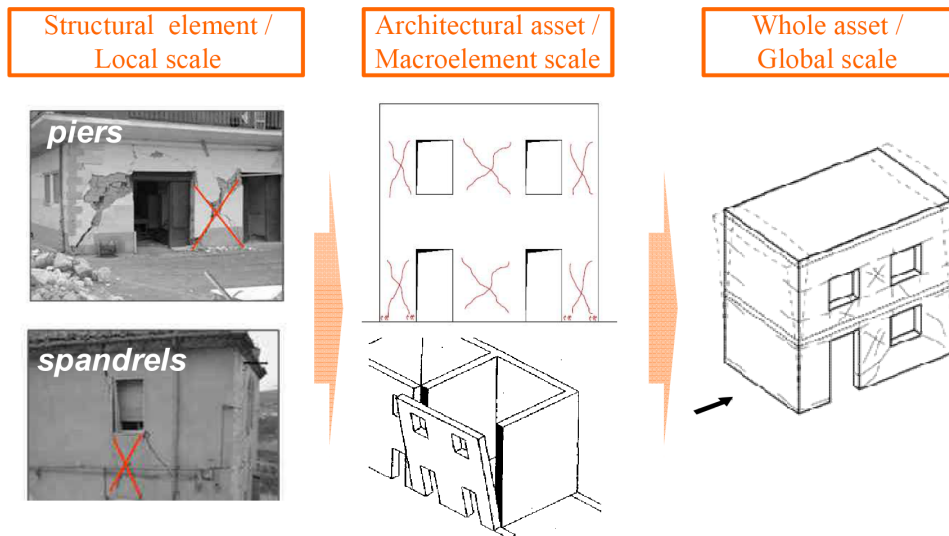
Figure 3.6: Damage assessment at different scales within the multiscale approach, adapted from [CLD+12].

the attainment of a DL is not effective to detect the actual behavior of complex existing URM buildings, that are often irregular in plan/elevation and with flexible diaphragms. Therefore, in order to overcome some of the drawbacks of traditional approaches adopted, within PERPETUATE European research project [LMP+10] a multicriteria approach, herein called *multiscale*, was proposed [CLD+12], [LC15b]. According to the multiscale approach, DLs are defined taking into account the asset response at different scales. However, in the present research, some limitations of the multiscale approach were highlighted, therefore both the method and the updates proposed are detailed in Section 3.2.4.

3.2.1   Global scale

According to the global approach, DLs are defined by tracking the evolution of the pushover curve and the decay rate of the overall building base shear. This is the approach proposed in both [EC804] and [NTC08] for the evaluation of the life safety limit state, and in [EC804] for the evaluation of damage limitation limit state as well. According to [EC804] the damage limitation limit state is related to the yield point of the equivalent bilinear curve representative of the building pushover curve. In Section 4.1 the concept of equivalent bilinear curve will be discussed in detail. However,

in this phase, the transformation of the pushover curve into an equivalent bilinear was not conducted because this transformation is mainly related to the evaluation of the inelastic displacement demand, and this issue, in the present research, is analyzed in a second phase (and discussed in Chapter 4). Therefore, as regards the evaluation of DL2 according to global scale, it was considered reached with the attainment of the pushover curve peak. More precisely, because a pushover curve may present an irregular shape and/or a long section with slope almost equal to zero before reaching its peak, DL2 was considered reached for a displacement in correspondence of 98% of maximum base shear. Then, for both [EC804] and [NTC08] the life safety limit states are evaluated as corresponding to the point of the pushover curve when the base shear decreases by 20%.

Within the multiscale approach the global scale was monitored for all the DLs considered, this is discussed more in detail in Section 3.2.4 and in Table 3.3 the threshold values assumed as reference are reported.

3.2.2 Macroelement scale

According to this criterion a given DL is considered reached when in a story (or level, l) of a wall (w) the interstory drift, $\theta_{w,l}$, exceeds a threshold. This is the method proposed in [NTC08] for the evaluation of the damage limitation limit state, where the limit $\theta_{w,l} = 0.3\%$ is given. No limits are given instead for the others DLs. For this reason, in order to apply this criterion for all DLs it is necessary to refer to the literature available. In [LC15a] and [Cal99] ranges of values for interstory drift limits are proposed; the thresholds values adopted in this research are summarized in Table 3.3.

It is worth mentioning the equation used to compute the interstory drift. In fact, in an existing URM building it should be taken into account also the displacement derived by the rotation of the piers, this may be done through the following equation:

$$\theta_{w,l} = \frac{D_{w,l} - D_{w,l-1}}{h_l} \pm \frac{\varphi_{w,l} + \varphi_{w,l-1}}{2} \qquad (3.4)$$

where h_l is the height of the story at level l, $D_{w,l}$ and $\varphi_{w,l}$ are respectively the average horizontal displacement and the rotation of the nodes located at level l (or l-1) of wall w. The $\pm$ depends on the sign of the rotation that is assumed positive if clockwise. In the presence of ring beams the

contribution of the rotation may be marginal, but this may not be the case in the presence of flexible diaphragms or weak spandrels (i.e. when they have a small flexural stiffens or they are not coupled with elements that may resist to tensile forces).

This criterion is rather easy to use in the professional engineering practice, however it has the limit that it requires a proper definition of the thresholds. In fact, it is difficult to define thresholds that can be adopted for all possible URM walls that are found in existing buildings that may have irregular openings distributions and, in the case of seismic loads, show different damage patterns. The damage pattern is influenced by characteristics such as the: geometry, slenderness, restrain conditions, compression level and masonry mechanical parameters. A change in the damage pattern (that may be dominated by a shear or flexural behavior) implies the attainment of different drift values for both piers and spandrels. In fact, as proposed in [NTC08], for piers the collapse drift limits are set to 0.4% and 0.8% in case of shear and flexural failures respectively. Since the pier drift limits may have such a wide range of variation this will influence the interstory drift as well. In order to overcome this issue, within the present research, a different criterion was studied for the safety checks at macroelement scale and was implemented in an updated version of the multiscale approach. This is based on the minimum damage level reached by the piers at a level in a wall and it is described in Section 3.2.4.

For the sake of completeness, the macroelement scale should comprise safety checks on the diaphragms as well, i.e. monitoring the amount of shear deformation. Currently both Italian and European codes, [NTC08] and [EC804], do not provide any procedure and/or threshold for this issue. Some indications are given in [ASC14] and [NZ217] but without the aim to define any specific PL. This is probably due to the fact that the experimental evidences about this problem are still limited (more information in [GDTI13] and [GWD+14]) and therefore this issue was not studied within the present research.

3.2.3 Local scale

This is the criterion adopted in [ASC14]. According to this criterion a DL is reached when a pier reaches the same DL. No safety checks are undertaken

for spandrels because they are considered as secondary components[2]. In [ASC14], differently from [NTC08] and [EC804], each action is classified as deformation controlled (ductile) or force controlled (non-ductile). In the case of URM walls, deformation-controlled in-plane actions include rocking and bed-joint sliding; force-controlled in-plane actions include toe crushing and diagonal tension that causes cracking through the masonry units. For the force-controlled actions no ductility is foreseen, therefore a DL is reached when the demand exceeds the capacity. Values of the deformation-controlled drift limits are proposed in Table 11-4 of [ASC14]. In [ASC14], for masonry elements force-deformation relations are proposed as well. However, one of the aims of the present research was to compare the criteria proposed in different codes and literature for the DLs evaluation, therefore, in order not to introduce further variables that could make the comparison more difficult to understand, also for the local scale checks, the multi-piecewise linear constitutive law described in Section 2.1 was adopted. Therefore, because the force-displacement relations proposed in [ASC14] are different from those described in Section 2.1, it was decided to use the procedure proposed in [ASC14] only for the evaluation of PL3 (i.e. the one corresponding to the life safety state limit), and some analogies were adopted that are outlined herein.

The first analogy refers to the flexural behavior of an URM pier. In [ASC14] two different mechanism are proposed to analyze the flexural behavior: rocking and toe-crushing (differently from [NTC08] and [EC804] where only one mechanism is proposed); the first is deformation-controlled, whereas the latter is force-controlled. This differentiation was studied through the level of compression in the piers. In fact, it was noticed that the equation proposed in [ASC14] for rocking is valid when the average compressive stress is below 7% the maximum compressive strength, otherwise the toe-crushing equation is used. Secondly, since in Tremuri it is not possible to run an analysis that considers simultaneously the diagonal tension and bed-joint sliding mechanism, for the sake of simplicity, only the diagonal tension mechanism was considered (that is consistent with the mechanism described in Section 2.1). Finally, since in the multi-piecewise

---

[2]In [ASC14] a secondary component is defined as: "an element that accommodates seismic deformations but is not required to resist the seismic forces it may attract for the structure to achieve the selected performance level".

linear constitutive law used for the piers a ductile behavior is adopted (Fig. 2.2), the issue arises if the attainment of a PL is considered corresponding to the displacement at the beginning or at the end of the upper *plateau* (i.e. the *plateau* in correspondence of DL2 in Fig. 2.2). The solution adopted was to study both possibilities, therefore with "Loc. min" is indicated the attainment of a drift in a pier in correspondence of the beginning of the *plateau* and with "Loc. max" the attainment of the *plateau* end. The drift limits for piers adopted to have a DL3 definition consistent with what proposed in [ASC14] are summarized in Table 3.2.

Table 3.2: Piers drift limits for the definition of a DL3 consistent with [ASC14] [*]

Damage level	Shear (diagonal tension)	Flexural	Mixed
Loc. min (when piers show toe crushing)	δ_2	δ_3	δ_3
Loc. min (when piers show rocking)	δ_2	δ_4 [**]	δ_3
Loc. max	δ_3	δ_4 [**]	δ_3

[*] the drift limits refer to the multi-piecewise linear constitutive law described in Section 2.1, and the values present in Table 2.1.

[**] in case of rocking there is not a strength reduction at the attainment of DL3 but only at DL4 (there is therefore a continuous *plateau* from DL2 to DL4.

3.2.4   Multiscale approach and developments proposed

As it is shown by the results present in Chapter 5, the global approach described in Section 3.2.1 is not accurate enough for complex masonry buildings with plan and/or elevation irregularities and without rigid diaphragms. In fact, in these cases, especially when low performance is demanded (i.e. for DL3 and DL4), a "significant damage in one single wall may not appear evident in the pushover curve of the whole structure in terms of strength decay" [LC15b]. Similarly, for the damage limitation limit state, it is acceptable to have some damage in some elements if the global stiffness

degradation is limited and the maximum shear strength is not reached, but an excessive spread of damage in the structural elements should be avoided. However, this spread of damage may not be clearly visible in the pushover curve. On the contrary, for existing URM buildings focus only on local scale may lead to overly conservative results, in fact also in [CNR14] it is stated: "masonry structures are characterized by a configuration that is irregular and complex in many cases; for this reason it is not meaningful to rely on a simple control of the ratio between demand and capacity at the level of the structural elements". Recently, in [KP16] the Authors came to a similar conclusion, in fact they observed that the criterion that fixes the attainment of a DL with the damage of a single piers provided over-conservative outputs. Taking into consideration all these observations, particularly in the presence of not rigid diaphragms, the adoption of a single criterion seems to be unreliable to detect all possible failure mechanism [LC15b].

Therefore a new proposal for the definition of the limit states was developed within the PERPETUATE project. According to this new procedure, called *multiscale approach* [LC15a], limit states are defined on the pushover curve through a multi-scale approach that analyzes the three scales introduced in Section 3.2. The original version of the method as proposed in [LC15a] and adopted in [CNR14] evaluates the position of a DL analyzing: a) the response at global level tracking the evolution of the pushover curve; b) the interstory drift in single walls; c) the exceedance of a predetermined level of drift in a number of structural elements (piers and spandrels). As previously said, the EDP adopted in this thesis is the control displacement, and the displacement corresponding to the attainment of DLk (k=1,..,4) is indicated with $D_{G,DLk}$, $D_{M,DLk}$, $D_{L,DLk}$ for the global, macroelement and local scale, respectively. Therefore the displacement corresponding to the attainment of DLk is computed as:

$$D_{DLk} = min(D_{G,DLk}, D_{M,DLk}, D_{E,DLk}) \quad k = 1, ..., 4 \qquad (3.5)$$

In the following subsections the procedure adopted in the original version of the multiscale approach as proposed in [LC15a] is detailed for all three scales defined. The limits of the method are pointed out and for the macroelement scale a new proposal to overcome the limits is suggested.

57

a) damage states at global scale

At global scale the variable chosen to monitor the attainment of $D_{G,DLk}$ is the rate κ_G of the total base shear over the maximum base shear of the pushover curve ($\kappa_G = V/V_{max}$). The thresholds used in this research for the different PLs are reported in Table 3.3. The use of this criterion allows to: 1) establish at global scale an ideal correspondence with the European macroseismic scale defined in [Ge98] 2) avoid overly conservative evaluations of DL1 and DL2. The thresholds adopted are summarized in Table 3.3, in particular for DL1 and DL2 they are defined in the growing part of the pushover curve, for DL3 and DL4 on the descending one.

It should be noted that for DL1 at global scale, differently from the other DLs, the limit of 50% of maximum building base shear, is a minimum limit (to avoid overly conservative position of DL1): it was assumed that DL1 may not be reached for a displacement smaller than the corresponding to DL1 at global scale. A similar limit was set for DL2: at global scale is is reached with the attainment of 98% of maximum building base shear, but also, to avoid overly conservative positions of DL2 a minimum displacement limit was set corresponding to the attainment of 60% of the building base shear.

b) damage states at macroelement scale

In the multiscale approach original proposal, the safety checks at macroelement scale are undertaken monitoring the interstory drift at each level of each wall of the building. Within the present research also this approach was adopted and the thresholds used for the different PLs are summarized in Table 3.3. Ranges for these thresholds are proposed in [LC15a] that are based on previous researches such as those in [Cal99]. However, the need for these thresholds is a limitation of this criterion, in fact the walls present in existing URM buildings may have very different geometries and openings distributions. Therefore it is difficult to choose proper thresholds for all the possible URM wall configurations. To overcome this limit, a new criterion was proposed to evaluate damage level at macroelement scale: the so called *DLmin* check. According to this criterion a DL (and consequently a PL) is reached when all piers in a story of a wall reach a DL equal to or higher than the considered one (Fig. 3.7). As for the interstory drift check,

(a) Example of a wall that did not reach DL3: at top story one pier is still presents DL2

(b) Example of a wall that reached DL3: at top story all the piers present DL3 or higher
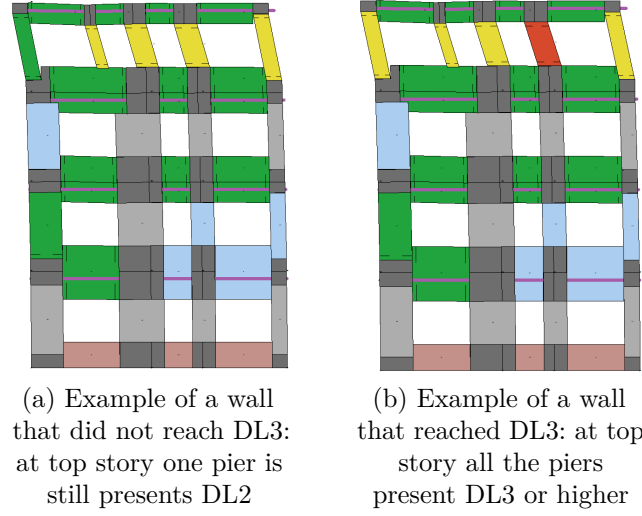
Figure 3.7: DLmin criterion for the damage level evaluation at macroelement scale, see Fig. 2.2 for the meaning of colors.

the aim of this criterion is to detect, if present, the trigger of a soft story mechanism. This criterion has the advantage that does not need to define interstory drift thresholds, but it is based only on piers behavior, for which it is possible to find more data in literature ([PB14], [VZPB17]) than for story mechanisms. In particular, considering the force-displacement relationship for piers introduced in Section 2.1, in this thesis the DLk (k = 1,...,4) was considered reached according to DLmin criterion when all piers at a level reached DLk, as shown in Fig. 3.7.

c) damage states at scale of the single elements

The criterion that monitors the evolution of damage at local scale within the multiscale approach uses a different philosophy than the one adopted in [ASC14]. In this case a DL is not reached when the first pier reaches a given DL, but cumulative rates of elements that reach a certain DLk ($\Lambda_{P,DLk}$ for piers and $\Lambda_{S,DLk}$ for spandrels) are introduced to check for the attainment of $D_{E,DLk}$.

The cumulative ranges of damage are defined in [LC15a], in particular $\Lambda_{S,DLk}$ is defined as the percentage of spandrels that reached or exceeded a given DLk (checked through the reaching of given drift thresholds δ_{DLk}

at structural element scale):

$$\Lambda_{S,DLk} = \frac{1}{N_s} \sum_{s=1}^{N_s} H\left(\frac{\delta_s}{\delta_{DLkk}} - 1\right) \quad kk = k + 2 \tag{3.6}$$

where the sum is extended to the total number of spandrels (s = 1,...,N_s) in the buildings and H is the Heaviside function (equal to 0 until the demand δ_S in the s-th spandrel does not reach the capacity δ_{DLkk}).

The cumulative rate of damage $\Lambda_{P,DLk}$ is defined as the percentage of piers that reached or exceeded a given DLk, weighted on the corresponding cross section A_p:

$$\Lambda_{P,DLk} = \frac{\sum\limits_{p=1}^{N_p} A_p H\left(\frac{\delta_p}{\delta_{DLkk}} - 1\right)}{\sum\limits_{p=1}^{N_p} A_p} \quad kk = k + 1 \tag{3.7}$$

where the sum is extended to the total number of piers (p=1,...,N_p).

Table 2.1 summarizes the values (in terms of drift limits) adopted as reference to define damage states in case of piers and spandrels [CLD+12].

It is worth noting that, according to Eq. 3.6 and 3.7, a higher damage level is accepted in spandrels than in piers. For example, "to check the attainment of DL2 (k=2) the reaching of damage levels 3 (kk=k+1) and 4 (kk=k+2) are checked at the scale of pier and spandrel elements, respectively. In case of DL4, only the attainment of DL 5 in piers is considered" [LC15a]. This difference is justified by their different role in the global response; in fact, as stated in [CLD+12]: "it is assumed that severe damage in spandrels does not compromise the seismic capacity of buildings in the same way as in piers" (which bear both static loads and seismic actions).

In [LC15a] for the local scale check a threshold of 3% was proposed. It means that in a building with a hundred piers when three piers reach DLk+1, the attainment of DLk is considered attained. As for the interstory drift check, a limit of this approach is in the definition of the threshold itself, which that is rather arbitrary. For example, during the present research it was noticed that a value of 3% was too high, because with that limit the local criterion was never decisive. Therefore a value of 2% was used for the building typologies analyzed.

Some further issues should now be considered. First, the in case of rather small buildings using the limit of 2 or 3% may bring to the threshold

of only one pier. For this reason, a further coefficient was introduced in the threshold that is equal to 1 over the number of piers (and spandrels), so also for small buildings the limit is not excessively small. Finally, only the damage derived by the seismic action should be considered. Therefore the threshold considers also the cumulative rate the damage due to the application of self weight. These last quantities are indicated with $\Lambda_{P,DLk,SW}$ and $\Lambda_{S,DLk,SW}$ for piers and spandrels respectively. Both these last two coefficients are reported in Table 3.3.

Summary of the adopted version of the multiscale approach

The original version of the multiscale approach was adopted using the thresholds reported in Table 3.3. Then, to overcome the limits in defining thresholds at macroelement scale an updated version of the method was used in which at the macroelement scale the DLmin criterion, described above, rather than the interstory-drift was adopted.

Table 3.3: Thresholds adopted for the multiscale approach with the interstory drift check.

Scale	Variable	PL1	PL2	PL3	PL4
Global	κ_G	0.5	0.98	0.8	0.6
	lower bound	0.5	0.6		
Macroelement	$\theta_{w,l}$	0.1%	0.3%	0.5%	0.7%
Local	$\Lambda_{P,DLk}$	$(0.02 + 1/N_P + \Lambda_{P,DLk,SW})$			
	$\Lambda_{S,DLk}$	$(0.02 + 1/N_S + \Lambda_{S,DLk,SW})$			

3.3   NDP: procedure adopted

In a nonlinear dynamic procedure (NDP) the seismic input is the acceleration time-history (TH) at the base of the structure. Due to issues related to the *record-to-record variability*, ten different records were used. They are compatible with the accelerations expected in L'Aquila (Italy), and they are conditioned to the spectral acceleration S_{ae} for the period T = 0.36s, assumed as representative of the main (first) modes of vibration of the considered buildings (Fig. 3.8). As it is outlined in Chapter 4, in this research the intensity measure adopted is the 5%-damped first-mode spectral
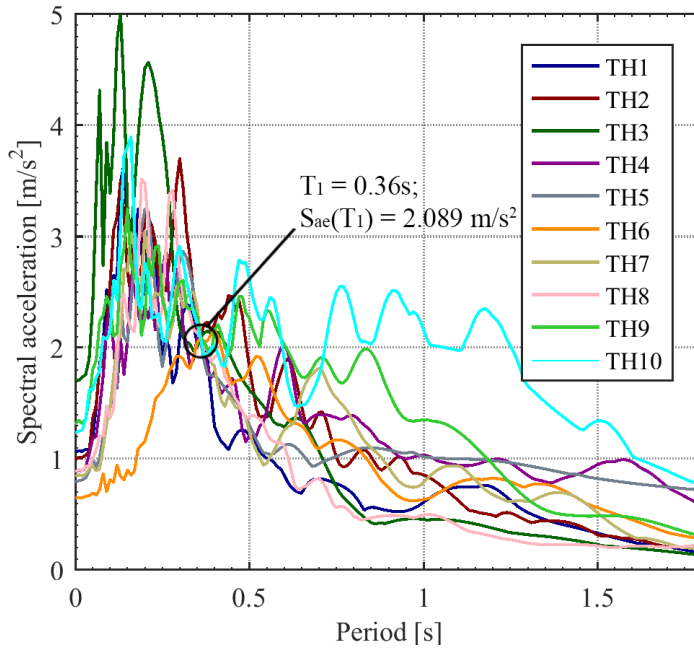
Figure 3.8: Elastic acceleration response spectra of the 10 time histories adopted.

acceleration $S_a(T_1, \xi = 5\%)$ (for the definitions of intensity measure see Chapter 4). However the results are shown in terms of PGA because it is a more intuitive quantity than $S_a(T_1)$. Fig. 3.9 depicts the average (50% percentile), 16% and 84% percentiles response spectra of the ten THs used up to a period of 2 s. They are compared with the Italian code response spectrum with unitary PGA, and it can be observed that it is close to the ten THs median spectra. More information on the THs used is available in Appendix B.

In order to have a consistency between static and dynamic analyses, the 50%, 16% and 84% response spectra from the 10 THs were used to evaluate the intensity measure with the NSP as well (Chapter 4).

In order to undertake the nonlinear dynamic analyses two possible procedures are available: the Multiple Stripe Analysis (MSA) described for example in [JC09], and the Incremental Dynamic Analysis (IDA) as defined in [VC02a]. A discussion of the advantages and disadvantages of the two techniques can be found in [Bak15]. In the present research the NDPs have been performed in the form of IDA. This procedure consists in
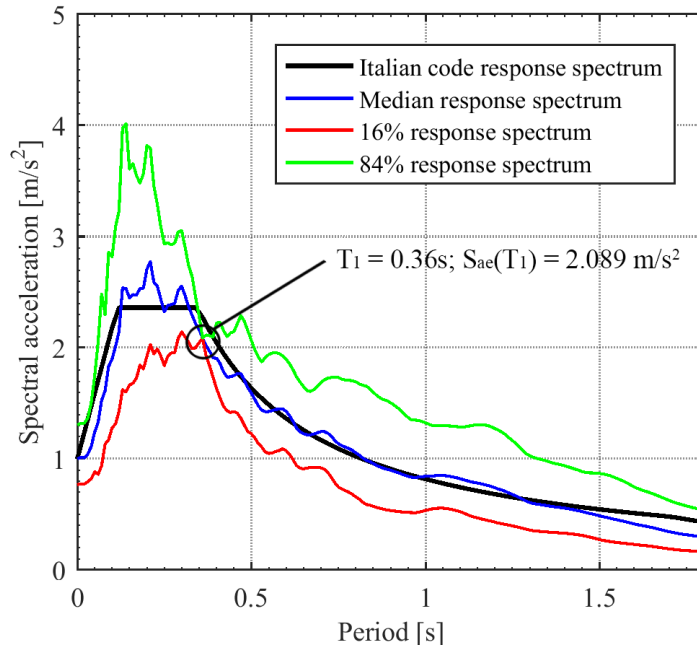
Figure 3.9: Median, 16% and 84% response spectra compared with code response spectrum with unitary PGA.

scaling each time history in order to obtain increasing intensity values of the seismic action, "ideally selected to cover the whole range from elastic to non-linear and finally to collapse of the structure" [VC02a]. In Section 4.3 the definition of IDA curves as well as the procedure adopted for the evaluation of IM with the NDP are detailed.

In Tremuri, it is possible to apply the time-history accelerograms for the three spatial components. However, in this research, in order to have a more consistent comparison with the results from NSPs, the THs were applied only in Y-direction. For each record, the analyses were conducted scaling the PGA of each TH with coefficients from 0.5 to 6 or 7 (considering the strength of the building and the characteristics of the TH) with step of 0.5. Although the uncertainties that may arise in using scaled time histories, this is a procedure commonly used due to the still limited number of time histories available (although always increasing). Furthermore, as discussed in [LB07] the issue of scaling records is limited when the scaling coefficient is rather small. Therefore it was controlled that this scaling factor was limited. In fact, for the most "critical" case study models (i.e. the "C" models, those

for which the procedure adopted by current Italian and European codes provides the less conservative results, see Chapter 5) the average scaling records factor was smaller than 2. For all the other models it was however smaller than 3.5 (at least up to PL3). Only for $A_{r,rig}$, $B_{r,rig}$, $A_{irr,rig}$ it almost reached the value of 4.

Rayleigh's coefficients adopted

In order to perform a nonlinear dynamic analysis a damping model needs to be adopted in order to reproduce the energy dissipation. In the present research the Rayleigh viscous damping model was assumed. According to this approach, the damping matrix is obtained as a linear combination of the stiffness and mass matrices of the MDOF model representative of the building under analysis:

$$\underline{C} = \alpha \underline{M} + \beta \underline{K} \tag{3.8}$$

where $\underline{M}, \underline{C}$ and $\underline{K}$ are the mass, damping and stiffness matrices respectively. The damping ratio for the n-th mode of such a system is the sum of a mass proportional and a stiffness proportional contribution [Cho95]:

$$\xi_n = \frac{\alpha}{2\omega_n} + \frac{\beta}{2}\omega_n \tag{3.9}$$

The coefficients α and β can be determined from specific viscous damping ratio ξ_1 and ξ_2 for two frequencies, ω_1 and ω_2 respectively. It is assumed that within this range of frequencies the viscous damping is almost constant and smaller than or equal to a selected value of critical damping. In this thesis this value was chosen to be equal to 0.03 (not higher to avoid overdamped models, see Fig. 3.10). The two frequencies ω_1 and ω_2 need to be chosen considering the features of the buildings analyzed, in particular ω_1 was associated to the elastic stiffness, and therefore equal to the frequency of the first natural mode; ω_2 is related to the secant stiffness in correspondence of the building that is close to a collapse condition. Therefore, ω_2 may be estimated by ω_1 using the following equation:

$$\omega_2 = \frac{\omega_1}{\sqrt{\mu}} \tag{3.10}$$

where μ is the ductility shown by the building when it is close to the collapse (more details about the ductility in Section 4.2.1), and in this research $\mu = 9$ was set.
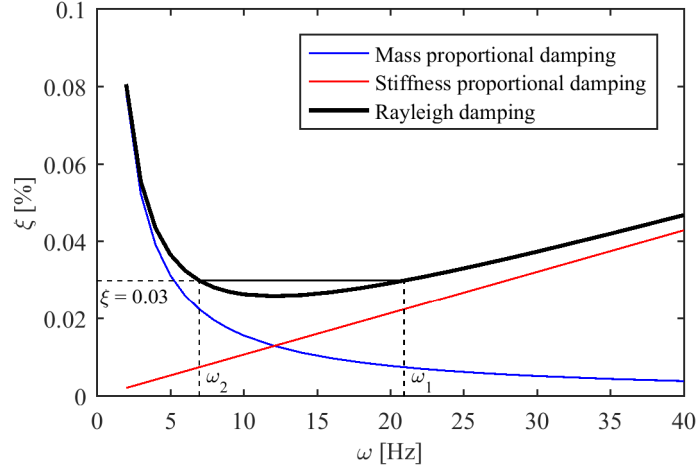
Figure 3.10: Variation of Rayleigh damping with frequency. The curves refer to the coefficients reported in Table 3.4 for $C_{irr,int}$ model. Very similar curves were developed applying the other coefficients present in Table 3.4.

Therefore from Eq. 3.9 it was possible to calculate α and β solving the following system:

$$\begin{cases} \xi = \dfrac{\alpha}{2\omega_1} + \dfrac{\beta}{2}\omega_1 = 0.03 \\[2mm] \xi = \dfrac{\alpha}{2\omega_2} + \dfrac{\beta}{2}\omega_2 = 0.03 \end{cases} \tag{3.11}$$

The values of ω_1 and ω_2 should be fitted for the different numerical models, however, for the sake of simplicity, it was decided to reduce this variability. This choice was supported from the results of modal analysis (Section 2.3), that are summarized in Table 3.4 and 3.5 for the A-type and B-type models respectively.

It may be observed that for both building types the average period of all *first modes* is similar and the global average is equal to 0.28 s. Then, because the period of some modes is smaller than 0.28s, the period corresponding to ω_1 was set to 0.25 s (Table 3.6). Regarding C-type models the periods varied in a wider range, therefore different values of ω_1 were adopted for each model and they are reported in Table 3.6. Then, the α and β values were computed solving the system shown in Eq. 3.11 for the ω_1 values adopted and they are summarized in Table 3.6. The coefficients used allowed to have a viscous damping less than 3% for periods corresponding to the

Table 3.4: *First modes* periods for A-type models

Model	Periods [s]					Av. period [s]
$A_{r,rig}$	Mode 1					
	0.296					0.296
$A_{r,int}$	Mode 1	Mode 4				
	0.324	0.215				0.270
$A_{r,flex}$	Mode 1	Mode 3	Mode 5	Mode 6		
	0.381	0.303	0.264	0.237		0.296
$A_{irr,rig}$	Mode 1	Mode 3				
	0.336	0.211				0.274
$A_{irr,int}$	Mode 1	Mode 3	Mode 4	Mode 6		
	0.359	0.273	0.208	0.173		0.253
$A_{irr,flex}$	Mode 1	Mode 2	Mode 4	Mode 6	Mode 7	
	0.384	0.360	0.302	0.219	0.201	0.293
				All A-type models		0.28 s

Table 3.5: *First modes* periods for B-type models

Model	Periods [s]				Average period [s]
$B_{r,rig}$	Mode 1				
	0.301				0.301
$B_{r,int}$	Mode 1	Mode 4			
	0.329	0.220			0.275
$B_{irr,rig}$	Mode 1	Mode 3			
	0.341	0.216			0.279
$B_{irr,int}$	Mode 1	Mode 3	Mode 4	Mode 6	
	0.364	0.278	0.212	0.176	0.258
			All B-type models		0.28 s

fundamental modes (both elastic and secant). For the higher modes (i.e. up to 0.1s for A and B models and 0.18s for C models) the damping never exceeded the 6%.

Table 3.6: Assumed threshold frequencies and α and β values for Rayleigh damping

Model	T_1 [s]	ω_1 [Hz]	T_2 [s]	ω_2 [Hz]	μ [-]	α	β
A, B	0.25	25.12	0.75	8.37	9	0.376991	0.001791
$C_{irr,rig}$	0.23	27.32	0.69	9.11	9	0.409773	0.001647
$C_{irr,int}$	0.30	20.94	0.90	6.98	9	0.314159	0.002149
$C_{irr,flex}$	0.44	14.40	1.31	4.80	9	0.216165	0.003123

3.3.1 Definition of the limit states

The definition of DLs from the results of nonlinear dynamic analyses is not straightforward. First proposals of DLs definition in relation to the results of nonlinear dynamic analyses are in [VC02a], where frame structures were analyzed and the identification of PLs was based on the analysis of: 1) the extent of damage; 2) the IDA curves (defined in Section 4.3.1). More recently, in [MRPM14] and [KP16], researchers proposed DLs definition for URM buildings when the NDP is applied. In [MRPM14], the Authors tested various approaches for the definition of limit states in case of NDPs, in particular, referring to the DL introduced in Section 3.2 they studied PL from 1 to 3 through the definition of DLs. In that research they decided not to study a PL comparable to DL4 because the definition of the near collapse PL may be a really difficult task that implies several issues such as "assumptions in the structural models, computer program used for the analysis, numerical convergence and stability of the solution" [MRPM14]. Therefore three DLs were analyzed, comparable to DL1, 2 and 3 of the present thesis, for DL1 one criterion was adopted whereas for DL2 and 3 three different criteria were examined with the idea behind to identify limit states which were not directly based on drift quantities. In that research this choice was motivated "to try and describe the global damage of the structure by means of some parameters that are truly representative of the evolution of the structural condition during the nonlinear dynamic

analysis". In case of DL1, the Authors suggest to adopt the displacement associated to the first pier reaching its maximum shear resistance. For DL2 and DL3 three criteria were proposed and summarized herein:

1. criterion 1 - identification of a DL from total base shear: the DL2 is reached at the attainment of the maximum base shear; DL3 in correspondence to the degradation to 80% maximum value of the force-displacement curve enveloping the response curves of all time-history analyses carried out.

2. criterion 2 - identification of a DL based on the percentage of pier area failing: the two DLs are identified based on the number and percentage of *piers* (spandrels are considered secondary elements) which achieve the maximum shear drift.

3. criterion 3 - identification of a DL tracking the evolution IDA curve slope: DL2 was identified at first significant change of slope; DL3 when the slope reaches 7% of the its initial value.

In their research they analyzed five case studies with rigid diaphragms and they run mono-dimensional analyses (the load was applied only in one direction). Criterion 2 has the limit in a definition of proper thresholds suitable for the different URM building typologies, furthermore the Authors noticed that this criterion showed a significant dependence on the record-to-record variability. About criterion 3 they noticed that its application appeared problematic for both DLs: for DL2 the difficulty arises on recognizing where exactly the first change of curvature occurs; for DL3 it is necessary to select a percentage of initial slope that represents a damage level adequate for the life safety limit states.

In [KP16] two main approaches were adopted in the DLs definition: one defined "local criterion" in which a DL was defined with reference to specific points of the moment-rotation backbone curve adopted by the Authors for the URM elements; then a second criterion defined "global criterion" in which a global damage index is assigned based on the number of piers damaged. The Authors noticed that using their "global criterion" the condition of 20% pier failures (condition that wanted to simulate the usual definition of structural failure in a code context) is not always reached and it confirmed that in presence of not rigid diaphragms "substantial

damage is localized in specific regions, leaving the rest of the elements nearly intact". From that research emerged that the definition of a general procedure for the DLs evaluation in case of NDPs of URM buildings is still an open issue. In fact, they concluded that "assigning the entire building to a certain damage state is much more an issue of engineering judgment than of accurate analysis" and as a general recommendation, "the qualified engineer ... should carefully examine the specific building at hand, assess ad hoc the implications of local failures (in particular with respect to life safety) and also carry out two or more sensitivity analyses invoking different global failure criteria" [KP16].

Finally, in the currently adopted codes, such as [EC804] and [NTC08], no specific recommendations for the PLs definition in case of NDPs are present.

Therefore, for the DLs definition two issues were considered: 1) the definition of a DL from the results of a nonlinear dynamic analysis is not straightforward and "no definitely convincing proposals can be found yet in literature" [MRPM14] and 2) in the present research the nonlinear dynamic analyses were used as a reference solution for the NSP. As a consequence, for NDPs, the position of DL was defined with the multiscale approach with a procedure as similar as possible to the one outlined in Section 3.2.4. In fact, as already discussed in [MRPM14] and [KP16], a procedure that invokes criteria at the different scales of a building is deemed as more robust. The differences between the multiscale approach adopted in the NSP and NDP are outlined herein:

- at element scale the same thresholds of NSP, and reported in Table 3.3, were adopted;

- for NDP, at macroelement scale it was not possible to use also the DLmin check, because using this criterion for each dynamic analysis the output is not a continuous number, but a "yes or no", and this does not allow to compute the median values of 10 THs; therefore only the interstory drift check was used with the thresholds reported in Table 3.3;

- the global scale check was used to give a maximum limit to the displacements: for every DL, the maximum displacement was computed from the pushover analysis considering all the LPs applied, and

this was considered as the maximum displacement threshold. As for the nonlinear static analyses, for DL1 and DL2 minimum displacement limits were set: for DL1 equal to the attainment of the 50% of maximum building base shear of pushover curves and DL2 in correspondence of 60% of maximum building base shear. The criterion proposed in [MRPM14] based on the identification of a DL from total base shear was not used because it presents difficulties when applied to models with flexible diaphragms, as outlined in Section 5.1.

It should be noted that, conceptually, these criteria are similar to what was recently proposed in [MRPM14] and [KP16].

3.4   Summary and main issues

For all the URM building models described in Chapter 2 both nonlinear static and dynamic analyses are conducted.

NSPs are conducted following the procedure outlined herein:

1. pushover analyses undertaken with different load patterns applied in Y-direction, proportional to the:

   - numerical model node's masses (*'uniform' LP*);
   - product of the node's masses for their heights (*'triangular' LP*);
   - first mode shape (1st *mode*);
   - SRSS combination of the *first modes* (*SRSS LP*);
   - CQC combination of the *first modes* (*CQC LP*);
   - $SRSS^+$ combination, only for building with elevation irregularity, see Section 3.1.1.

     Note: the *uniform* and *triangular* LPs are the most commonly adopted for an assessment according to [NTC08] and [EC804]; the 1st *mode* LP is the only LP to be applied according to [ASC14].

2. for every pushover analysis, a pushover curve is plotted that presents in the horizontal axis the *control displacement* (average displacement
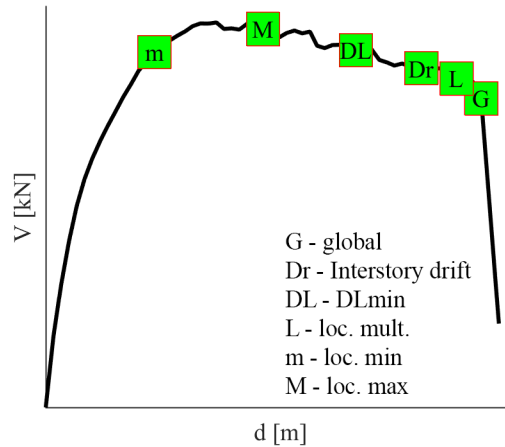
Figure 3.11: Example of a pushover curve with highlighted the position of a PL applying the methodologies described in Section 3.3.1.

of all nodes at top floor weighted by their masses) and in the vertical axis the base shear of the building (Fig. 3.11);

3. various DL (or correspondingly PLs) are evaluated, according to what was proposed in the *multiscale* approach and in the currently adopted codes such as [NTC08], [EC804] and [ASC14], in particular for the different DLs:

   - DL1: multiscale approach;

   - DL2: multiscale approach and as proposed in [NTC08],[EC804];

   - DL3: multiscale approach and as proposed in [NTC08],[EC804] and in [ASC14];

   - DL4: multiscale approach.

An example of a pushover curve with highlighted all the PL studied is shown in Fig. 3.11.

Subsequently, **NDPs** are conducted following the procedure outlined herein:

1. for each numerical model 10 THs are applied in their Y-direction, in the form of Incremental Dynamic Analysis (IDA);

2. the position of PLs was evaluated using the multiscale approach as for the NSP, with some differences at macroelement and global scale:

   - macroelement scale, the interstory drift criterion rather than the DLmin is adopted (the motivation is pointed out in 3.3.1);

   - global scale, it is used with displacement limits given by the nonlinear static analyses, in particular: for DL1 the global check sets a *minimum* displacement limit corresponding to 50% of pushover maximum base shear; for DL2 sets both a *minimum* displacement limit corresponding to 60% of pushover maximum base shear and a *maximum* limit at the attainment of 98% of pushover maximum base shear; for DL3 and DL4 sets maximum displacement limits as for the NSP.

Finally, in this chapter some issues are outlined that will be analyzed and discussed in Chapter 5:

- the LP proportional to 1st mode may not be accurate if applied to URM buildings with flexible diaphragms;

- the definition of PLs based on safety checks at only one scale may give not conservative results in irregular URM buildings, in particular if they have not rigid diaphragms;

- the thresholds currently proposed for the PL evaluation may be arbitrary and not suitable to capture the variety of configurations present in existing URM buildings (see interstory drift and local scale for multiscale approach).

Chapter 4

Procedure: evaluation of the performance

Performance-Based Seismic Assessment (PBSA) of an existing building checks if the structure is able to attain some selected Performance Levels (PLs) in case of an occurrence of earthquake hazard levels, defined by the annual rate of exceedance λ (or return period $T_R \approx 1/\lambda$) [LC15b]. The severity of the input motion is characterized by the so called *intensity measure* - IM. There are various quantities that may be adopted as IM: the peak ground acceleration (PGA) is the most frequently adopted IM due to the large amount of information and models that are available. Other possible IMs are the spectral acceleration for a significant period of vibration, the maximum spectral displacement, Arias intensity and Housner intensity ([LC15b], [DSU$^+$15]). As anticipated in Section 3.3, in this research the intensity measure adopted is the 5%-damped first-mode spectral acceleration $S_a(T_1, \xi = 5\%)$, but the results are shown in terms of PGA because it is a more intuitive quantity than $S_a(T_1)$. In fact, the latter require the knowledge of the spectra shape. Once a proper intensity measure (IM) has been selected as the one better correlated with the building capacity, "the maximum IM compatible with the fulfillment of each PL that has to be checked (IM_{PLk}, k=1,..,4 if four PLs are considered) is adopted as relevant outcome of the assessment" [LC15b]. Therefore the IM_{PL} is the maximum value of the intensity measure that is compatible with the fulfillment of each target PL [LC15a].

As already discussed in Section 3.2, for the seismic assessment of exist-

ing buildings it is preferred to compare capacity and demand in terms of displacements rather than forces. Furthermore, since for long return period earthquakes a nonlinear behavior is expected, it is necessary to calculate the *nonlinear* displacement demand. In the literature two main methodologies are adopted to evaluate the non-linearity, through the use of: 1) inelastic spectra (as in the *N2 method*, Section 4.2.1 and *Coefficient Method*, Section 4.2.3); 2) overdamped spectra (*Capacity Spectrum Method*, Section 4.2.4).

The N2 method is the procedure currently adopted in both Italian [NTC08] and European [EC804] codes. However, this method was conceived and developed for the seismic design of regular RC buildings; as a consequence, this method presents some drawbacks when applied for the seismic assessment of existing irregular URM buildings. In this chapter the main issues of the method are analyzed, and an original procedure to evaluate the nonlinear displacement demand is proposed that takes into account very recent literature proposals (Section 4.2.2).

The NSP, regardless the procedure applied to evaluate the nonlinear displacement demand, needs that the pushover curve representative of the MDOF system capacity be transformed into a *capacity curve* of an equivalent SDOF and that is the topic of Section 4.1.

Finally in Section 4.3 the procedure to evaluate the IM_{PL} using the NDP is outlined.

4.1 NSP: from MDOF to equivalent SDOF systems

The NSPs are based on some rough assumptions such as: 1) the response of the structure depends mainly on one vibration mode; 2) the behavior of a structure with *multiple degrees of freedom* (MDOF) subject to seismic ground motion can be estimated from the response of an oscillator with a *single degree of freedom* (SDOF). Concerning the last assumption, it should be noted that the seismic capacity of a building is calculated on a MDOF model representative of its structural elements. Then, this capacity needs to be compared with the seismic demand expected in the region where the building is located and to this aim the codes provide the response spectra (in terms of acceleration, velocity and displacement). However, the

response spectra, by definition, represent the peak response of SDOF models subjected to ground motions. For this reason it is necessary to transform the MDOF response deriving from the pushover analysis to an equivalent SDOF response. Therefore the capacity of the structure is connected to a SDOF model response and it motivates the assumptions above mentioned.

In the case of nonlinear static analysis, the capacity of a MDOF model is represented by a pushover curve (see Section 3.1). In some procedures this curve is often simplified as an equivalent bilinear formed by two sections: an elastic phase (up to the yielding point that has coordinates D_y, V_y) and the plastic phase up to the ultimate displacement D_u. Different procedures are proposed in codes and literature to generate this equivalent bilinear diagram: a general overview and the procedure adopted in both Italian and European codes is given in Section 4.2.1, whereas the procedure adopted in [ASC14] is outlined in Section 4.2.3. Fig. 4.1a shows an example of a pushover curve and a possible equivalent bilinear approximation. Subsequently, the transformation of the pushover curve (or the equivalent bilinear) into a *capacity curve*, representative of a SDOF system is made through the use of participation factor Γ, as proposed in [Faj00]. This coefficient is discussed in detail in Appendix C for the dynamic response of an elastic system. In that case it is necessary to compute as many Γ coefficients as the number of natural modes to be considered. In case of a NSP, the procedure is slightly different, in fact the participation factor adopted is function of the nodal displacements due to the application of forces. Therefore, the equations adopted to compute Γ coefficients in X and Y directions are reported herein:

$$\Gamma_X = \frac{\underline{\phi}^T \underline{M} \underline{t_X}}{\underline{\phi}^T \underline{M} \underline{\phi}} \quad ; \quad \Gamma_Y = \frac{\underline{\phi}^T \underline{M} \underline{t_Y}}{\underline{\phi}^T \underline{M} \underline{\phi}} \tag{4.1}$$

where $\underline{\phi}$ is the normalized reference deformed shape representative of the pushover analysis under consideration, $\underline{t_X}$ ($\underline{t_Y}$) is the vector that allows to apply the seismic action in the X (Y) direction and $\underline{M}$ is the mass matrix of the MDOF model. In case of modal analysis $\underline{\phi} = \underline{\phi_n}$, i.e. the modal shape of the n-th mode (see Appendix C), in case of nonlinear static analysis it is necessary to choose a reference deformed shape. Currently, in both national and international codes such as [ASC14], [EC804] and [NTC08] it is proposed to use the first mode shape normalized by the ordinate at the roof (control node), regardless of the load pattern applied to the

numerical model. However, in existing URM buildings, the presence of not rigid diaphragms may produce relevant differences in the computation of Γ coefficients (as well as m^*, discussed subsequently in this section), therefore, in order to detect the URM building features, the deformed shape obtained by the pushover analysis at the first steps (i.e. in the initial elastic phase) was used as reference deformed shape [LC15a]. Although in this research one-dimensional analyses were undertaken, and therefore the loads were applied only in the Y-direction (Fig. 2.4), these forces caused small nodal displacements in direction X as well. Therefore the equation to calculate the participation factors to take into account also their contribution was modified and herein reported not using the vectors (as in Eq. 4.1), but the sum of all nodes:

$$\Gamma_Y = \frac{\Sigma m_{j,y}\phi_{j,y}}{\Sigma m_{j,y}\phi_{j,y}^2 + \Sigma m_{j,y}\phi_{j,x}^2} \tag{4.2}$$

where $m_{j,x}$, $m_{j,y}$ are the dynamic mass of node j in direction X and Y respectively, $\phi_{j,x}$, $\phi_{j,y}$ are the normalized displacements of node j in direction X and Y respectively, due to the application of the given horizontal load (that as said in these research was always in Y direction).

From Eqs. 4.1 and 4.2, it should be observed that Γ coefficient depends on the normalization adopted to evaluate $\underline{\phi}$ from the deformed shape. In this research the deformed shape was normalized to the control displacement, defined in Section 3.1 as the average displacement of all nodes at top floor weighted by their masses. The equations used to transform the pushover curves into capacity curves are given herein:

$$F_y^* = \frac{V_y}{\Gamma} \quad ; \quad d_y^* = \frac{D_y}{\Gamma} \tag{4.3}$$

where the "*" indicates that the quantity refers to a SDOF system. Examples of capacity curves (derived directly from the pushover curve or by the equivalent bilinear) are shown in Fig. 4.1b.

4.1.1 Response spectra in the acceleration-displacement format

The capacity curves need to be compared with a consistent response spectrum. To this aim, the traditional acceleration and displacement response

(a) Example of a pushover curve and an equivalent bilinear representative of the curve

(b) Capacity curve derived from a pushover curve and equivalent bilinear
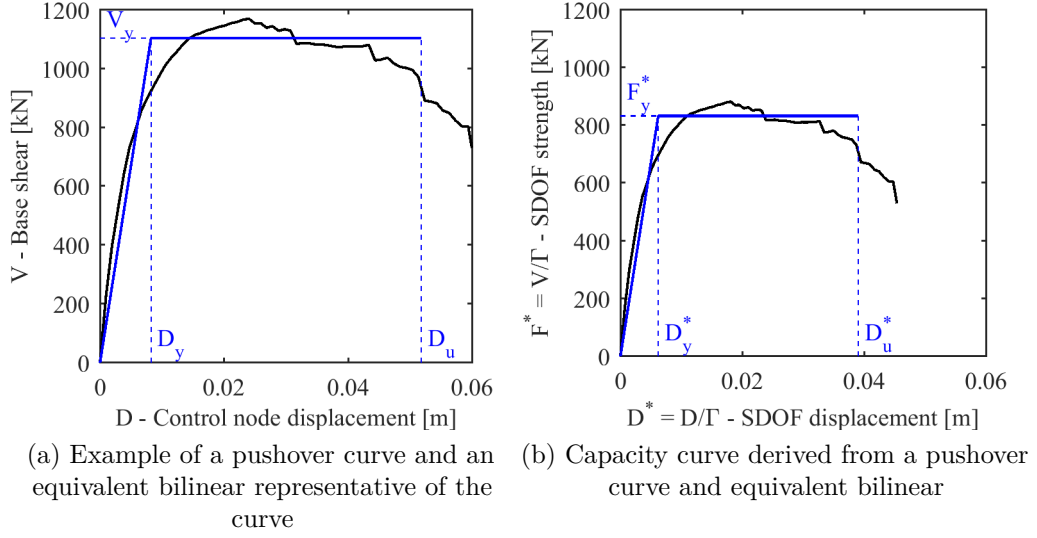
Figure 4.1: Examples of pushover (MDOF) and capacity (SDOF) curves

spectra need to be converted to the so called acceleration-displacement response spectra (ADRS); an overview of this conversion is given in [ATC96]. This conversion is relatively easy to undertake using the equation herein that links the acceleration and displacement spectral quantities:

$$S_{Ae}(T) = \left(\frac{2\pi}{T}\right)^2 S_{De}(T) = \omega^2 S_{De}(T) \tag{4.4}$$

where S_{Ae} is the elastic spectral acceleration at period T, S_{De} is the elastic spectral displacement at period T and $\omega = 2\pi/T$ is the frequency corresponding to the period T. In this format, lines passing through the origin of the axes and a point of the spectra indicate the period corresponding to the acceleration and displacement of that point (Fig. 4.2). Herein, the equation used to evaluate the period:

$$T = 2\pi\sqrt{\frac{S_{De}}{S_{Ae}}} \tag{4.5}$$

An example of the derivation of an ADRS is shown in Fig. 4.2, and it is possible to observe that as in the acceleration-displacement (AD) space the periods are indicated by lines passing through the origin.

However, the curves depicted in Fig. 4.1b cannot be compared with the spectra in the AD format, in fact in Fig. 4.1b on the Y axis there is
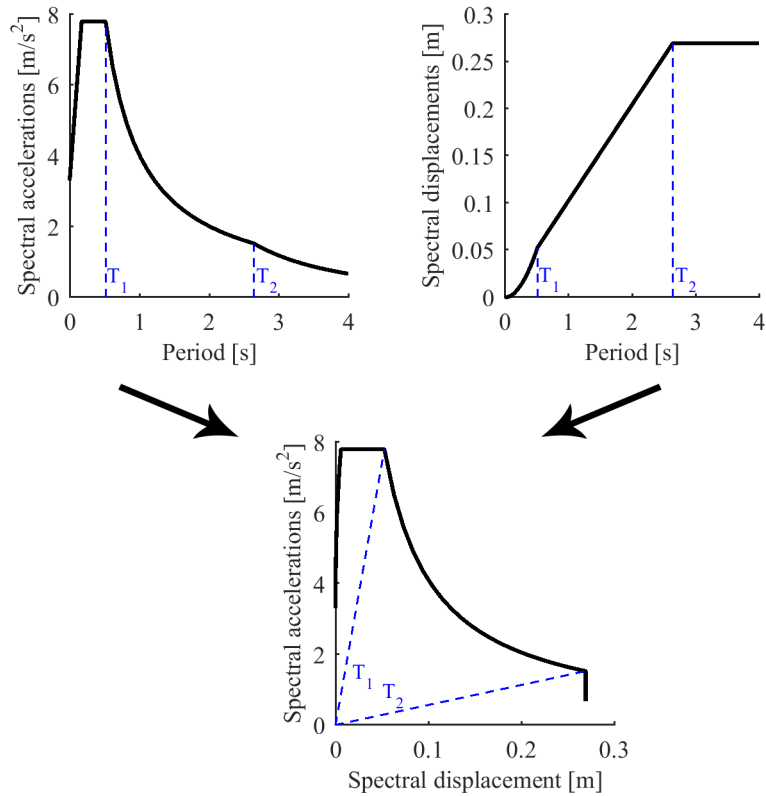
Figure 4.2: Derivation of an acceleration-displacement response spectrum

a force instead of an acceleration. Therefore, in order to have a consistent comparison, the forces represented on the Y axis need to be divided by a representative mass of the equivalent SDOF system. This is computed similarly to the *equivalent mass* of the n-th mode as outlined in Appendix C. The equation used to compute m_X^* is reported herein:

$$m_X^* = \underline{\phi}^T \underline{\underline{M}} \underline{t_X} \tag{4.6}$$

with the meaning of symbols defined above, a similar equation, but with $\underline{t_Y}$ is used to compute m_Y^*.

An example of capacity curve in the AD space is depicted in Fig. 4.3. To underline that quantities refer to the AD space, they are not written with capital letters, therefore the displacements are indicated with "d" instead of "D" as in the pushover curves.
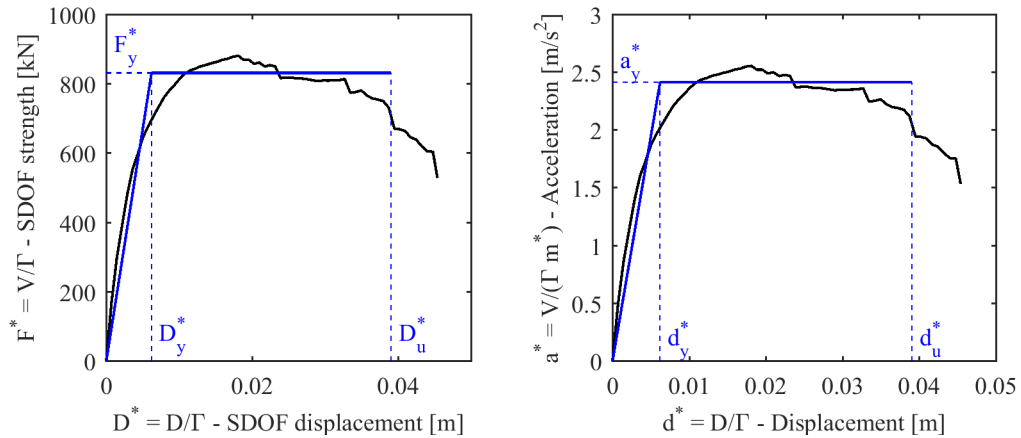
(a) Capacity curve and equivalent bilinear in a force-displacement space

(b) Capacity curve and equivalent bilinear in the AD space

Figure 4.3: Examples of pushover (MDOF) and capacity (SDOF) curves.

4.2 Intensity measure calculated with the nonlinear static analysis

4.2.1 N2 method

The N2 method was firstly proposed by Fajfar and Fischinger [FF88] and then developed, initially for the planar analysis of regular RC structures [FG96], [Faj99] and [Faj00], and subsequently by considering also higher mode effects in both plan and elevation ([KF11] and [KF12]). This is the method adopted to evaluate the inelastic displacement demand, and hence the IM, in the NSP according to the Italian code [NTC08] and Eurocode 8-1 [EC804]. In the N2 method the evaluation of the seismic demand is based on the use of inelastic spectra, instead of highly damped elastic spectra, as done through the Capacity Spectrum Method (see Section 4.2.4).

The name of the method derives from the proposals to use two distinct nonlinear models: for the materials and the response spectra. The first hypothesis requires the adoption of nonlinear constitutive models for the materials and the use of nonlinear static analysis (Chapter 2), then to comply the second hypothesis inelastic spectra are used. In fact, since the buildings may be subjected also to extended damage during the earthquake, their capacity should not be compared with the elastic spectra but with

spectra which consider that part of the energy that is dissipated in the damaging process. For this reason the concept of *ductility* was introduced, that is the capacity of a structure to deform beyond the material elastic limit of its load bearing elements. Specifically, ductility (μ) is defined as the ratio between actual inelastic displacement and the displacement corresponding to the end of the elastic phase. The *control displacement* corresponding to the end of the elastic phase is usually called *yield displacement* (D_y). Pushover analyses investigate the behavior of structures beyond their elastic limits, through the application of incremental forces applied at each step i of the analysis. To each applied force corresponds a control displacement and therefore a ductility μ_i (Fig. 4.4). The same procedure may be applied in the case of elasto-plastic force-displacement relationship and in this case usually only one value of ductility is considered, i.e. the ratio between the ultimate displacement (D_u) and the yield displacement (Eq. 4.7 and Fig. 4.4).

$$\mu = \frac{D_u}{D_y} \qquad (4.7)$$

It is possible to evaluate the inelastic displacement of an *inelastic SDOF*
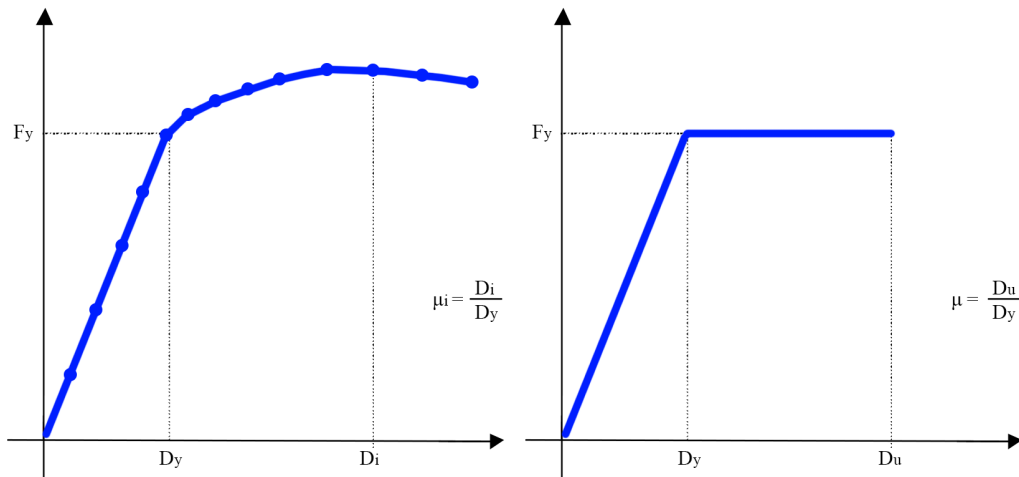
Figure 4.4: Ductility definition. Left, in case of a pushover analysis, the ductility is evaluated at each step of the analysis, right the ductility in case of an elasto-platic force-displacement relationship.

system with a bilinear force-displacement relationship that presents a *given*

ductility. It is known that for an elastic SDOF system, in the elastic phase, force (F) and displacement (D) are related through the equations herein:

$$F = KD = m\omega^2 D \tag{4.8}$$

where K is the elastic stiffness of the SDOF system and ω is its natural frequency. From the equation of motion of a SDOF model, it is known that $\omega^2 = K/m$, where m is the mass of the SDOF system. Therefore at yielding:

$$F_y = m\omega^2 D_y \tag{4.9}$$

From the definition of ductility (Eq. 4.7) and considering Eq. 4.9 it is possible to write the ultimate displacement D_u of a SDOF system:

$$D_u = \mu D_y = \frac{\mu F_y}{m\omega^2} \tag{4.10}$$

Evaluation of inelastic response spectra

Since the behavior of buildings subjected to strong earthquakes is typically inelastic, they may reach a given displacement with a reduced value of strength if compared with the strength developed if they behaved elastically (Fig. 4.5). In last decades numerous researches were conducted on nonlinear SDOF models with elasto-plastic force-displacement relationship ([VN60],[VNC65] and [NR80]). It was concluded that the response depends on the period of the SDOF system. In particular, in the medium and long period range the displacements of elastic systems were very similar to the displacements of the inelastic ones; in the case of short-period structures the inelastic displacements were larger than the elastic ones [Faj00]. The first behavior has been called as *equal displacement approximation*, the latter as *equal energy approximation*. The latter name derives from the fact that it is possible to compute the ultimate displacement considering approximately equal areas under the elastic and inelastic relationship. Sometimes these rules are called "principles", although they are not based on a rigorous theoretical framework but on numerical simulations[1]. Fig. 4.5 shows an example of these behaviors. The ratio between the elastic and inelastic

---

[1]However, these rules seem reliable to the scientific community, in fact as stated in [FD14]: "A lot of research has been done over the last five decades on the relations between elastic and inelastic demand quantities. [...] extensive research has not devalued
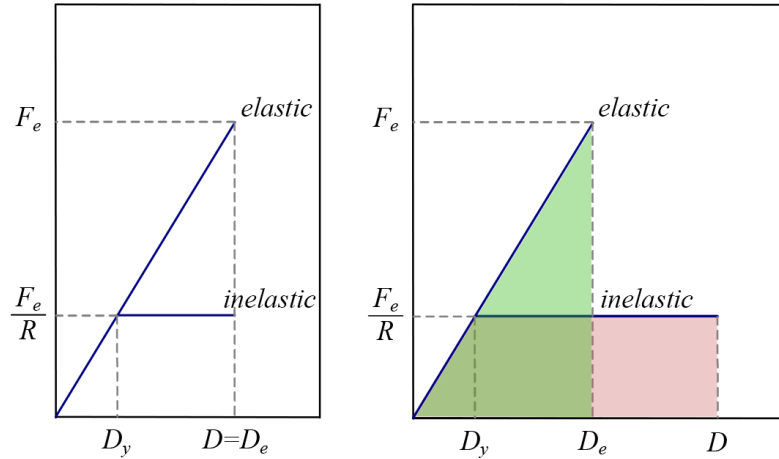
Figure 4.5: Equal displacement (left) and equal energy (right) principles

strength is here defined as:

$$R = \frac{F_e}{F_y} = \frac{mS_{ae}}{F_y} \qquad (4.11)$$

where m is the mass of the SDOF model and S_{ae} is the value of the elastic (pseudo) acceleration spectrum. F_y is often named as *yield strength*, because it is the force at "yield" of the elasto-plastic system. Newmark and his collaborators firstly proposed to link the elastic strength reduction to ductility, through the use of coefficients [VN60], [VNC65]. From geometrical considerations on the force-displacement relationships in Fig. 4.5 the following equations were derived:

$$R = \mu \qquad \text{(medium- and long-period range)} \qquad (4.12a)$$

$$R = \sqrt{2\mu - 1} \quad \text{(short-period range)} \qquad (4.12b)$$

There are different proposal in literature for the definition of a threshold between the short and medium/long period region. In [NTC08] this limit is given by T_c that is defined as the transition period where the constant acceleration segment of the response spectrum (the short-period range) passes to the constant velocity segment spectrum (the medium-period range) [Faj00].

the simple equal displacement rule. On the contrary, at least in the case of SDOF structures on firm sites with a fundamental period in the medium (velocity controlled) or long- period (displacement controlled) range, with relatively stable and full hysteretic loops, the equal displacement rule has proved to be an adequate assumption."

Regarding the N2 method, after numerous numerical analyses, in [VFF94] the researchers proposed a coefficient that relates the inelastic with the elastic strength through the ductility and called it the *strength reduction factor* (R_μ). This coefficient is used to evaluate the inelastic strength for a given ductility μ. For the medium- and long- period region maintained the equality with the ductility and an empirical linear relationship was proposed for the short-period region. The latter was subsequently simplified in [Faj00] and reported herein:

$$R_\mu = \mu \qquad \text{(medium- and long-period range)} \qquad (4.13a)$$

$$R_\mu = (\mu - 1)\frac{T}{T_c} + 1 \quad \text{(short-period range)} \qquad (4.13b)$$

Applying the strength reduction factor it is possible to compute the inelastic spectra (S_d and S_a), representative of the response of a bilinear elasto-plastic SDOF system, from the elastic ones using the equations proposed in [VFF94] and [Faj99]. Applying Eq. 4.11 and then Eq. 4.4 in Eq. 4.10:

$$D_u = \frac{\mu F_e}{R_\mu m \omega^2} = \frac{\mu S_{ae}}{R_\mu \omega^2} = \frac{\mu}{R_\mu} S_{de} = S_d \qquad (4.14)$$

Therefore the inelastic acceleration spectrum and displacement spectrum can be determined as ([Faj99]):

$$S_a = \frac{S_{ae}}{R_\mu} \qquad (4.15a)$$

$$S_d = \frac{\mu}{R_\mu} S_{de} = \frac{\mu}{R_\mu} \frac{T^2}{4\pi^2} S_{ae} = \mu \frac{T^2}{4\pi^2} S_a \qquad (4.15b)$$

It should be noted that the inelastic spectra are computed for a *given ductility* that together with elastic spectra are *input* of the problem. Both Italian and European codes ([NTC08] and [EC804]) adopt the inelastic spectra, and examples of inelastic spectra for increasing level of ductility are depicted in Fig. 4.6. The same spectra are plotted in both the traditional $T - S_a$ format (Fig. 4.6a) and in the AD space (Fig. 4.6b). The period T_C (considered as the threshold between short-period and medium- long-period structures) as well as T_d are highlighted. The latter indicates the beginning of the constant displacement part of the spectra.

Knowing the elastic spectra, to compute the inelastic spectra for a given ductility does not present difficulties (simply using equations 4.13

(a) T - S_a spectra   (b) Spectra in AD space
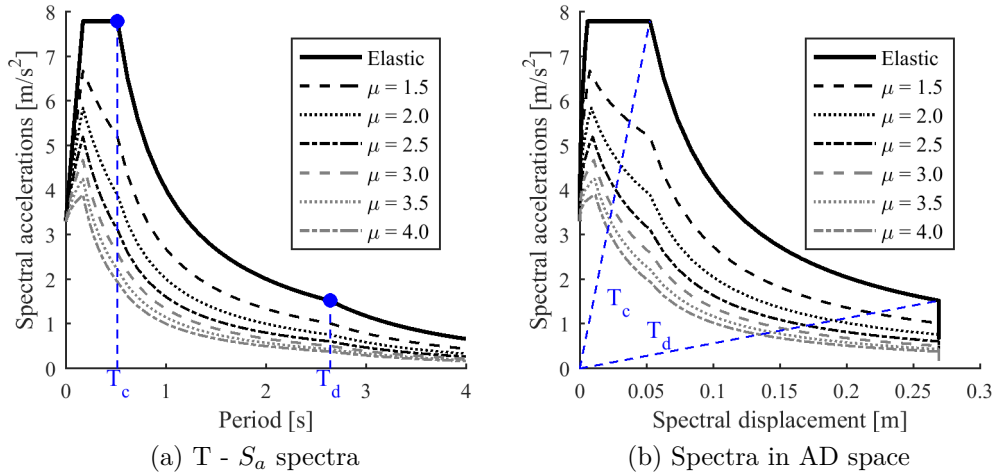
Figure 4.6: Examples of inelastic spectra for increasing level of ductility

and 4.15). However, this method presents the limitation that elastic spectra for specific accelerograms should not be used, but only response spectra with a "regular" shape, as the code spectra. Moreover, spectra which for different reasons deviate from the actual spectral shape should not be used [Faj99]. Furthermore, in [Faj00] is pointed out that the inelastic demand spectra, are not appropriate for hysteretic loops with significant pinching or stiffness and/or strength deterioration, and unfortunately it is not uncommon to observe this kind of behavior in URM buildings. In a subsequent research, the N2 method was extended in order to make it applicable to infilled RC frames [DF04b]. Therefore, a multi-linear idealization of the pushover curve, which takes into account the strength degradation which occurs after the infill fails was introduced. However, also in that procedure, the nonlinear displacement demand evaluation is based on the equivalent period T^* (defined in the next subsection) and in the present research this is considered as one of the principal issues of the procedure.

Evaluation of equivalent SDOF bilinear force-displacement relationship

In the N2 method, to evaluate the seismic demand it is necessary to define a characteristic period of the building under analysis. To this aim, the force-displacement relationship of the pushover curve is transformed into
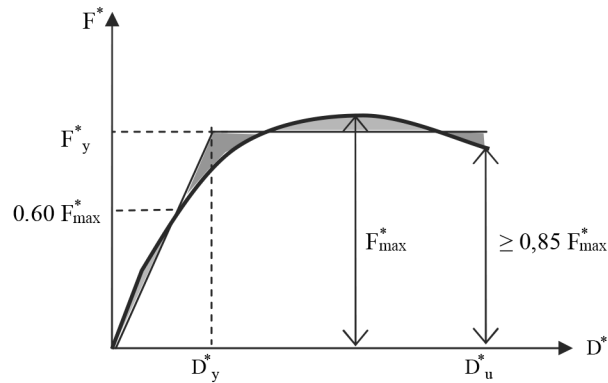
Figure 4.7: Equivalent SDOF system elasto-plastic force-displacement relationship as proposed in [Cir09]

an elastic-perfectly plastic form. Therefore, the representative period of the building is function of the elastic phase stiffness of the bilinear relationship. However, a standardized procedure for this transformation is not defined. In [Faj99] is stated that "engineering judgment has to be used" but also that the methodologies proposed in codes may be adopted , such as [FEM97], where it is required that the effective lateral stiffness shall be taken as the secant stiffness calculated at a force equal to 60% of the *yield strength*. Other codes, such as [OPC03], suggests to adopt as yield strength the maximum force registered during the pushover analysis and to compute the secant stiffness through the equivalence of the areas under the pushover curve and the bilinear approximation. Currently, in the Italian code first is evaluated the stiffness as the secant stiffness at a force equal to 60% of the *maximum base shear*, then the yield strength is computed through the equivalence of the areas under the pushover curve and the bilinear approximation for a displacement up to 15% base shear decay (Fig. 4.7). In this research the latter approach has been adopted, with two slight differences: 1) to compute the secant stiffness at a force of 70% of the maximum base shear, 2) consider the pushover curve up to 20% base shear decay (as proposed in [Cir09] for existing URM buildings and to be consistent with the DL3 defined in Section 3.2). Fig. 4.7 shows an example of the evaluation of the equivalent bilinear. The period of the idealized bilinear system T^* is

85

therefore computed with the following equation:

$$T^* = 2\pi \sqrt{\frac{m^* D_y}{V_y}} = 2\pi \sqrt{\frac{m^* d_y^*}{F_y^*}} \qquad (4.16)$$

Where m^* is the mass of the equivalent SDOF system as introduced in Section 4.1 and the couples of values (D_y, F_y) (d_y^*, F_y^*) represent the yield displacement and strength of the MDOF and equivalent SDOF respectively. The identity of the ratios under the two roots is due to the fact that the participation factor Γ (Section 4.1) applies for the transformation of both displacement and forces.

It should be noted that the use of an equivalent bilinear system for the representation of the nonlinear behavior of a building is a limit of the N2 method. In fact the period of the idealized bilinear system T^* is a constant for all the PLs considered, although it is expected that when damage increases the stiffness reduces. This issue, was recognized by the proposer of the method himself: "under incrementally increasing loads various structural elements yield sequentially. Consequently, at each event, the structure experience a loss in stiffness" [Faj00]. To overcome this limit the procedure was improved, computing a different equivalent bilinear system for all the PLs analyzed (and eventually for each step of the analysis to compute ISA curves, Section 4.2.5). This procedure is outlined is Section 4.2.2.

IM_{PL} computation

The final step of the procedure is to evaluate the intensity measure (IM) that causes the attainment of a given PLk (IM_{PLk}). As outlined in Section 3.2, it is possible to evaluate a displacement corresponding to every DL, D_{PL}, then, the PGA that causes the D_{PLk} (or the equivalent d_{PLk} in the AD space) is used to represent the IM_{PLk} (as discussed at the beginning of the chapter). It is hence necessary to evaluate the inelastic displacement demand, that is computed for both models with periods $T \geq T_c$ and $T < T_c$. In the European code [EC804] and in the Italian code commentary [Cir09] equations are proposed that express the inelastic displacement demand for an equivalent SDOF system (d_{max}^*) to elastic displacement spectra. The use of strength reduction factors reported in Eq. 4.13. Eq. 4.13b may be

rearranged to evaluate the ductility:

$$\mu = (R-1)\frac{T_c}{T^*} + 1 \tag{4.17}$$

note that R instead of R_μ is reported to underline that R is now an input variable of the problem. Applying Eqs. 4.13a and 4.17 to Eq. 4.15b:

$$d_{max}^* = \frac{d_{e,max}^*}{R}\left[1 + (R-1)\frac{T_c}{T^*}\right] \geq d_{e,max}^* \quad (T^* < T_C) \tag{4.18a}$$

$$d_{max}^* = d_{e,max}^* = S_{de}(T^*) \qquad \text{(during the elastic phase and for } T^* \geq T_C) \tag{4.18b}$$

The IM_{PLk} that for which the demand d_{max}^* is equal to the d_{PLk}. Therefore to evaluate the IM for PLs that are still in the elastic phase of the equivalent bilinear or for bilinear with period $T^* > T_C$, starting from Eq. 4.18b:

$$d_{PLk} = d_{max}^* = S_{de}(T^*) = c_{PGA}S_{ae}(T^*)\frac{T^{*2}}{4\pi^2} \tag{4.19}$$

where c_{PGA} is the coefficient that multiplies the original values of the spectra defined in Section 3.3. Since the 50 percentile spectra has a PGA equal to 1 m/s^2, the multiplicative coefficient c_{PGA} corresponds to the IM. Therefore:

$$IM_{PLk} = c_{PGA} = \frac{d_{PLk}}{S_{ae}(T^*)}\frac{4\pi^2}{T^{*2}} \quad \text{(during the elastic phase and for } T \geq T_C) \tag{4.20}$$

Same procedure is adopted when $T^* < T_C$, therefore from Eq. 4.18a and 4.11:

$$d_{PLk} = d_{max}^* = \frac{S_{de}(T^*)}{\frac{m^*c_{PGA}S_{ae}(T^*)}{F_y^*}}\left[1 + \left(\frac{m^*c_{PGA}S_{ae}(T^*)}{F_y^*} - 1\right)\frac{T_C}{T^*}\right] \tag{4.21}$$

where $F_y^* = V_y/\Gamma$ (see Section 4.1), then considering Eq. 4.4 here reported:

$$S_{de}(T^*) = \frac{c_{PGA}S_{ae}(T^*)T^{*2}}{4\pi^2} \tag{4.22}$$

we get:

$$d_{PLk} = d_{max}^* = \frac{F_y^*T^*}{4\pi m^*}\left[1 + \left(\frac{m^*c_{PGA}S_{ae}(T^*)}{F_y^*} - 1\right)\frac{T_C}{T^*}\right] \tag{4.23}$$

87

applying Eq. 4.5

$$d_{PLk} = d^*_{max} = \frac{F^*_y}{k^*} \left[1 + \left(\frac{m^* c_{PGA} S_{ae}(T^*)}{F^*_y} - 1 \right) \frac{T_C}{T^*} \right] \tag{4.24}$$

finally, with $F^*_y / k^* = d^*_y$, c_{PGA} is equal to:

$$IM_{PLk} = c_{PGA} = \frac{F^*_y}{\Gamma m^*} \frac{1}{S_{ae}(T^*)} \left[1 + \frac{T^*}{T_C} \left(\frac{d_{PLk} \Gamma}{d^*_y} - 1 \right) \right] \text{(for } T < T_C \text{)} \tag{4.25}$$

As it is possible to observe from Eq. 4.20 and 4.25, if the equivalent bilinear representation of the capacity curve is fixed, as well as the period T^*, IM_{PLk} depends only on the displacement d_{PLk}. As a consequence, IM_{PLk} increases with d_{PLk}, and with a linear relationship if $T^* \geq T_C$. This is a limit of the method, especially when damage increases. In fact, as shown in Section 4.3.1, when subjected to increasing dynamic loading the IM a building can support does not increase linearly with the displacement demand.

This is the procedure currently adopted in both Italian and European codes. However, this formulation does not consider issues derived by the presence of in-plan and/or elevation irregularities. As anticipated at the beginning of the section, in more recent researches the N2 method was developed to consider higher modes effects in both plan and elevation ([KF11] and [KF12]). In the procedure proposed, the contributions of the higher modes are determined by using correction factors that increase the demand. These coefficients (one for the higher mode effects in elevation and one for the higher mode effects in plan) were tested on models: $A_{irr,rig}$, $C_{irr,rig}$, $A_{irr,flex}$ and $C_{irr,flex}$. It was observed that the coefficients computed for these buildings presented a wide range of variation, in particular for the models with flexible diaphragms where also a value equal to 5 was reached. Therefore this approach was not further studied in the present research.

4.2.2 N2 method: improvements proposed

Equation 4.18a may be rewritten as follows:

$$d^*_{max} = \frac{d^*_{e,max}}{R} \left[1 + (R - 1) \frac{T_c}{T^*} \right] = d^*_y \mu_{R,N2} \tag{4.26}$$

where

$$d_y^* = \frac{d_{e,max}^*}{R} \tag{4.27a}$$

$$\mu_{R,N2} = 1 + (R-1)\frac{T_c}{T^*} \tag{4.27b}$$

and $\mu_{R,N2}$ is the *ductility demand* for a given R and d_y^* is the yield displacement of the equivalent SDOF introduced in the previous section. As reported in the previous section, a limit of the method is to adopt only one equivalent bilinear system wherever the position of the limit states, as a consequence T^* is constant. Considering Eq. 4.26 it is evident that the inelastic displacement demand derives from the elastic one and it is modified by the coefficient R and the ratio T_C/T^*. Also coefficient R (introduced by Eq. 4.11) depends on the definition of the equivalent bilinear. Therefore, in order to get a more precise inelastic displacement demand prediction it was decided to update the equivalent bilinear for each step of the pushover analysis. The "adaptive" bilinear curves are computed adopting the rules herein:

- up to the point corresponding to the peak of the curve, V_y^* is equal to the shear of the pushover curve for the given step of the analysis and the stiffness is calculated by the equivalence of the areas under the pushover curve and the bilinear approximation (Fig. 4.8a);

- in the post-peak phase, the stiffness remains constant and equal to the stiffness of the peak and the base shear decreases in order to have the equivalence of the areas under the pushover curve and the bilinear approximation (Fig. 4.8b).

Examples of the equivalent bilinears before and after the attainment of the pushover curve peak are shown in Fig. 4.8. It was possible to observe that to compute the equivalent bilinear using this new procedure improved the precision of N2 method, this improvement was however small, especially for higher ductility demands. In fact, with the "updated" bilinears, when the base shear strength is reached, the stiffness remained constant from that step on. However, it is likely that the pushover curve base shear reductions corresponds to a decrease of building's stiffness. Therefore a further methodology to define the equivalent bilinears for the post peak

(a) Before the pushover curve peak   (b) After the pushover curve peak
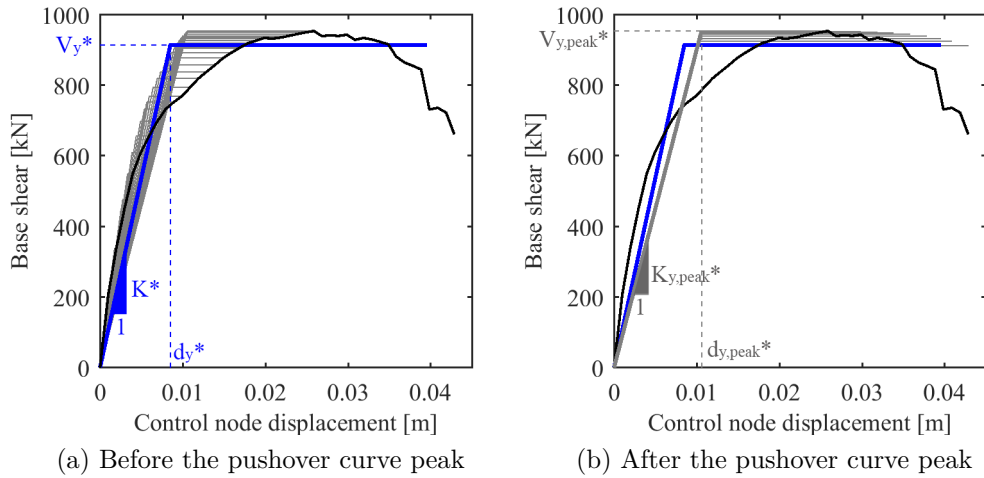
Figure 4.8: Examples of equivalent bilinears for a given pushover curve (in black): in blue the equivalent bilinear as proposed in [NTC08], in grey the "adaptive" bilinears proposed
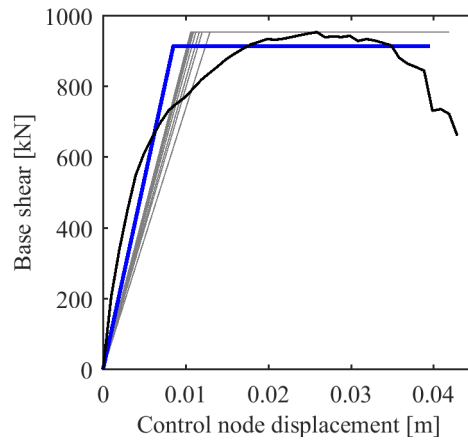
Figure 4.9: Post-peak phase, final proposal for the equivalent bilinears (in grey): yield strength constant and stiffness reduces (in blue the equivalent bilinear as proposed in [NTC08]).

phase was adopted: the yield strength is kept constant and equal to the maximum pushover base strength, then the stiffness is computed through the equivalence of the areas. In this way also in the post peak phase the stiffness reduces as shown in Fig. 4.9.

Recently, further developments to the N2 method were studied as in

[GGPM17] where an equation for the estimation of earthquake-induced nonlinear displacement demand was proposed, with particular attention on short-period masonry structures (i.e. with fundamental periods between 0.1 and 0.5 s). The equation proposed in [GGPM17] was developed by the analysis of SDOF models representative of the response of low-rise URM structures (see [GPBM14] and [GPM16]). The Authors pointed out that inelastic displacement demands depend on the oscillator's hysteretic behavior, being generally larger for less dissipative systems [GGPM17]. However, as alredy said, the current NSP formulation present in [EC804] and [NTC08] descends from the N2 method that does not consider this hysteresis dependence, but gives only explicit consideration of structural period and ductility [GGPM17]. In the research undertaken in [GGPM17], several hysteretic response were adopted for the SDOF oscillators and from the analysis of the main results a new equation relating maximum inelastic and elastic displacements for $R \geq 1$ was proposed and it is reported herein:

$$d^*_{max} = \frac{d^*_{e,max}}{R} \left[\frac{(R-1)^{c_G}}{\left(\dfrac{T^*}{T_{hyst}} + a_{hyst}\right) \left(\dfrac{T^*}{T_C}\right)^{b_G}} + R \right] \qquad (4.28)$$

where a_{hyst}, b_G, c_G, T_{hyst}, are parameters calibrated with the dynamic response of the SDOF oscillators as described in [GGPM17]. Defining $\mu_{R,G}$ as:

$$\mu_{R,G} = \left[\frac{(R-1)^{c_G}}{\left(\dfrac{T^*}{T_{hyst}} + a_{hyst}\right) \left(\dfrac{T^*}{T_C}\right)^{b_G}} + R \right] \qquad (4.29)$$

It is possible to rewrite Eq. 4.28 in the same form of Eq. 4.26. For the calibrated parameters the values proposed in [GGPM17] are reported in Table 4.1 where FD indicates *flexure-dominated* and SD *shear-dominated* systems, ξ_h indicates the hysteretic dissipation; more details about this parameter are given in Section 4.2.4.

This approach improves the N2 method because it includes the effects of hysteretic dissipation, but it presents a limit in the complexity of the equation itself that includes a series of coefficients whose effect is difficult

Table 4.1: Calibrated parameters as proposed in [GGPM17]

Case	a_{hyst} [-]	b_G [-]	c_G [-]	T_{hyst} [s]
Mainly FD $13\% \leq \xi_h < 15\%$	0.7	2.3	2.1	0.055
Intermediate $15\% \leq \xi_h \leq 18\%$	0.2	2.3	2.1	0.030
Mainly SD $18\% < \xi_h \leq 20\%$	0.0	2.3	2.1	0.022

to interpret. For this reason, a simpler procedure, that maintains a similar format to the current equation proposed in the codes, was studied and proposed in this research and written herein:

$$d^*_{max} = \frac{d^*_{e,max}}{R} R^c = d^*_y R^{(c-1)} \qquad (4.30)$$

where

$$c = \frac{1}{ln4}\left(1 + 3b\frac{T_C}{T^*}\right) \geq 1 \qquad (4.31)$$

and b is a coefficient related to the dissipative capacity and strength degradation of the system under analysis. With the limit of $c \geq 1$ this equation is applicable also for T^* values greater than T_C. Therefore for this new proposal $\mu_R = R^c$. The equation for the coefficient c derives from the consideration reported in [GGPM17]: "the current formulation generally underestimates the demand when the ductility is larger than 4 and in particular this issue is more evident for short-periods oscillators". In fact, for low ductility demands, the N2 method provides conservative results. Then the new equation provides larger inelastic displacement demands than the N2 method in case of higher ductility demands. Hence, the equivalence in the inelastic displacement demand between the new proposal and the N2 method was set for ductility demands of 4 (or correspondingly setting R = 4). This choice was supported by the results present in [GGPM17] as those depicted in Fig. 4.10. In the graphs reported the gray dots represent the data derived from both nonlinear static and dynamic analyses on nonlinear SDOF systems. On the X-axis the Italian code ductility demand for short-period structure is reported (Eq. 4.17), on the Y-axis the ductility demand from NLTH analysis. As stated in [GGPM17], Fig.4.10 shows that "the current formulation generally underestimates the demand when the ductility is larger than 4, as indicated by data points cumulating above the bisector". In particular, this issue is more evident for short-period oscilla-
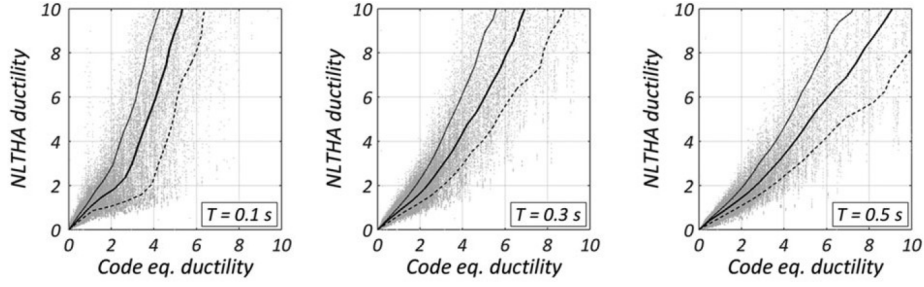
Figure 4.10: Comparison between ductility demands from N2 equation and nonlinear time-history analyses (NLTHA) undertaken on nonlinear SDOF oscillators with different idealized elastic periods, from [GGPM17].

tors (i.e. when their own period is from 0.1 to 0.3 s). Already for models with period 0.5s this issue is less evident.

Therefore the equivalence was set for a ductility demand of 4 and Eq. 4.31 was defined through the following steps:

$$d^*_{max,N2} = d^*_y \left[1 + (R-1)\frac{T_c}{T^*} \right] = d^*_y R^c = d^*_{max,new} \tag{4.32}$$

Setting R = 4:

$$d^*_y \left[1 + 3\frac{T_c}{T^*} \right] = d^*_y 4^c \tag{4.33}$$

we can now divide both terms by d^*_y and apply the natural logarithms:

$$ln\left(1 + 3\frac{T_c}{T^*} \right) = ln(4^c) \tag{4.34}$$

considering the properties of logarithms it is possible to get the coefficient c and Eq. 4.31.

$$c = \frac{1}{ln4} ln\left(1 + 3\frac{T_c}{T^*} \right) \tag{4.35}$$

Finally the b coefficient was added to the equation (it multiplies the ratio T_C/T^*) in order to consider the dissipative capacity and strength degradation of the system under analysis. Statistical analyses need to be undertaken for a proper calibration of this coefficient. However, for a preliminary study, b = 1.5 was set, in order to have the best fit with [GGPM17] results that are based on a wide statistical study.

4.2.3 Coefficient method

In the past two decades, the [ATC96], [FEM97], [FEM00] and [FEM05] reports were issued. These documents present similar approaches: they are essentially the same when it comes to generating the pushover curve, but they differ in the technique used to calculate the inelastic displacement demand [FEM05]. [ATC96] utilizes the Capacity Spectrum Method (outlined in Section 4.2.4), the other documents adopt a procedure known as the Coefficient Method (CM). This procedure has been refined afterwards and its last version is proposed in [ASC14] and studied in the current research.

The CM approach modifies the linear elastic response of the equivalent SDOF system by multiplying it by a series of coefficients to generate an estimate of the maximum inelastic global displacement, which is termed the *target displacement* [FEM05]. As for N2 method, this approach begins with an idealized force-deformation curve obtained from the pushover curve (Fig. 4.11). For the development of this curve the procedure outlined in [ASC14] has been adopted and it is reported herein. As stated in [ASC14] "the first line segment of the idealized force-displacement curve shall begin at the origin and have a slope equal to the effective lateral stiffness, K_e. The effective lateral stiffness, K_e shall be taken as the secant stiffness calculated at a base shear force equal to 60% of the effective yield strength of the structure. The effective yield strength, V_y, shall not be taken as greater than the maximum base shear force at any point along the force-displacement curve". As reported in [FEM05], it should be noted that the selection of 60% of the yield strength to define this slope is based purely on judgment. The second line segment shall represent the positive post-yield slope ($\alpha_1 K_e$), determined by a point (V_d, D_d) and a point at the intersection with the first line segment such that the areas above and below the actual curve are approximately balanced. (V_d, D_d) shall be a point on the actual force-displacement curve at the target displacement, or at the displacement corresponding to the maximum base shear, whichever is least. The third-line segment shall represent the negative post-yield slope ($\alpha_2 K_e$), determined by the point at the end of the positive post-yield slope (V_d, D_d) and the point at which the base shear degrades to 60% of the effective yield strength. Note that the symbols that indicate the displacements were changed from the original Δ to D for consistency with the symbols adopted in this thesis.

Contrary to the N2 method, this procedure has the advantage that the
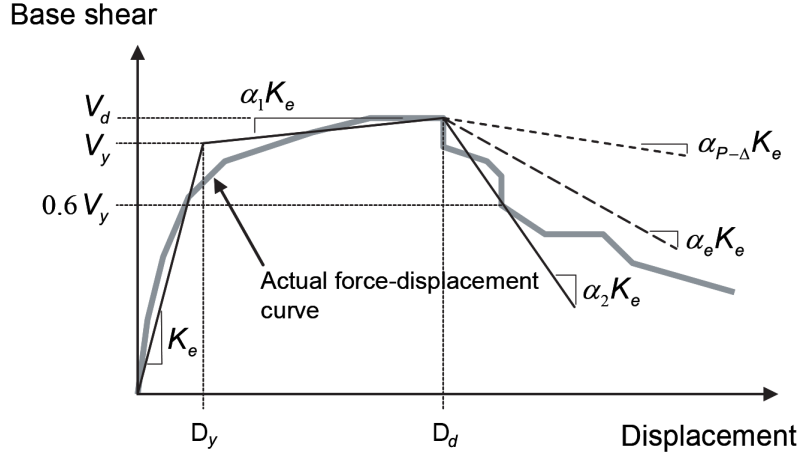
Figure 4.11: Idealized force-displacement curve for nonlinear static
analysis as proposed in [ASC14] (adapted from [FEM05])

idealized force-deformation curve is not fixed for any displacement demand, but it is updated with it (Fig. 4.12). However, since there are two unknowns (the point D_y, V_y and the stiffness K_e) and only one conditions to define the curve up to the point (D_d, V_d), i.e., the balance of the areas, it needs the implementation of an iterative algorithm that may cause difficulties for professional uses of the procedure.

For each idealized force-displacement curve is then calculated the effective fundamental period. In [ASC14] it is suggested to use the equation herein:

$$T_e = T_i \sqrt{\frac{K_i}{K_e}} \tag{4.36}$$

where T_i is the elastic fundamental period (in seconds) in the direction under consideration calculated by elastic dynamic analysis; K_i is the elastic lateral stiffness of the building in the direction under consideration and K_e is the effective lateral stiffness of the building in the direction under consideration. However, for simplicity and for a better consistency with the other methodologies studied, in this research T_e has been calculated directly from the idealized force-displacement curve using equation herein:

$$T_e = 2\pi \sqrt{\frac{D_y m^*}{V_y}} = 2\pi \sqrt{\frac{D_y^* m^*}{V_y^*}} \tag{4.37}$$

where D_y is effective yield displacement and V_y is the effective yield strength

95
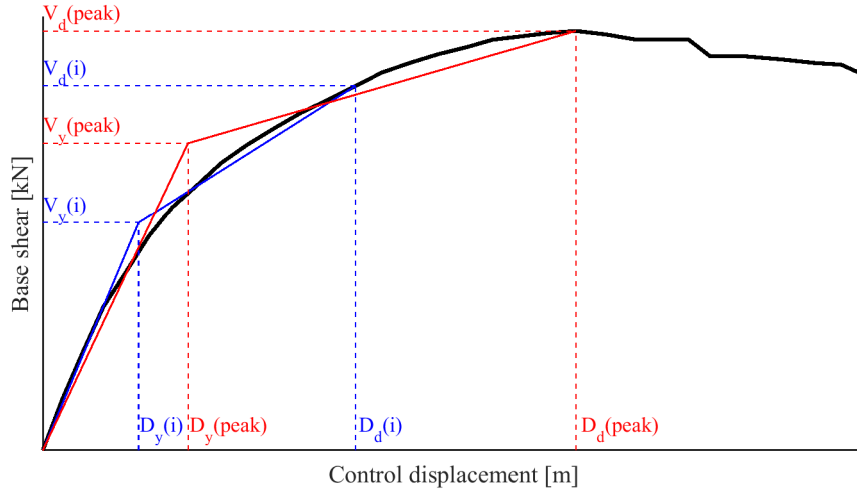
Figure 4.12: Examples of idealized force-displacement curve adopting CM as proposed in [ASC14] for the step "i" and the step in correspondence of the peak of the curve

previously introduced, m^* is the equivalent SDOF mass as defined in Section 4.1.

Finally, the target displacement is calculated from the linear elastic response of the equivalent SDOF system by multiplying it by a series of coefficients (Eq. 4.38).

$$\delta_t = C_0 C_1 C_2 S_{de}(T_e) = C_0 C_1 C_2 S_{ae}(T_e) \frac{T_e^2}{4\pi^2} \qquad (4.38)$$

The coefficient C_0 is a modification factor to relate (convert) spectral displacement of the equivalent SDOF system to the control displacement of the building MDOF system. Therefore, C_0 is equivalent to the participant factor Γ introduced in Section 4.1. In [ASC14] it is suggested to calculate C_0 from the first mode or the mass participation factors. Alternatively in Table 7-5 of the document values for modification factor C_0 are proposed that are function of the building typology and the number of stories. However, for a better comparison with the other methodologies studied in this research the equivalence $C_0 = \Gamma$ has been adopted.

The coefficient C_1 is the modification factor to relate expected maximum *inelastic* displacement to displacement calculated with *linear elastic* response. As stated in [FEM05], it should be noted that the inelastic dis-

placements refer to a SDOF oscillator with *non-degrading* hysteretic behavior. As for N2 method, this modification depends on the effective period of the SDOF:

$$C_1 = 1 + \frac{\mu_{strength} - 1}{a_s(0.2)^2} \quad (T_e < 0.2s) \tag{4.39a}$$

$$C_1 = 1 + \frac{\mu_{strength} - 1}{a_s T_e^2} \quad (0.2 \leq T_e \leq 1s) \tag{4.39b}$$

$$C_1 = 1 \quad (T_e > 1s) \tag{4.39c}$$

where a_s is a site class factor and $\mu_{strength}$ is the ratio of elastic strength demand to yield strength coefficient. Three values (60, 90 and 130) are proposed in [ASC14] for the site class factor that are function of the site class. However, since the effects due to different soil conditions are not object of this study, the average value $a_s = 90$ has always been used. Then, $\mu_{strength}$ is calculated as:

$$\mu_{strength} = \frac{S_{ae}(T_e)M_{dyn}C_m}{V_y} \tag{4.40}$$

where M_{dyn} is the effective seismic weight (i.e. the dynamic mass of MDOF system) and C_m is the effective mass factor to account for higher modal mass participation effects. Therefore C_m depends on the number of stories of the building and values are proposed in Table 7-4 of the document. However, for URM buildings, regardless of the number of stories always a coefficient equal to 1 is proposed. This choice was not considered consistent therefore the following equation has been used to compute C_m:

$$C_m = \frac{\Gamma M^*}{M_{dyn}} \tag{4.41}$$

Considering its definition, coefficient C_1 is equivalent to the coefficients in Eq. 4.18, but in this case the limit of the equal-displacement approximation is at a period of 1 s, regardless of the shape of the acceleration spectra. Previously, in [FEM00], this limit was set differently, in fact the equations proposed were function of T_s, characteristic period of the response spectrum, defined as the period associated with the transition from the constant-acceleration segment of the spectrum to the constant-velocity segment of the spectrum. Therefore T_s was the equivalent of T_C of Italian and European codes. Although the limit of 1s seems crude, it has the advantage not to

be very small, in fact, to adopt as a limit T_C, in case of firm soils, it may lead to the equal displacement rule adoption already for periods of 0.4s. Another difference is that in [FEM00] C_1 was limited to 1.5.

As stated in [ASC14], the coefficient C_2 is a modification factor to represent the effect of pinched hysteretic shape, stiffness degradation, and strength deterioration on the maximum displacement response. In fact, as said, coefficent C_1 assumes the SDOF oscillator has a non-degrading hysteretic behavior. This aspect is not taken into account in the N2 method, and, as it will be shown in Chapter 5, this is a limitation of the method, especially for high ductility demands. In [FEM00] values of C_2 are proposed in a table, and they depend on the type of structural framing system and structural performance levels being considered (i.e., immediate occupancy, life safety and collapse prevention). In [ASC14] an equation is proposed to compute C_2, that was already recommended as proposal for a code development in [FEM05]. The equation is reported herein:

$$C_2 = 1 + \frac{1}{800}\left(\frac{\mu_{strength} - 1}{T_e}\right)^2 \quad (T_e \leq 0.7s) \qquad (4.42\text{a})$$

$$C_2 = 1 \qquad\qquad\qquad (T_e > 0.7s) \qquad (4.42\text{b})$$

This equation was proposed "since the studies do not include the effects of the duration of shaking that may be important for structures subject to cyclic strength degradation" [CAG$^+$04], such us URM buildings.

In [FEM97] a further coefficient C_3 was proposed to adjust for second-order geometric nonlinearity. In [FEM05] it was pointed out that global displacement demand is not significantly amplified by degrading strength until a critical point at which dynamic instability may occur. This point is related to the initial strength and period of the oscillator as well as the magnitude of the negative post-elastic (yield) stiffness caused by in-cycle strength degradation. Therefore, this coefficient was eliminated, and in [ASC14] it is replaced with a limit on a minimum strength (maximum $\mu_{strength}$ permitted to avoid dynamic instability).

$$\mu_{max} = \frac{D_d}{D_y} + \frac{|\alpha_e|^{-h}}{4} \qquad (4.43)$$

where D_d is the lesser of the target displacement, δ_t, or displacement corresponding to the maximum base shear, D_y is the displacement at effective

yield strength, $h = 1 + 0.15 ln T_e$ and α_e is the effective negative post-yield slope ratio. As stated in [FEM05], these coefficients "are empirical and were derived primarily from statistical analysis studies of the nonlinear response-history analyses of SDOF oscillators and adjusted using engineering judgment".

A drawback of the method is that it is not easy to understand the origin of the coefficients used. In fact "the coefficients are typically derived empirically from series of nonlinear response-history analyses of oscillators with varying periods and strengths" [FEM05].

IM_{PL} computation

As already done for N2 method, the final step of the procedure is to evaluate the IM_{PLk} that causes the attainment of D_{PLk}. Similarly, when $\delta_t = D_{PLk}$, PL_k is reached. Therefore substituting Eq. 4.39 and 4.42 in Eq. 4.38 and considering $C_0 = \Gamma$ it is possible to write:

$$D_{PLk} - \Gamma \left[1 + \left(\frac{c_{PGA} S_{ae}(T_e) M_{dyn} C_m}{V_y} - 1 \right) \frac{1}{90 T_e^2} \right]$$
$$\left[1 + \left(\frac{c_{PGA} S_{ae}(T_e) M_{dyn} C_m}{V_y} - 1 \right)^2 \frac{1}{800 T_e^2} \right] \frac{c_{PGA} S_{ae}(T_e) T_e^2}{4\pi^2} = 0$$
(4.44)

The result is a complex equation with c_{PGA} as the unknown. No closed form solution was determined, but c_{PGA} was evaluated numerically.

4.2.4   Capacity Spectrum Method

The Capacity Spectrum Method (CSM) was first introduced in the 1970s by Freeman [Fre78], developed in the decades afterwards [Fre98],[Fre04], and adopted in international standards such as [ATC96]. The basic assumption of the method is that "the maximum inelastic deformation of a nonlinear SDOF system can be approximated from the maximum deformation of a linear SDOF system that has a period and a damping ratio that are larger than the initial values of those for the nonlinear system" [FEM05].

Similarly to the N2 method and CM, the procedure compares the capacity of the structure with the demand on it in the form of a response spectrum (demand response spectrum), but the assumption above reported

implies two main differences in the procedure if compared with the other methods: 1) the period of the equivalent linear system is assumed as the *secant* (rhater than the initial elastic) period and 2) the maximum non-linear displacement demand is based on *overdamped* (and therefore not inelastic) spectra. To compute the overdamped spectra, it is assumed that the equivalent damping "is related to the area under the capacity curve associated with the inelastic displacement demand" [FEM05].

In fact, an advantage of this method is that there is no need to transform the pushover curve in an equivalent bilinear. Indeed, the capacity is expressed in the form of capacity curve that is the representation of the pushover curve in the AD format (see Section 4.1). The graphical intersection of the capacity curve and the overdamped spectrum approximates the response of the structure. Then, by determining the point, where this capacity curve *breaks through* the earthquake demand (expressed in terms of overdamped spectrum), "engineers can develop an estimate of the spectral acceleration, displacement and damage that may occur for specific structure responding to a given earthquake" [Fre04]. This intersection is called in Freeman's article the *performance point* (PP) and represents "the condition for which the seismic capacity of the structure is equal to the seismic demand imposed on the structure by the specific ground motion" [ATC96]. However, it should be noted that the concept of performance point and target displacement used in the other procedures discussed is equivalent.

The basic idea of the method is that during the excursion in the nonlinear range the energy of the earthquake is partially absorbed by hysteretic damping, thus the elastic spectrum is reduced to take into account this phenomenon. Figure 4.13 represents an example of this reduction, the procedure adopted for the reduction is outlined in the subsection IM_{PL} *computation*. The black line represents the capacity curve and the thickest blue line the elastic (5 percent-damped) demand spectrum. The intersection of the two curves, indicated by the red square, is not the performance point, since the demand spectrum intersects the capacity curve in an advanced nonlinear phase. As a consequence, the elastic spectrum and the capacity curve, at the initial intersection, do not present equal dynamic and damping characteristics. In fact, to reach this level of damage some energy must be dissipated by the structure, and therefore the damping must be increased from the initial 5 percent (concept of hysteretic damping);

hence, the demand spectra must be reduced using higher values of equivalent damping and the intersection point anticipates. Therefore, in order to account for nonlinear inelastic behavior of the structural system, equivalent viscous damping values (ξ) are applied to reduce the linear-elastic response spectrum. The equivalent viscous damping is considered as the sum of the initial elastic viscous damping and the hysteretic damping. In the literature relationships between structural displacement and equivalent damping are proposed and discussed in the following subsection. The performance point corresponds to the intersection of capacity curve and demand spectrum when both present the same level of equivalent damping. This is an iterative procedure because it is not know *a priori* this value of the equivalent damping. There may be more than one performance points, it depends on the number of performance levels considered, and, as discussed in Section 3.2, in this research four PL are analyzed.
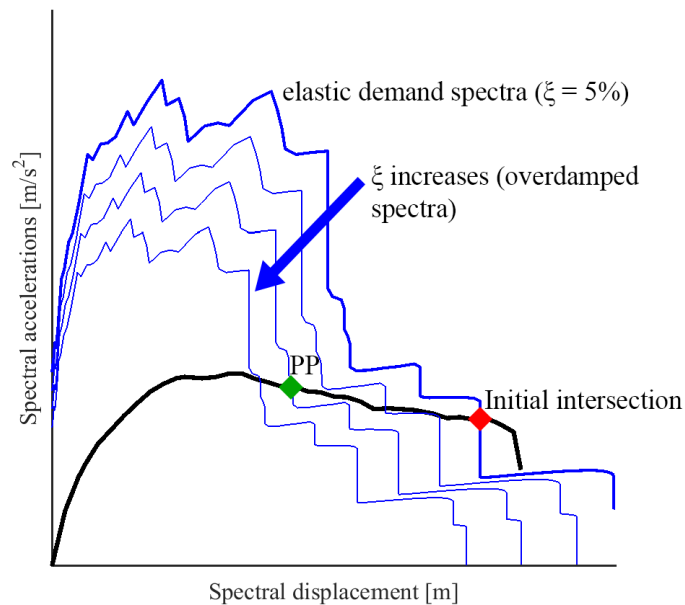
Figure 4.13: Capacity curve and overdamped spectra

In the next section the procedure adopted to calculate the equivalent viscous damping values and the spectral reduction factors is outlined.

Equivalent viscous damping and spectral reduction factors

The values of equivalent viscous damping can be estimated from analytical expressions proposed in literature for similar assets [Cal99], [BP05], [PCK07], [SC13], as the following expression adapted from [LC15a]:

$$\xi = \xi_0 + \xi_{h,max} \left(1 - \frac{1}{\mu^\zeta} \right) \tag{4.45}$$

where ξ_0 is the elastic viscous damping, $\xi_{h,max}$ is the asymptote of the hysteretic damping (see Fig. Fig. 4.14), $\mu = d/d_{PL2}$ is the ductility corresponding to the displacement d (of the control displacement) and ζ is a free parameter coefficient that influences the rate of increase of hysteretic damping with ductility (reference values for both $\xi_{h,max}$ and ζ are in [LC15a]. The concept of ductility makes sense only when the model is not in its linear phase anymore, and therefore when d>d_{PL2}, before that point the equivalent viscous damping is equal to the elastic damping (see Fig. 4.14). For URM buildings, usually (ξ_0) values between 3 and 5% are assumed [LC15a]. In [CL13b] some expressions specifically calibrated for existing masonry buildings have been proposed on the basis of cyclic pushover analyses on different configurations that exhibited various global failure mechanisms [LC15b].

An alternative approach is to calculate ξ_h directly from cyclic pushover analyses, evaluating the hysteretic dissipation as a function of the current displacement. For each model four cyclic pushover analyses were conducted, one for every PL and for each analysis the displacement corresponding to the given PL was assumed as maximum displacement. These four analyses were undertaken with two different load patterns: the uniform and the inverted triangular. The hysteretic damping was not calculated with the other "modal" LPs, for all them the values calculated with the inverted triangular LP were used. It should be noted that usually the displacement corresponding to the attainment of a given PL was different if the forces were applied in the positive or negative directions. As a consequence, it often happened to have asymmetric loops.

For each analysis the hysteretic contribution was calculated with the following equation:

$$\xi_h = \frac{1}{2\pi} \frac{E_d}{E_{S0+} + E_{S0-}} \tag{4.46}$$

where E_d is the energy dissipated by damping (area of enclosed by hysteresis loops), E_{S0+} and E_{S0-} are the maximum strain energy in positive and negative direction and correspond to the area of the blue triangles in Fig. 4.14. More information on the origin of this equation can be found in [ATC96]. This method has the advantage to consider the seismic behavior of the building under analysis with a reasonable computational effort. The equivalent viscous damping is then the sum of the elastic viscous damping (ξ_0) with the hysteretic contribution (ξ_h), see Fig. 4.14.

Figure 4.15 reports an example of spectral displacement and equivalent viscous damping relationship defined through the use of cyclic pushover analyses. It starts with the value of 5% (elastic damping) and then increases at the attainment of each PL. To avoid a sharp drop at the attainment of PL1, in this research the hysteretic contribution was added starting from half the displacement corresponding to the PL1 (Fig. 4.15). Table 4.2 reports the equivalent viscous damping values adopted for the numerical models analyzed (values in %) and they are consistent with the experimental values discussed in [CL13b].
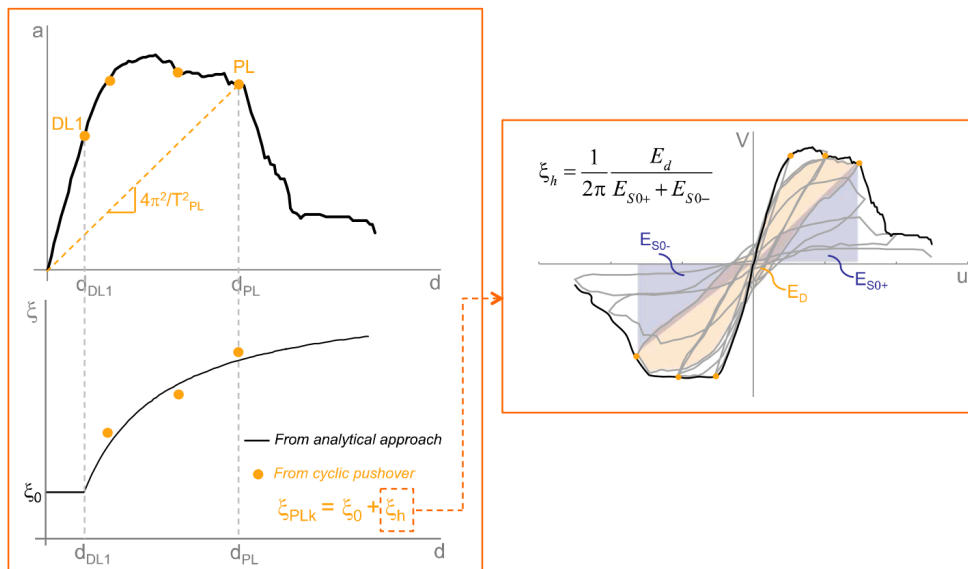
Figure 4.14: Evaluation of equivalent viscous damping through analytical approach and use of cyclic pushover (from [LC15a])
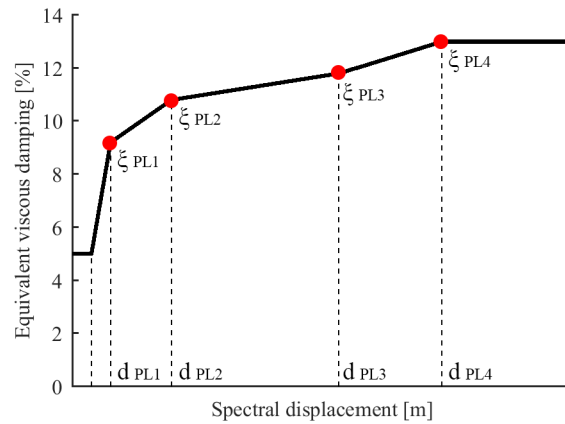
Figure 4.15: Example of equivalent viscous damping calculated through use of cyclic pushover

Table 4.2: Values adopted for the equivalent viscous damping [%]

Diaphragm stiffness	Model	Uniform				Modal			
		PL1	PL2	PL3	PL4	PL1	PL2	PL3	PL4
Rigid	A_r	8.50	10.1	15.5	15.6	8.20	12.6	15.0	16.7
	B_r	7.81	12.2	14.5	14.5	7.50	10.9	13.4	13.4
	A_{irr}	7.96	13.3	14.7	14.7	8.60	10.8	13.1	22.6
	B_{irr}	5.80	9.40	14.3	14.3	6.20	11.2	11.2	13.4
	C_{irr}	8.00	13.3	14.7	14.7	8.60	10.8	13.1	22.6
Intermediate	A_r	7.00	12.4	15.0	16.0	7.30	12.0	13.0	15.0
	B_r	6.90	11.1	14.0	15.0	7.00	10.8	12.5	12.5
	A_{irr}	8.62	12.4	13.4	13.0	9.20	10.8	11.8	13.0
	B_{irr}	6.80	7.30	12.2	12.8	7.30	14.2	14.7	15.2
	C_{irr}	8.60	12.4	13.5	14.2	9.20	10.8	11.8	13.0
Flexible	A_r	7.20	9.80	12.2	12.4	7.00	9.50	11.1	11.3
	A_{irr}	9.50	11.8	13.0	13.6	9.50	11.7	11.7	11.9
	C_{irr}	9.80	11.8	13.0	13.6	9.50	11.7	12.2	12.7

IM_{PL} computation

The evaluation of the displacement demand using the CSM requires an iterative procedure, but the evaluation of the seismic input that produces a given displacement (that is the adopted outcome of the assessment, IM_{PL})

is straightforward, once the corresponding equivalent viscous damping (ξ_{PL}) is known [LC15b]. The first step is to define a period-damping relationship. In the previous subsection possible relationship between displacement and damping were outlined. For every PL considered it is then possible to calculate from the displacement the secant period corresponding to its attainment (T_{PL}) using the following equation (see Fig. 4.14):

$$T_{PL} = 2\pi\sqrt{\frac{d_{PL}}{a_{PL}}} \tag{4.47}$$

where a_{PL} and d_{PL} are the acceleration and the displacement in the AD space at the attainment of the PL considered. Therefore for every PL considered is possible both the secant period and the equivalent viscous damping are known. To reduce the elastic response spectrum considering higher values than 5% the equation proposed in [NTC08] and [EC804] codes was used:

$$\eta = \sqrt{\frac{10}{5 + \xi}} \tag{4.48}$$

where η is the damping correction factor with reference value of $\eta = 1$ for 5% equivalent viscous damping. [NTC08] states that this factor can not be lower than 0.55 that corresponds to $\xi = 28\%$. However, the damping values used were always smaller (see Table 4.2). It is worth noting that if $\xi = 10\%$, $\eta \approx 0.82$ and if $\xi = 15\%$, $\eta \approx 0.71$. Since this coefficient reduces linearly the spectral values, it means that these two values indicate a reduction of the elastic spectra by almost 20 and 30%. Applying this reduction the elastic spectral accelerations (S_{ae}) are transformed in the overdamped spectral accelerations (S_a). It is then possible to calculate the corresponding spectral displacement with the equation:

$$S_d = \frac{S_a T^2}{4\pi^2} \tag{4.49}$$

Therefore the overdamped demand spectra ($S_d - S_a$) are now known. If it is regular and the spectral displacement demand increases monotonically with the period T (or remains constant), IM_{PL} can be simply evaluated as the IM for which the spectral displacement demand $S_{dPL}(T_{PL},\text{IM},\xi_{PL})$ is equal to d_{PL}, being d the displacement of the capacity curve (that is the original displacement D of the pushover curve properly converted in the SDOF system, see Section 4.1).

The procedure here outlined for the application of CSM still presents issues in the evaluation of IM_{PL} when: 1) the demand spectra has irregular shape; 2) the capacity curves present strength degradation. These are two distinct problems, but the solution is similar, i.e. to consider the maximum IM reached up to the point of the curve of interest. More information about the first issue is in [LC15a] and [LC15b], about the latter herein.

In case of URM buildings it is quite common that the pushover curve shows strength degradation, consequently it may happen that higher displacement demands are caused by lower values of IM. Figure 4.16 shows an example of this phenomenon. In the Figure an example of capacity curve is depicted in black with highlighted the position of four PL. The red shapes on the black curve indicate the spectral displacement at the attainment of PL, the shapes on the ordinate indicate the IM (in this case the PGA) that caused the attainment of PL (the values are reported in the legend). PL1 is represented by red circles and PL2 by red triangles. Due to the sudden drop in strength after PL3, the demand spectra that intersects the capacity curve in correspondence of PL4 (drawn with dashed blue line) has a lower IM_{PL} value than the demand spectra that intersects the capacity curve in correspondence of PL3. This is something physically not admissible, therefore for a given PL the IM_{PL} is here considered as the maximum IM reached in all points of the capacity curve before its attainment.

4.2.5   ISA curves

From Section 4.2.1 to 4.2.4 several procedures were discussed to evaluate the IM that caused the attainment of a PL. However, the NSP requires to run a pushover analysis in which the independent variable is the control displacement, and the variation in base shear due to the control displacement are tracked. Therefore, it is possible to calculate the IM_{PL} not only in correspondence of the limit states, but it could be calculated for each displacement of the pushover curve. With this procedure the ISA (incremental static analysis) curves are obtained, that can be defined as "the IM that causes a given displacement D as a function of D" [LC15b]. ISA curves are the static counterpart of the better known IDA curves discussed in Section 4.3.1. First attempts to represent ISA curve with N2 method
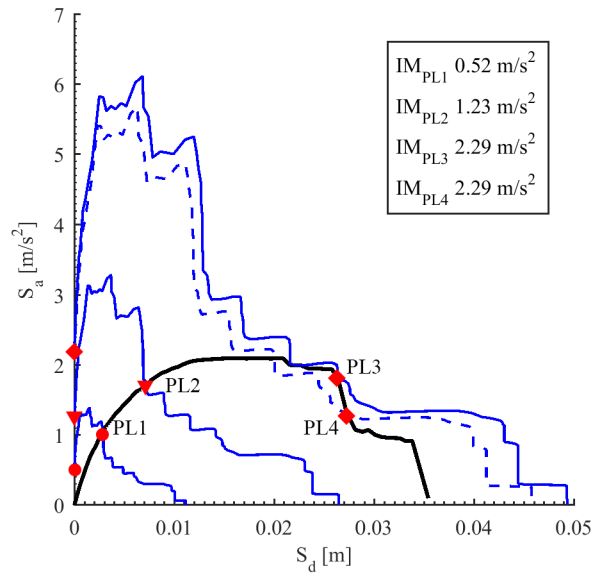
Figure 4.16: Evaluation of IM_{PL} in case of capacity curves characterized by base shear decays

are in [DF04a], and Fig. 4.17 shows examples of ISA curves developed with the method above discussed.

In ISA curve graphs the control displacement is reported on the X-axis, and on the Y-axis the corresponding IM. It should be noted that on the X-axis the MDOF control displacement instead of the equivalent SDOF displacement is reported. In fact these curves will be compared with IDA curves that derive from dynamic analyses, for which it does not make sense to compute a participant factor and transform the MDOF response into an equivalent SDOF one.

4.3 Intensity measure calculated through nonlinear dynamic analysis

In case of NDPs the procedure is reversed if compared with NSP. The analyses are conducted at a given IM (scaling the PGAs of the different THs used from 0.5 to 6 or 7 times their actual values, until collapse is reached) and then the corresponding control displacements are evaluated, i.e. the maximum value of the control displacement attained during the
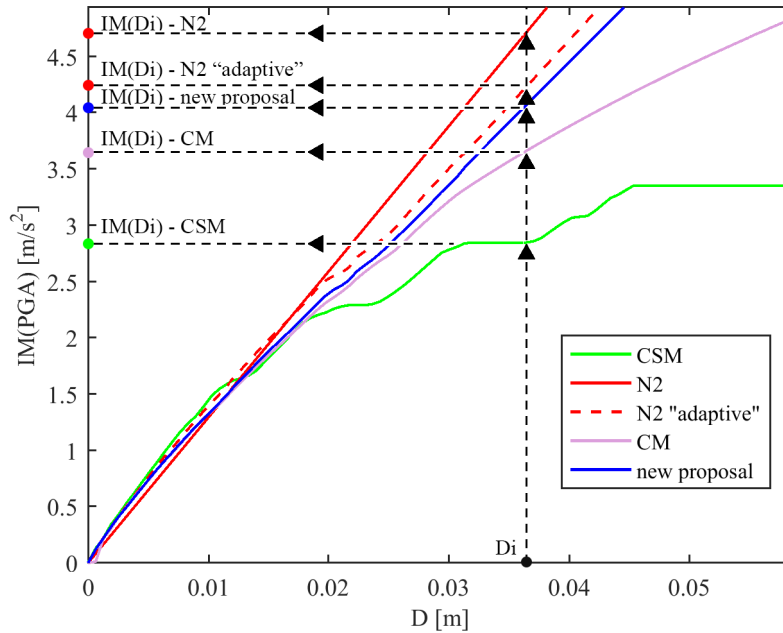
Figure 4.17: Examples of ISA curves developed with the procedures discussed from Section 4.2.1 to 4.2.4

NLTH analysis. This procedure could be applied to evaluate the position of a single PL, or it could be "extended" continuously and define the IDA curves that are discussed in the next Section.

4.3.1 IDA curves

IDA curves were introduced by Vamvatsikos and Cornell in 2002 [VC02a], and they are a plot where in the abscissa depicts the engineering demand parameter (EDP) and the ordinate one (or more) IMs that characterize the applied scaled accelerogram. The result of one nonlinear dynamic analysis is a point on the IDA curve. Each of these points has the vertical coordinate equal to the IM used to undertake the nonlinear dynamic analysis; the abscissa is the maximum value of control displacement reached during the analysis. Then, IDA curves are drawn linking those points. Fig. 4.18 shows an example of ten IDA curves (in grey) obtained applying the ten time-histories described at Section 3.3 to a case study model. In the same figure, the median, 16% and 84% percentiles IDA curves are shown.
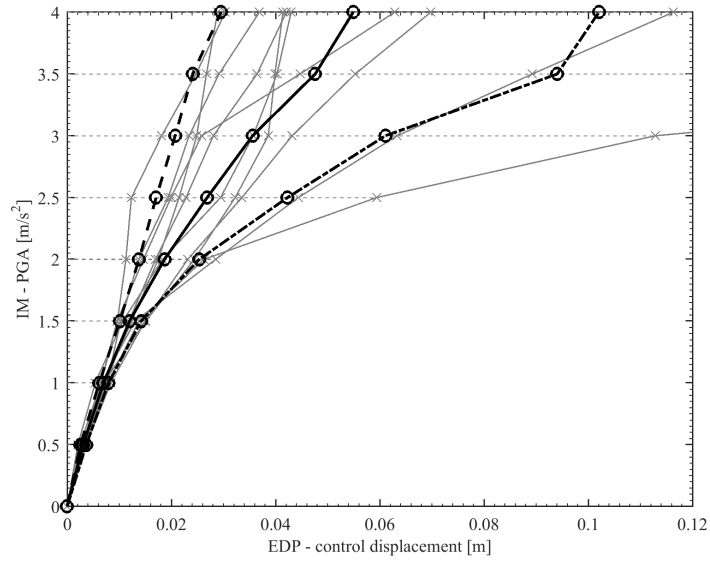
Figure 4.18: Examples of ten IDA curves (in gray) and the median (full black line), 16% (dashed black line) and 84% (dashed-dotted black line) percentiles

In IDA curves the independent variable is the IM plotted on the vertical axis. The reason of this choiche is given in [VC02a]: "as per standard engineering practice, such plots often appear 'upside-down' as the independent variable is the IM which is considered analogous to 'force' and plotted on the vertical axis as in stress-strain or force-deformation graphs". It is worth noting that often IDA curves could be drawn interpolating using a spline or a piecewise linear approximation as shown in [VC02b]. However, in this research IDA curve were developed using a linear interpolation.

IDA curves are not always monotonic, but hardening is something often observed. This is a counter-intuitive feature, in fact it means that a system "may exhibit the same or even lower response when subjected to higher seismic intensities" [VC02a]. Possible explanation of this phenomenon is given in [VC02a]: "it is the *pattern* and the *timing* rather than the intensity that make the difference. As the accelerogram is scaled up, weak response cycles in the early part of the response time history become strong enough to inflict damage thus altering the properties of the structure for the subsequent, stronger cycles, [...], perhaps due to period elongation". It is possible to observe this phenomenon also in some IDA curves of Fig. 4.18. As a

consequence of this fact IDA curves do not represent bijective functions. In fact, if any value of IM produces a single value of EDP, for a given EDP there is at least one ore more IMs that generate it.

Finally, IDA curves allow to detect the onset of dynamic instability, that is defined as "the point where deformations increase in an unlimited manner for vanishingly small increments in the IM. The curve then flattens out in a plateau of the maximum value in IM as it reaches the *flatline* and EDP moves towards 'infinity'"[VC02a].

IM_{PL} computation

As said in the previous section, in nonlinear dynamic analysis the IM is the independent variable, however for each model and each PL n values of IM_{PL} derive from the analyses, one for each TH (and in particular in this research 10 THs were used). It is therefore necessary to adopt a statistical approach to evaluate one value of IM_{PL}. To this aim IM_{PL} is computed under the hypothesis that the IM distribution may be assumed as lognormal [VC02a]. Therefore IM_{PL} is the median value of all IMs, i.e. the 50% fractile or the antilog of the mean of the logarithms, and the standard deviation of the logarithms is a measure of the dispersion. An example is given in Fig. 4.19, where the blue dots on the vertical axis indicate the IM for different TH applied, the horizontal blue dashed line indicates the position of the median IM_{PL} and its intersection with the IDA curves provide the position of the control displacement corresponding to the attainment of the PL_k, D_{PLk}. Three values of D_{PLk} were studied, that derive from the median, 16% and 84% percentile IDA curves.

4.4   Summary and main issues

The method to compute the nonlinear (inelastic) displacement demand currently adopted by the Italian [NTC08] and European [EC804] codes, is based on the coefficients T_C and T^*. T_C sets the limit between the *equal energy* and the *equal displacement* rules, T^* is the period of the equivalent bilinear curve representative of the original MDOF system. In particular if $T^* \geq T_C$ the *equal displacement* rule is used. This method, if applied to existing URM buildings presents the following issues:
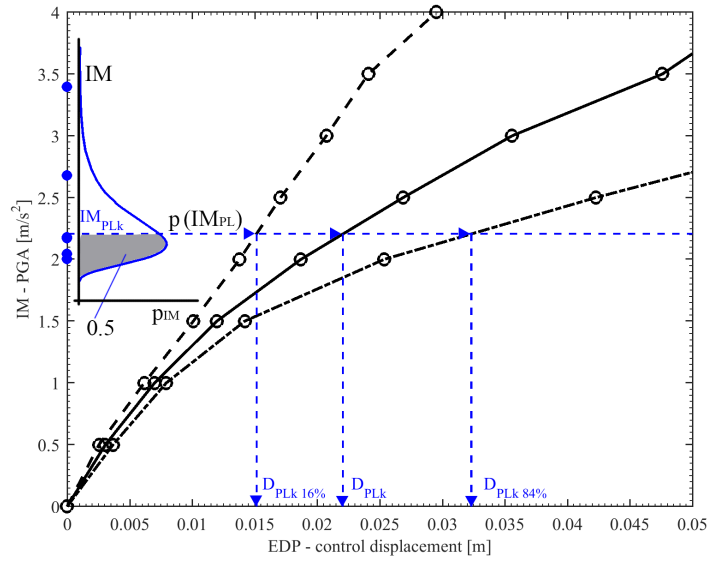
Figure 4.19: Evaluation of IM_{PL} as median value of IM, D_{PLk} values derived by the intersection of IM_{PL} with IDA curves

- in firm soils T_C may assume a small value and as a consequence the *equal displacement* rule may be applied for URM buildings, and this assumption, as it is shown by the results of Chapter 5, is often not conservative. In fact in that case the IM grows linearly with the displacement demand, but this trend is not confirmed by the dynamic results;

- regardless of the PL analyzed, the equivalent bilinear curve does not change, as a consequence it is not possible to evaluate the change in stiffness due to the evolution of damage;

- the equation adopted to compute the target displacement (Eq. 4.18) does not take into account damping-related issues as well as strength degradation (that are common in URM buildings);

- this method should not be applied for specific accelerograms, but only response spectra with a "regular" shape, as the code spectra, may be used.

With the aim to find a methodology that allows to overcome these issues, further procedures proposed in the literature and in current codes were

studied, and they were integrated with an original one developed within the present research. The procedures are listed herein:

- N2 method (based on inelastic spectra);

- Coefficient method, that takes into account the strength degradation issue;

- Capacity spectrum method (based on overdamped spectra), if care is paid, this method allows to use also non-smooth response spectra;

- recently developed methods: 1) as proposed in [GGPM17]; 2) a new method proposed within this research work. Both these methods are based on the use of inelastic spectra but taking into account the damping issue as well.

For all of these procedures the nonlinear displacement demand as well as the IM were evaluated, following the steps herein:

1. transform the pushover curve into a capacity curve representative of an equivalent SDOF. The capacity curve may be in the form of a bilinear (N2, CM, and new proposals) or not (CSM) - *capacity*;

2. the nonlinear displacement demand is evaluated (for each method studied) - *demand*;

3. for all the PLs considered the IM is calculated, comparing capacity and demand, as the seismic input that causes the attainment of a given PL. In the present research the IM adopted is the PGA;

4. for all the aforementioned methodologies the ISA curves were developed.

Subsequently the IM_{PL}, as well as the IDA curves were evaluated through an NDP and compared with the static result. The static result is indicated with $IM_{PL,st}$, the dynamic with $IM_{PL,dyn}$.

Chapter 5

Non-linear analyses main results

In this chapter the main results derived from both nonlinear static and dynamic analyses are compared and discussed. In particular the attention is pointed out on three "decisions" that need to be taken in undertaking a NSP: 1) the load patterns (LPs) to apply to undertake the pushover analysis; 2) the performance levels (PLs) definition and 3) the procedure to use in order to compute the inelastic displacement demand and the consequent evaluation of the intensity measure (IM) that caused its attainment.

The effect of different LPs is discussed regarding: the global force-displacement response (Section 5.1), the evolution of the damage (Section 5.2) and on the DLs evaluation (Section 5.3). Indications on the most suitable LPs are given and subsequently the focus switches to the effects of the procedures used to compute the inelastic displacement demand. First it is necessary to convert the pushover curve into the capacity curve, to this aim transformation coefficients are needed and this topic is discussed in Section 5.4. The step forward is the IM evaluation, first in terms of IDA-ISA curves comparison (Section 5.5), then the attention is focused on the final outcome of a seismic analysis, i.e. on the IM that causes the attainment of a given PL (Section 5.6), in this thesis indicated with IM_{PL}. The latter aims to provide in a synthetic way the outcome of the seismic assessment procedure regardless of the complexity of the method of analysis. Hence, the outcome derived from a static procedure, $IM_{PL,st}$ is compared with the output from

113

the more complex dynamic procedure, $IM_{PL,dyn}$ and the main results are commented in Section 5.6.

5.1 Comparison in terms of force-displacement response

The global response of a building may be studied analyzing the force-displacement response outcome of both static and dynamic nonlinear analyses. An example of this comparison is given in Fig. 5.1 where the control displacement (defined in Section 3.1) and the building base shear are plotted on the X and Y axis respectively.
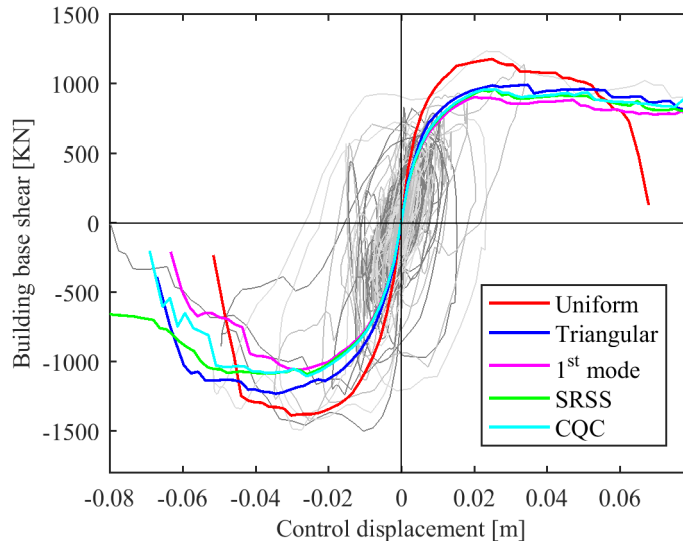
Figure 5.1: Comparison between pushover curves derived applying different LPs and the force-displacement loops from NLTHs for scaled values of the PGA. $A_{irr,rig}$ model, TH5 PGA up to 0.47g.

It is worth reminding that the control displacement adopted in this research was the average displacement of all nodes at top floor weighted by their masses (the reasons for this choice are detailed in Section 3.1), therefore it is not the displacement of a physical node. If in presence of rigid diaphragms this is not an issue, when the stiffness of the diaphragms reduces the curves from the dynamic analyses may assume a not very regular shape, as it is shown in Fig. 5.2.

114

(a) TH4, PGA 0.27 g (b) TH7, PGA 0.26 g
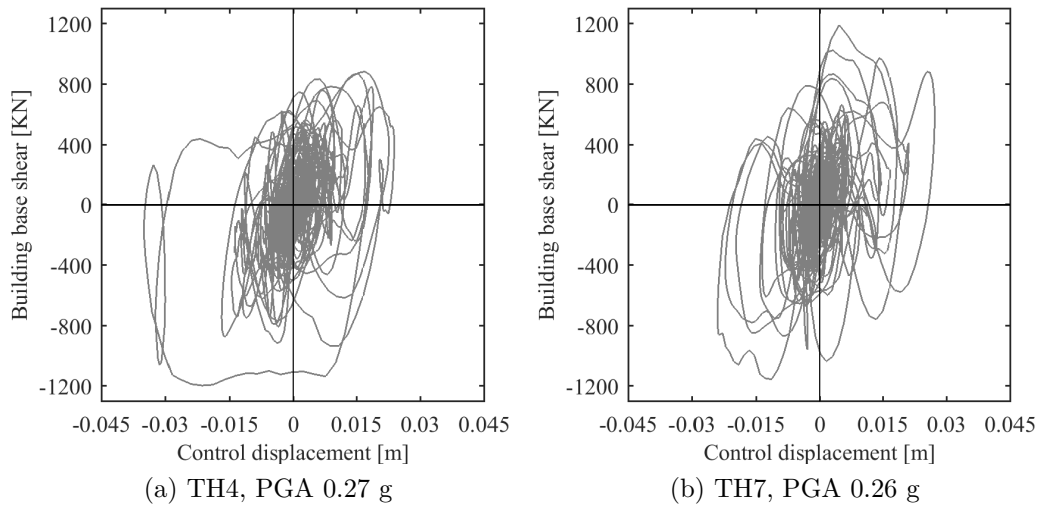
Figure 5.2: $A_{irr,flex}$ model, examples of force-displacement loops from nonlinear dynamic analysis at the attainment of DL4.

Due to this issue, in the presence of flexible diaphragms, it is hard to evaluate the attainment of a limit state through checks at global scale as proposed in [MRPM14]. Therefore, for the limit states attainment evaluation, it justifies the adoption of the criteria proposed for local and macroelement scale defined in Section 3.3.1. In addition, nonlinear dynamic analyses produce a very large amount of data that may be difficult to interpret. Therefore some researchers prefer to compare the result from the nonlinear static analyses with the nonlinear dynamic through their peak seismic response, as recently done in [NDG+17], where the mean peak top displacements and mean peak interstory drifts between the static and dynamic analyses were compared.

A characteristic that was often possible to observe was that the best estimation of the dynamic base shear strength capacity was provided by the uniform load pattern and that its force-displacement relationship was always very different from the other LPs (as shown in Fig. 5.1). This points to the need to use the uniform LP. However, to use only the uniform load pattern may lead to not conservative results when it is applied to buildings with elevation irregularities, such as the C-type models described in Chapter 2. An example of that is reported in Fig. 5.3: the pushover

curves with the different LPs adopted are shown, together with the NLTH force-displacement loops up to the PGA that caused the attainment of PL4 for $C_{irr,rig}$ model. It is possible to observe that the pushover curve developed with the uniform LP strongly overestimates the actual building base shear. This is because the uniform LP forces a story mechanism at ground floor, whereas in case of elevation irregularities, with the dynamic analysis, it is possible to observe that damage is concentrated at top story (i.e. corresponding to the stiffness reduction of the walls), see Section 5.2. Therefore, due to the damage development at top story, the piers at ground level do not reach their shear capacity, as it happens when in the static procedure the uniform LP is applied. As a consequence, the total base shear derived by the dynamic analysis is lower than that evaluated when the static analysis with the uniform LP is undertaken (Fig. 5.3). However, the uniform LP for the other models is often the most conservative LP, especially at ultimate PLs (see Section 5.6 and Fig. 5.35).
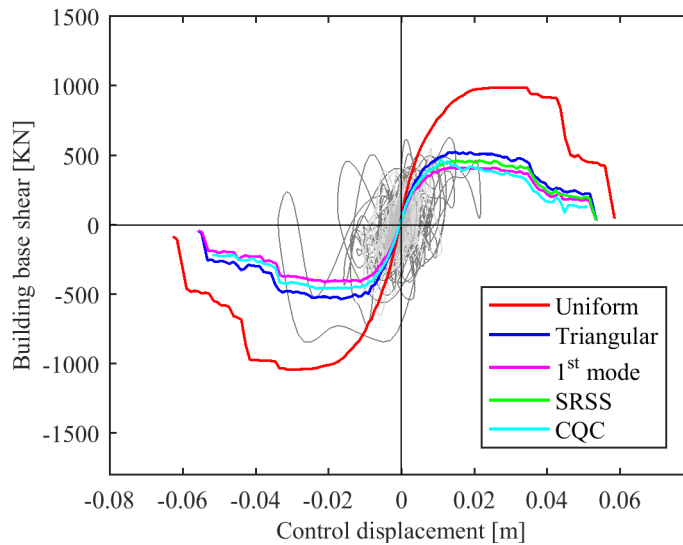
Figure 5.3: Comparison between pushover curves and the force-displacement loops from nonlinear dynamic analysis for scaled values of the PGA. $C_{irr,rig}$ model, TH4 PGA up to 0.14g.

With regard to the LP proportional to the 1st mode shape, its use in buildings with flexible diaphragms is discouraged for two main reasons: (a)
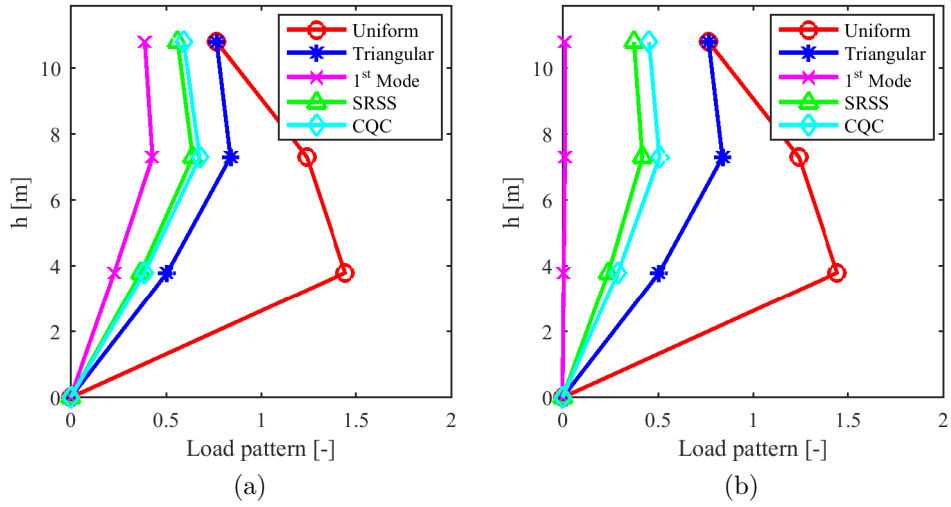
Figure 5.4: Comparison between the different load patterns used for the pushover analyses (kept invariant during the analysis), considering a specific wall (wall 2) of the $A_{irr,rig}$ model (a) and $A_{irr,flex}$ (b).

the walls that have their own period of vibration far from the 1st mode one could not receive any force; (b) it activates a small percentage of mass.

Fig. 5.4 clarifies what stated in point (a). In fact, in model $A_{irr,flex}$, wall 2 receives almost zero forces, since its displacements are close to zero in the 1st mode of the model (see Fig. A.33 in Appendix A). Another consequence of this issue is that the damage prediction is not correct. This further issue is discussed Section 5.2.

The consequences of point (b) are shown in Fig. 5.5, where the pushover and capacity curves for the $A_{r,flex}$ model are shown. Although the use of LP proportional to 1st mode provides the pushover curve with the smallest base shear, it becomes the curve with the highest capacity when transformed into the capacity curve (representative of the equivalent SDOF, see Section 4.1). This happened because in order to get the capacity curve in the acceleration-displacement format, the base shear needs to be divided for the mass of the equivalent SDOF that is very small if compared with the ones obtained from the other LPs (see Section 5.4). Finally, the use of 1st mode LP may lead to even less conservative results if it is combined with a PL evaluation defined according to what is currently proposed in codes
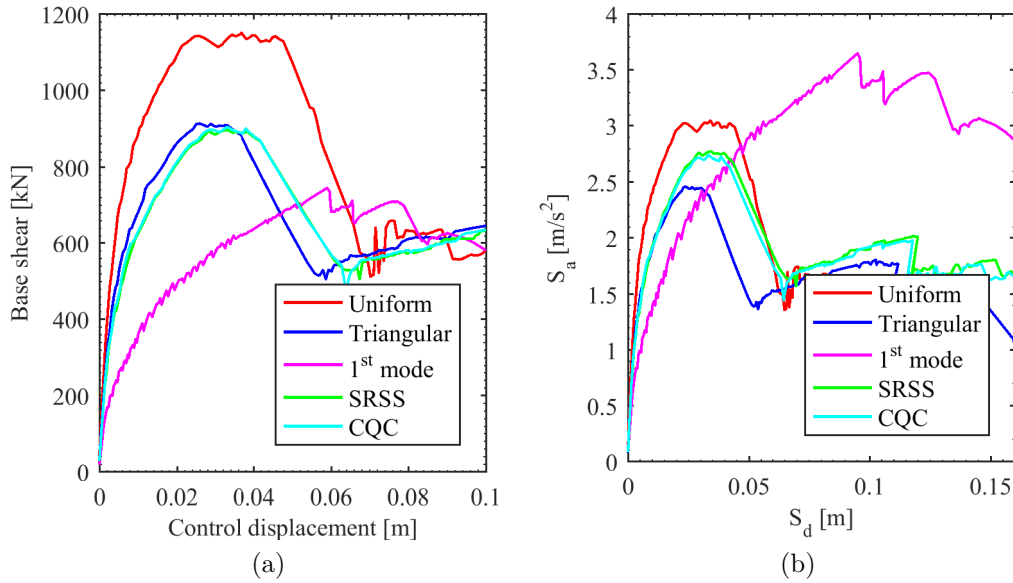
Figure 5.5: $A_{r,flex}$ model: pushover (a) and capacity (b) curves associated to the different LPs used for the NSPs

such as [NTC08] and [EC804], as it is discussed in Section 5.6 (see Fig. 5.35).

As a final remark about the LPs, it should be noted that the differences in the pushover curves observed are also a consequence of the resultant force point of application. In fact, the lowest position of the point of application is with the uniform LP, and it implies the maximum strength and the lowest displacement at the failure. On the contrary with the triangular and other "modal" distributions the point of application is at a higher position than the uniform and it implies less strength, but larger displacements at failure.

5.2 Extent of damage

From the analysis of damage extent after the nonlinear analyses observations may be made on the effects of: diaphragm stiffness, construction details and LP applied.

As it was already shown by the modal analysis, Section 2.3, in the presence of rigid diaphragms all the walls of a building move together. As

a consequence, in nonlinear static analysis, regardless of the LP applied, when a PL is reached all the walls show a similar extent of damage. On the contrary, when diaphragms are flexible they cannot redistribute forces between the walls and therefore, especially when a LP proportional to the 1st mode is applied, the walls may show damage patterns that are not similar. Fig. 5.6 depicts an example of this issue: in Figs. 5.6a, 5.6b, 5.6c, 5.6d the damage pattern of walls 4,5,6 and 2 at the attainment of DL3 is shown. It is possible to observe that only walls 5 and 6 present a significant damage. This is consistent with the 1st mode of the model, in which only wall 5 and (slightly) 6 are activated. However, this damage pattern is not consistent with the dynamic results, as it is shown in Figs. 5.6e, 5.6f, 5.6g, 5.6h. In fact, when a TH is applied to a building model all walls are activated by the base acceleration.

(a) Wall 4 NSP   (b) Wall 5 NSP   (c) Wall 6 NSP   (d) Wall 2 NSP

(e) Wall 4 NDP   (f) Wall 5 NDP   (g) Wall 6 NDP   (h) Wall 2 NDP
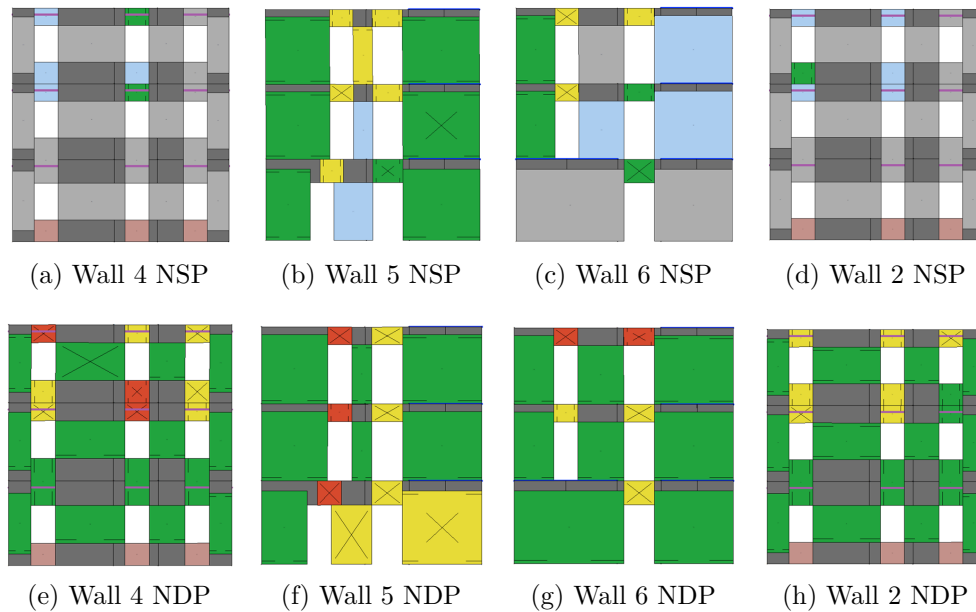
Figure 5.6: $A_{r,flex}$ model, damage in the walls at the attainment of DL3 applying a LP proportional to 1st mode (from a to d) and at the end of a NLTH analysis (from e to h). See Fig. 2.2 for the meaning of colors and symbols.

Fig. 5.7 shows a damage pattern comparison that takes into account the effect of the structural details. In particular, the damage pattern for $A_{irr,int}$ and $B_{irr,int}$ models at the attainment of DL4 is depicted. It is

possible to observe that: 1) the model with tie rods (A) presents a higher degree of damage in spandrels than the model with ring beams (B); 2) as a consequence of 1), in the B-type model it is more common to observe story mechanisms. Both these characteristics are due to the presence of ring beams, in fact they increase spandrel strength and stiffness, they reduce the rigid node rotations and therefore cause a shift of damage from spandrels to piers.

In Fig. 5.7 it is also possible to observe the effect of the LP applied. Figs. from 5.7a to 5.7h show a damage state at the attainment of DL4 when the triangular LP is applied, whereas Figs. 5.7i to 5.7p show the damage condition when the uniform LP is applied. It is possible to observe that the two damage patterns are very different: the uniform LP often leads to the activation of a story mechanism at ground floor, whereas the triangular LP stresses mainly the upper stories. The other "modal" LPs (proportional to 1st mode or based on the SRSS or CQC combinations), lead to a damage pattern similar to the triangular. Therefore this observation provides an indication of the two LPs to choose: the uniform LP and one LP between the triangular and the other "modal" LPs.

However, as already discussed, it is not sufficient to use only the uniform LP, in fact, especially in the case of elevation irregularities (C-type models), it is expected that the failure is at the level of the irregularity. Applying the *uniform* LP to C-type models the DLs were reached for the attainment of damage limit at top story as well. However, due to the shape of *uniform* pattern (that stresses mainly the lower stories) the DLs were reached for higher displacement values than the other LPs (see Sections 5.3.3, 5.3.4 and Figs. 5.12d, 5.14b). Moreover, the ISA curves developed applying the *uniform* LP to models with elevation irregularity overestimate the IDA curve (see Section 5.5 and Fig. 5.32a).

5.3 DLs position comparison

In this section the control displacement values at the attainment of the different DLs considered are analyzed. As in previous, also in this section it is was preferred to refer to DLs instead of PLs because the results show displacements that monitor the evolution of damage at the scales introduced in Section 3.2, but there is no comparison with the inelastic seismic demand,

(a) $A_{irr,int}$, wall 4
triangular LP

(b) $A_{irr,int}$, wall 5
triangular LP

(c) $A_{irr,int}$, wall 6
triangular LP

(d) $A_{irr,int}$, wall 2
triangular LP

(e) $B_{irr,int}$, wall 4
triangular LP

(f) $B_{irr,int}$, wall 5
triangular LP

(g) $B_{irr,int}$, wall 6
triangular LP

(h) $B_{irr,int}$, wall 2
triangular LP

(i) $A_{irr,int}$, wall 4
uniform LP

(j) $A_{irr,int}$, wall 5
uniform LP

(k) $A_{irr,int}$, wall 6
uniform LP

(l) $A_{irr,int}$, wall 2
uniform LP

(m) $B_{irr,int}$, wall 4
uniform LP

(n) $B_{irr,int}$, wall 5
uniform LP

(o) $B_{irr,int}$, wall 6
uniform LP

(p) $B_{irr,int}$, wall 2
uniform LP

Figure 5.7: Damage comparison between $A_{irr,int}$ and $B_{irr,int}$ models at the attainment of DL4. See Fig. 2.2 for the meaning of colors and symbols.

that is analyzed in Sections 5.5 and 5.6. However, always in Section 3.2 it is pointed out that the PLs are defined herein on the basis of DLs.

For all the numerical models studied, to undertake the NDP, ten THs were applied, therefore, there are ten displacement values corresponding to the attainment of a given DL. As detailed in Section 3.3, a statistical approach was adopted, therefore the median (50% percentile), 16% and 84% percentiles values of the ten THs were calculated. These values are compared with those deriving from the NSP, and therefore for each model, five different displacements were computed for each DLk, one for each LP. For the different DLs the main results are summarized in the following subsections.

5.3.1 DL1

Using the static method the displacement values obtained with all the LPs are always conservative if compared with the dynamic result (sometimes also overly conservative). For this DL only the multiscale approach was used (see Section 3.4). The results for $A_{r,flex}$ and $C_{irr,rig}$ models are depicted in Fig. 5.8. $A_{r,flex}$ is the only model in which a LP (i.e. that proportional to 1st mode) with the static method provides not conservative results. Since this is the only case for all the models and all the LPs, it is likely that this is a consequence of using the LP proportional to 1st mode in a building with flexible diaphragms. This is a further confirmation that this LP is not suitable to be applied in buildings with flexible diaphragms. Fig. 5.8b shows the results for $C_{irr,rig}$ model, that is one of the cases in which the static method is overly conservative. The optimum outcome of a static analysis would be to predict exactly the dynamic response, i.e. D_{DLk} computed with the static approach approximately equal to that computed with the dynamic. However, also a prediction within the 16% - 84% may result acceptable, with the preference of displacements smaller than the 50% dynamic response.

For this DL, as well as for all the other DLs, both the multiscale approach with macroelement check based on interstory drift checks and DLmin were analyzed. For almost all the case study models the attainment of DL1 was ruled by the global scale. It is worth reminding that for DL1 the global scale fixes a minimum displacement limit that is equal to the one corresponding

(a) $A_{r,flex}$ model   (b) $C_{irr,rig}$ model
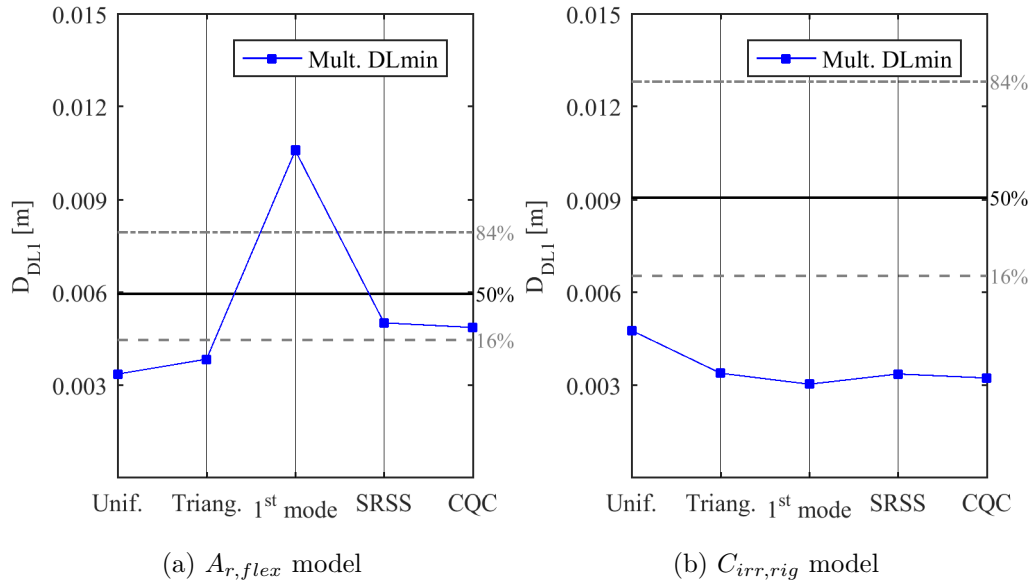
Figure 5.8: Control displacement at the attainment of D_{DL1} with the different LPs applied. The horizontal lines indicate the dynamic result.

to 50% of the maximum base shear. As a consequence, for DL1 it was not possible to observe any differences between the two versions of the multiscale approach.

The scales that controlled the attainment of DLs for all the models analyzed, and all the LPs applied, are summarized in the format shown in Fig. 5.9. In both parts of the figure the average result is depicted that is differentiated for the different diaphragm stiffness and model type in Fig. 5.9a and 5.9b respectively. It is possible to observe that in almost all cases the global scale ruled the attainment of DL, therefore with the other scales the position of the DL was evaluated at a very early stage of the analysis.

5.3.2 DL2

For the evaluation of DL2 both the multiscale approach and the procedure proposed in [NTC08], [EC804] were applied. In particular, with regard to the procedure adopted in the European codes, DL2/PL2 is considered reached when either the pushover curve reaches its peak (or more precisely
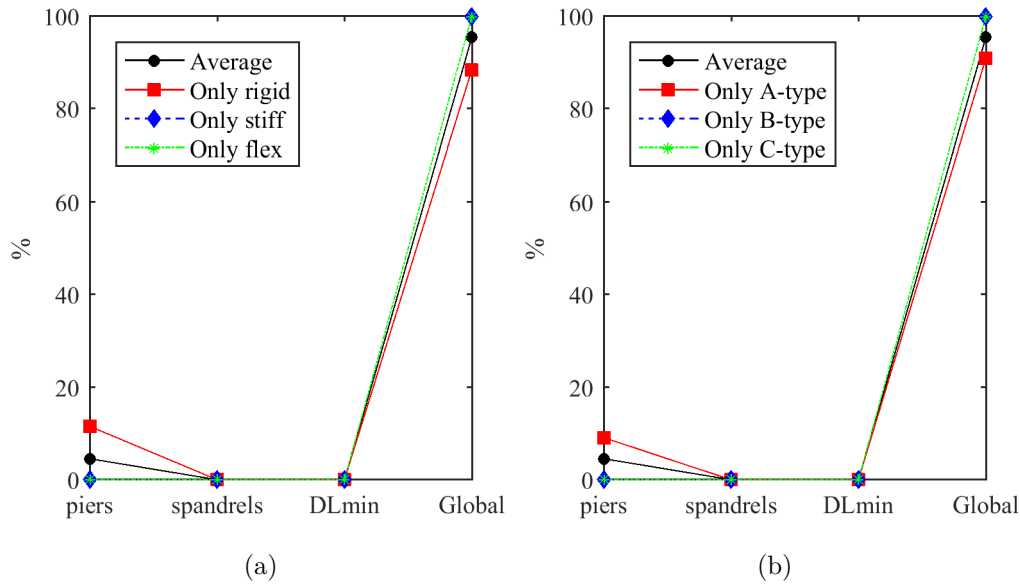
Figure 5.9: Control that caused the attainment of D_{DL1}

in this research the 98% of the maximum building base shear) or in any wall an interstory drift of 0.3% is reached.

It was possible to observe that the method proposed in the European codes provides conservative results (i.e. control displacement values smaller than dynamic displacement) for the models regular and with rigid diaphragms. On the contrary, with the introduction of irregularities this approach tends to overestimate the dynamic result. Although in some models ($B_{irr,rig}$,$C_{irr,rig}$,$B_{irr,int}$,$C_{irr,int}$,$A_{irr,flex}$, see Figs. 5.10a and 5.10b), considering the minimum displacement between two LPs (as the uniform and the triangular) the static method provides conservative results, for other models such as $A_{irr,int}$ and $C_{irr,flex}$ (see Figs. 5.10c and 5.10d) it is not possible to get conservative displacement values. Instead, the multiscale approach (considering the minimum between two LPs) provides displacement values corresponding to DL2 smaller than the dynamic approach for all models. In most cases, there are no significant differences in using the multiscale approach with the interstory drift or the DLmin criteria at macroelement scale. Two of the few exceptions are shown in Figs. 5.10b and 5.10d. In these two cases, as well as the other cases in which there is a significant difference between the two criteria, use of the DLmin check provides more

conservative results. This is due to the need to define a threshold for the interstory drift criterion that, as said for DL2, was set equal to 0.3%. In fact, as discussed in Section 5.3.5, this limit is too high for this type of buildings. As a confirmation of this issue: 1) in the new version Italian code, very recently issued [NTC18], the limit for the maximum interstory drift is set to 0.2%; 2) in [KP16] the Authors adopted for PL2 a drift limit of 0.1%, and this is a value more similar to the results obtained in this thesis and discussed in Section 5.3.5. Finally, in Fig. 5.10a the displacement evaluated with the procedure according to the European codes provides lower values because in that procedure there is not a minimum displacement limit as in the multiscale approach, that, for DL2, it is equal to the displacement corresponding to 60% of the maximum building base shear.

Another difference noticed between the use of the interstory or DLmin criteria at macroelement scale is in the scale that controlled the attainment of DL2. In fact, if the DLmin check is adopted this is in most cases the dominant criterion (see Figs. 5.11a and 5.11b). On the contrary, when the interstory drift check is used, also the local scale (and in particular the damage check in spandrels) and the global scale are often critical (see Figs. 5.11c and 5.11d). If this, on one hand, means that all criteria are well balanced, on the other proves again the sensibility in the choice of the threshold. In fact, at the beginning of the present research a higher threshold was adopted for the local scale and it was found that the use of this scale was never significant.

5.3.3 DL3

For the evaluation of DL3, in addition to the criteria adopted for DL2, a further procedure, consistent with what proposed in [ASC14] was adopted, as described in Section 3.2.3.

The main results are depicted in Fig. 5.12, where it is possible to observe: a) a further confirmation that the 1st mode LP is not suitable for URM buildings with flexible diaphragms , in fact, since only one (or few) wall(s) receive(s) the major part of the forces, it will reach a high level of damage before the other walls reach their shear resistance. As a consequence the 20% building base shear strength degradation is reached for very high displacement values; b) the criteria based only on the extent of damage

125

(a) $A_{irr,flex}$ model

(b) $C_{irr,int}$ model

(c) $A_{irr,int}$ model

(d) $C_{irr,flex}$ model
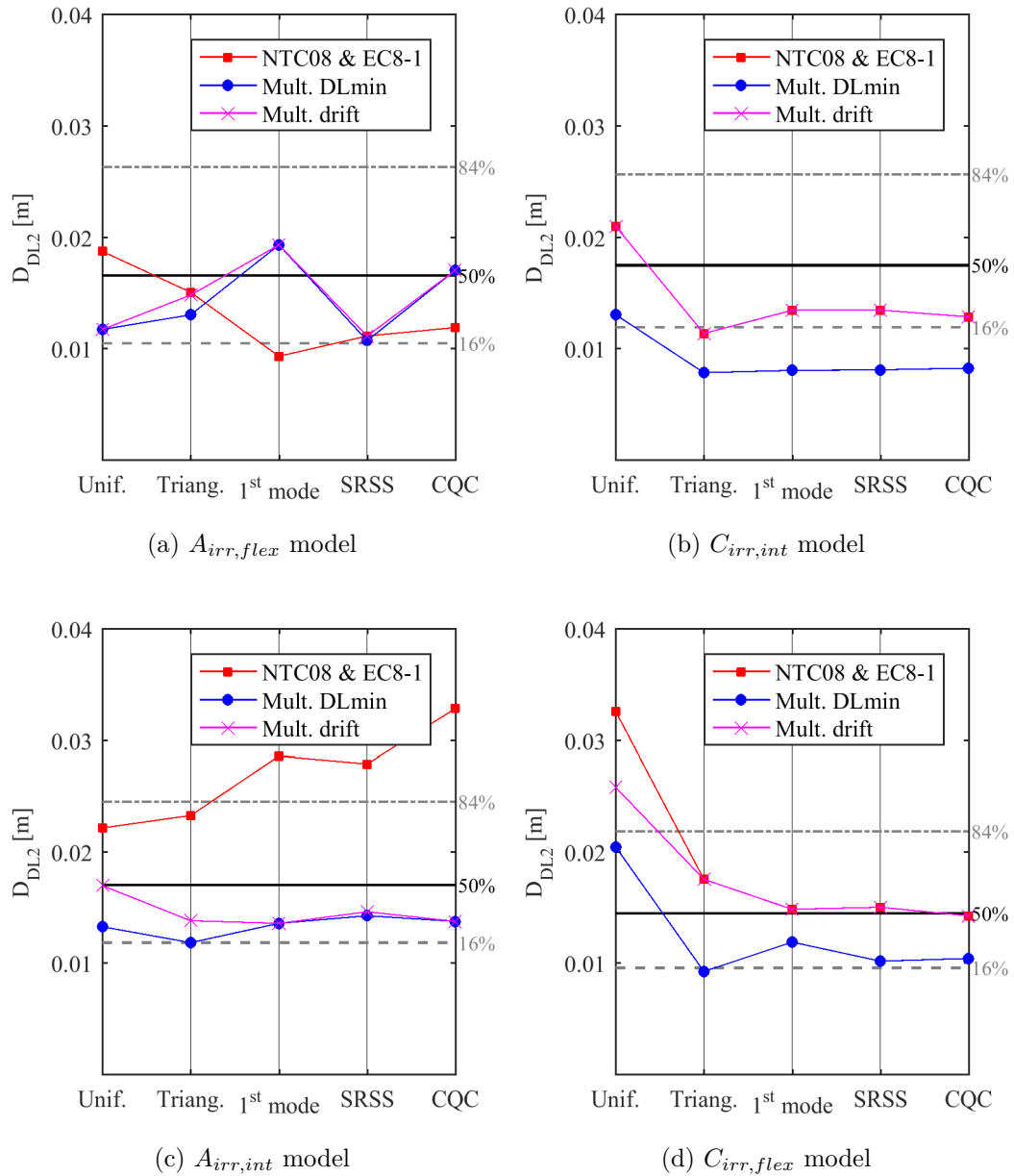
Figure 5.10: Control displacement at the attainment of D_{DL2} with the different LPs applied. The horizontal lines indicate the dynamic result.

(a) Macroelement scale: DLmin

(b) Macroelement scale: DLmin

(c) Macroelement scale: drift

(d) Macroelement scale: drift
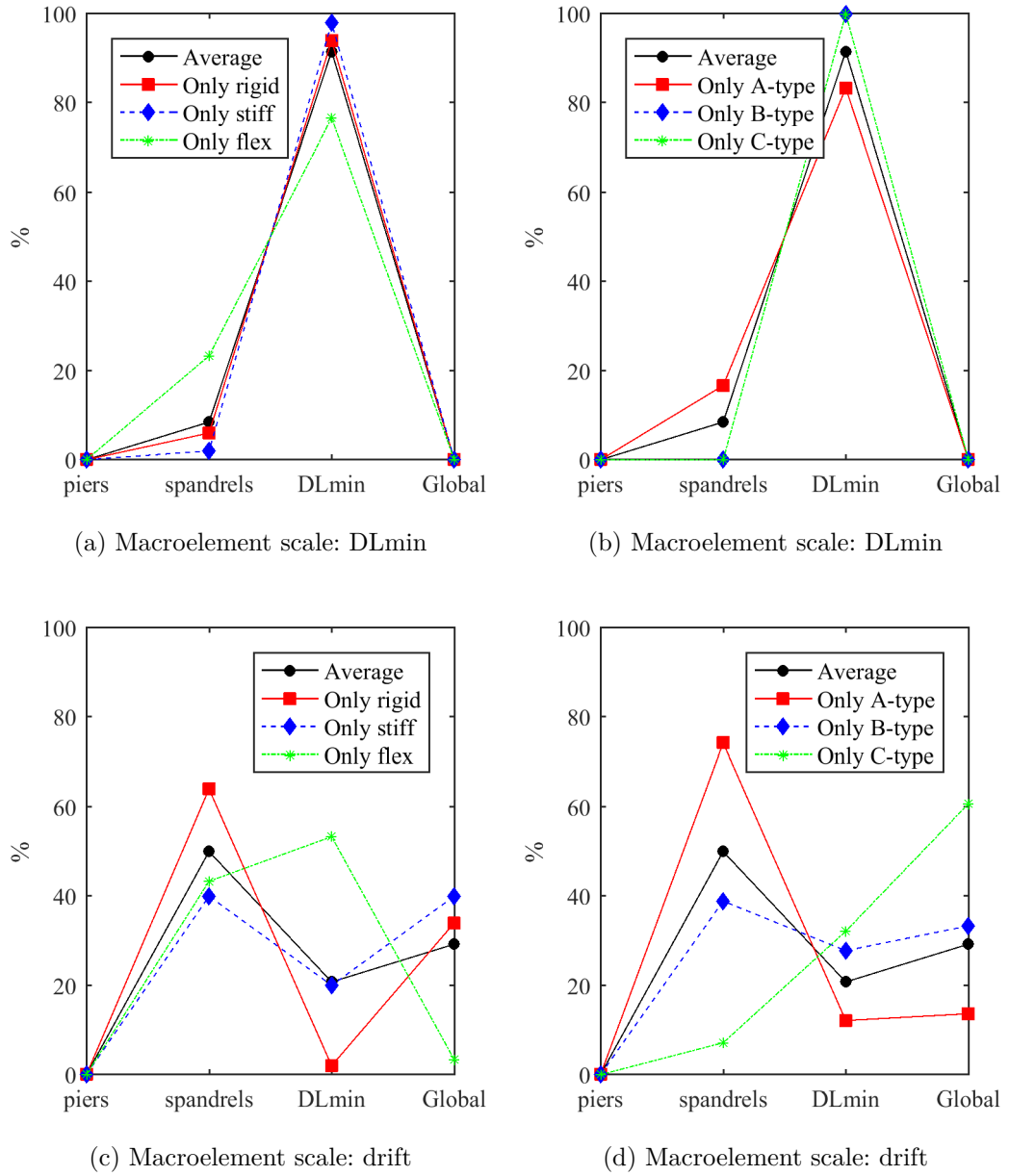
Figure 5.11: Control that caused the attainment of D_{DL2}

at local scale (as the procedure adopted in [ASC14], may result overly conservative, and this is true in particular for the *Loc. min* criterion; the criterion adopted in [NTC08] and [EC804] based on checks at global scale often does not provide conservative results, if in some cases to consider the minimum between the uniform and triangular distribution helps in approximating the dynamic result (Fig. 5.12c) in other cases this is not enough, as it is shown in Fig. 5.12d. Finally, always Fig. 5.12d shows that the uniform LP may provide very unsafe results when applied to buildings with elevation irregularities.

Fig. 5.13 shows the scale that controlled the attainment of DL3. It is possible to observe that in this case there are no notable differences in using, at macroelement scale, the interstory drift or DLmin checks. This proves that the interstory drift threshold of 0.5% is suitable for the buildings analyzed in the present research.

5.3.4 DL4

Also for DL4, if the minimum of two LPs is evaluated, the static procedure provides displacement capacities that are smaller than the dynamic ones. Only for the models with elevation irregularities the static method provides results slightly less conservative than the dynamic (Fig. 5.14). It is possible to observe that if in some cases, as in Fig. 5.14a, to adopt the SRSS LP may help in obtaining a smaller displacement capacity than the dynamic, in other cases this is not enough, as it is shown in Fig. 5.14b, however the overestimation is small, and only when using the DLmin criterion.

Finally, similarly to DL3, there is not much difference in the scales that governed the attainment of this DL if the DLmin or the interstory drift criteria were adopted.

5.3.5 Drift vs DLmin check

In this section the positions of the different DLs evaluated with only the DLmin and the interstory drift check are discussed. The aim of this comparison was to understand whether the two criteria are comparable/interchangeable. To this aim, for all the numerical models, the displacement ratio (at the attainment of every DL) for the two criteria was computed. In particular, if this ratio is higher than one it means that a given DL was reached for a

(a) $A_{r,flex}$ model

(b) $A_{irr,rig}$ model

(c) $B_{irr,int}$ model

(d) $C_{irr,rig}$ model
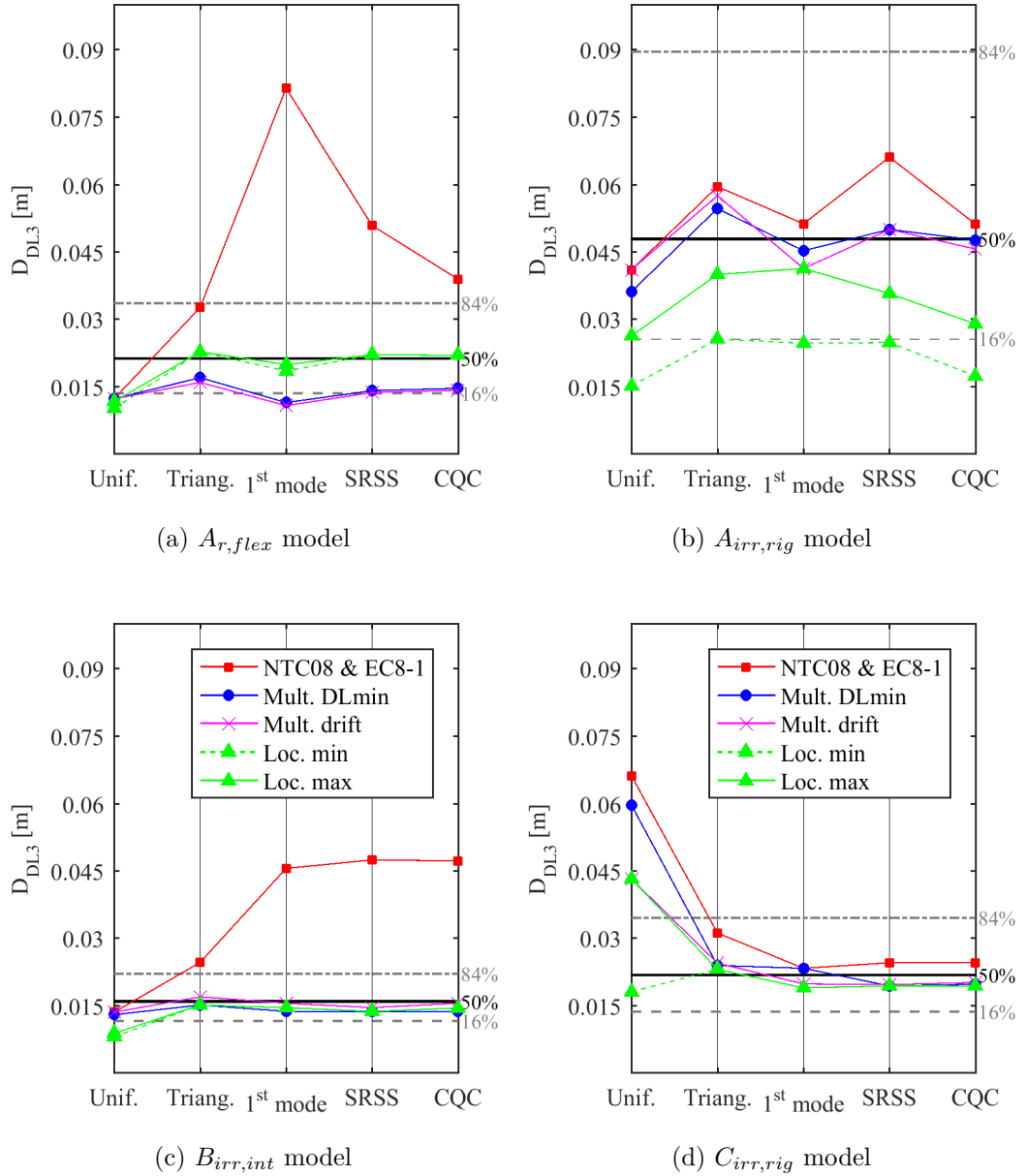
Figure 5.12: Control displacement at the attainment of D_{DL3} with the different LPs applied. The horizontal lines indicate the dynamic result. Sub-figures a) and b) have the same legend of sub-figures c) and d).
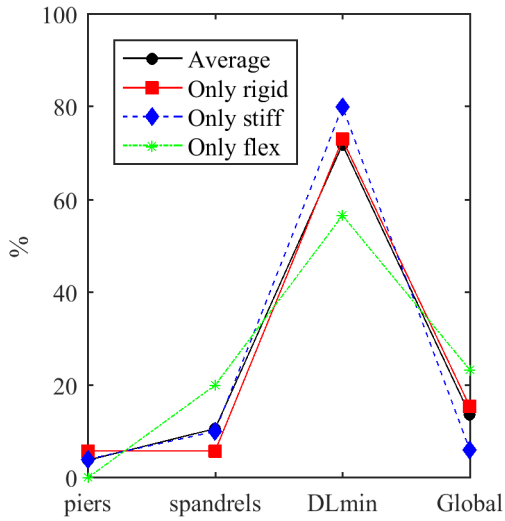
(a) Macroelement scale: DLmin
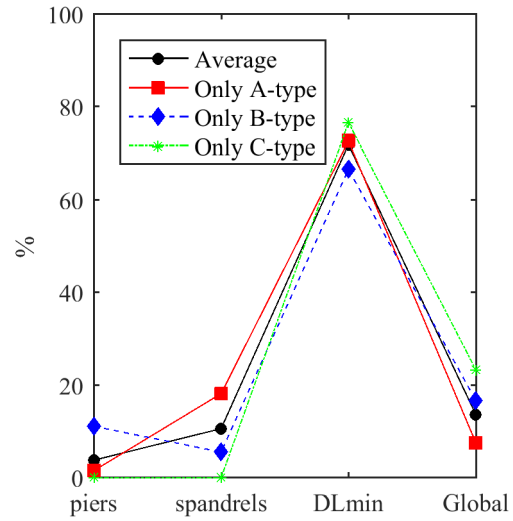
(b) Macroelement scale: DLmin
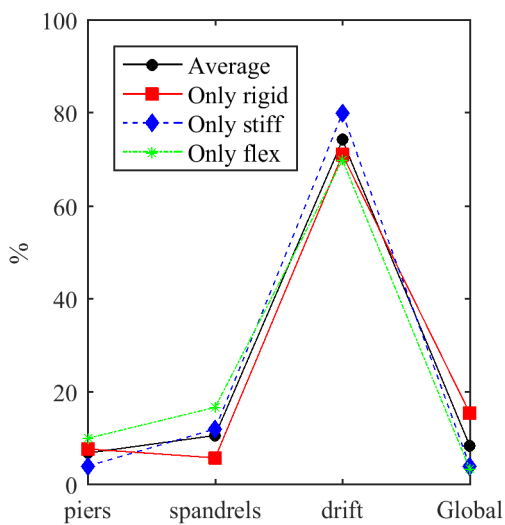
(c) Macroelement scale: drift
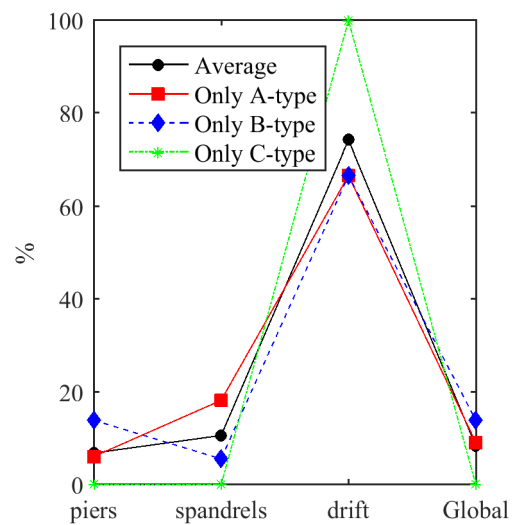
(d) Macroelement scale: drift

Figure 5.13: Control that caused the attainment of D_{DL3}

(a) $C_{irr,flex}$ model

(b) $C_{irr,int}$ model
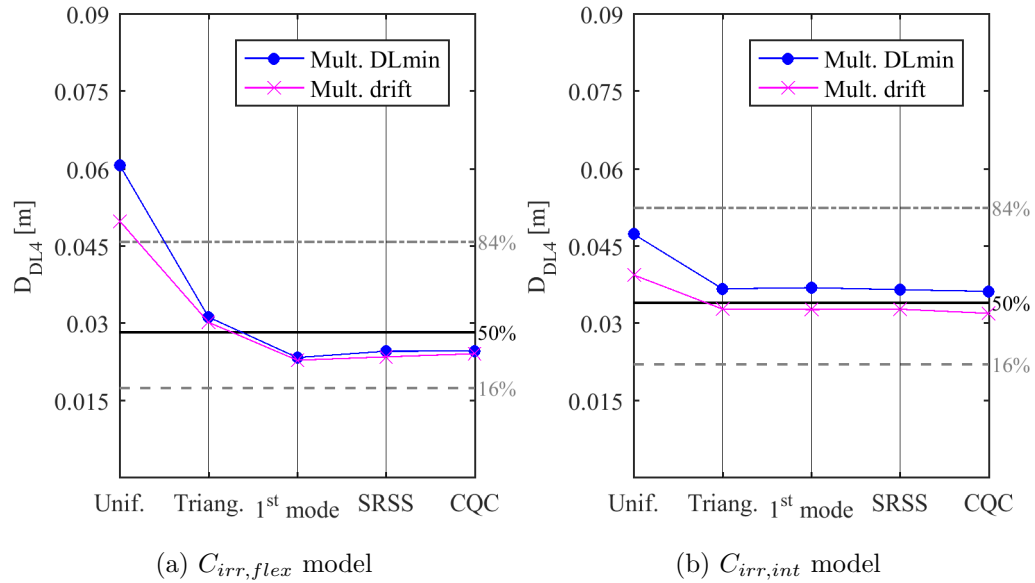
Figure 5.14: Control displacement at the attainment of D_{DL4} with the different LPs applied. The horizontal lines indicate the dynamic result.

larger displacement with the DLmin criterion than the interstory drift (See Fig. 5.15). As anticipated by the results in the previous sections, it was possible to observe that the two criteria provide very close results for DL3 and DL4, whereas using the DLmin criterion the stages DL1 and DL2 were reached for smaller displacements, if compared with the interstory drift criterion. Fig. 5.15a shows clearly this trend: regardless of the load pattern applied for DL3 and DL4 this ratio is close to unity. On the contrary, the ratios for DL1 and DL2 are between 0.3 and 0.4. This means that with the DLmin criterion there is a strong anticipation of the location at which the DL is reached. This trend was confirmed also by the other models, in which the displacement ratio was in almost all cases below 0.6. Fig. 5.15b shows one of the few cases in which the DLmin criterion provided higher displacement values than the interstory drift check, and also that applying the DLmin, in some cases, DL1 may be attained for very small displacement values. This demonstrates the major difficulty in the calibration of proper interstory drift thresholds for DL1 and DL2. In fact, for these DLs the interstory drift depends mainly on characteristics such as geometry and stiffness of the elements that may be very variable.

(a) $B_{irr,rig}$ model

(b) $C_{irr,rig}$ model
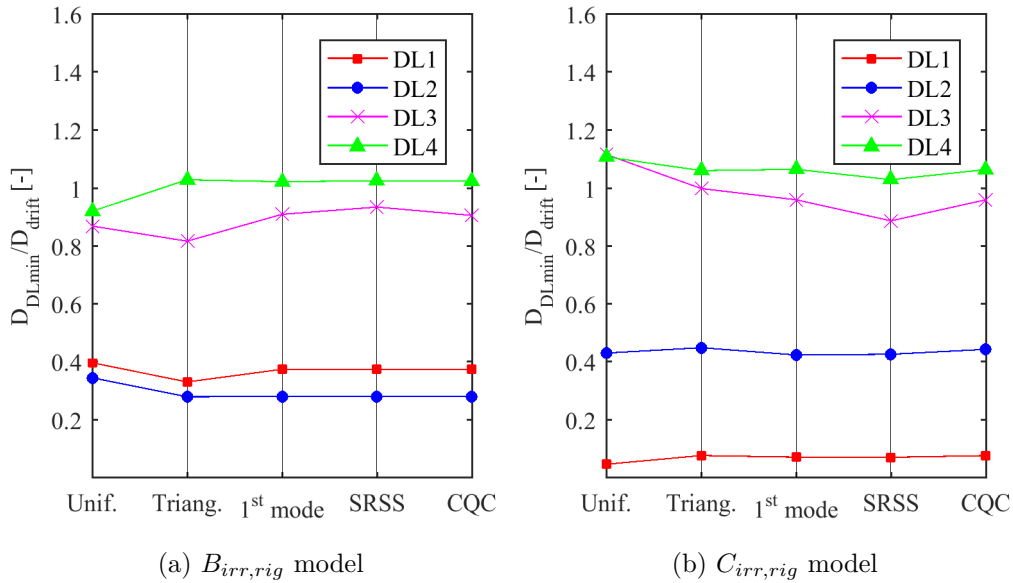
Figure 5.15: Ratio of the displacement at the attainment of the different DLs evaluated with DLmin and interstory drift criteria.

Finally, it is worth reminding that if the DLmin criterion provides overly conservative results, in the framework of multiscale approach minimum limit displacement values are provided for DL1 and DL2.

5.3.6 Ductility for DL3 and DL4

In this section the ductility exploited for DL3 and DL4 is discussed. In the N2 method the ductility is used to compute the inelastic spectra, therefore it is a very important parameter. To compute the ductility the displacement corresponding to the attainment of DL3 and DL4 was divided by a displacement corresponding to the end of the elastic phase. Two different elastic limits were adopted: 1) the "traditional" yield displacement introduced in Section 4.1, i.e. the D_Y is computed with the procedure proposed in [NTC08] and [EC804]; 2) the displacement corresponding to the attainment of DL2.

Fig. 5.16 and Fig. 5.17 show the ductility attained at the attainment of DL3 with the procedure 1) and 2) respectively. It is possible to observe that the ductility is strongly influenced by the presence of structural irregularities

and by the stiffness of the diaphragms. In particular it decreases in the presence of in plan irregularity and together with the diaphragms stiffness, being the latter more relevant. In fact, the models with rigid diaphragms show the highest ductility values that exceed 5. Regarding "C" models, their behavior is different, in particular the ductility decrease due to the diaphragms stiffness reduction is less evident. This is probably due to the fact that for "C" models the DLs are reached with a mechanism at top story that is less influenced by diaphragm stiffness. In the model analyzed, the presence of tie rods or ring beams does not significantly influence the ductility. DL4 presents a trend similar to DL3 (Fig. 5.18 and Fig. 5.19).

Finally, it is possible to observe that computing the ductility using D_{DL2}, approximately, provides smaller ductility values than when computed using D_Y. It means that on average D_Y is smaller than D_{DL2}.
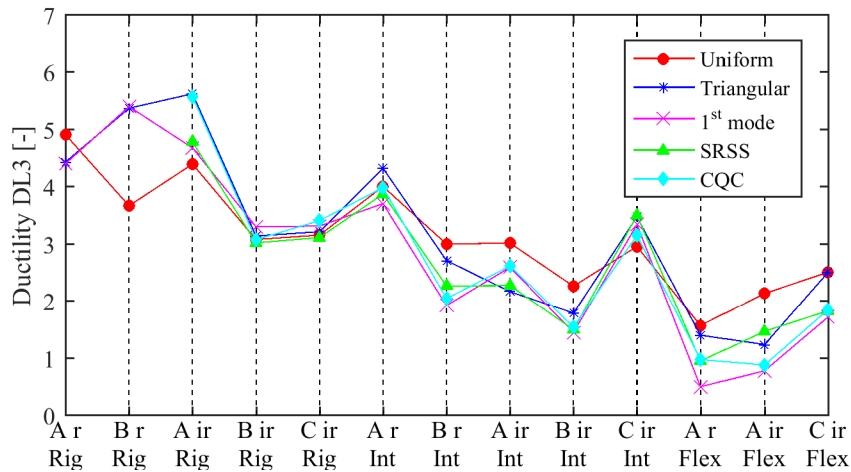
Figure 5.16: Ductility exploited at the attainment of DL3. Computed as D_{DL3}/D_Y.

From the analysis of the results it is worth pointing out that the ductility demand to reach DL3 and DL4 for the URM buildings under analysis was not small with peaks of 5 and 6 for DL3 and DL4 respectively. It is a further proof that it is necessary to have NSP that are reliable also in the presence of high ductilities. Fig. 5.20 shows the comparison between the ductility at the attainment of DL3 and DL4 when the uniform and the triangular LPs are applied. It is possible to observe that when the uniform LP is applied: a) the buildings analyzed show smaller ductility if compared
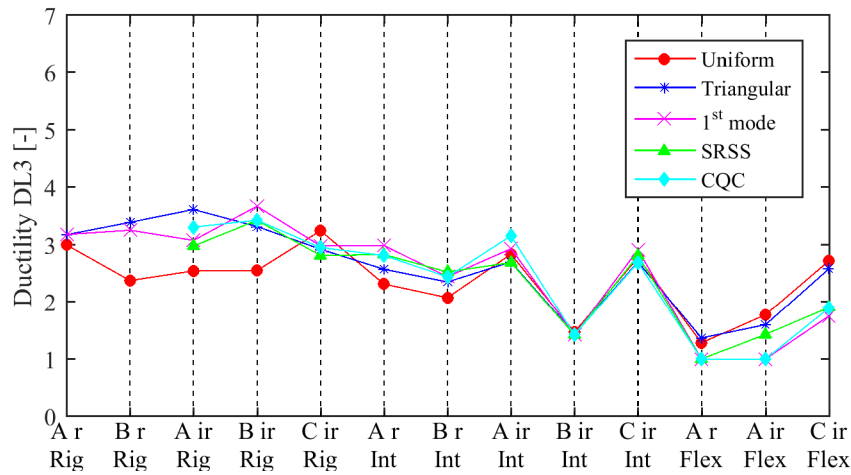
Figure 5.17: Ductility exploited at the attainment of DL3. Computed as D_{DL3}/D_{DL2}.
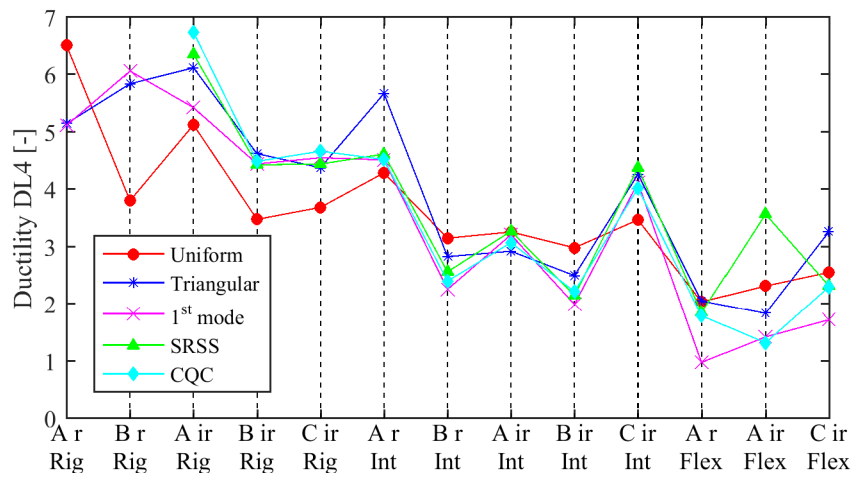
Figure 5.18: Ductility exploited at the attainment of DL4. Computed as D_{DL4}/D_Y.

with the triangular LP; b) the failure mechanism results more brittle being the ductility corresponding to DL3 and DL4 closer. The comparison with SRSS LP is not reported, however, the SRSS LP trend is very similar to the triangular one.
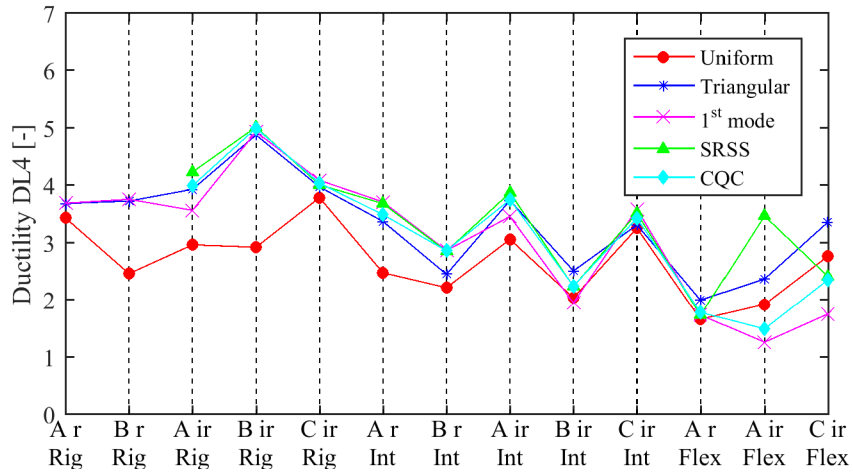
Figure 5.19: Ductility exploited at the attainment of DL4. Computed as D_{DL4}/D_{DL2}.
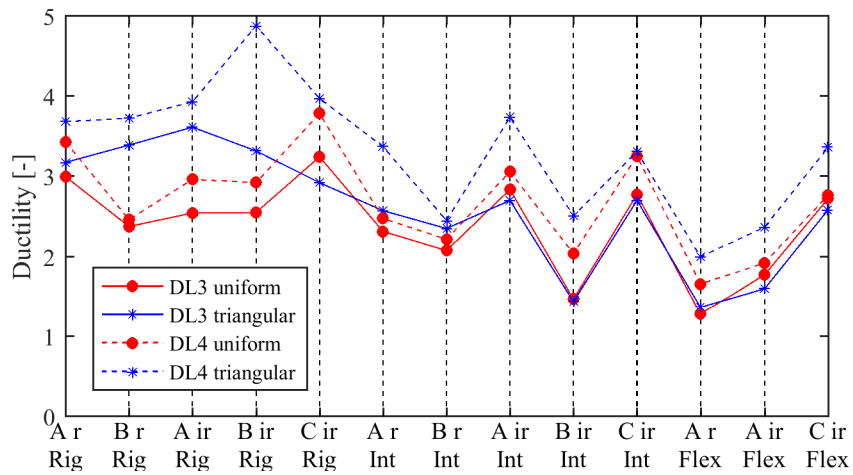
Figure 5.20: Comparison between the ductility exploited at the attainment of DL3 (D_{DL3}/D_{DL2}) and DL4 (D_{DL4}/D_{DL2}).

5.4 Evolution of transformation coefficients

Figs. 5.22, 5.23 and 5.24 show the evolution of e^* coefficient for the case study buildings when the *uniform*, 1st *mode* and *SRSS* LPs respectively are applied. The models analyzed are reported on the abscissa and e^* is reported on the ordinate. Similarly, Figs. 5.25, 5.26 and 5.27 show the evolution of Γ_Y coefficient. Note that in Figs. 5.24 and 5.27 for models

$A_{r,rig}$ and $B_{r,rig}$ the results shown refer to the *triangular* LP because for these models the *SRSS* LP was not applied (see Section 3.1.1). The results reported are the average between the Y+ and Y- directions.

As expected, the LP that involves the highest percentage of mass is the *uniform* LP (Fig. 5.22). Fig. 5.23 shows clearly that when the LP proportional to the 1st *mode* is applied the mass of the building involved reduced significantly. In particular when the diaphragms are flexible this LP activates only the 50% of the total dynamic mass, or less. This issue may be overcome using the *SRSS* LP, as it is shown in Fig. 5.24, for all the models at least 65% of the dynamic mass is triggered in the initial phase of pushover analysis. When *SRSS* LP is adopted, the percentage of mass participation is higher in the initial phase of pushover analysis than what was computed at the stage DL1 is reached. The "C" models show a lower mass participation than the other models and this is attributed to their different failure mode. In fact, in these models the damage concentrated at top story. Probably for the same reason the Γ_Y coefficients for these buildings are higher than in if compared with the other models. In fact Γ coefficient is linked to the vertical deformed shape of a buildings (see Section C.1 in Appendix C), and it assumes higher values when the vertical deformed shape is far from the story mechanism (as in the "C" models). However, unlike what happens with e^*, it is more difficult to link the Γ coefficient with the mode shapes when the diaphragms are not rigid. Furthermore it has not a numerical limit (as e^* that cannot be higher than 1) and it may be both less or greater than 1. In Fig. 5.21 is shown that Γ is approximately equal to 1 when a soft story mechanism at ground story develops. However, as it is shown in Figs. 5.25, 5.26 and 5.27 it may be also less than 1. In particular in the presence of flexible diaphragms when the 1st *mode* LP is applied Γ coefficient is less than 1 (even significantly) also at the initial phase of the analysis. This is a not conservative behavior, in fact to compute the displacement of the equivalent SDOF model is necessary to divide the actual control displacement by Γ coefficient; therefore if $\Gamma < 1$ it means that the equivalent SDOF model has a higher displacement capacity than the original MDOF model. It is therefore worth reminding that in [ASC14] it is proposed to apply only one LP proportional to the 1st mode deformed shape.
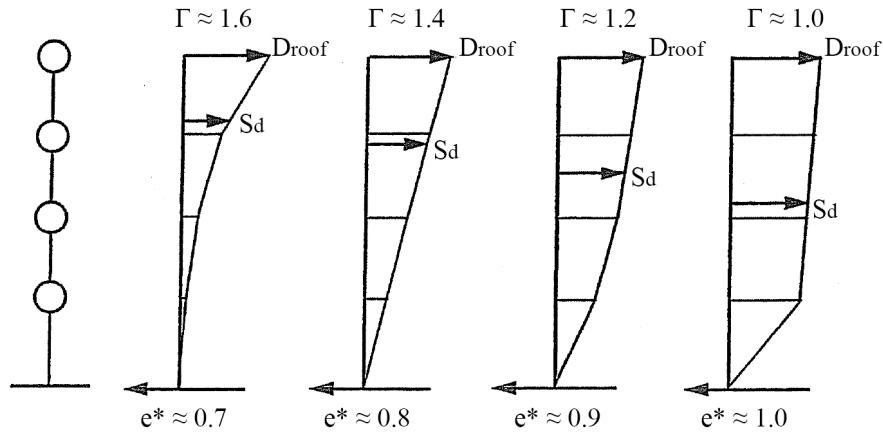
Figure 5.21: Example modal participation factors and modal participant masses (adapted from [ATC96])
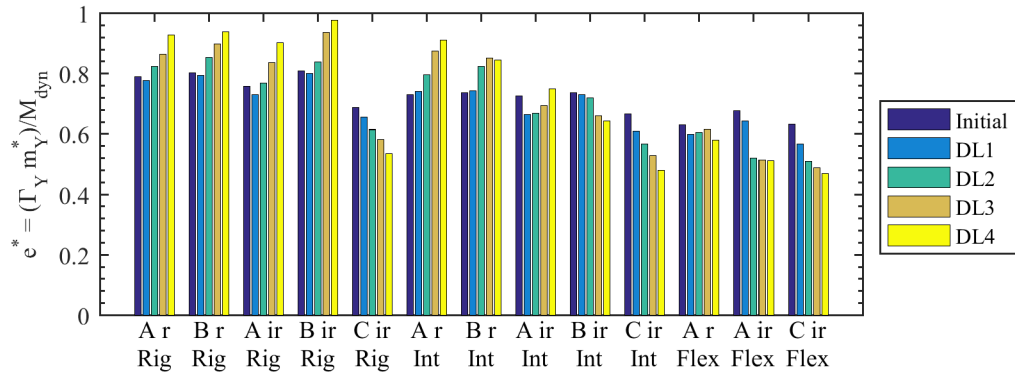
Figure 5.22: Uniform LP, e^* evolution.
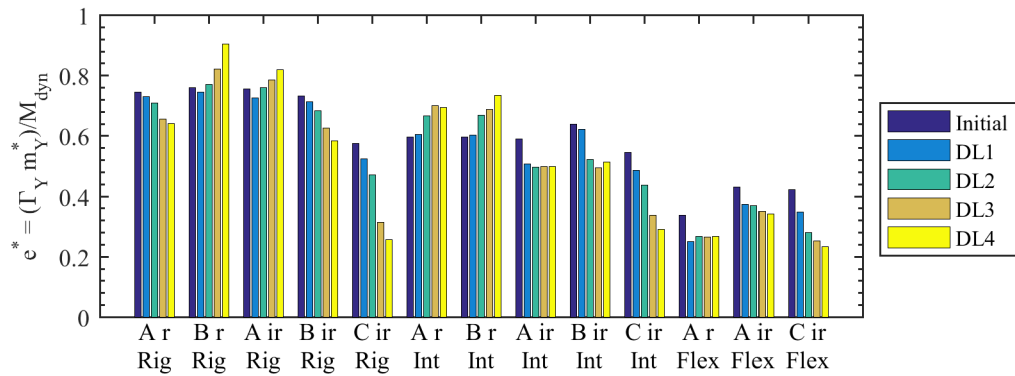
Figure 5.23: 1st *mode* LP, e^* evolution.
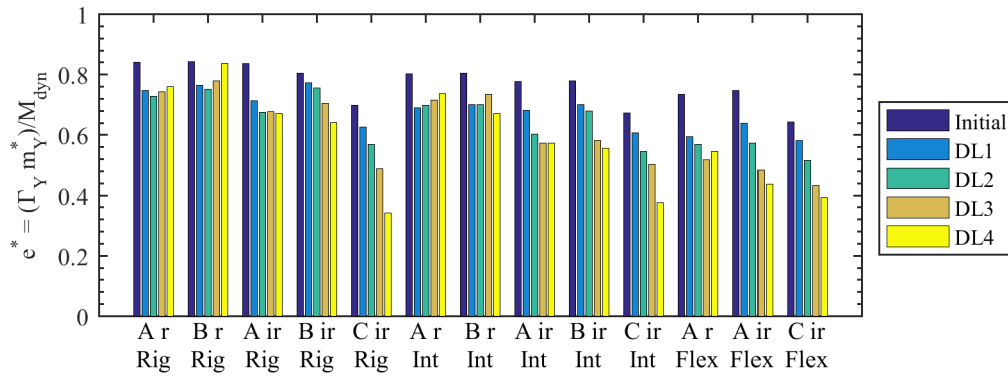
Figure 5.24: SRSS LP, e^* evolution (note for $A_{r,rig}$ and $B_{r,rig}$ the results refer to the triangular distribution).
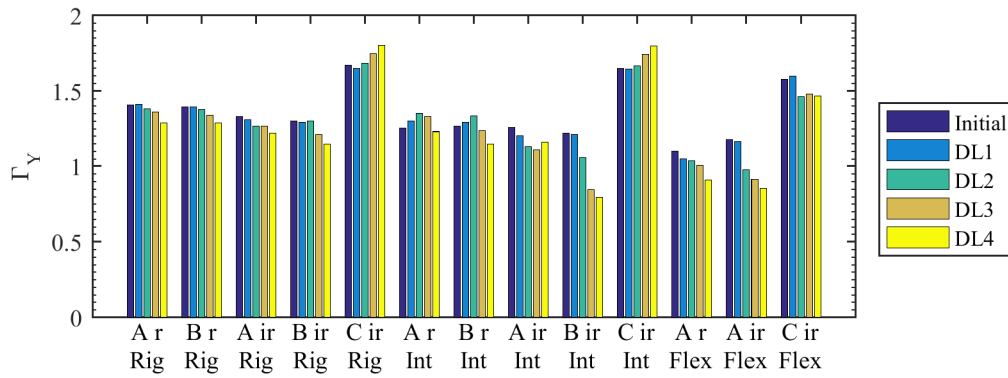
Figure 5.25: Uniform LP, Γ_Y evolution.
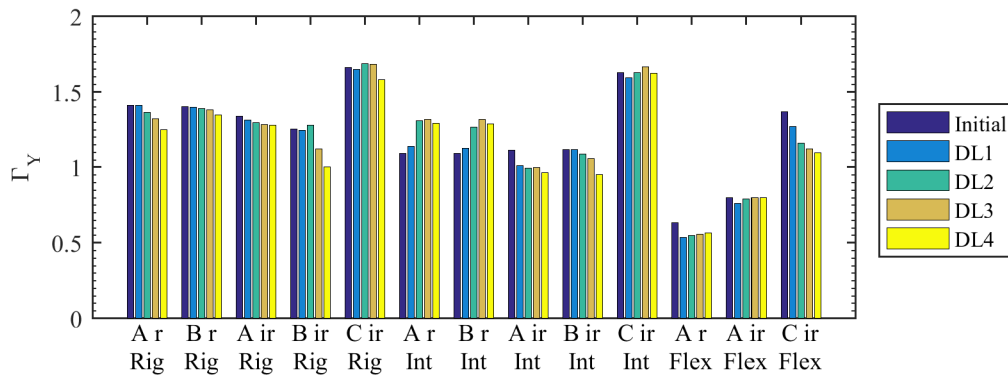
Figure 5.26: 1st *mode* LP, Γ_Y evolution.
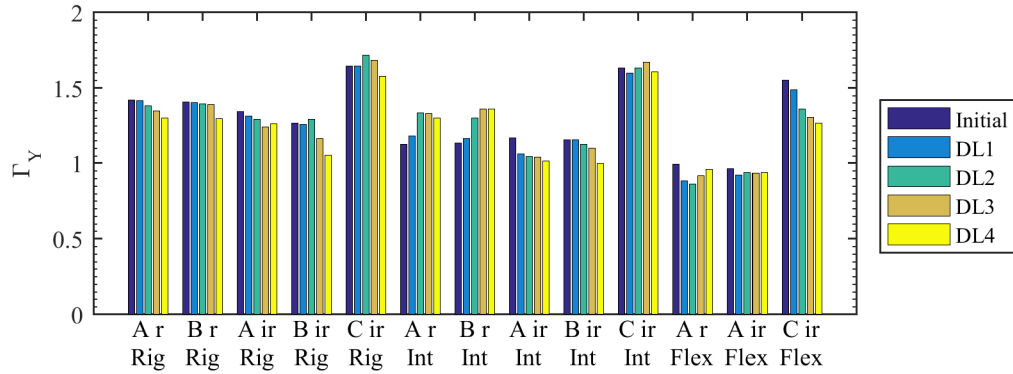
Figure 5.27: SRSS LP, Γ_Y evolution (note for $A_{r,rig}$ and $B_{r,rig}$ the results refer to the triangular distribution).

5.5 IDA-ISA curves comparison

In this section the comparison between the IDA and ISA curves (introduced in Section 4.3.1 and 4.2.5 respectively) is discussed.

It is worth highlighting that since IDA curves derive from nonlinear dynamic analyses, they consider the model's seismic response in the positive and negative direction. On the contrary when a NSP is conducted, the LP is monotonically increased either in the positive or negative direction. As a consequence, in order to draw an ISA curve, for each control displacement value considered, the minimum IM between the positive and negative direction was considered. It is worth reminding that in NSPs the displacements are monitored and subsequently the acceleration that caused it is computed; on the contrary for NDPs the input is a time-history accelerogram with its own PGA and subsequently the maximum displacement attained during the analysis is considered as the corresponding control displacement (Fig. 5.28).

For each LP several ISA curves were developed, one for each of the procedures discussed in Chapter 4. Both IDA and ISA curves show on the X-axis the control displacement (as defined in Section 3.1) and on the Y-axis the corresponding intensity measure. In the graphs presented in this section, the IM is reported in terms of PGA because it is more intuitive to understand than the $S_a(T_1)$. Thanks to the IDA-ISA curves comparison it is possible to understand if possible differences between the $IM_{PL,st}$ and $IM_{PL,dyn}$ derive from the procedure adopted to compute the IM (that

139
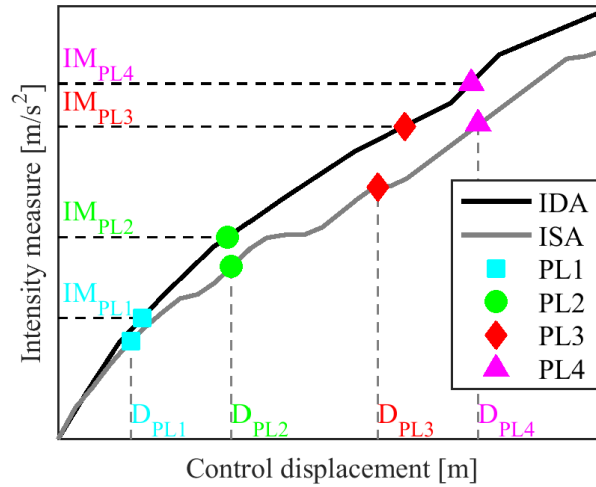
Figure 5.28: Example of a comparison of IDA-ISA curves. The horizontal and vertical lines indicate the attainment of four PLs in the IDA curves (defined in terms of Intensity Measure - IM_{PL}) and in the ISA curves (defined in terms of displacement - D_{PL}), respectively.

influences the shape of ISA curve) or if it is more important the evaluation of the displacement corresponding to the PLs. It is worth pointing out that starting from this section it is preferred to refer to performance levels rather than damage levels because the capacity is now compared with the demand.

The IDA-ISA curves are represented also in a normalized space, i.e. the ductility and the ratio IM/a_y^* are represented on the X and Y-axis respectively. The meaning of a_y^* is explained in Section 4.1.1, and the ductility is computed dividing the actual control displacement (see X-axis of Fig. 5.29a) by D_y^* (more information in Section 4.1.1). An example of an IDA-ISA comparison in this "normalized" space is depicted in Fig. 5.29b, where the results for $A_{irr,rig}$ model subjected to the SRSS LP are reported. Therefore Fig. 5.29a and 5.29b show the same results in two different spaces. The four vertical dashed lines indicate the displacements corresponding to the four PLs considered that were evaluated applying the NSP; the four horizontal dashed lines indicate the IM that caused the attainment of the PLs considered with the NDP. In Fig. 5.29a the position of PL3 is highlighted and it is possible to observe that a (single) displacement

value implicates very different values of IM (shown with different colors for the different procedures studied, the legend is reported in Fig. 5.31). This is even more evident for PL4, in fact the intersection between the vertical dashed line that indicates the position of PL4 with the red ISA that represent the N2 method is not included in the graph. In this case the IM computed with the "N2 adaptive" and the *new procedure* proposed provide the same results and they therefore coincide. In these figures some characteristics that are recurrent for almost all the models and all LPs are present: a) the CSM is the most conservative static procedure and the ISA curves obtained with this method are in almost all the cases below the IDA curves, there are few exceptions that will be outlined shortly; b) the N2 method provides unsafe results in almost all cases, especially for the higher PLs, in fact up to PL2 there are no significant differences between the different procedures adopted, but this is not the case for PL3 and PL4; c) the CM, the N2 "adaptive" and the *new procedure* proposed usually are located between the N2 method and CSM.

Fig. 5.29a shows also another issue: the NSP, in order to provide conservative results, should provide an ISA curve close as much as possible to the IDA curve, but also a close prediction of PL position. In fact it is possible to observe that the blue curve (that indicates the *new procedure*) matches well the IDA curve (in black), however the IM_{st} computed is slightly bigger than IM_{dyn}. This is because with the NDP the displacement evaluated corresponding to PL3 is (slightly) smaller than that computer with the NSP.

A reverse situation is depicted in Fig. 5.30. In Fig. 5.30a the ISA curves were derived by the application of the uniform LP, whereas in Fig. 5.30b the triangular LP was applied. They both refer to $B_{r,rig}$ model. When the uniform LP is applied the CM overestimates the dynamic response that is well matched by the *new procedure*; on the contrary, when the triangular LP is applied the best match with the IDA curve is given by the CM. In both cases, with respect to PL3 and PL4 the ISA curves (with the exception of the CSM, in green) exceed the IDA (with very different responses and also in this case both N2 and N2 "adaptive" methods provide the most unsafe results). However, when the uniform LP is applied, PL3 and PL4 are reached for very smaller displacements if compared with the dynamic, as a consequence the NSP still provides conservative results.

(a) Actual control displacement (X-axis) and IM (Y-axis)

(b) IDA-ISA curves in the normalized space
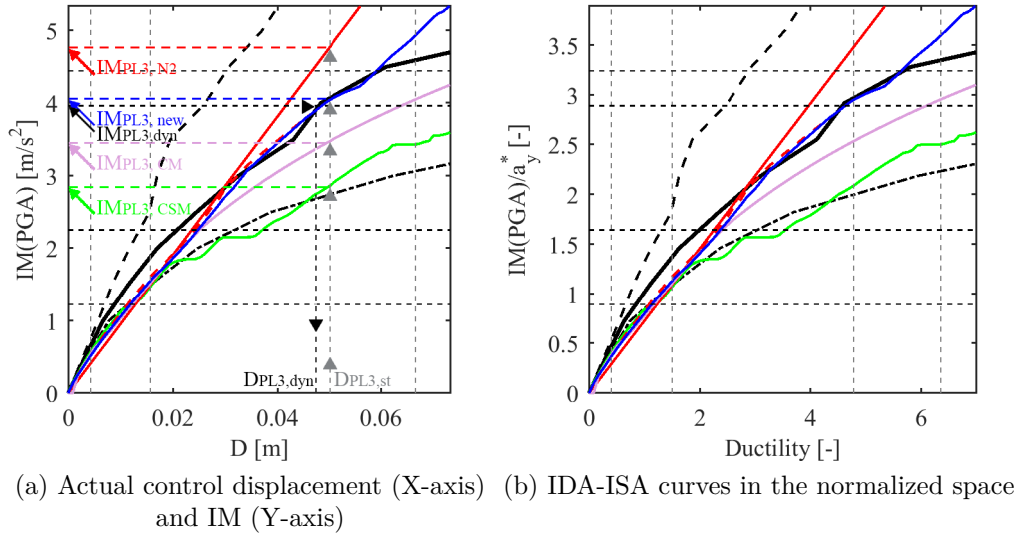
Figure 5.29: $A_{irr,rig}$ model, SRSS LP, IDA-ISA curves comparison (the legend is reported in Fig. 5.31).

It should be noted that $B_{r,rig}$ model is regular both in plan and in elevation and has rigid diaphragms, therefore the requirements needed to apply the NSP as currently proposed in the European codes are fulfilled, however applying the N2 method the inelastic seismic displacement demand is underestimated.

The unsuitability of N2 method for the seismic assessment of this type of buildings is attributed to: a) the equation itself of the method (Eq. 4.18) that does not consider strength reduction and b) the evolution of damping caused by the damage increase for higher seismic demands. On the contrary, each building under analysis is represented by an equivalent bilinear system that has a constant period T^*, therefore the IM increases linearly with the displacement demand. This issue is even more evident in the *equal displacement rule* range. In N2 method, the *equal displacement rule* is applied when T^* overcome T_C, but in presence of soils with good mechanical properties T_C is small and therefore the *equal displacement rule* may be applied also for URM buildings. The use of an equivalent bilinear with a constant period T^* presents another drawback, i.e. in presence of flexible diaphragms T^* may be high and therefore the N2 method may results over conservative (Fig. 5.31).

(a) Uniform LP (b) Triangular LP
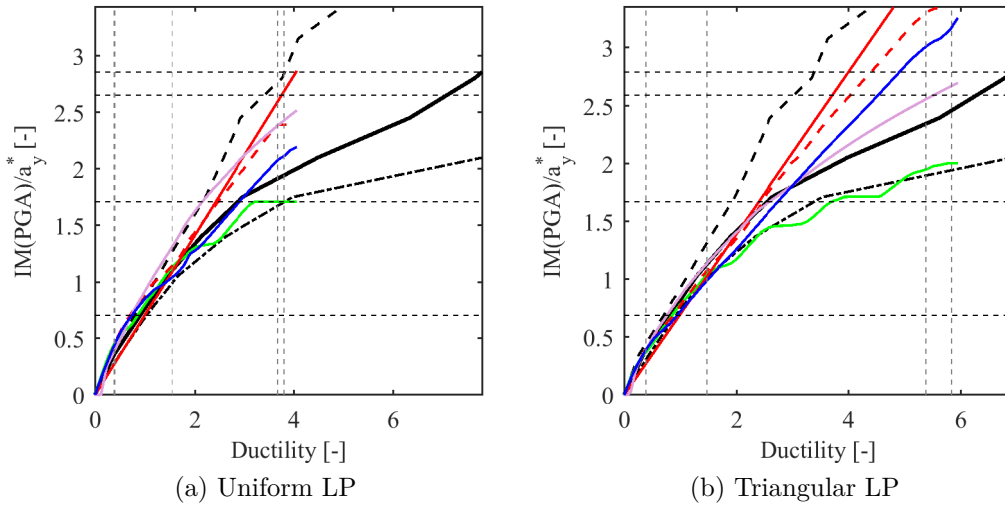
Figure 5.30: $B_{r,rig}$ model, IDA-ISA curves comparison (the legend is reported in Fig. 5.31).

(a)
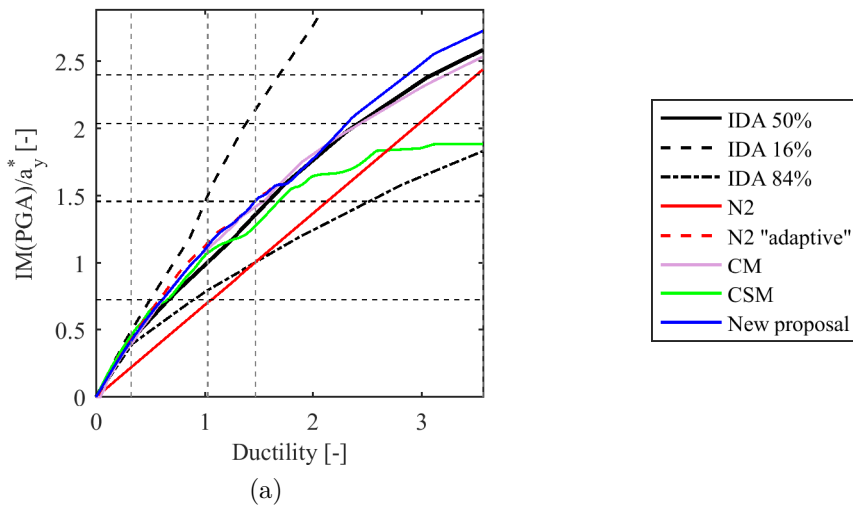
Figure 5.31: $A_{irr,flex}$ model, SRSS LP, the ISA curve computed with N2 method underestimates the dynamic response.

These drawbacks are present because the N2 method was conceived and developed for the seismic design of RC buildings that it is expected they reach the target displacement for a lower ductility if compared with existing URM buildings. In fact, existing URM buildings may develop high ductilities, and for all the models analyzed the ISA curve derived by the N2 method distanced the IDA curve for ductilities comprised between 2 and 3 (and in same cases also for ductilities minor than 2).

Fig. 5.32 shows the IDA-ISA curves comparison for $C_{irr,rig}$ model. As anticipated, it is possible to observe that for buildings with elevation irregularity the uniform LP does not provide conservative results, indeed, regardless the procedure adopted to compute the inelastic displacement demand, all ISA curves are far from IDA curve. The triangular and SRSS LPs improve the NSP prediction, however only the CSM provides conservative results, the other ISA curves are still far from the IDA curve. Therefore it was thought that, for this building typology, the main issue was not in the procedure adopted to compute the inelastic displacement demand, but that the LPs applied were not able to detect the most vulnerable part of the building (i.e. the story where the elevation irregularity is located). Therefore the $SRSS^+$ LP was applied (see Section 3.1.1) and the results are reported in Fig. 5.32d. It is possible to observe that applying the $SRSS^+$ LP together with CM or with the *new proposal* to compute the inelastic displacement demand, the ISA curves are now close to the IDA and therefore the NSP provides more reliable results.

With regard to CQC LP, it was possible to observe that ISA curves computed with the application of this LP were often similar to those derived with the application of SRSS LP. Therefore the major complexity in the calculation of CQC LP did not provide an increase of response prediction.

5.6 Comparison in terms of IM

In the previous section it was shown that in a NSP, each displacement value corresponds to the attainment of an IM, vice versa when a NDP is conducted. In this section, for the four PLs studied in the present research, the IM computed with the NSP ($IM_{PL,st}$) is compared with the IM computed with the NDP ($IM_{PL,dyn}$). In particular, for each model and each PL the ratio $IM_{PL,st}/IM_{PL,dyn}$ is computed and the results are presented in

(a) Uniform LP

(b) Triangular LP

(c) SRSS LP

(d) $SRSS^+$ LP
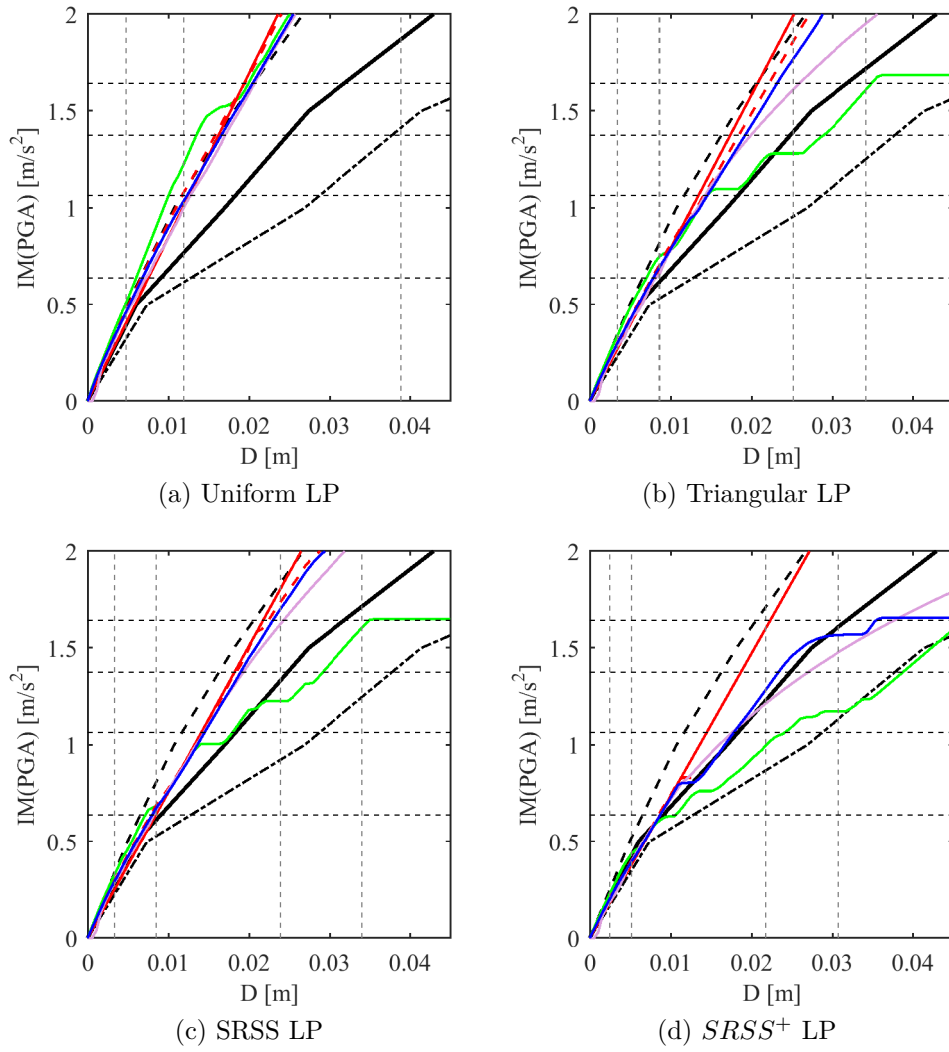
Figure 5.32: $C_{irr,rig}$ model, IDA-ISA comparison for different LPs applied (the legend is reported in Fig. 5.31).

diagrams as shown in Fig. 5.33. If the ratio $IM_{PL,st}/IM_{PL,dyn}$ is less than 1 it means that with the static procedure it was computed that a PL was reached for an IM value smaller than what was computed with the dynamic analysis, and therefore the static procedure was assumed as *conservative*. The opposite if $IM_{PL,st}/IM_{PL,dyn} > 1$, and this "unsafe" region is marked in light red. On the X-axis of these diagrams all the models analyzed are reported with the symbols defined in Chapter 2 and the main properties are summarized in Table A.1 presented in Appendix A.
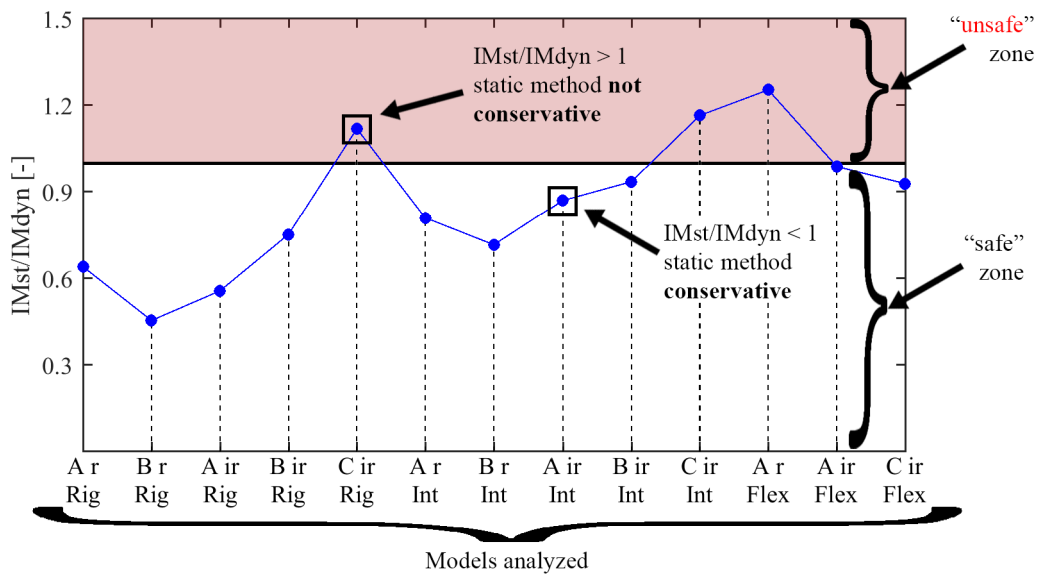
Figure 5.33: Example of an IM_{st}/IM_{dyn} ratio diagram, each of them refers to a given PL.

For each model and each PL one value of $IM_{PL,dyn}$ was computed following the procedure outlined in Section 4.3. These "exact" values are reported on the top of diagrams in Fig. 5.34 and Fig. 5.35 for PL2 and PL3 respectively. In the next subsections the effect of: 1) load patterns (Section 5.6.1); 2) performance level definition (Section 5.6.2) and 3) inelastic displacement demand evaluation together with the pushover into capacity curve transformation (Section 5.6.3) are discussed.

5.6.1 LPs effect

In this section the effect of applying different LPs in the IM computation is discussed. In Fig. 5.34 and Fig. 5.35 the results for PL2 and PL3 respectively are reported. The IMs were computed with both the PL definition and the inelastic displacement demand procedure proposed in [EC804] and [NTC08] that are reported below each figure for clarity. PL1 and PL4 are not discussed in this section because limits to define them quantitatively are not set in [EC804] and [NTC08]. They will be discussed in Section 5.6.3.

It is possible to observe that for both PLs there is not a single LP that provides always conservative results. As a consequence, the provision of [ASC14] to use only one LP (and in particular the LP proportional to the 1st mode shape) is not conservative. This finding confirms what is stated in [LC15a]: "usually codes propose to assume at least two LPs, because the inertial force distribution changes, with the occurrence of damage, from an initial *modal* distribution to patterns that are proportional to the deformed shape, which at collapse is closer to the *uniform* one".

It should be noted that in [ASC14] the PL and the displacement demand are defined differently. However, the results, in terms of IM, deriving applying the whole procedure present in [ASC14] are not conservative for all the buildings analyzed (as discussed in Chapter 7 and shown in Fig. 6.1). Furthermore, although for the majority of the case study buildings the procedure presented in [ASC14] provides conservative results, this is due to the combination of a not conservative LP applied together with an overly conservative procedure for the PL definition. Therefore in many cases the whole procedure is conservative, but it is formed by a sum of not convincing substeps. On the contrary, a solid procedure should consist of properly arranged steps for the building typology under analysis. In fact, it is worth reminding that all findings of this research are applicable only for URM buildings that are formed by elements (piers and spandrels) with their specific mechanical behavior that is significantly different from the behavior of columns and beams in RC or steel buildings.

For PL2 to consider the minimum IM of two different LPs (i.e. the minimum between the uniform and the triangular LP or the minimum between the uniform and SRSS LP) for the majority of the cases provides conservative results. For PL3 the seismic performance predicted using a

NSP is far inferior to that from the NDP regardless of the LP applied. As a consequence the issues of the method are not only in the LP definition.
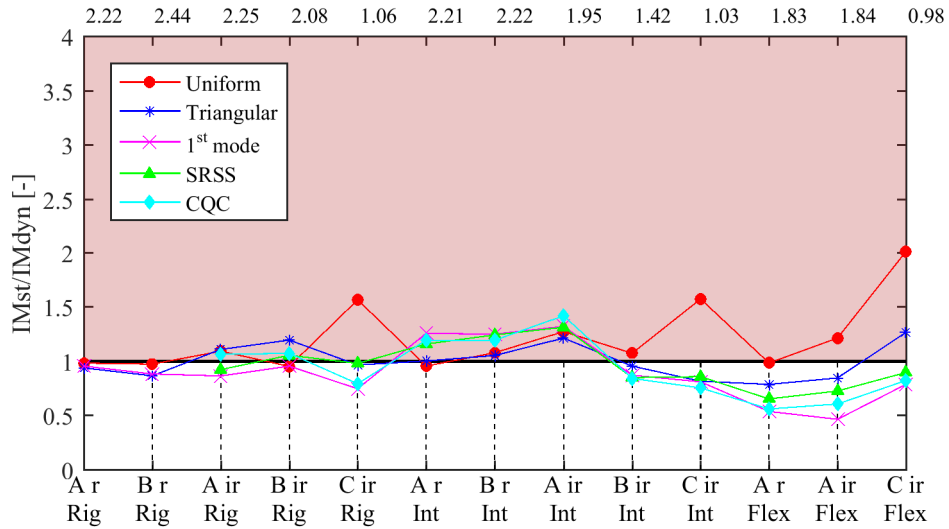
Figure 5.34: PL2 IM_{st}/IM_{dyn} ratio, effect of LPs. PL reached for an interstory drift of 0.3%, displacement demand computed with the N2 method. Above the $IM_{PL,dyn}$ (in m/s^2) that caused the PL attainment.
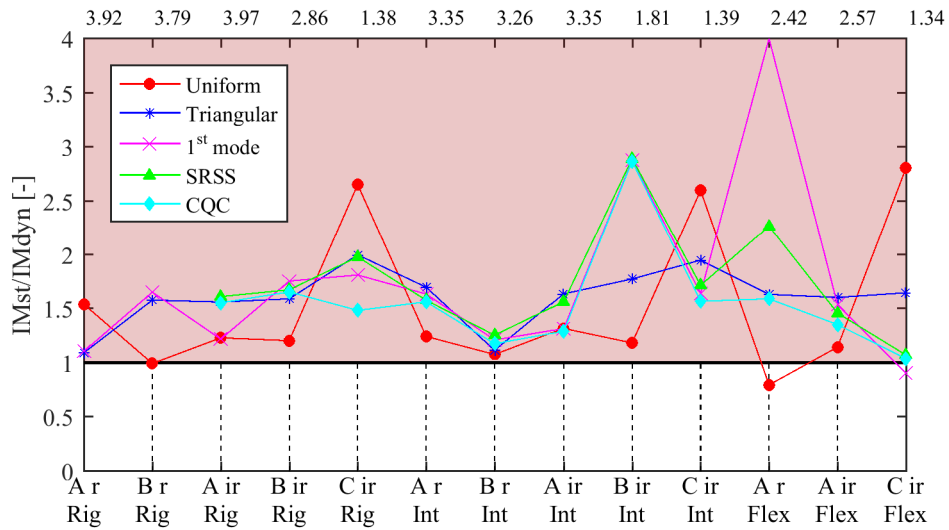
Figure 5.35: PL3 IM_{st}/IM_{dyn} ratio, effect of LPs. PL reached for a base shear reduction of 20%, displacement demand computed with the N2 method. Above the $IM_{PL,dyn}$ (in m/s^2) that caused the PL attainment.

5.6.2 PLs definition effect

In this section the effect of the procedure used in the definition of performance levels is discussed. Figs. 5.36 and 5.37 show the results for PL2, whereas Figs. 5.38 and 5.39 show the results for PL3. For both PL2 and PL3 first it is shown the diagram reporting the minimum IM between the *uniform* and *triangular* LPs, secondly the diagram reporting the minimum IM between the uniform and *SRSS* LPs. Since the *SRSS* LP was not applied for $A_{r,rig}$ and $B_{r,rig}$, in Figs. 5.37, 5.39 the IM values were set equal to one.

For PL2 the procedure proposed in [EC804] and [NTC08] does not provide conservative results for all the case study buildings, as the multiscale approach does. For some models the multiscale approach also turned out to be very conservative, however, it should be noted that in the dynamic results, the macroelement scale was monitored using the interstory drift, whereas the DLmin criterion was used for NSP and it was observed (Section 5.3.5) a rather significant difference in the prediction of PL2 using the two approaches.

For PL3 there is not a criterion that provides conservative results for all the case study buildings. To use the multiscale approach improves the prediction if compared with the procedure proposed in the European codes (Fig. 5.38) and to use the SRSS LP helps in improving the response (in particular for the models with elevation irregularity, as shown in Fig. 5.39). Both procedures adopted to be consistent with what is proposed in [ASC14] show some issues. In fact for many case study models they both provide very conservative results but still for two models with elevation irregularity the dynamic response is overestimated.

5.6.3 Effect of the approach adopted to estimate the nonlinear displacement demand

In this section the effect in considering different procedures to compute the inelastic displacement demand is discussed. These procedures are detailed from Section 4.2.1 to 4.2.4. Figs. 5.40, 5.41, 5.42, 5.43 show the results for PL1, 2, 3, and 4 respectively. In all these figures the IM values are computed considering: the minimum between the uniform and SRSS LP
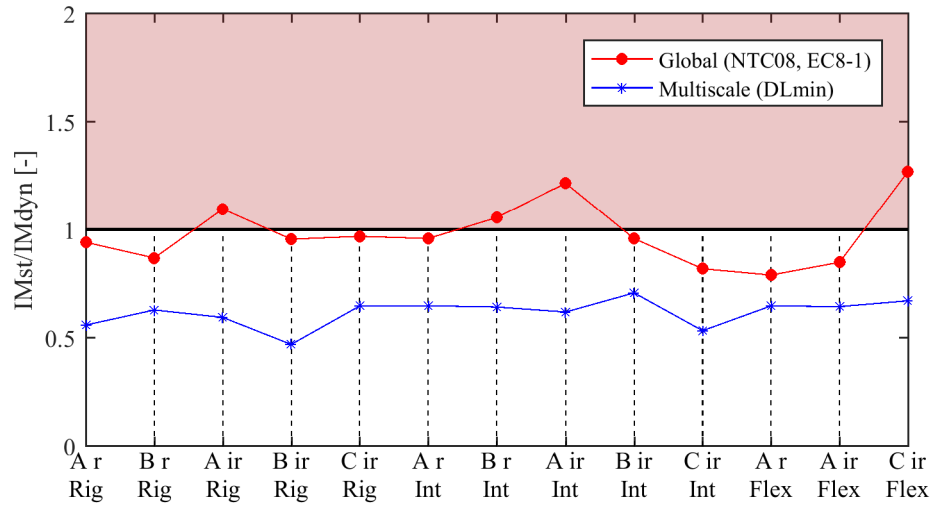
Figure 5.36: PL2 IM_{st}/IM_{dyn} ratio, minimum between uniform and triangular LPs, effect of PLs definition.
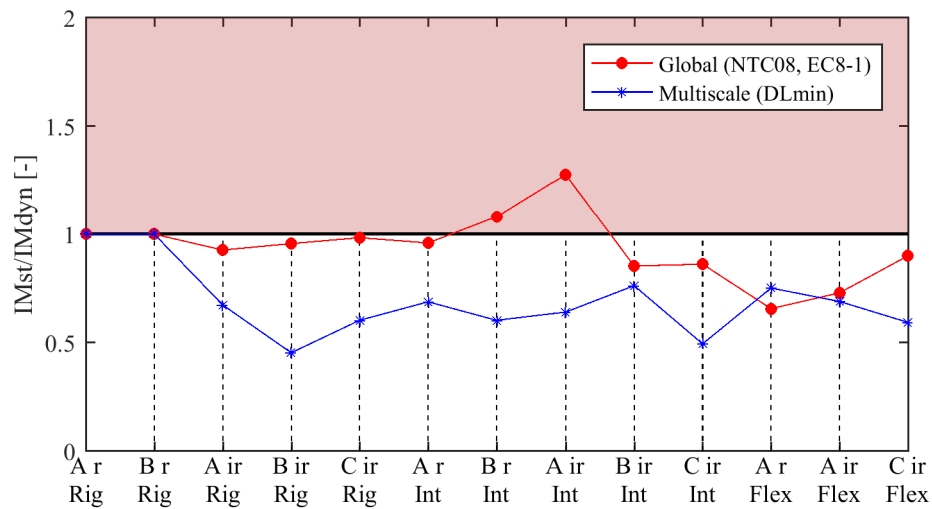
Figure 5.37: PL2 IM_{st}/IM_{dyn} ratio, minimum between uniform and SRSS LPs, effect of PLs definition.

and the PLs are computed using the multiscale approach with the DLmin check at macroelement scale.

For both PL1 and PL2 it is possible to observe that the different procedures do not provide significantly different outcomes. However it is worth pointing out that for PL1 the N2 method as adopted in [EC804] and
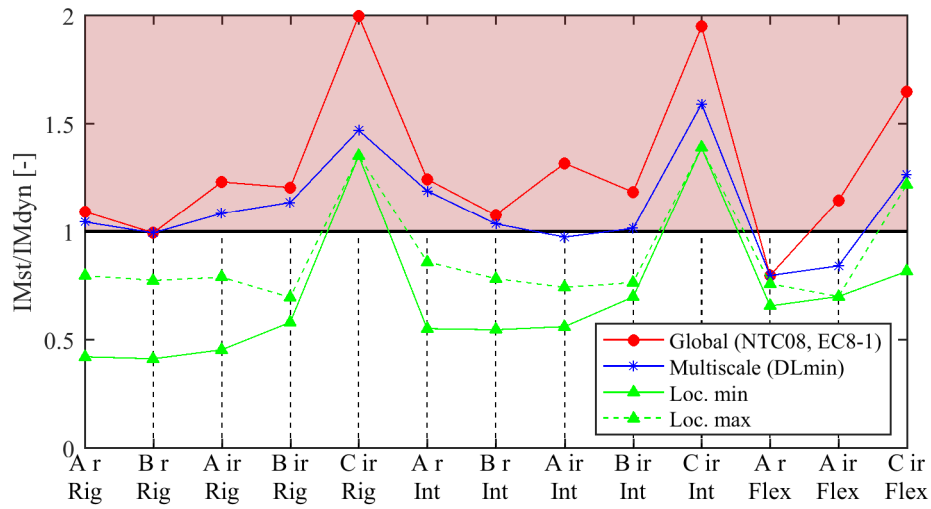
Figure 5.38: PL3 IM_{st}/IM_{dyn} ratio, minimum between uniform and triangular LPs, effect of PLs definition.
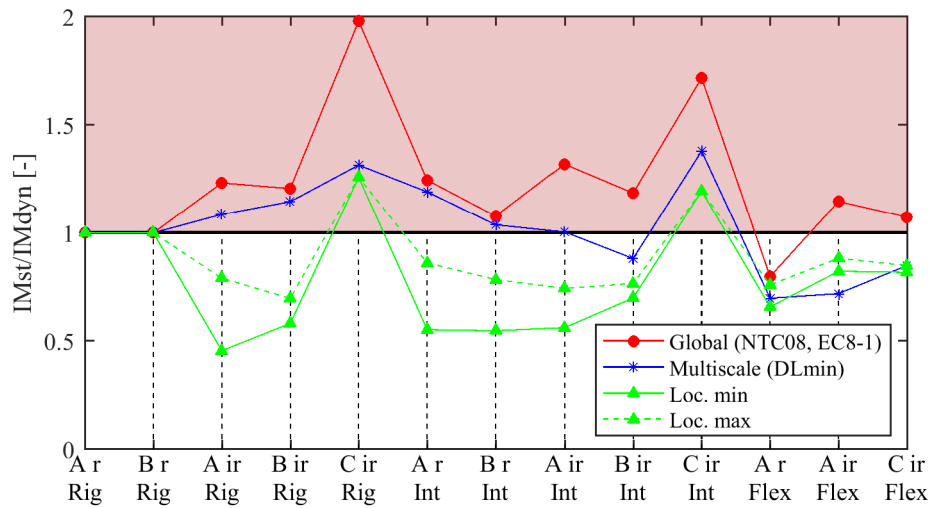
Figure 5.39: PL3 IM_{st}/IM_{dyn} ratio, minimum between uniform and SRSS LPs, effect of PLs definition.

[NTC08] is, for all the case study buildings, the most conservative, being in some cases over-conservative since it provides a static response lower than 0.4 the dynamic. This issue was already detected when IDA-ISA curves were compared (see Figs. 5.29, 5.31). In fact, to use a single equivalent bilinear system regardless of the PL considered leads to overestimating the

demand for the PL corresponding to an elastic behavior and to underestimating it when the building behavior is strongly nonlinear. For the same reason this issue is less significant for PL2 (intermediate situation between an elastic and a strongly elastic performance).
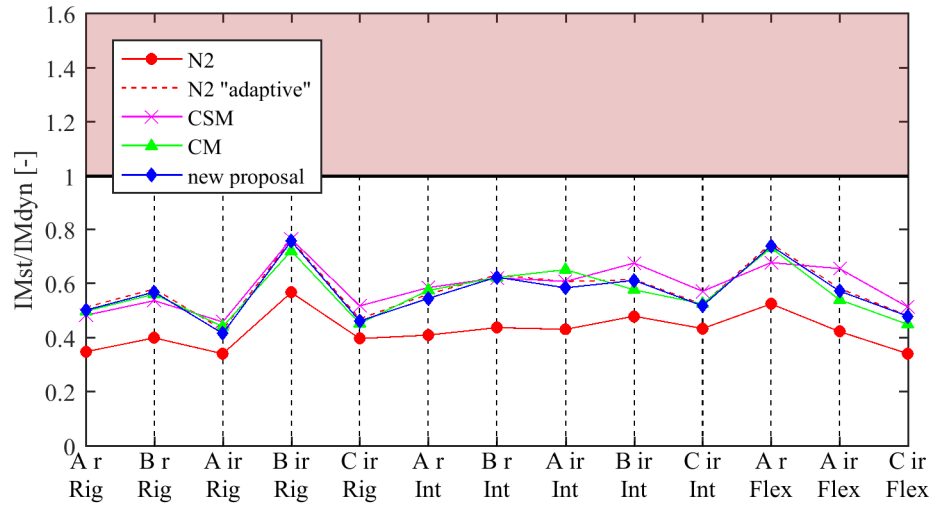
Figure 5.40: PL1 IM_{st}/IM_{dyn} ratio, minimum between uniform and SRSS LPs, PLs evaluated with the multiscale approach.
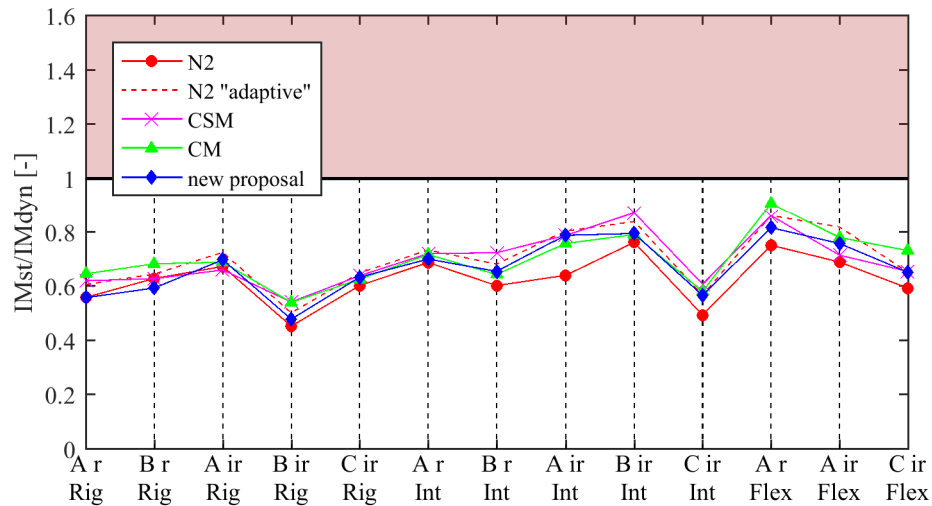
Figure 5.41: PL2 IM_{st}/IM_{dyn} ratio, minimum between uniform and SRSS LPs, PLs evaluated with the multiscale approach.

For PL3 and PL4 the differences between the methods used are significant, however the methods show a similar trend for both PLs. The CSM is, for all models, the most conservative procedure and it always provides IM values smaller than the dynamic ones. On the contrary, the N2 method as currently adopted in [EC804] and [NTC08] is the procedure that most overestimates the dynamic response. Updating the equivalent bilinear as discussed in Section 4.2.2 the static prediction moves closer to the dynamic (see Figs. 5.42 and 5.43). The CM and the *new procedure* discussed in Section 4.2.2 provide similar results, but the latter is preferable because: 1) it is slighter more conservative and for some models this conducts to results in the "safe" zone; 2) it is simpler to use. However, as already discussed in Section 4.2.2, this *new procedure* needs a wider statistical validation.
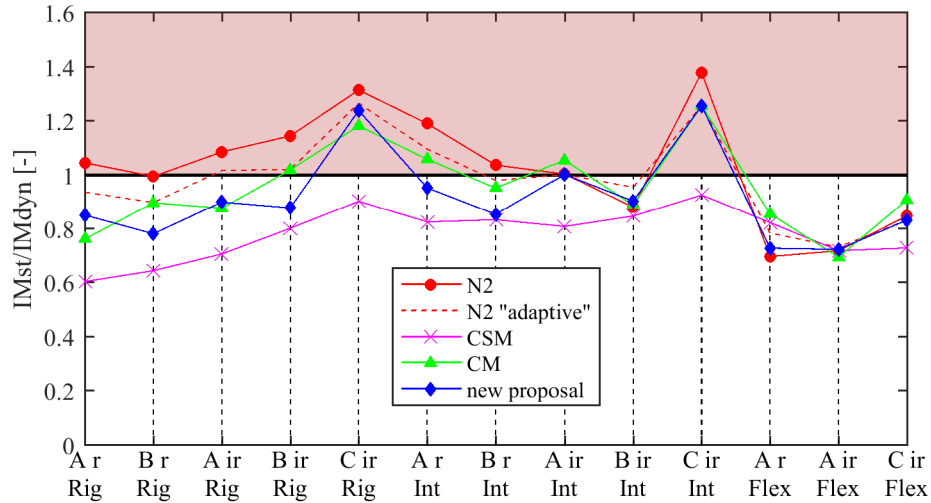
Figure 5.42: PL3 IM_{st}/IM_{dyn} ratio, minimum between uniform and SRSS LPs, PLs evaluated with the multiscale approach.

For two models with elevation irregularity ("C" models) also the *new procedure* is not enough in providing conservative results. Therefore, it was thought to apply the $SRSS^+$ LP, because, as discussed in Sections 3.1.1 and 5.2 both the uniform and the SRSS LPs were not able to detect the actual (dynamic) damage evolution. The results derived from the application of $SRSS^+$ LP to "C" models are depicted in Fig. 5.44. It is possible to observe that for both PL3 and PL4 for all the case study buildings, applying the *new procedure* discussed in Section 4.2.2, the static method provides
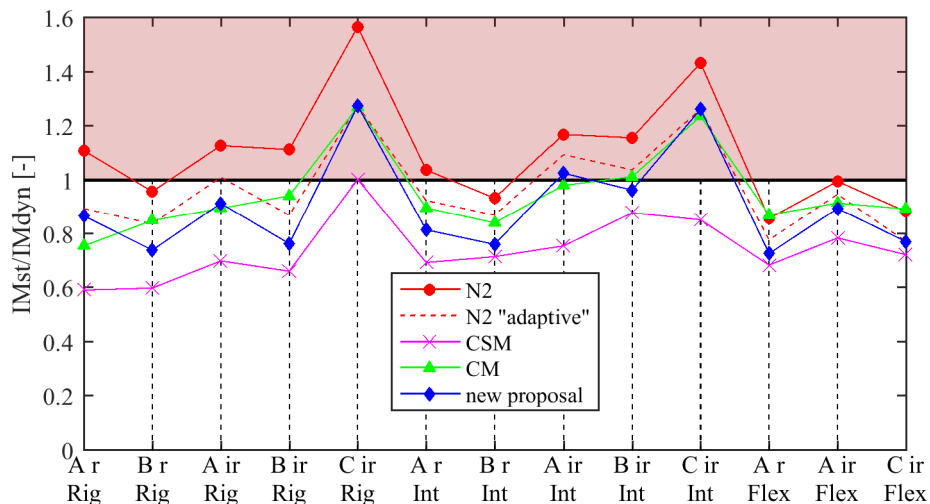
Figure 5.43: PL4 IM_{st}/IM_{dyn} ratio, minimum between uniform and SRSS LPs, PLs evaluated with the multiscale approach.

conservative results (only for two cases the static result overestimates the dynamic, however very slightly).
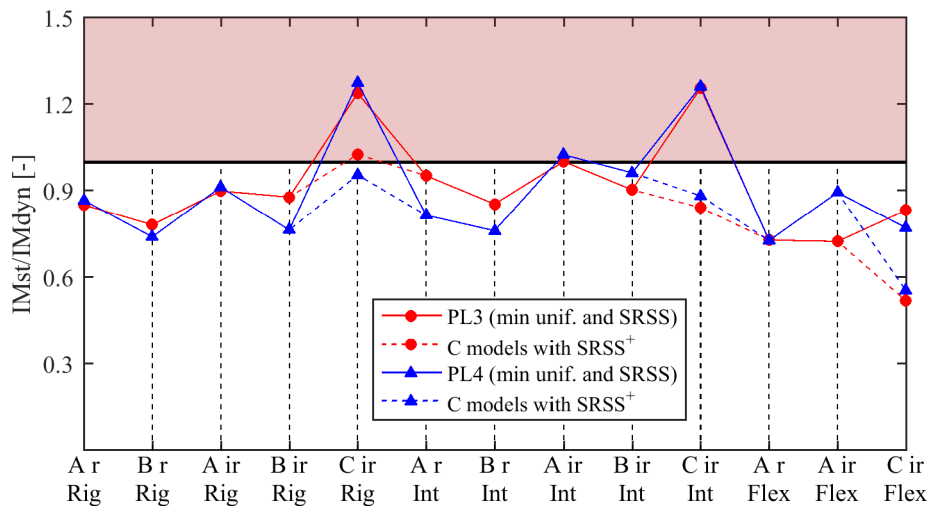
Figure 5.44: Effect of $SRSS^+$ LP when applied to models with elevation irregularity. IM computed with the multiscale approach and the *new procedure* was used to compute the displacement demand.

5.7 Summary of the main results

The main results derived from the nonlinear analyses are summarized in Chapter 6. They are subdivided in the three steps of a NSP that were considered as the most critical in the present thesis: 1) the load patterns (LPs) to apply; 2) the performance levels (PLs) definition; 3) the nonlinear displacement demand and the consequent IM evaluation.

Chapter 6

Summary of the nonlinear static procedure proposed

The comparison of the results derived by the application of NSP and NDP to the case study buildings, presented in Chapter 5, allowed to choose the best options for each of the steps which form the NSP and that were studied in the present research.

Thanks to this comparison, the main limitations of NSPs adopted by current codes were outlined and from those refinements were proposed. These limitations are clearly shown in Fig. 6.1 (in Section 6.4): applying the NSP proposed in Italian and European codes ([NTC08] and [EC804]) the results are not conservative if compared with those deriving from NDP. Therefore refinements were needed. These refinements did not have the aim to turn upside-down the current NSPs, but to develop a NSP which takes into account also the particular features that are often present in existing URM buildings: flexible diaphragm, in plan and elevation irregularities, strong nonlinear behavior of the structural elements and significant strength degradation when they are subjected to seismic actions. In fact, the NSP adopted by current codes was conceived and developed for the seismic design of regular RC buildings, whereas a systematic validation of the procedure for existing URM buildings still lacks in the literature.

Three steps of a NSP were considered as the most critical in the present thesis for this kind of buildings and the main outcomes are summarized in next sections: 1) the load patterns (LPs) to apply (Section 6.1); 2)

the performance levels (PLs) definition (Section 6.2); 3) the nonlinear displacement demand and the consequent IM evaluation (Section 6.3).

6.1 Load patterns

With regard to the load patterns, from the comparison with nonlinear dynamic analyses, the most reliable choice was found to be the use of the uniform distribution combined with another load pattern representative of the dynamic behavior of the structure in the initial phase. In fact, it was possible to observe that there is not a single LP that is able to predict correctly the dynamic behavior for all the models analyzed. As a consequence, the prescription present in [ASC14] to use only one LP (and in particular the LP proportional to the 1st *mode* shape) is not conservative. Herein the main features of each LP are summarized.

1. The *uniform* LP showed different pushover curves and distribution of damage in comparison with the other LPs. Therefore its use is encouraged, however it may provide very unsafe results when applied to buildings with elevation irregularities.

2. The *triangular* LP may be adopted as a proper secondary LP, however its use may lead to unreliable results in the presence of significant elevation irregularities, in particular when the deformed shape is far from linear.

3. The use of a LP proportional to 1st *mode* deformed shape is discouraged when not rigid diaphragms are present because:

   - it activates a small percentage of mass and it influences also the transformation coefficients, therefore the equivalent SDOF capacity curve may overestimate the building's actual strength;

   - walls that have their own period of vibration far from the 1st mode may receive very little forces, therefore the damage distribution is very different from a damage pattern that may be obtained with a dynamic analysis;

   - since same walls may receive little forces, the use of this LP is not compatible with a purely global PL definition, as currently

foreseen in European codes, because it leads to overestimation of the capacity.

4. The *SRSS* LP provided, for the case study buildings, more reliable results if compared with the triangular LP and above all with the LP proportional to the 1st mode. This is more evident when diaphragms are not rigid, therefore its use is suggested as secondary LP.

5. The *CQC* LP did not improve significantly the response given by SRSS LP, therefore its use is not suggested due to its complexity.

6. The $SRSS^+$ LP may help in presence of elevation irregularity;

It is therefore suggested to use at least two different LPs, in particular the *uniform* and the *SRSS* LP. In presence of elevation irregularities the *SRSS* LP may be substituted with the $SRSS^+$ LP.

6.2 Definition of PL position

Regarding the performance levels definition, it was noted that the main issue was related to the currently adopted criterion (in [NTC08] and [EC804]) that monitors only the global force-displacement curve. On the contrary, to relate the attainment of a PL with the damage of a single structural element (as in [ASC14]) may be overly conservative. Herein the main outcomes regarding the definition of PLs position are summarized.

1. For almost all configurations, the attainment of DL1 was conditioned by the minimum displacement defined at the global scale.

2. Italian and European codes do not always provide conservative results, whereas the multiscale approach improves the prediction. Using the DLmin criterion DL1 and DL2 are reached for displacements believed as more reliable than those computed by adopting the interstory drift criterion; in fact using the DLmin criterion it is not necessary to define thresholds as for the interstory drift criterion.

3. the multiscale approach provided reliable results and:

159

- no significant differences were noticed in using the drift or DLmin criteria at macroelement scale for PL3 and 4; instead, for PL2 the use of DLmin criterion showed that the interstory drift limit of 0.3% currently set is high.

- At macroelement scale the use of interstory drift check (as currently adopted in [NTC08] and [EC804]) is discouraged because existing URM buildings may present very different geometries of the walls, therefore it is difficult to set a threshold that is always suitable. It is hence suggested to substitute the interstory drift criterion with the DLmin criterion that has the same aim, i.e. to detect, if present, the trigger of a soft story mechanism.

- For the sake of simplicity in the engineering practice, the checks at local scale may be omitted because: a) existing URM buildings are very variable and it is hard to evaluate proper thresholds and, as said, to relate the attainment of a PL with the damage of a single structural element may result overly conservative; b) the application of the criterion may be rather time consuming.

4. If at least two different LPs are applied (as those suggested in Section 6.1), the static method provides conservative results. Small overestimation of the dynamic response was found for buildings with elevation irregularities.

It is therefore suggested to adopt a combined criterion based on checks at global (monitoring the pushover curve evolution) and macroelement (using DLmin check) scales. In this way it is possible to detect local developments of damage that may not significantly influence the global pushover curve.

6.3   Intensity measure

With regard to the evaluation of nonlinear displacement demand, from both the IDA-ISA curves comparison and the analysis of IM_{st}/IM_{dyn} it was possible to observe that:

1. the CSM is the most conservative method and for all the configurations analyzed provided conservative results. From the analysis of

the results the reason why the CSM is more conservative seems attributable to the use of the secant stiffness (rather than the equivalent elastic) that allows detecting buildings' strength reduction. Moreover, the CSM has the advantage that does not require the definition of an equivalent bilinear, but it needs the definition of an equivalent viscous damping - displacement relationship; this may be computed conducting cyclic pushover analyses, but they need the definition of cyclic force-displacement constitutive laws.

2. The CM provided a good prediction of the dynamic response however it has the disadvantage to be a rather complex and iterative procedure that requires the use of a series of coefficients whose interpretation is not straightforward. In fact "the coefficients are typically derived empirically from a series of nonlinear response-history analyses of oscillators with varying periods and strengths" [FEM05].

3. The N2 method, as adopted in [NTC08] and [EC804], is not suitable for this building typology, in fact it provides conservative results only for small ductility demands (i.e. for PL2 and in some cases for PL3). The reason was attributed to two main issues of the procedure:

   - the equation of the method is linear, therefore when the displacement demand increases the corresponding IM increases linearly and does not take into account effects derived from strength degradation and variation in damping that are due to the distribution of damage. In fact the displacement demand depends only on the period T^* of the equivalent bilinear that is constant throughout the analysis;

   - it adopts the *equal displacement rule* when the period T^* exceeds T_C, but in the presence of soils with good mechanical characteristics T_C may be small and therefore the *equal displacement rule* is applied also to URM buildings.

4. A refinement was proposed for the N2 method, i.e. to use an adaptive bilinear (the N2 "adaptive"), and with this procedure the IM evaluation improved, however it is still not accurate enough to predict correctly the dynamic response.

5. The new equation proposed to compute the IM (the results were labeled as *new proposal*) provides a good prediction of the dynamic response. The prediction is more accurate than that of the CM and it has the further advantage to be simpler to apply and therefore more suitable for practical use. However this equation (see Eq. 4.30) and the coefficient *b* related to the dissipative capacity and strength degradation (see Eq. 4.31) need to be validated through a more extensive numerical application.

6.4 Comparison of the new procedure with those adopted by current codes

Finally, in Fig. 6.1 the results derived by the application of the procedures currently proposed in [NTC08], [EC804] and [ASC14] are compared with the new proposal developed in the present research.
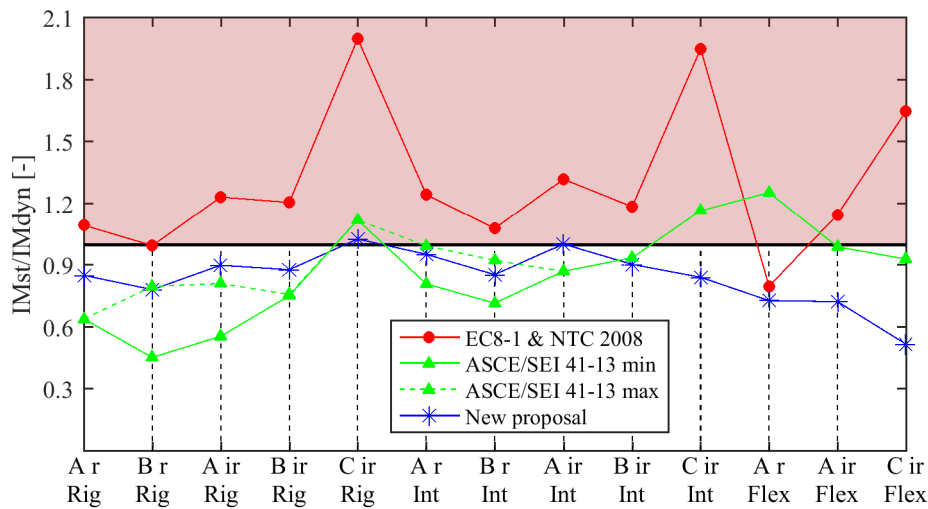
Figure 6.1: Comparison in terms of IM_{st}/IM_{dyn} ratio. The procedures currently adopted in European and American codes are compered with the new procedure proposed.

As already discussed, this new proposal is inserted in the framework of other NSPs already developed and tested for other building typologies. It consists in:

- the application of the uniform and SRSS LPs (in the presence of elevation irregularity use the $SRSS^+$ LP, Eq. 3.3), then the minimum value between the two LP is considered;

- the performance levels are defined using the multiscale approach with the DLmin criterion at macroelement scale (for the sake of simplicity the analysis according to local criterion may be neglected);

- evaluation of the nonlinear displacement demand using Eq. 4.30.

It should be noted that the procedures adopted by current codes lead to not conservative when applied to the building typology studied in the present research, whereas the improvements listed above allow the new procedure proposed to predict well the dynamic response of the studied buildings.

Chapter 7

Conclusions and further developments

The applicability of nonlinear static procedure for the seismic assessment of irregular URM buildings has been investigated by a systematic comparison with the results provided by nonlinear dynamic analyses, assumed as actual reference solution. The attention was focused only on the so called *global response* of URM buildings, i.e. based only on the in-plane response of URM walls. Therefore it was assumed that proper connections prevent the activation of local failure modes mainly associated with the out-of-plane response of walls.

The applicability of NSP also in the case of irregular masonry buildings is an important result for the engineering practice because, at present, a systematic validation of its reliability when applied to this type of buildings is still lacking in literature. Furthermore, the use of NDP for professional practice is still problematic, due to a number of reasons outlined in the present thesis. Therefore the choice to focus on the improvement of NSP rather than NDP derived by the aim to work on a practice-oriented procedure.

Several configurations have been considered, defined in order to be representative of existing URM buildings, starting from a regular building with rigid floors and introducing in plan and elevation irregularities and reducing the in-plane shear stiffness of the diaphragms.

It was possible to observe that the procedures proposed in the currently adopted European and Italian codes do not provide conservative results. The procedure proposed in [ASC14] was studied as well, but the results

obtained were rather inconclusive: for some models they resulted very conservative and for others not conservative. Moreover, often, the procedure provided conservative results as a combination of the application of a not appropriate LP with a very conservative definition of limit states. However, a robust procedure should be formed by different steps, each of them reliable.

The present research focused in particular on three steps of nonlinear static procedures that were considered as the most relevant for a proper prediction of the results: the load patterns to apply; the limit state definition and the evaluation of nonlinear displacement demand. The refinements to currently adopted procedures were outlined in Chapter 6 and it was possible to observe that the new procedure proposed predicts well the dynamic response of the studied buildings.

The application of the NSP to several case study models provided important results. However, the conclusions about the reliability of nonlinear static approach should be supported by the application to other irregular configurations. For example, buildings with a strong in-plan irregularity that for a given mode significant torsional effects are present should be studied. In [CNR14] a limit is set to define this type of buildings, i.e. when the ratio between the minimum and maximum participation factors is greater than 10%. For the models analyzed, this ratio was always smaller (see Table 2.7), and this allowed to conduct the analysis in only one direction.

In the new procedure proposed there are steps conducted in an original way that need a more extensive validation. Firstly, the $SRSS^+$ LP was proposed if a building presents an elevation irregularity. However, in the present research only three models presented this irregularity. Moreover for the model $C_{irr,flex}$ it provided rather conservative results. It should be noted that the new procedure proposed gave the most conservative results also for the other two models with very flexible diaphragms. This issue is part of the still open debate on whether in the presence of very flexible diaphragms it may be more appropriate to analyze each wall separately rather than the whole building. Secondly, due to practical issues it was not possible to apply the DLmin criterion in NDPs, its application in the dynamic analyses would be very interesting. Then a new equation was

166

proposed to compute the inelastic displacement demand (Eq. 4.30) that contains a coefficient related to the dissipative capacity and strength degradation of the system. A statistical calibration/validation of that coefficient is needed.

Finally, although the NSP is becoming more popular in the professional practice, the present research highlighted that its use may present issues when applied to irregular URM buildings. In fact, it was noticed that the presence of flexible diaphragms, structural irregularities (in plan and/or in elevation) and strength degradation require that engineers assume a certain number of choices that are not all adequately detailed in current codes. Therefore it is desirable that the new version of the codes provide more information on the issues outlined in the present thesis for the application of the NSP, it is in fact a complex task that should not be left to the choice of individuals.

Bibliography

[AKS15]   S.A. Anagnostopoulos, M.T. Kyrkos, and K.G. Stathopoulos. Earthquake induced torsion in buildings: critical review and state of the art. *Earthquakes and Structures, 8(2): 305-377,* 2015.

[AMM94]   A. Anthoine, G. Magonette, and G. Magenes. Shear-compression testing and analysis of brick masonry walls. In *Proceedings of the 10th European conference on earthquake engineering,* Wien, Austria, 1994.

[AÖ10]   M.N. Aydinoğlu and G. Önem. *Evaluation of analysis procedures for seismic assessment and retrofit design, pp. 171-198, in: Earthquake engineering in Europe.* A. Ansal and M. Garevski Eds., 2010.

[AP04a]   S. Antoniou and R. Pinho. Advantages and limitations of adaptive and non-adaptive force-based pushover procedures. *Journal of Earthquake Engineering, 8(4): 497-522,* 2004.

[AP04b]   S. Antoniou and R. Pinho. Development and verification of a displacement-based adaptive pushover procedure. *Journal of Earthquake Engineering, 8(5): 643-661,* 2004.

[ASC14]   *ASCE/SEI 41-13, Seismic Evaluation and Retrofit of Existing Buildings.* Reston, Virginia, 2014.

[ATC96]   *ATC-40, Seismic evaluation and retrofit of concrete buildings.* Redwood City, California, 1996.

169

[Bak15]   J.W. Baker. Efficient analytical fragility function fitting using dynamic structural analysis. *Earthquake Spectra, 31(1): 579-599*, 2015.

[Bey12]   Katrin Beyer. Peak and residual strengths of brick masonry spandrels. *Engineering Structures, 41: 533-547*, 2012.

[BM13]   K. Beyer and S. Mangalathu. Review of existing strength models for spandrels. *Bulletin of Earthquake Engineering, 11(2): 521-542*, 2013.

[BP05]   C.A. Blandon and M.J.N. Priestley. Equivalent viscous damping equations for direct displacement based design. *Journal of Earthquake Engineering, 9(Special Issue 2): 257-278*, 2005.

[BPP12]   A. Brignola, S. Pampanin, and S. Podestà. Experimental evaluation of the in-plane stiffness of timber diaphragms. *Earthquake Spectra, 28(4):1687-1909*, 2012.

[BTPP15]   K. Beyer, M. Tondelli, S. Petry, and S. Peloso. Dynamic testing of a four-storey building with reinforced concrete and unreinforced masonry walls: prediction, test results and data set. *Bulletin of Earthquake Engineering, 13(10): 3015-3064*, 2015.

[CAG+04]   C.D. Comartin, M. Aschheim, A. Guyader, R. Hamburger, R. Hanson, W. Holmes, W. Iwan, M. Mahoney, E. Miranda, J. Moehle, C. Rojahn, and J. Stewart. A summary of FEMA 440: improvements of nonlinear static seismic analysis procedures. In *Proceedings of the 13th world conference on earthquake engineering*, Vancouver, B.C., Canada, 2004.

[Cal99]   Gian Michele Calvi. A displacement-based approach for vulnerability evaluation of classes of buildings. *Journal of Earthquake Engineering, 3(3): 411-438*, 1999.

[CCD+14]   S. Cattari, A. Chioccariello, H. Degée, C. Doneux, S. Lagomarsino, and C. Mordant. Seismic assessment of masonry buildings from shaking table tests and nonlinear dynamic simulations by the proper orthogonal decomposition (POD). In

Proceedings of the Second European conference on Earthquake Engineering and Seismology, Istanbul, Turkey, 2014.

[CCDA⁺12] C. Calderini, S. Cattari, S. Degli Abbati, S. Lagomarsino, D. Ottonelli, and M. Rossi. Modelling strategies for seismic global response of building and local mechanisms. Technical report, PERPETUATE (EU-FP7 Research Project), Deliverable D26 (www.perpetuate.eu/D26/), 2012.

[CCL09a] C. Calderini, S. Cattari, and S. Lagomarsino. In plane seismic response of unreinforced masonry walls: comparison between detailed and equivalent frame models. In *Proceedings of the second COMPDYN conference*, Rhodes Island, Greece, 2009.

[CCL09b] C. Calderini, S. Cattari, and S. Lagomarsino. In-plane strength of unreinforced masonry piers. *Earthquake Engineering and Structural Dynamics, 38(2): 243-267*, 2009.

[CCL⁺17] D. Camilletti, S. Cattari, S. Lagomarsino, D. Bonaldo, G. Guidi, S. Bracchi, A. Galasco, G. Magenes, CF. Manzini, A. Penna, and A. Rota. RINTC project: nonlinear dynamic analyses of italian code-conforming urm buildings for collapse risk assessment. In *Proceedings of the COMPDYN 2017*, Rhodes Island, Greece, 2017.

[CCL18] D. Camilletti, S. Cattari, and S. Lagomarsino. In plane seismic response of irregular urm walls through equivalent frame and finite element models. In *Proceedings of the 16th European conference on earthquake engineering*, Thessaloniki, Greece, 2018.

[CCLR10] C. Calderini, S. Cattari, S. Lagomarsino, and M. Rossi. Review of existing models for global response and local mechanisms. Technical report, PERPETUATE (EU-FP7 Research Project), Deliverable D07 (www.perpetuate.eu/D07/), 2010.

[CG02] A.K. Chopra and R.K. Goel. A modal pushover analysis procedure for estimating seismic demands for buildings. *Earthquake Engineering and Structural Dynamics, 31:561-582*, 2002.

[CGLP06] S. Cattari, A. Galasco, S. Lagomarsino, and A. Penna. Aspetti critici nell'analisi sismica statica non lineare degli edifici esistenti in muratura (in italian). In *Proceedings of "Wondermasonry, workshop on design for rehabilitation of masonry structures"*, Florence, Italy, 2006.

[Cho95] A. K. Chopra. *Dynamics of structures. Theory and applications to earthquake engineering.* Prentice Hall, Englewood Cliffs, New Jersey, 1995.

[Cir09] *Circolare C.S.Ll.Pp. No. 617 of 2/2/2009: Istruzioni per l'applicazione delle nuove norme tecniche per le costruzioni di cui al Decreto Ministeriale 14 gennaio 2008. G.U. S.O. n. 27 of 26/2/2009, No. 47.* Rome, Italy, 2009.

[CL08] S. Cattari and S. Lagomarsino. A strength criterion for the flexural behavior of spandrel in un-reinforced masonry walls. In *Proceedings of the 14th world conference on earthquake engineering*, Beijing, China, 2008.

[CL13a] S. Cattari and S. Lagomarsino. Analisi non lineari per la simulazione del danno di un fabbricato in san felice sul panaro. In *Proceedings of the 15th ANIDIS conference*, Padua, Italy, 2013.

[CL13b] S. Cattari and S. Lagomarsino. *Masonry structures, pp. 151-200, in: Developments in the field of displacement based seismic assessment.* IUSS Press and EUCENTRE, Pavia, Italy, 2013.

[CLD+12] S. Cattari, S. Lagomarsino, D. D'Ayala, V. Novelli, and V. Bosiljkov. Correlation of perfomance levels and damage states for types of buildings. Technical report, PERPETUATE (EU-FP7 Research Project), Deliverable D17 (www.perpetuate.eu/D17/), 2012.

[CNR14] *Guide for the Probabilistic Assessment of the Seismic Safety of Existing Buildings.* Rome, Italy, 2014.

[CP03] R. Clough and J. Penzien. *Dynamics of structures.* Computers & Structures, Berkeley, California, 2003.

[CRL08] S. Cattari, S. Resemini, and S. Lagomarsino. Modelling of vaults as equivalent diaphragms in 3d seismic analysis of masonry buildings. In *Proceedings of the 6th SAHC Conference*, Bath, UK, 2008.

[DF04a] M. Dolšek and P. Fajfar. IN2 - a simple alternative for IDA. In *Proceedings of the 13th world conference on earthquake engineering*, Vancouver, B.C., Canada, 2004.

[DF04b] M. Dolšek and P. Fajfar. Simplified non-linear seismic analysis of infilled reinforced concrete frames. *Earthquake Engineering and Structural Dynamics, 34(1): 49-66*, 2004.

[DK79] Armen Der Kiureghian. On response of structures to stationary excitation. Technical report, University of California, 1979.

[DSM15] M. De Stefano and V. Mariani. *Pushover analysis for plan irregular building structures, pp. 429-448, in: Perspectives on European Earthquake Engineering and Seismology*, volume 1. Atilla Ansal Ed., Instambul, Turkey, 2015.

[DSU+15] J. Douglas, D.M. Seyedi, T. Ulrich, H. Modaressi, E. Foerster, K. Pitilakis, D. Pitilakis, A. Karatzetzou, G. Gazetas, E. Garini, and M. Loli. Evaluation of seismic hazard for the assessment of historical elements at risk: description of input and selection of intensity measures. *Bulletin of Earthquake Engineering, 13(1): 49-65*, 2015.

[EC804] *CEN, "Eurocode 8: Design of structures for earthquake resistance, Part 1: General rules, seismic actions and rules for buildings"*. Brussels, Belgium, 2004.

[EC817] *CEN, "Eurocode 8: Design of structures for earthquake resistance, Part 1: General rules, seismic actions and rules for buildings (draft)"*. Brussels, Belgium, 2017.

[Faj99] Peter Fajfar. Capacity Spectrum Method based on inelastic demand spectra. *Earthquake Engineering and Structural Dynamics, 28(9):979-993*, 1999.

[Faj00]   Peter Fajfar. A nonlinear analysis method for performance based seismic design. *Earthquake Spectra, 16(3):573-592*, 2000.

[Faj17]   Peter Fajfar. Analysis in seismic provisions for buildings: past, present and future. *Bulletin of Earthquake Engineering, published online*, 2017.

[FD14]   P. Fajfar and M. Dolšek. *Pushover-based analysis in Performance-Based Seismic Engineering - A view from Europe, pp. 265-277, in: Performance-Based Seismic Engineering: Vision for an Earthquake Resilient Society.* M. Fischinger Ed., 2014.

[FEM97]   *FEMA 273, NEHRP guidelines for the seismic rehabilitation of buildings.* Washington, D.C, 1997.

[FEM00]   *FEMA 356, Prestandard and commentary for the seismic rehabilitation of buildings.* Washington, D.C, 2000.

[FEM05]   *FEMA 440, Improvement of nonlinear static seismic analysis procedures.* Washington, D.C, 2005.

[FF88]   P. Fajfar and M. Fischinger. N2 - a method for non linear seismic damage analysis of rc buildings. In *Proceedings of the 9th world conference on earthquake engineering, Maruzen, Tokyo, vol V, pp 111-116*, Kyoto, Japan, 1988.

[FG96]   P. Fajfar and P. Gašperšić. The N2 method for the seismic damage analysis of RC buildings. *Earthquake Engineering and Structural Dynamics, 25(1): 31-46*, 1996.

[Fre78]   Sigmund A. Freeman. Prediction of response of concrete buildings to severe earthquake motion, 1978. Douglas McHenry International Symposium on Concrete and Concrete Structures, SP-55, American Concrete Institute, Detroit, Michigan, pp. 589-605.

[Fre98]   Sigmund A. Freeman. The capacity spectrum method as a tool for seismic design. In *Proceedings of the 11th European Conference of Earthquake Engineering*, Paris, France, 1998.

[Fre04]   Sigmund A. Freeman. Review of the development of the capacity spectrum method. *ISET Journal of Earthquake Technology, Paper No. 438, 41(1): 1-13*, 2004.

[Gal06]   Alessandro Galasco. *Analisi sismica degli edifici in muratura.* PhD thesis, University of Genoa, 2006. In Italian.

[GDTI13]   I. Giongo, D.Y. Dizhur, R. Tomasi, and J.M. Ingham. In-plane assessment of existing timber diaphragms in urm buildings via quasi-static and dynamic in-situ tests. *Advanced Materials Research, 778: 495-502*, 2013.

[Ge98]   G. Grünthal (editor). European macroseismic scale EMS. Technical report, European seismological commission, 1998.

[GGPM17]   G. Guerrini, F. Graziotti, A. Penna, and G. Magenes. Improved evaluation of inelastic displacement demands for short-period masonry structures. *Earthquake Engineering and Structural Dynamics, 46: 1411-1430*, 2017.

[GLP06]   A. Galasco, S. Lagomarsino, and A. Penna. On the use of pushover analysis for existing masonry buildings. In *Proceedings of the First European conference on earthquake engineering and seismology*, Geneva, Switzerland, 2006.

[GPBM14]   F. Graziotti, A. Penna, E. Bossi, and G. Magenes. Evaluation of displacement demand for unreinforced masonry buildings by equivalent SDOF systems. In *Proceedings of the 9th international conference on structural dynamics - EURODYN*, Porto, Portugal, 2014.

[GPM16]   F. Graziotti, A. Penna, and G. Magenes. A nonlinear SDOF model for the simplified evaluation of the displacement demand of low-rise URM buildings. *Bulletin of Earthquake Engineering, 14(6): 1589-1612*, 2016.

[GWD+14]   I. Giongo, A. Wilson, D.Y. Dizhur, H. Derakhshan, R. Tomasi, M.C. Griffith, P. Quenneville, and J.M. Ingham. Detailed seismic assessment and improvement procedure for vintage flexible

timber diaphragms. *Bulletin of the New Zealand Society for Earthquake Engineering, 47(2): 97-118*, 2014.

[JC09]   F. Jalayer and C.A. Cornell. Alternative non-linear demand estimation methods for probability-based seismic assessments. *Earthquake Engineering and Structural Dynamics, 38(8): 951-972*, 2009.

[KF11]   M. Kreslin and P. Fajfar. The extended N2 method taking into account higher mode effects in elevation. *Earthquake Engineering and Structural Dynamics, 40:1571-1589*, 2011.

[KF12]   M. Kreslin and P. Fajfar. The extended N2 method considering higher mode effects in both plan and elevation. *Bulletin of Earthquake Engineering, 10(2):695-715*, 2012.

[KK04]   E. Kalkan and S.K. Kunnath. Lateral load distribution in nonlinear static procedurs for seismic design. In *Proceedings of the Structures Conference*, Nashville, Tennessee, US, 2004.

[KP16]   A.J. Kappos and V.K. Papanikolaou. Nonlinear dynamic analysis of masonry buildings and definition of seismic damage states. *The Open Construction and Building Technology Journal, 10 (suppl 2, M2): 192-209*, 2016.

[KS97]   H. Krawinkler and G.D.P.K. Seneviratna. Pros and cons of a pushover analysis of seismic performance evaluation. *Engineering Structures, 20: 452-464*, 1997.

[Kun04]   S. K. Kunnath. Identification of modal combinations for nonlinear static analysis of building structures. *Computer-Aided Civil and Infrastructure Engineering, 19: 246-259*, 2004.

[Lag17]   S. Lagomarsino. Modellazione, analisi e verifiche di sicurezza di edifici esistenti in muratura: uno strumento di conoscenze per il progetto di consolidamento sismico. In *Proceedings of the 17th ANIDIS conference*, Pistoia, Italy, 2017.

[LB07]   N. Luco and P. Bazzurro. Does amplitude scaling of ground motion records result in biased nonlinear structural drift re-

sponses? *Earthquake Engineering and Structural Dynamics, 36(13): 1813-1835*, 2007.

[LBB⁺17]   S. Lu, K. Beyer, V. Bosiljkov, C. Butenweg, D. D'Ayala, D. Degee, M. Gams, J. Klouda, S. Lagomarsino, A. Penna, N. Mojsilovic, F. Da Porto, L. Sorrentino, and E. Vintzileo. Amendment of masonry chapter of eurocode 8. In *Proceedings of the 16th world conference on earthquake engineering*, Santiago, Chile, 2017.

[LC15a]   S. Lagomarsino and S. Cattari. Perpetuate guidelines for seismic performance-based assessment of cultural heritage masonry structures. *Bulletin of Earthquake Engineering, Vol. 13(1): 13-47*, 2015.

[LC15b]   S. Lagomarsino and S. Cattari. *Seismic performance of historical masonry structures through pushover and nonlinear dynamic analyses, pp. 265-292, in: Perspectives on European Earthquake Engineering and Seismology*, volume 2. Atilla Ansal Ed., Instanbul, Turkey, 2015.

[LMP⁺10]   S. Lagomarsino, H. Modaressi, K. Pitilakis, V. Bosiljkov, C. Calderini, D. D'Ayala, D. Benouar, and S. Cattari. PERPETUATE project: The proposal of a performance-based approach to earthquake protection of cultural heritage. *Advanced Materials Research, 133-134: 1119-1124*, 2010.

[LPGC13]   S. Lagomarsino, A. Penna, A. Galasco, and S. Cattari. TREMURI program: an equivalent frame model for the nonlinear seismic assessment of masonry buildings. *Engineering Structures, 56: 1787-1799*, 2013.

[MCL⁺16]   S. Marino, S. Cattari, S. Lagomarsino, J.M. Ingham, and D. Dizhur. Modelling of two damaged unreinforced masonry buildings following the canterbury earthquakes. In *Proceedings of the 2016 NZSEE Conference*, Christchurch, New Zealand, 2016.

[ML11]   R. Marques and P.B. Lourenço. Possibilities and comparison of structural component models for the seismic assessment

of modern unreinforced masonry buildings. *Computers and Structures, 89: 2079-2091*, 2011.

[MM80] W. Mann and H. Müller. Failure of shear-stressed masonry - an enlarged theory, tests and application to shear-walls. In *Proceedings of the international symposium on load-bearing brickwork, pp. 1-13*, London, UK, 1980.

[MPKF93] J.A. Mahaney, T.F. Paret, B.E. Kehoe, and S.A. Freeman. The capacity spectrum method for evaluating structural response during the loma prieta earthquake. In *Proceedings of 1993 national earthquake conference on earthquake hazard reduction in the Central and Eastern United States: a time for examination and action*, Oakland, CA, USA, 1993.

[MRPM14] A. Mouyiannou, M. Rota, A. Penna, and G. Magenes. Identification of suitable limit states from nonlinear dynamic analyses of masonry structures. *Journal of Earthquake Engineering, 18(2): 231-263*, 2014.

[NDG+17] Y. Nakamura, H. Derakhshan, M.C. Griffith, G. Magenes, and A.H. Sheikh. Applicability of nonlinear static procedures for low-rise unreinforced masonry buildings with flexible diaphragms. *Engineering Structures, Vol. 137: 1-18*, 2017.

[NR80] N.M. Newmark and R. Riddell. Inelastic spectra for seismic design. In *Proceedings of the 7th world conference on earthquake engineering, vol IV, pp. 129-136*, Istanbul, Turkey, 1980.

[NTC08] *NTC, "Norme tecniche delle costruzioni"*. Rome, Italy, 2008.

[NTC18] *NTC, "Norme tecniche delle costruzioni"*. Rome, Italy, 2018.

[NZ217] *The Seismic Assessment of Existing Buildings*. Wellington, New Zealand, 2017.

[OPC03] *OPCM 3274, "Norme tecniche per il progetto, la valutazione e l'adeguamento sismico degli edifici"*. Rome, Italy, 2003.

[PB14]   S. Petry and K. Beyer. Influence of boundary conditions and size effect on the drift capacity of URM walls. *Engineering Structures, Vol. 65: 76-88*, 2014.

[PCK07]   M.J.N. Priestley, G.M. Calvi, and M.J. Kowalsky. *Displacement-based seismic design of structures.* IUSS Press, Pavia, Italy, 2007.

[PSGM16]   A. Penna, I.E. Senaldi, A. Galasco, and G. Magenes. Numerical simulation of shaking table tests on full-scale stone masonry buildings. *International Journal of Architectural Heritage, 10(2-3): 146-163*, 2016.

[QMC17]   E. Quagliarini, G. Maracchini, and F. Clementi. Uses and limits of the equivalent frame model on existing unreinforced masonry buildings for assessing their seismic risk: A review. *Journal of Building Engineering, 10: 166-182*, 2017.

[RC11]   J.C. Reyes and A.K. Chopra. Evaluation of three-dimensional modal pushover analysis for unsymmetric-plan buildings subjected to two components of ground motion. *Earthquake Engineering and Structural Dynamics, 40: 1475-1494*, 2011.

[RCL15]   M. Rossi, S. Cattari, and S. Lagomarsino. Performance-based assessment of the Great Mosque of Algiers. *Bulletin of Earthquake Engineering, 13(1): 369-388*, 2015.

[SC13]   T. Sullivan and G.M. Calvi. *Development in the field of displacement based seismic assessment.* IUSS Press, Pavia, Italy, 2013.

[SSC⁺17]   R. Siano, V. Sepe, G. Camata, E. Spacone, P. Roca, and L. Pelá. Analysis of the performance in the linear field of equivalent-frame models for regular and irregular masonry walls. *Engineering Structures, 145: 190-210*, 2017.

[S.T16]   S.T.A.Data. 3muri program, release 10.5.0.1 (www.3muri.com), 2016.

[VC02a]   D. Vamvatsikos and C.A. Cornell. Incremental dynamic analysis. *Earthquake Engineering and Structural Dynamics, 31: 491-514*, 2002.

[VC02b]   D. Vamvatsikos and C.A. Cornell. The incremental dynamic analysis and its application to performance-based earthquake engineering. In *Proceedings of the 12th European Conference of Earthquake Engineering*, London, UK, 2002.

[VFF94]   T. Vidic, P. Fajfar, and M. Fischinger. Consistent inelastic design spectra: strength and displacement. *Earthquake Engineering and Structural Dynamics, 23: 507-521*, 1994.

[VN60]   A.S. Veletsos and N.M. Newmark. Effect of inelastic behavior on the response of simple systems to earthquake motions. In *Proceedings of the 2nd world conference on earthquake engineering, vol II, pp. 895-912*, Tokyo, Japan, 1960.

[VNC65]   A.S. Veletsos, N.M. Newmark, and C.V. Chelapati. Deformation spectra for elastic and elastoplastic systems subjected to ground shock and earthquake motions. In *Proceedings of the 3rd world conference on earthquake engineering, vol II, pp. 663-682*, Wellington, New Zealand, 1965.

[VZPB17]   F. Vanin, D. Zaganelli, A. Penna, and K. Beyer. Estimates for the stiffness, strength and drift capacoty of stone masonry walls based on 123 quasi-static cyclic tests reported in literature. *Bulletin of Earthquake Engineering, 15: 5435-5479*, 2017.

Appendix A

Modal analysis for the case study buildings

The main results derived from the modal analysis of the case study buildings are reported in the next pages. Different acronyms were used to refer to the case study buildings. In table A.1 the meaning of the acronyms with the main features of the models is reported; DS, PR and ER stand for diaphragms stiffness, in plan regularity and elevation regularity respectively.

Table A.1: Acronyms used to indicate the case study buildings.

	DS	PR	ER	Constructive details
$A_{r,rig}$	rigid	yes	yes	tie-rods
$B_{r,rig}$	rigid	yes	yes	ring beams
$A_{irr,rig}$	rigid	no	yes	tie-rods
$B_{irr,rig}$	rigid	no	yes	ring beams
$C_{irr,rig}$	rigid	no	no	tie-rods
$A_{r,int}$	intermediate	yes	yes	tie-rods
$B_{r,int}$	intermediate	yes	yes	ring beams
$A_{irr,int}$	intermediate	no	yes	tie-rods
$B_{irr,int}$	intermediate	no	yes	ring beams
$C_{irr,int}$	intermediate	no	no	tie-rods
$A_{r,flex}$	flexible	yes	yes	tie-rods
$A_{irr,flex}$	flexible	no	yes	tie-rods
$C_{irr,flex}$	flexible	no	no	tie-rods

$A_{r,rig}$ model

Table A.2: $A_{r,rig}$ model, modes characteristics

	T [s]	M_x [%]	M_y [%]
mode 1	0.30	0.00	82.8
mode 3	0.22	6.04	0.37
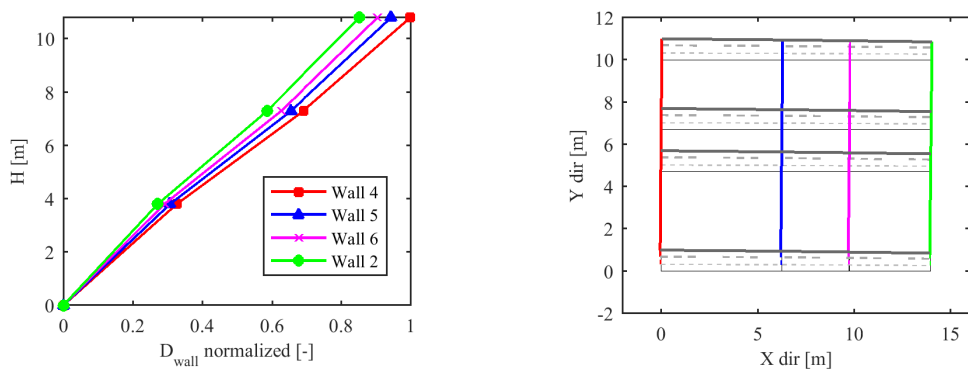
Figure A.1: Mode 1, elevation (left) and plan (right) deformed shape
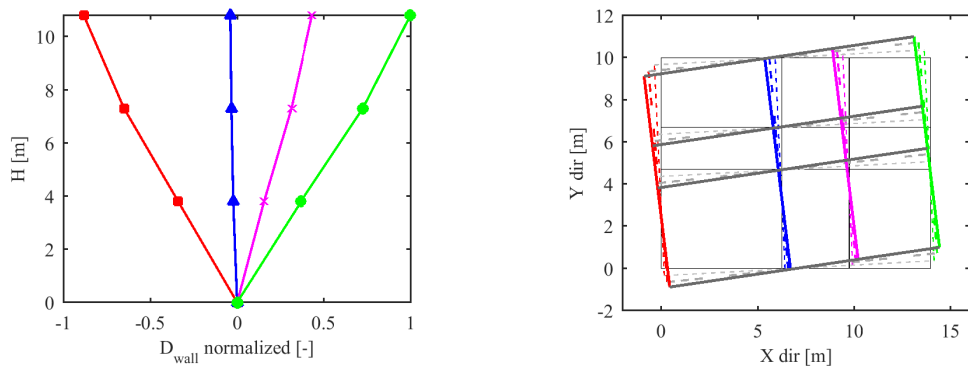
Figure A.2: Mode 3, elevation (left) and plan (right) deformed shape

$B_{r,rig}$ model

Table A.3: $B_{r,rig}$ model, modes characteristics

	T [s]	M_x [%]	M_y [%]
mode 1	0.30	0.00	82.9
mode 3	0.22	6.15	0.40
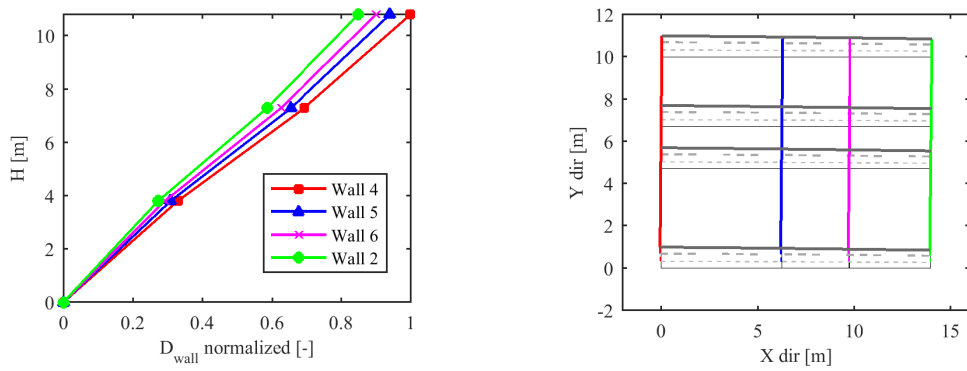
Figure A.3: Mode 1, elevation (left) and plan (right) deformed shape
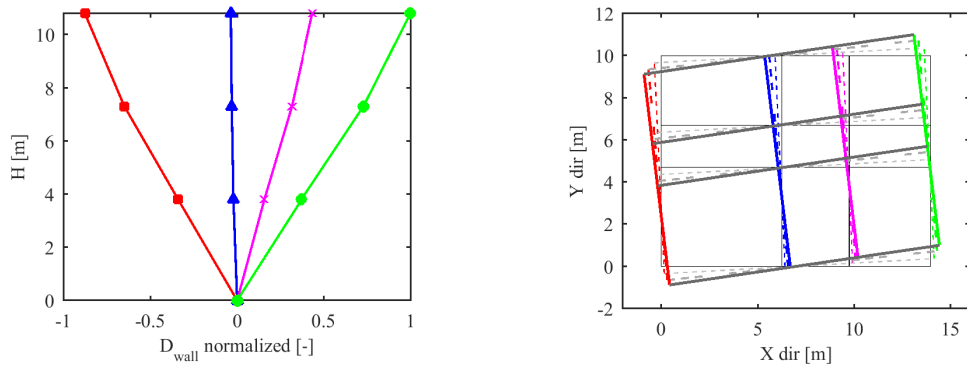
Figure A.4: Mode 3, elevation (left) and plan (right) deformed shape

$A_{irr,rig}$ model

Table A.4: $A_{irr,rig}$ model, modes characteristics

	T [s]	M_x [%]	M_y [%]
mode 1	0.34	0.12	71.4
mode 3	0.21	3.39	11.1
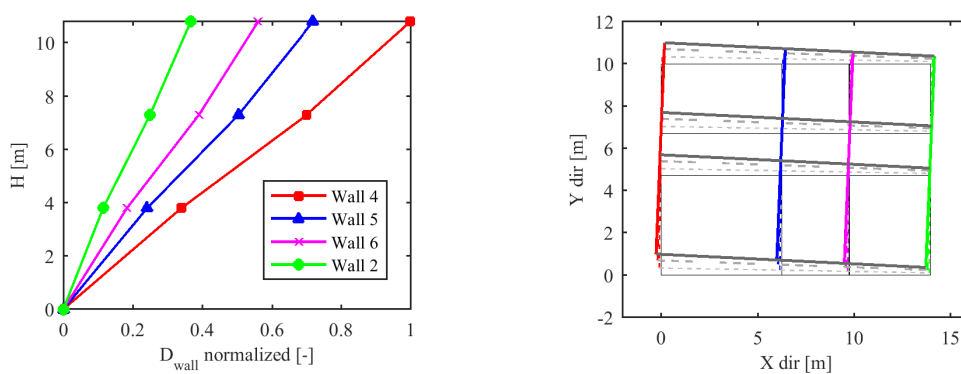
Figure A.5: Mode 1, elevation (left) and plan (right) deformed shape
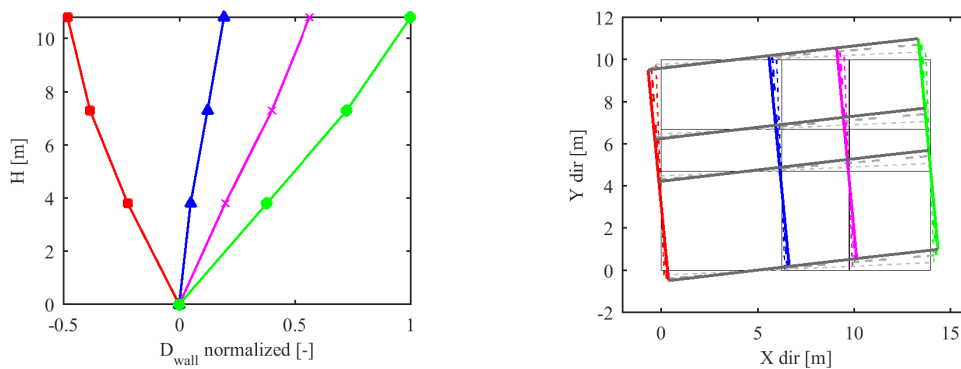
Figure A.6: Mode 3, elevation (left) and plan (right) deformed shape

$B_{irr,rig}$ model

Table A.5: $B_{irr,rig}$ model, modes characteristics

	T [s]	M_x [%]	M_y [%]
mode 1	0.34	0.12	71.4
mode 3	0.22	3.33	11.4
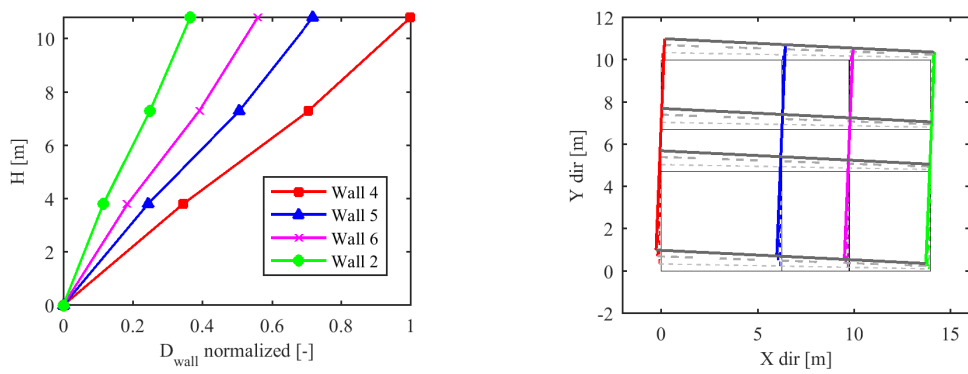
Figure A.7: Mode 1, elevation (left) and plan (right) deformed shape
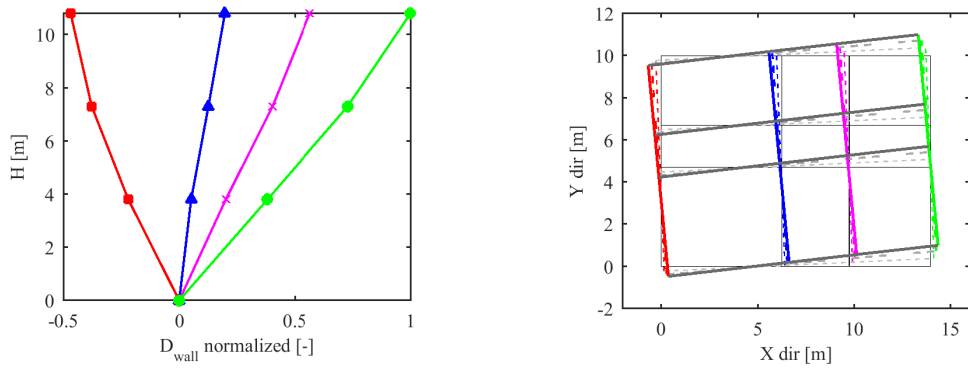
Figure A.8: Mode 3, elevation (left) and plan (right) deformed shape

$C_{irr,rig}$ model

Table A.6: $C_{irr,rig}$ model, modes characteristics

	T [s]	M_x [%]	M_y [%]
first modes			
mode 1	0.42	0.04	62.1
mode 3	0.23	0.77	15.0
second modes			
mode 4	0.19	0.02	12.0
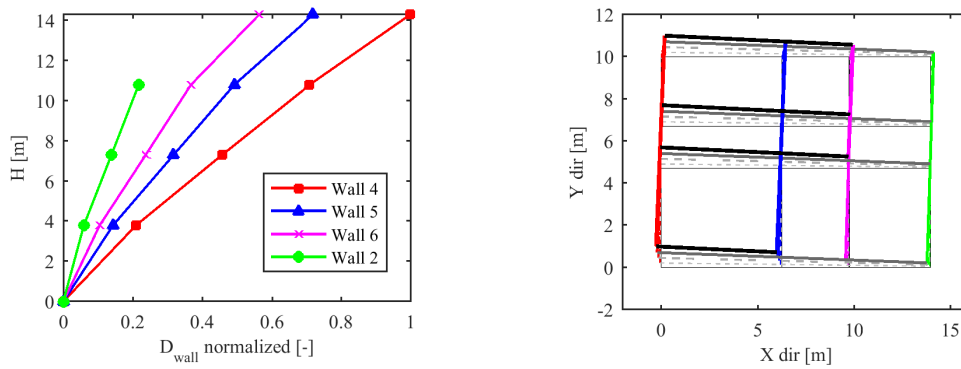
Figure A.9: Mode 1, elevation (left) and plan (right) deformed shape
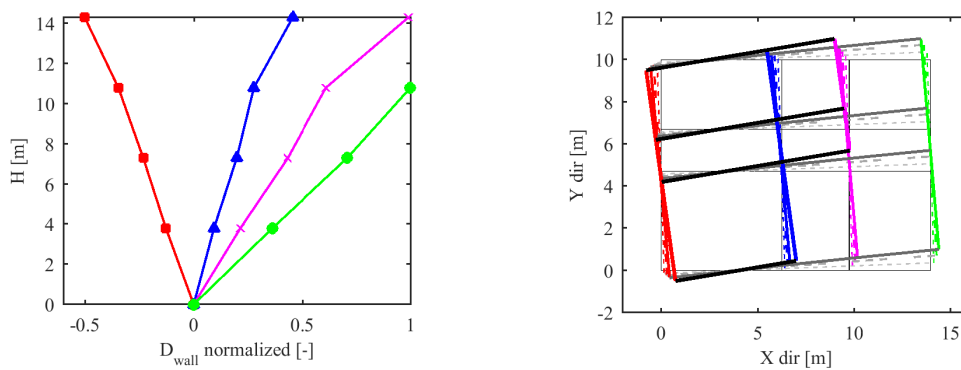
Figure A.10: Mode 3, elevation (left) and plan (right) deformed shape

186
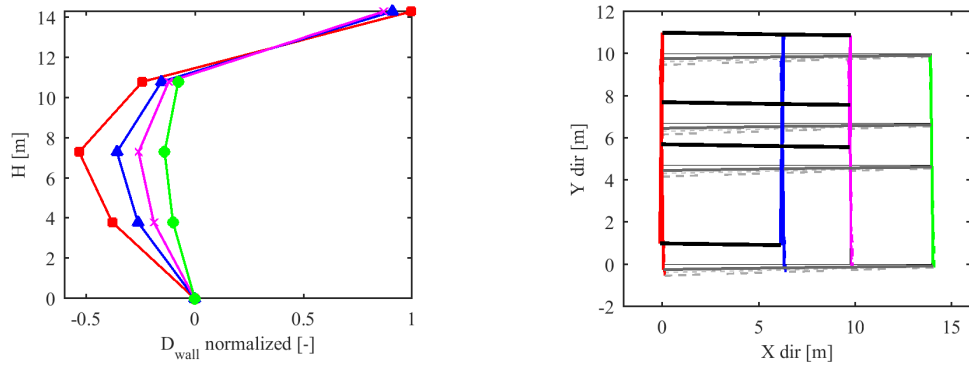
Figure A.11: Mode 4, elevation (left) and plan (right) deformed shape

$A_{r,int}$ model

Table A.7: $A_{r,int}$ model, modes characteristics

	T [s]	M_x [%]	M_y [%]
mode 1	0.32	0.04	70.6
mode 4	0.22	0.00	11.8
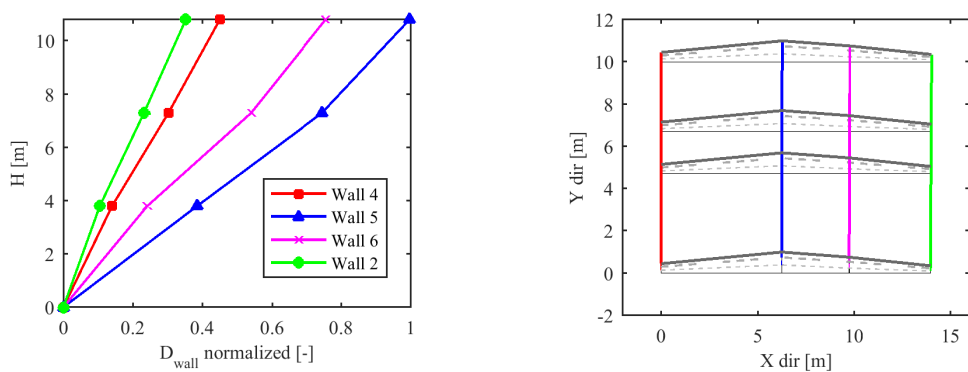
Figure A.12: Mode 1, elevation (left) and plan (right) deformed shape
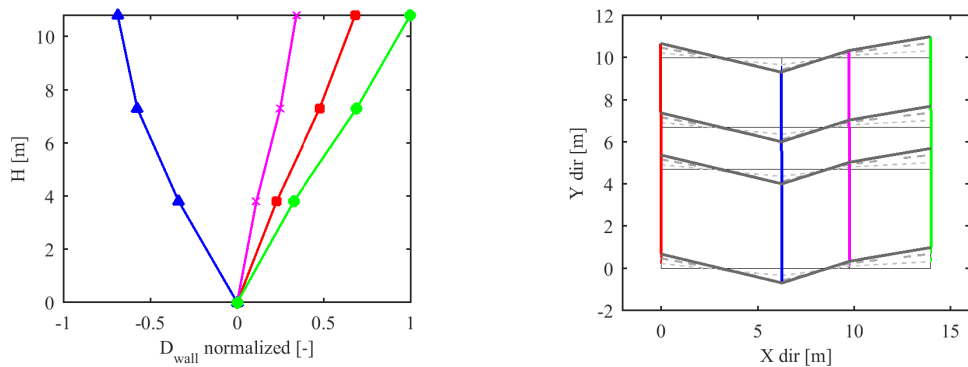
Figure A.13: Mode 4, elevation (left) and plan (right) deformed shape

$B_{r,int}$ model

Table A.8: $B_{r,int}$ model, modes characteristics

	T [s]	M_x [%]	M_y [%]
mode 1	0.33	0.03	70.6
mode 4	0.22	0.00	12.0
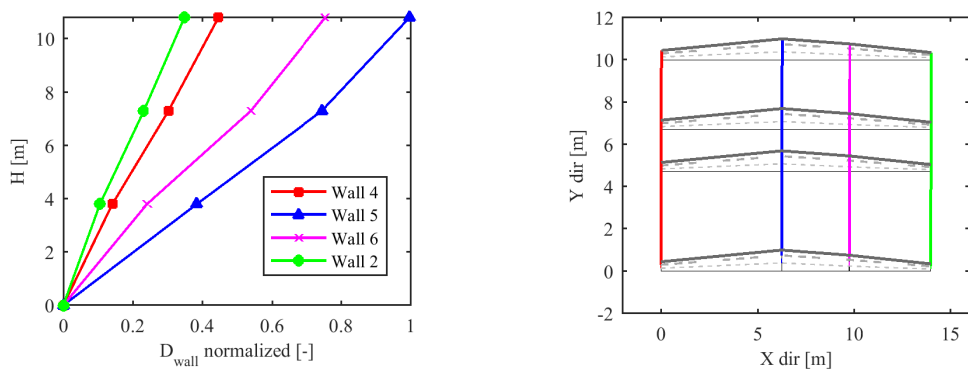
Figure A.14: Mode 1, elevation (left) and plan (right) deformed shape
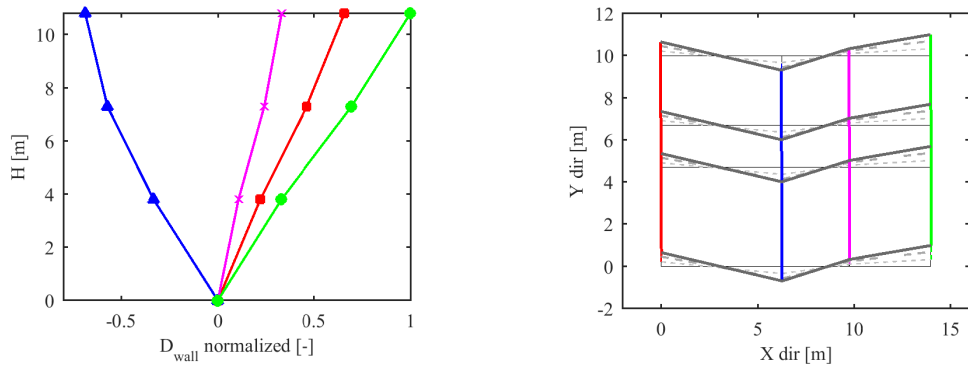
Figure A.15: Mode 4, elevation (left) and plan (right) deformed shape

189

$A_{irr,int}$ model

Table A.9: $A_{irr,int}$ model, modes characteristics

	T [s]	M_x [%]	M_y [%]
mode 1	0.36	0.03	66.1
mode 3	0.27	7.93	4.42
mode 4	0.21	0.00	8.81
mode 6	0.17	0.10	3.16
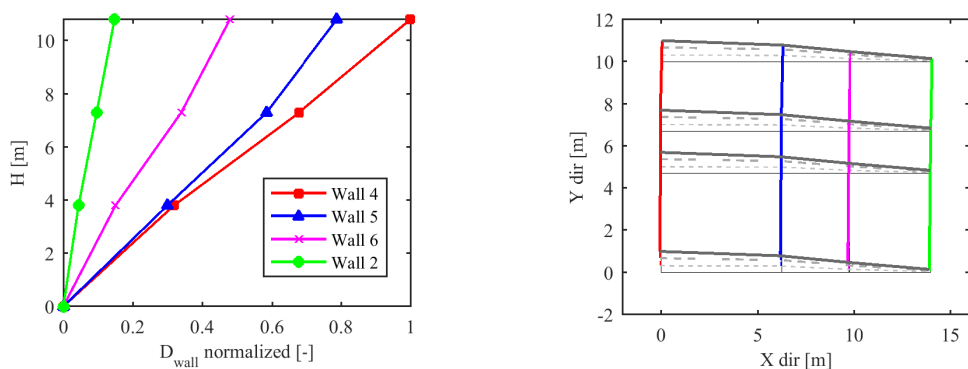
Figure A.16: Mode 1, elevation (left) and plan (right) deformed shape
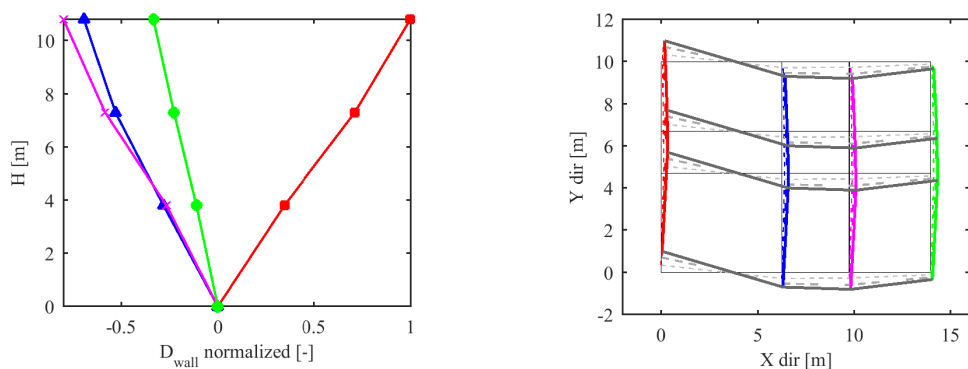
Figure A.17: Mode 3, elevation (left) and plan (right) deformed shape
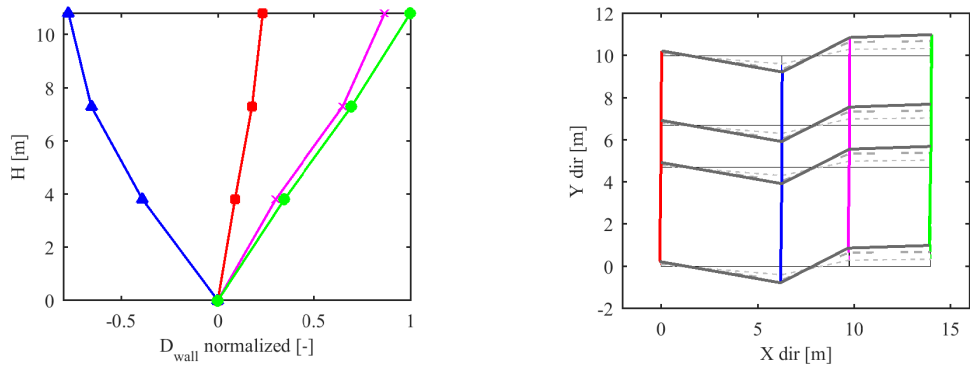
Figure A.18: Mode 4, elevation (left) and plan (right) deformed shape
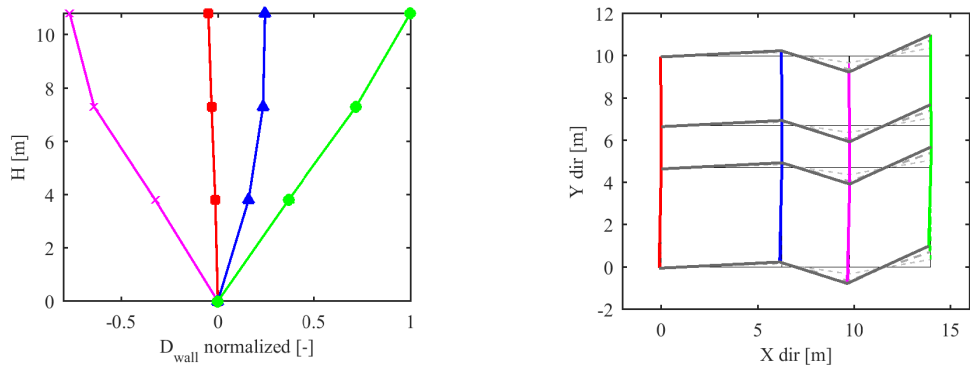
Figure A.19: Mode 6, elevation (left) and plan (right) deformed shape

$B_{irr,int}$ model

Table A.10: $B_{irr,int}$ model, modes characteristics

	T [s]	M_x [%]	M_y [%]
mode 1	0.36	0.03	66.1
mode 3	0.28	9.77	4.32
mode 4	0.21	0.00	9.04
mode 6	0.17	0.08	3.13
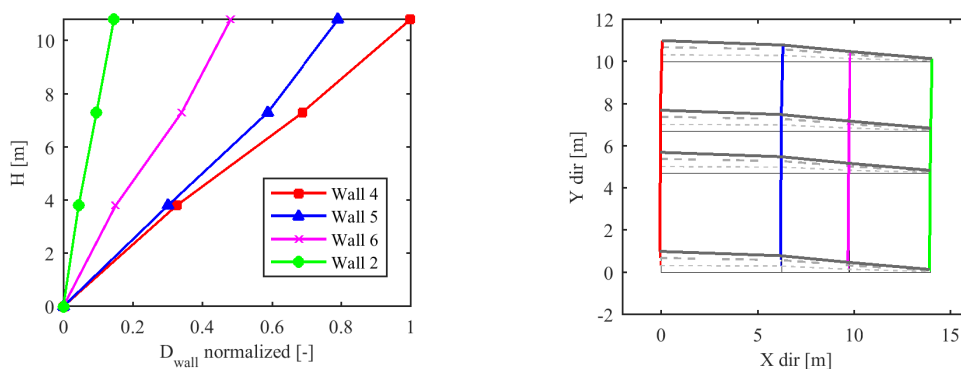
Figure A.20: Mode 1, elevation (left) and plan (right) deformed shape
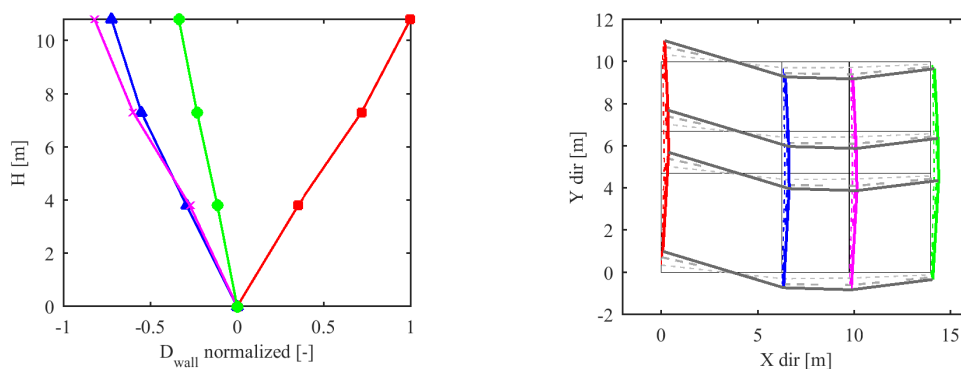
Figure A.21: Mode 3, elevation (left) and plan (right) deformed shape
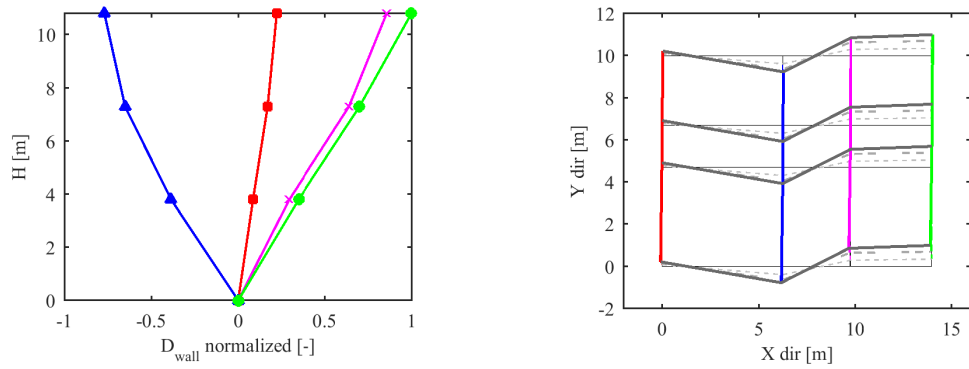
Figure A.22: Mode 4, elevation (left) and plan (right) deformed shape
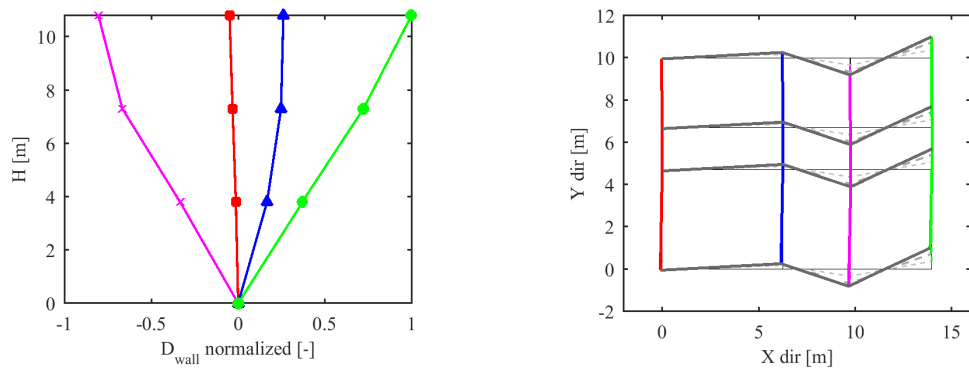
Figure A.23: Mode 6, elevation (left) and plan (right) deformed shape

$C_{irr,int}$ model

Table A.11: $C_{irr,int}$ model, modes characteristics

	T [s]	M_x [%]	M_y [%]
first modes			
mode 1	0.46	0.03	58.2
mode 3	0.30	6.23	5.80
second modes			
mode 4	0.21	0.53	15.5
mode 5	0.20	0.13	3.27
mode 7	0.18	3.17	2.91
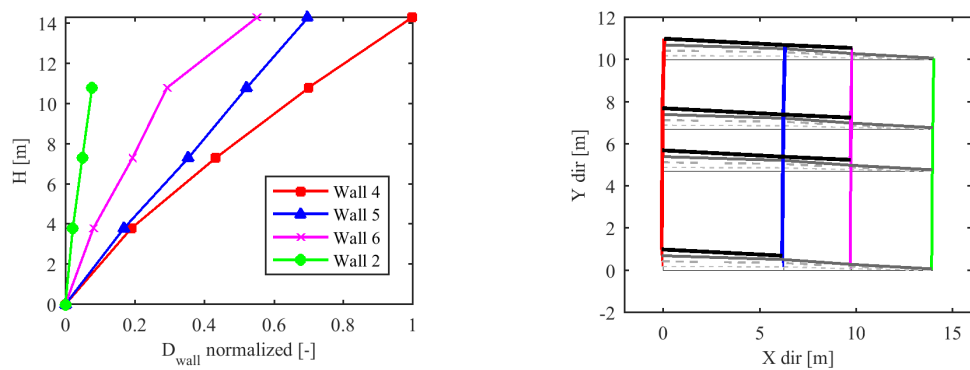
Figure A.24: Mode 1, elevation (left) and plan (right) deformed shape
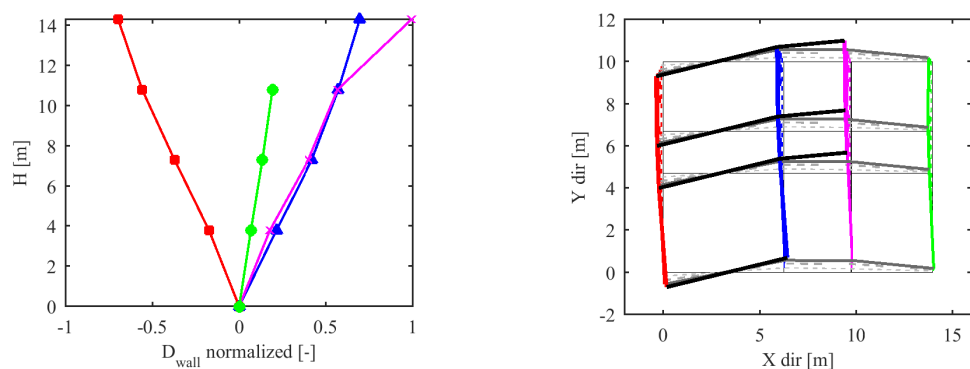
Figure A.25: Mode 3, elevation (left) and plan (right) deformed shape
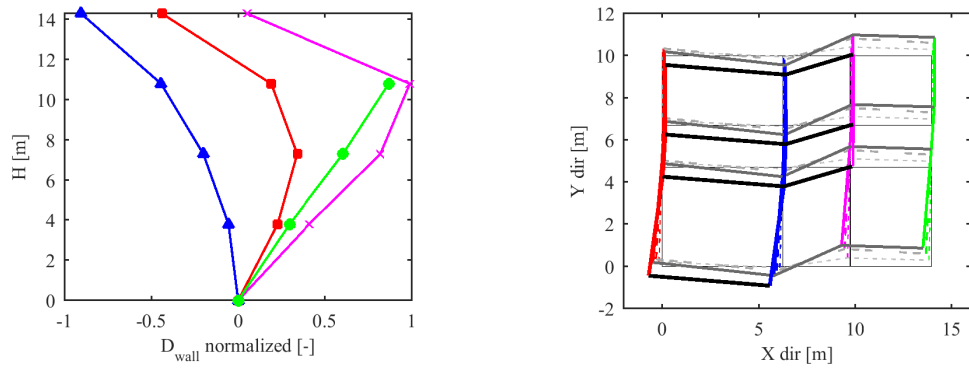
Figure A.26: Mode 4, elevation (left) and plan (right) deformed shape
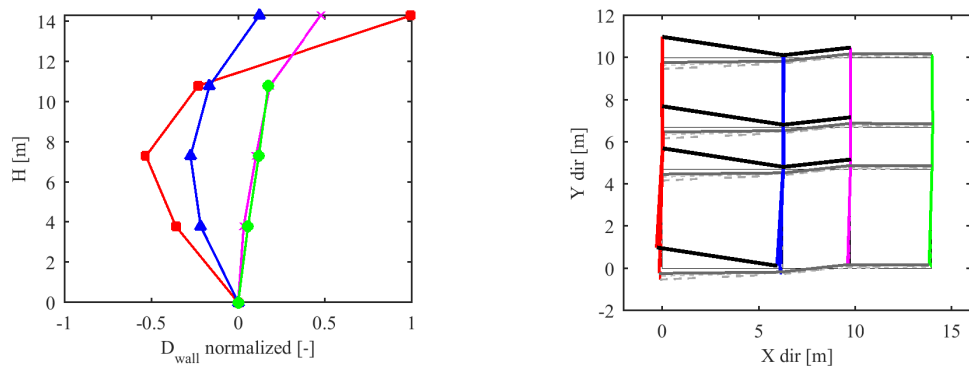
Figure A.27: Mode 5, elevation (left) and plan (right) deformed shape
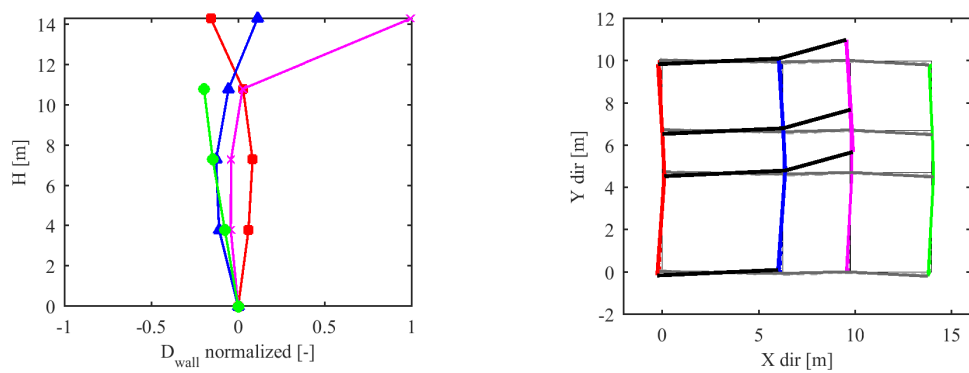
Figure A.28: Mode 7, elevation (left) and plan (right) deformed shape

195

$A_{r,flex}$ model

Table A.12: $A_{r,flex}$ model, modes characteristics

	T [s]	M_x [%]	M_y [%]
mode 1	0.38	0.04	36.4
mode 3	0.30	0.01	10.4
mode 5	0.26	1.62	18.5
mode 6	0.24	1.18	17.4
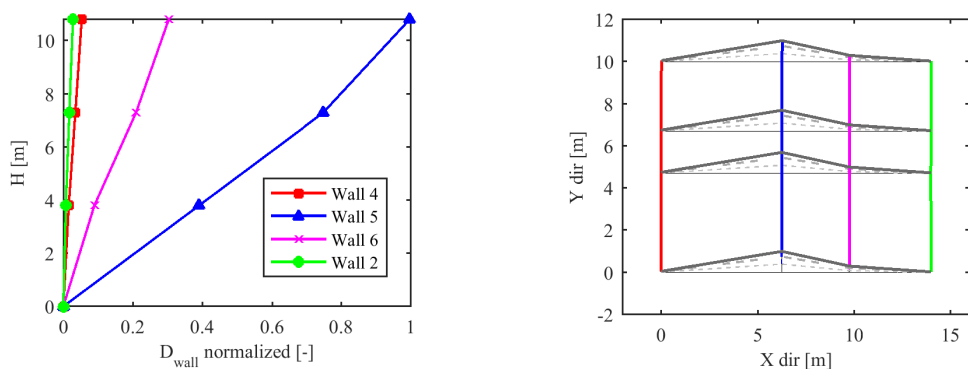
Figure A.29: Mode 1, elevation (left) and plan (right) deformed shape
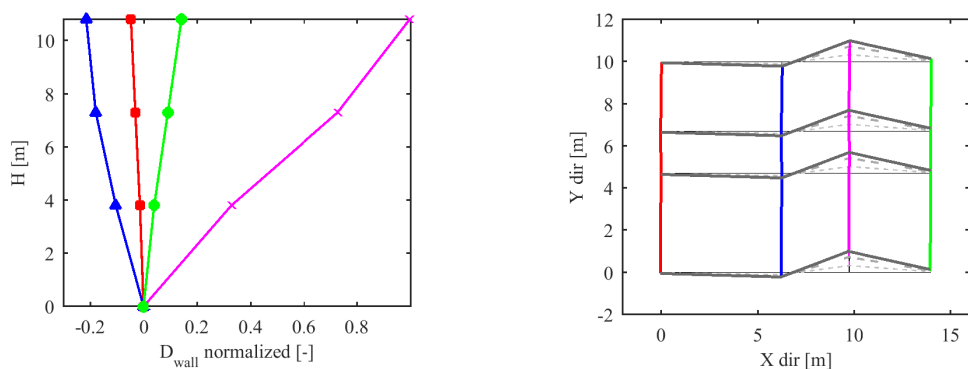
Figure A.30: Mode 3, elevation (left) and plan (right) deformed shape

196
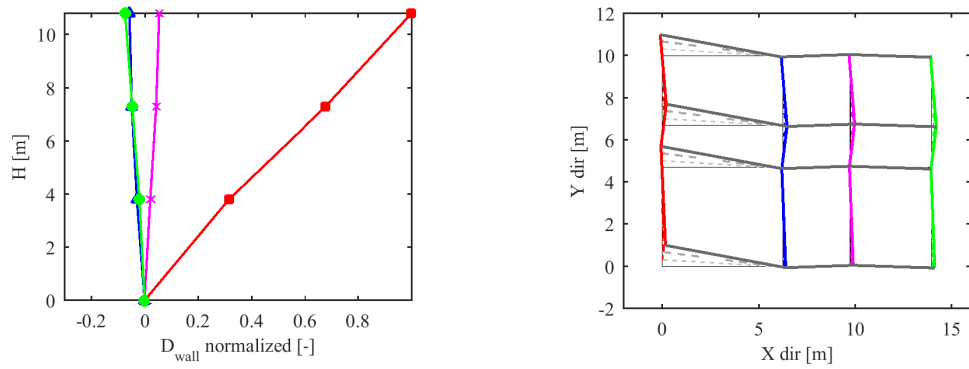
Figure A.31: Mode 5, elevation (left) and plan (right) deformed shape
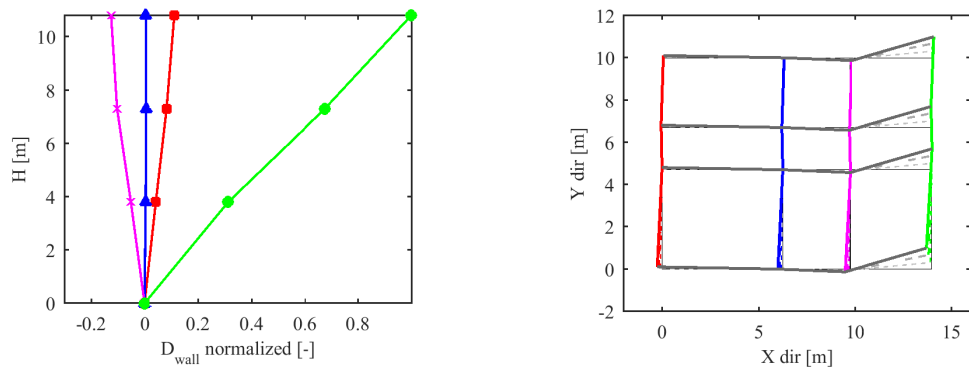
Figure A.32: Mode 6, elevation (left) and plan (right) deformed shape

$A_{irr,flex}$ model

Table A.13: $A_{irr,flex}$ model, modes characteristics

	T [s]	M_x [%]	M_y [%]
mode 1	0.38	0.01	50.6
mode 2	0.36	2.96	3.65
mode 4	0.30	0.00	11.7
mode 6	0.22	7.58	9.00
mode 7	0.20	13.3	7.21
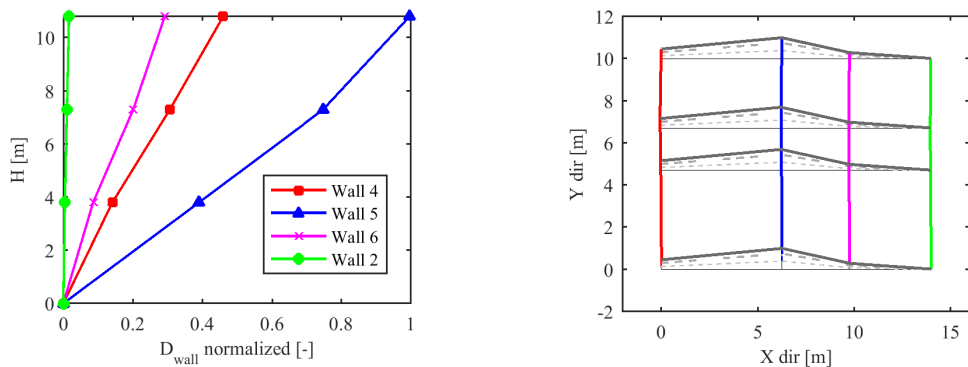
Figure A.33: Mode 1, elevation (left) and plan (right) deformed shape
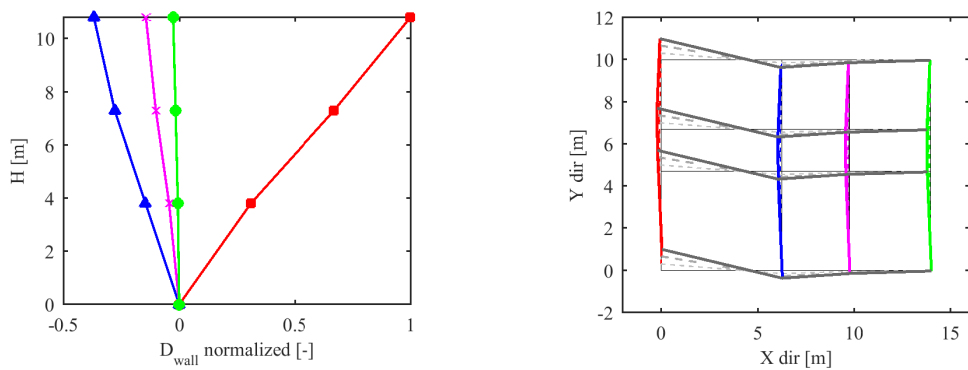
Figure A.34: Mode 2, elevation (left) and plan (right) deformed shape
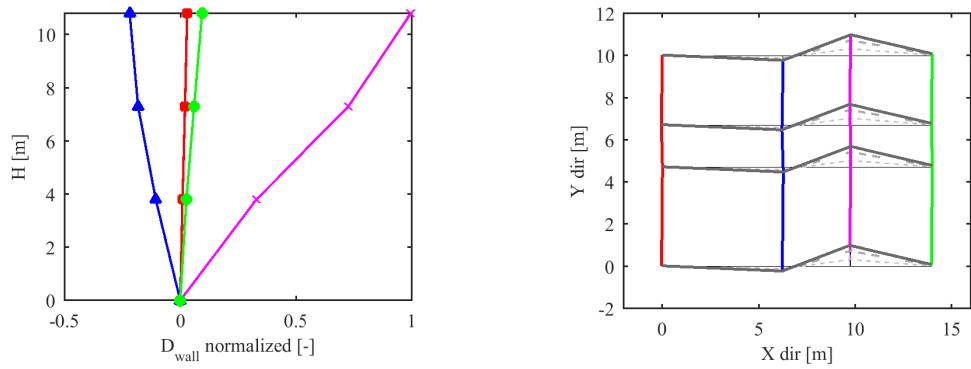
Figure A.35: Mode 4, elevation (left) and plan (right) deformed shape
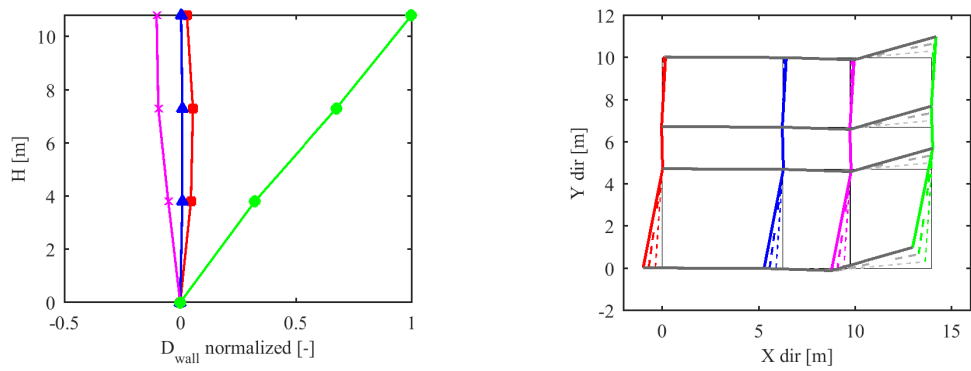
Figure A.36: Mode 6, elevation (left) and plan (right) deformed shape
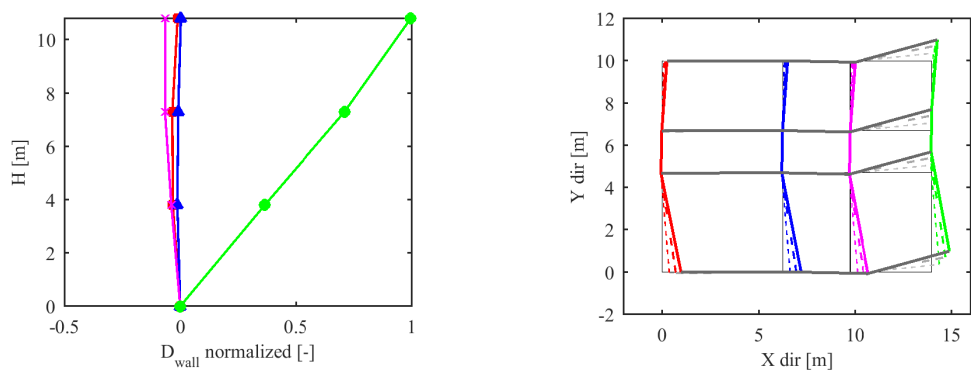
Figure A.37: Mode 7, elevation (left) and plan (right) deformed shape

$C_{irr,flex}$ model

Table A.14: $C_{irr,int}$ model, modes characteristics

	T [s]	M_x [%]	M_y [%]
first modes			
mode 1	0.49	0.15	43.9
mode 2	0.44	0.15	10.2
mode 4	0.33	0.28	7.83
mode 6	0.24	13.1	1.65
second modes			
mode 7	0.22	0.90	7.04
mode 8	0.21	6.20	6.07
mode 11	0.18	0.06	2.91
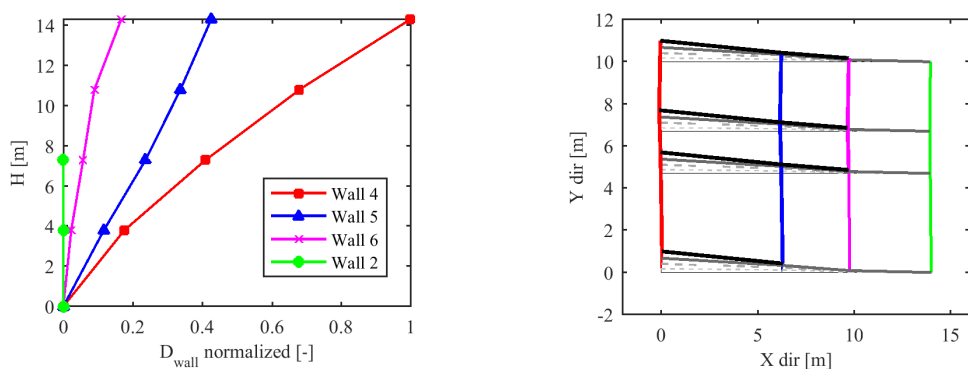
Figure A.38: Mode 1, elevation (left) and plan (right) deformed shape
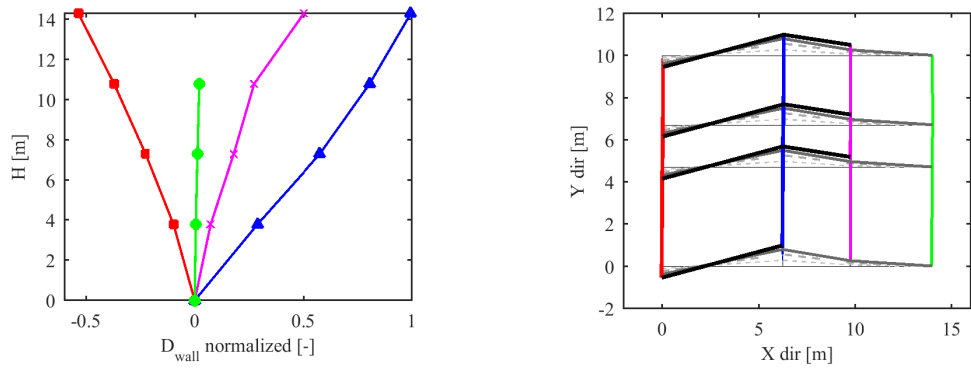
Figure A.39: Mode 2, elevation (left) and plan (right) deformed shape
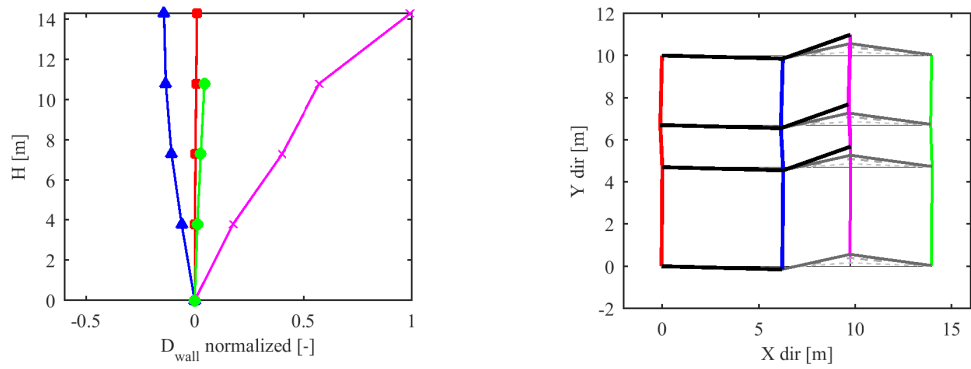
Figure A.40: Mode 4, elevation (left) and plan (right) deformed shape
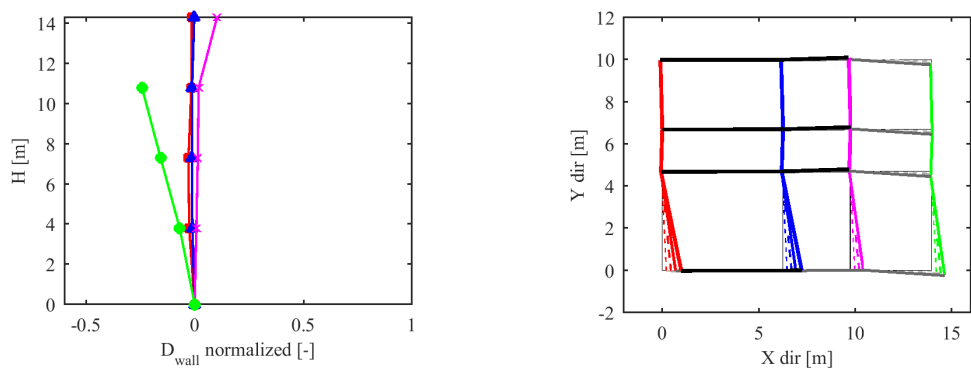
Figure A.41: Mode 6, elevation (left) and plan (right) deformed shape
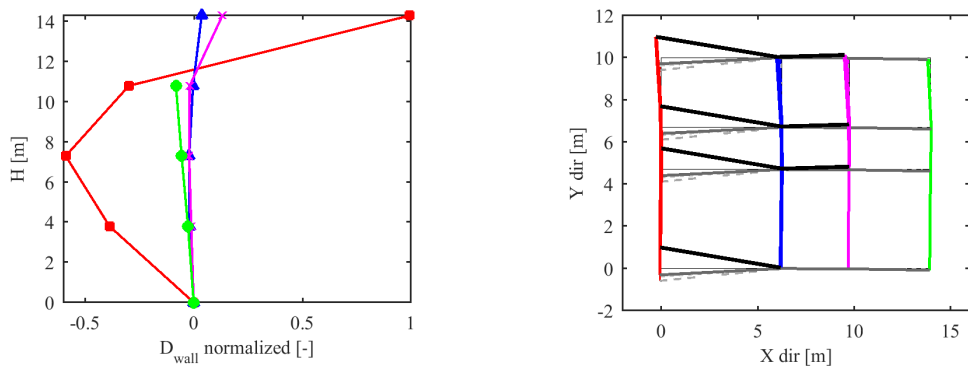
Figure A.42: Mode 7, elevation (left) and plan (right) deformed shape
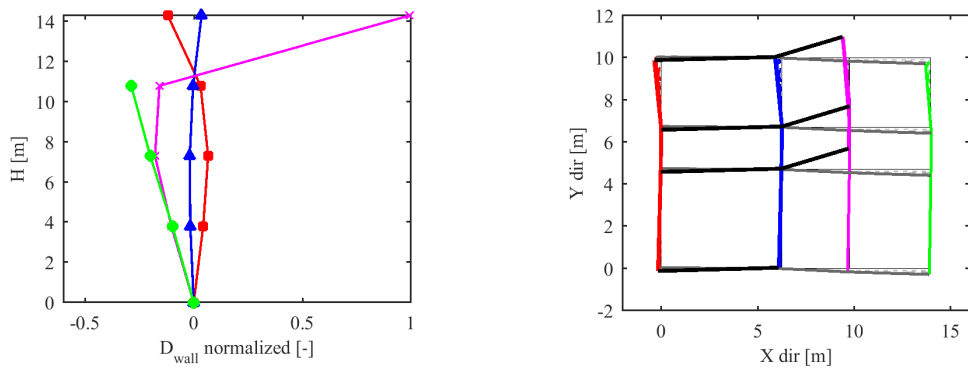
Figure A.43: Mode 8, elevation (left) and plan (right) deformed shape
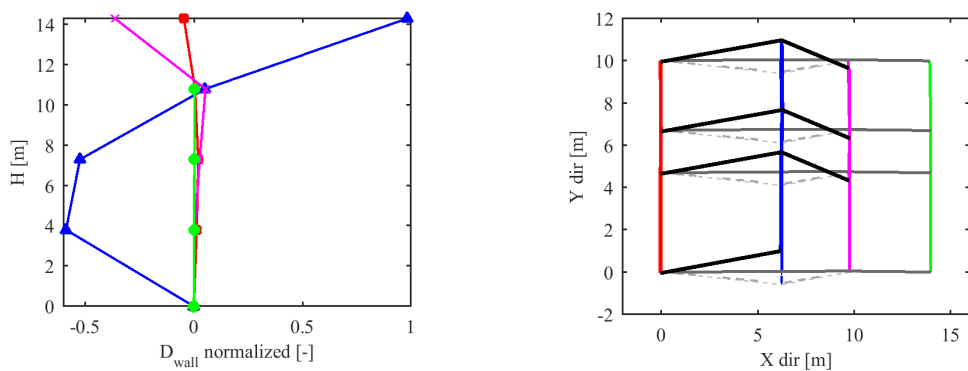
Figure A.44: Mode 11, elevation (left) and plan (right) deformed shape

Appendix B

Time histories adopted for the NDPs

Since each seismic event has specific features and can produce different effects on the same structure (record to record variability), ten artificial time histories have been used, compatible with the accelerations expected in L'Aquila (Italy).

The records were conditioned in order to have the same spectral acceleration for the period of 0.35s, assumed as representative of the main modes of vibration of the considered buildings (see Appendix A).

The resulted median response spectrum (see Fig. 3.9) has $T_c = 0.3$ s.

Table B.1: Main characteristics of the time histories adopted.

Time history	Time step [s]	Length of the signal	PGA $[m/s^2]$
TH1	0.01	3300	1.062
TH2	0.01	4800	0.992
TH3	0.005	3250	1.711
TH4	0.01	5500	0.877
TH5	0.01	5500	0.765
TH6	0.01	3000	0.650
TH7	0.01	5500	0.843
TH8	0.01	2999	0.886
TH9	0.01	2999	1.312
TH10	0.01	5500	1.234
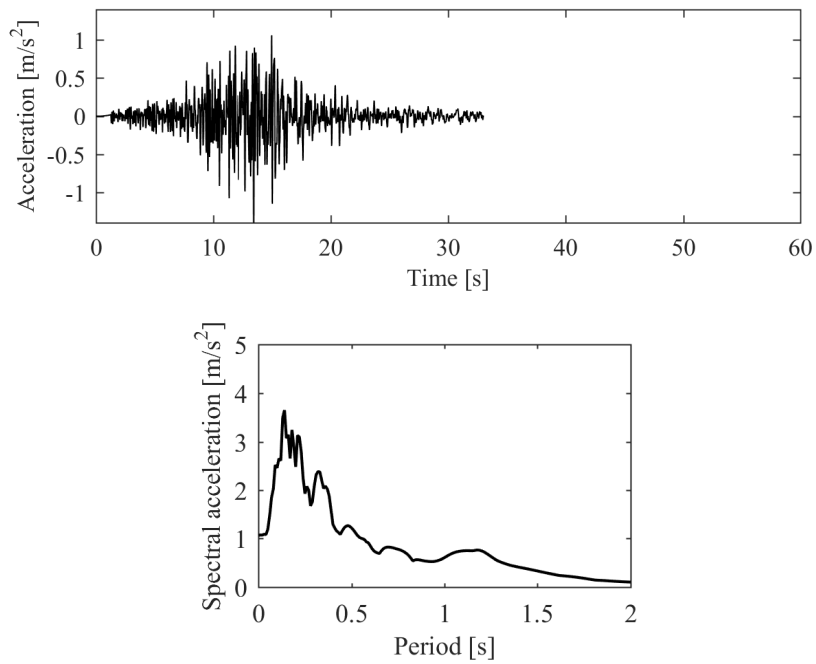
Figure B.1: Time history 1 and corresponding response spectrum
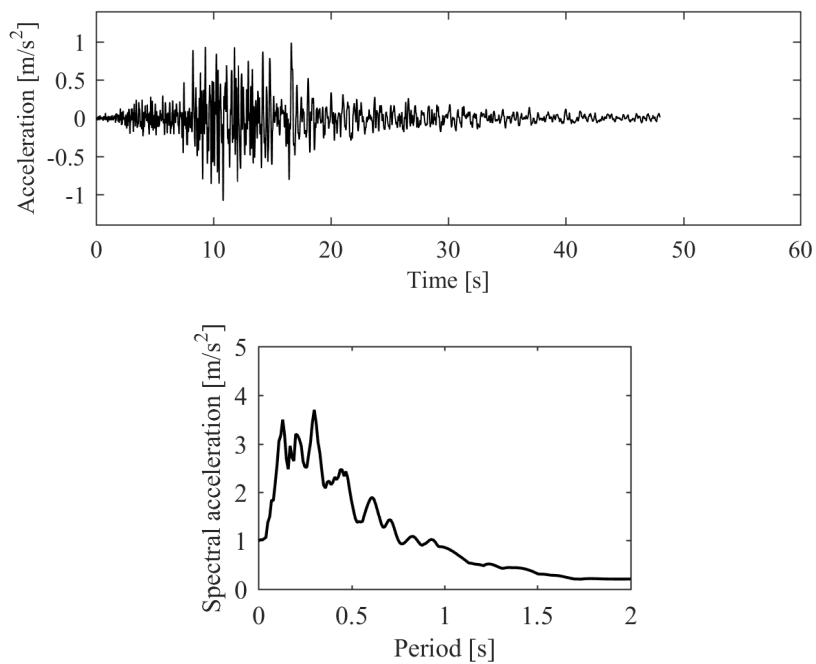
Figure B.2: Time history 2 and corresponding response spectrum
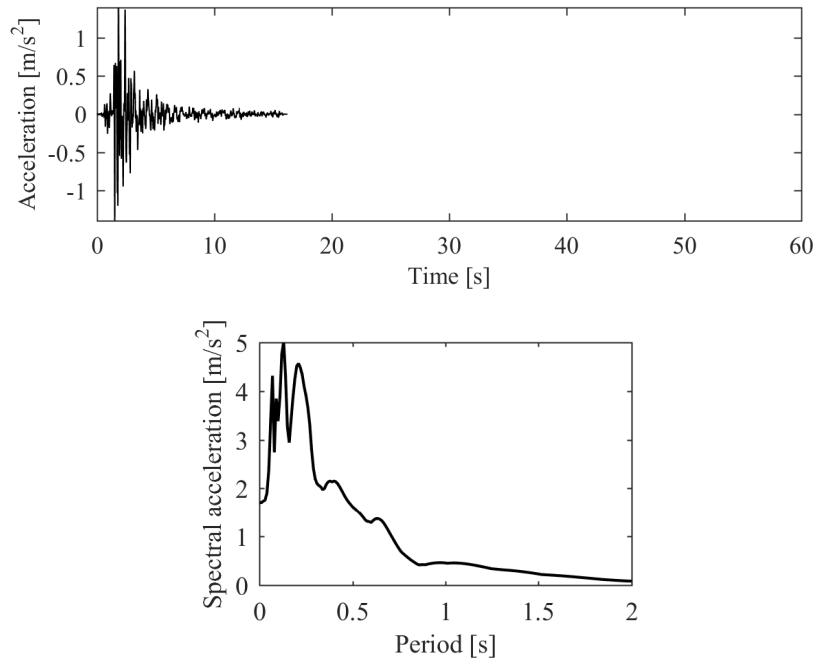
Figure B.3: Time history 3 and corresponding response spectrum
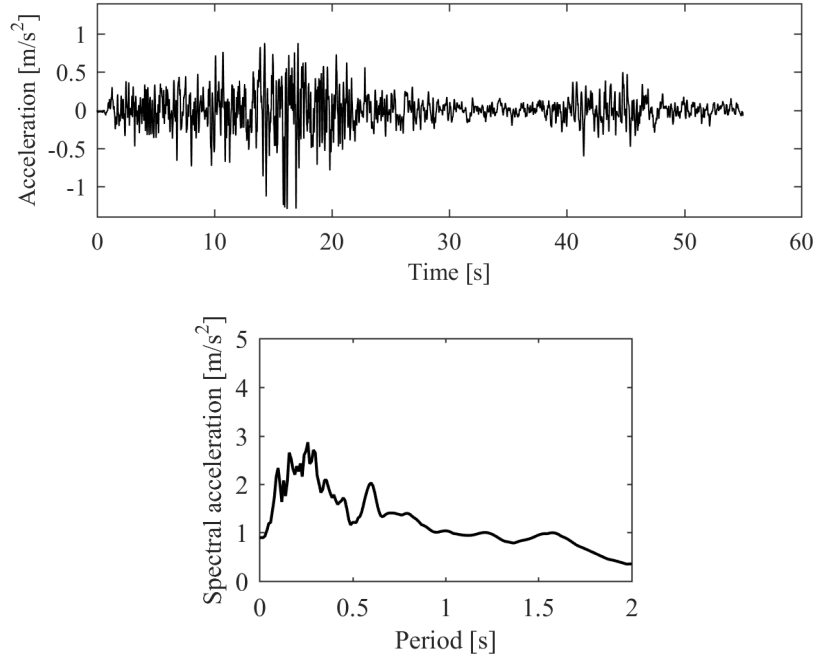
Figure B.4: Time history 4 and corresponding response spectrum
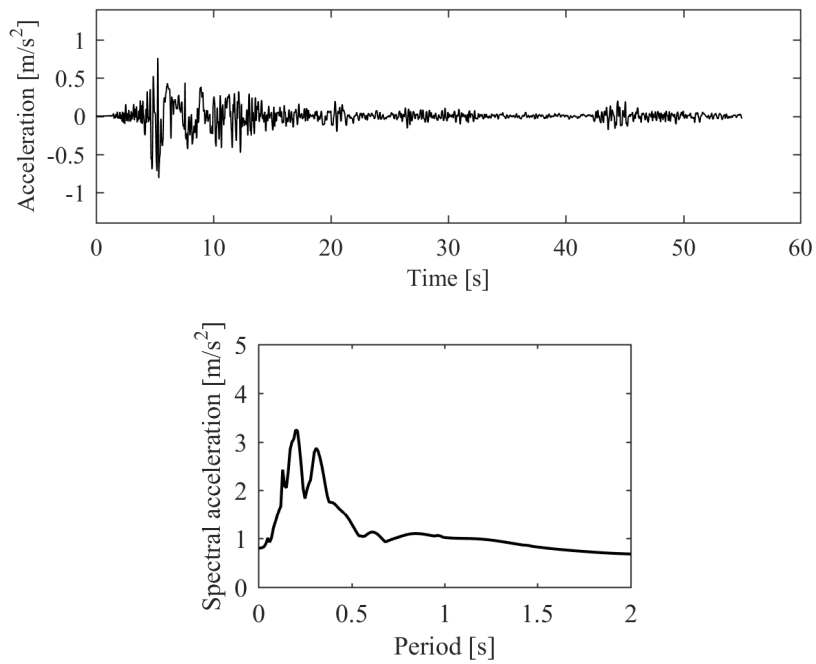
Figure B.5: Time history 5 and corresponding response spectrum
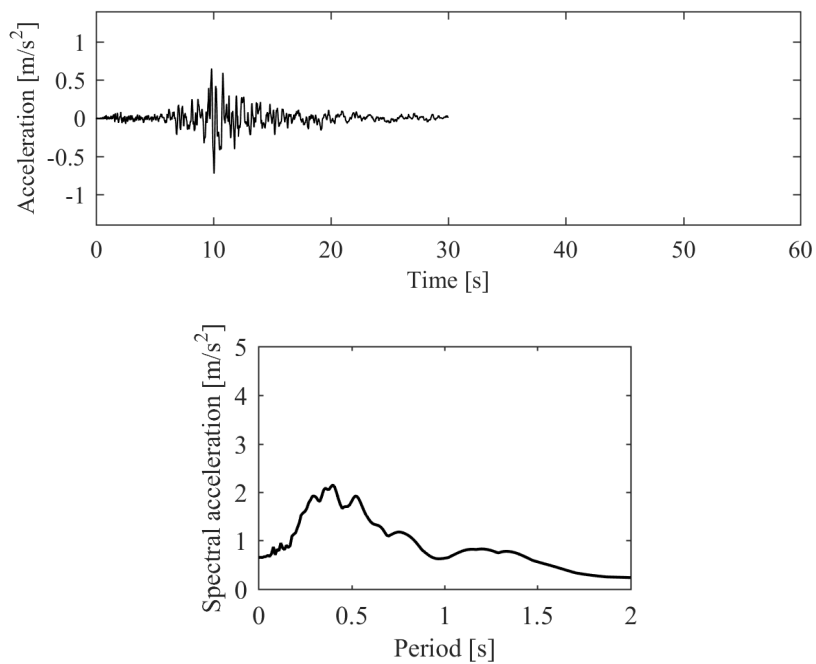
Figure B.6: Time history 6 and corresponding response spectrum
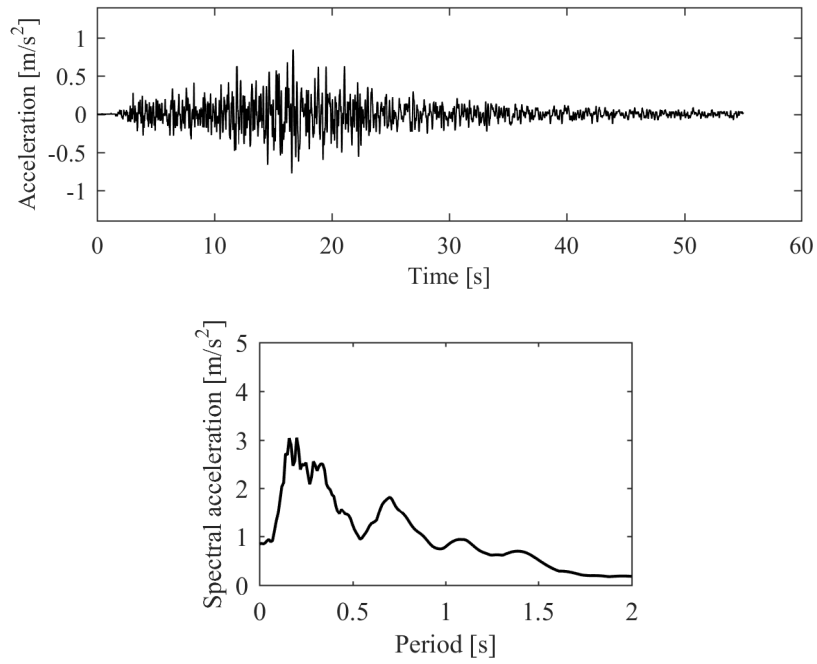
Figure B.7: Time history 7 and corresponding response spectrum
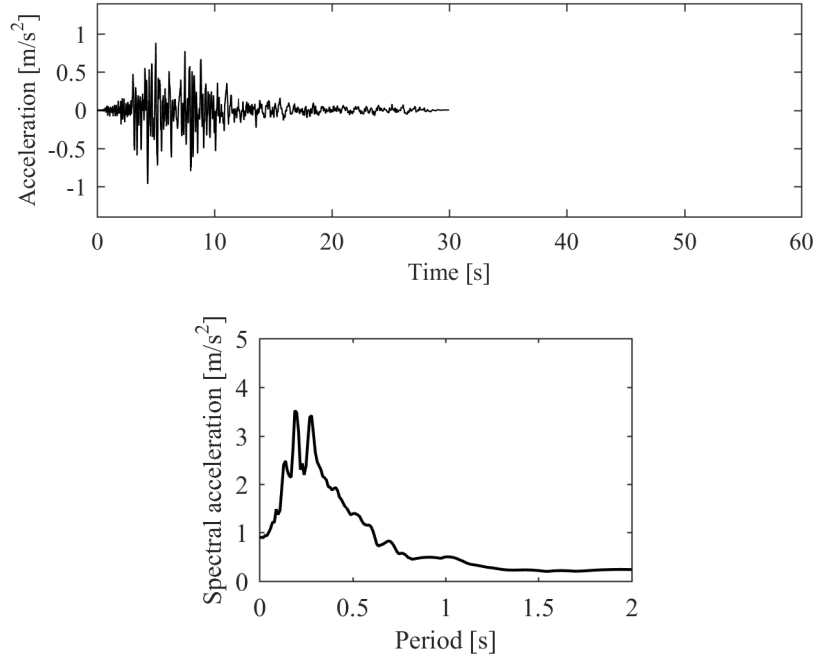
Figure B.8: Time history 8 and corresponding response spectrum
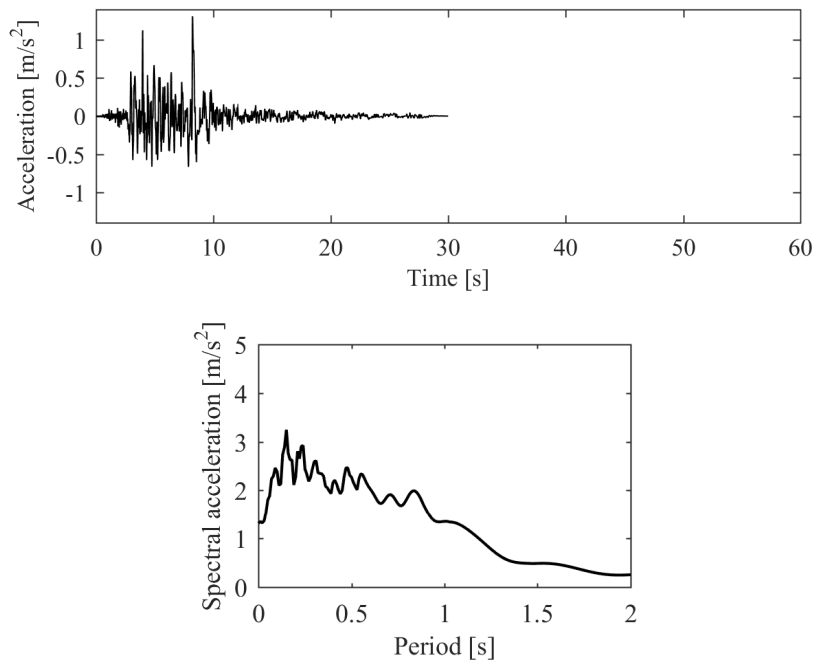
Figure B.9: Time history 9 and corresponding response spectrum
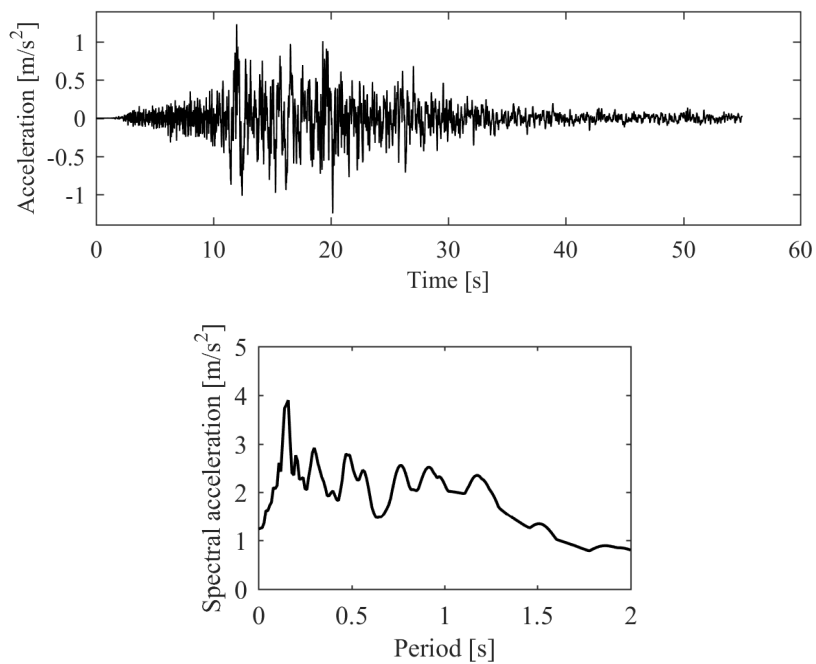
Figure B.10: Time history 10 and corresponding response spectrum

Appendix C

Dynamic response of linear MDOF systems

The equations of motions for a *linear* MDOF system subjected to external forces varying in time t, $\underline{p}(t)$, are:

$$\underline{M}\underline{\ddot{u}}(t) + \underline{C}\underline{\dot{u}}(t) + \underline{K}\underline{u}(t) = \underline{p}(t) \tag{C.1}$$

where $\underline{M}, \underline{C}$ and $\underline{K}$ are the mass, damping and stiffness matrices respectively. All these matrices are input of the problem, the unknown is the vector $\underline{u}$(t) that represents the displacements of the nodes of the model during the application of the external forces.

It is known, that the displacements $\underline{u}$(t) of a MDOF system can be evaluated as the linear composition of the vectors representing its modal shapes. Thus the dynamic response of a system can be expressed as:

$$\underline{u}(t) = \sum_{r=1}^{N} \underline{\phi}_r q_r(t) = \Phi \underline{q}(t) \tag{C.2}$$

where N is the number of modes, $\underline{\phi}_r$ is the vector that represents the modal shape of the r mode (known from the modal analysis) and the N modal coordinates $q_r(t)$ are unknowns (called as *modal coordinates* in [Cho95]). Substituting Eq. C.2 in Eq. C.1, then premultiplying each term of Eq. C.1 by $\underline{\phi}_n{}^T$ gives:

$$\sum_{r=1}^{N} (\underline{\phi}_n{}^T \underline{M} \underline{\phi}_r) \underline{\ddot{q}}_r(t) + \sum_{r=1}^{N} (\underline{\phi}_n{}^T \underline{C} \underline{\phi}_r) \underline{\dot{q}}_r(t) + \sum_{r=1}^{N} (\underline{\phi}_n{}^T \underline{K} \underline{\phi}_r) \underline{q}_r(t) = \underline{\phi}_n{}^T \underline{p}(t) \tag{C.3}$$

because of the orthogonality of modes, and if the system has classical damping (more information in [Cho95]) all terms in each of the summations vanish, except the r = n term, reducing the equation to:

$$(\underline{\phi_n}^T \underline{M} \underline{\phi_n}) \ddot{q}_n(t) + (\underline{\phi_n}^T \underline{C} \underline{\phi_n}) \dot{q}_n(t) + (\underline{\phi_n}^T \underline{K} \underline{\phi_n}) q_n(t) = \underline{\phi_n}^T \underline{p}(t) \qquad (C.4)$$

or

$$M_n \ddot{q}_n(t) + C_n \dot{q}_n(t) + K_n q_n(t) = \underline{\phi_n}^T \underline{p}(t) = P_n(t) \qquad (C.5)$$

where

$$M_n = \underline{\phi_n}^T \underline{M} \underline{\phi_n}; \quad C_n = \underline{\phi_n}^T \underline{C} \underline{\phi_n}; \quad K_n = \underline{\phi_n}^T \underline{K} \underline{\phi_n} \qquad (C.6)$$

Eq. C.5 may be interpreted as the equation governing the response $q_n(t)$ of a SDOF system with mass M_n, damping C_n and stiffness K_n. Fig. C.1 shows an example of such a system. Therefore, M_n is called the *generalized mass* for the n-th natural mode, C_n is called the *generalized damping* for the n-th natural mode and K_n the *generalized stiffness* for the n-th mode. These parameters "depend only on the n-th mode $\underline{\phi_n}$, thus if we know only the n-th mode, we can write the equation for q_n and solve it without even knowing the other modes" [Cho95]. In fact, in case of seismic analysis, M_n, C_n and K_n derive from the geometry of the model, whereas $\underline{p}(t)$ is the ground motion input. The only unknown in the equation is $q_n(t)$, and there are N such equation, one for each mode.
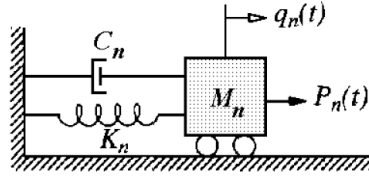
Figure C.1: Generalized SDOF system for the n-th natural mode (from [Cho95])

C.1   Modal participation factor

Dividing by M_n Eq. C.5 we get.

$$\ddot{q}_n(t) + 2\zeta \omega_n \dot{q}_n(t) + \omega_n^2 q_n(t) = \frac{\underline{\phi_n}^T \underline{p}(t)}{M_n} \qquad (C.7)$$

where ω_n is the natural frequency of mode n, and

$$\zeta = \frac{C_n}{2M_n\omega_n} \tag{C.8}$$

where ζ is the *damping ratio* or *fraction of critical damping* and is a property of the system that also depends on its mass and stiffness [Cho95].

The load vector $\underline{p}(t)$ may be caused by any external load mechanism, and in general it may vary with time both in amplitude and in spatial distribution. However, it is here assumed that the load distribution does not vary with time so that only the amplitude is time varying. This type of external loading applies to many practical situations, including earthquake excitations [CP03]. The effective earthquake loading vector is generally expressed as:

$$\underline{p}(t) = -\underline{\underline{M}}\,\underline{t}\,\ddot{u}_g(t) \tag{C.9}$$

where "$\ddot{u}_g(t)$ is the earthquake acceleration history applied at the structure's supports, and $\underline{t}$ is a displacement transformation vector that expresses the displacement of each structure degree of freedom due to application of a unit support displacement" [CP03]. Substituting Eq. C.9 in Eq. C.7 we get:

$$\ddot{q}_n(t) + 2\zeta\omega_n\dot{q}_n(t) + \omega_n^2 q_n(t) = \frac{\phi_n{}^T\underline{\underline{M}}\,\underline{t}}{M_n}\ddot{u}_g(t) \tag{C.10}$$

The ratio shown on the right side of Eq. C.10 is defined the *modal participation factor* for the mode n:

$$\Gamma_n = \frac{\phi_n{}^T\underline{\underline{M}}\,\underline{t}}{M_n} = \frac{\phi_n{}^T\underline{\underline{M}}\,\underline{t}}{\underline{\phi_n}{}^T\underline{\underline{M}}\,\underline{\phi_n}} \tag{C.11}$$

In case of three dimensional model of a building, using vector $\underline{t}$ is possible to apply the seismic action in one of the three spatial directions (X,Y,Z):

$$\Gamma_{nX} = \frac{\phi_n{}^T\underline{\underline{M}}\,\underline{t_X}}{M_n} \tag{C.12}$$

The denominator in these expressions is the effective modal mass previously introduced. Regarding the numerator, it is evident that it will be relatively large for the first mode because the first-mode shape is all positive. On the contrary, "for higher modes the product will be much smaller because these mode shapes include both positive and negative zones" [CP03]. However,

for the higher modes also the denominator will decrease, therefore Γ may not be small. The numerator is often indicated with the symbol m_n^*, and it is called *equivalent mass* of the mode (that should not be confused with the *generalized mass* M_n).

$$m_n^* = \underline{\phi_n}^T \underline{M} \underline{t_X} \tag{C.13}$$

Therefore the dynamic response of a linear MDOF model may be studied solving N uncoupled differential equations as the following:

$$\ddot{q}_n(t) + 2\zeta\omega_n\dot{q}_n(t) + \omega_n^2 q_n(t) = \Gamma_n \ddot{u}_g(t) \tag{C.14}$$

Eq. C.14 has the same form of a SDOF system equation here reported:

$$\ddot{u}(t) + 2\zeta\omega\dot{u}(t) + \omega^2 u(t) = \ddot{u}_g(t) \tag{C.15}$$

Comparing Eq. C.14 and C.15 gives [CP03]:

$$q_n(t) = \Gamma_n u(t) \tag{C.16}$$

or

$$u(t) = \frac{q_n(t)}{\Gamma_n} \tag{C.17}$$

Eq. C.17 links the modal coordinates intensity with the displacement of a SDOF system. This relation will be used to transform the pushover curves deriving from pushover analyses into capacity curve in the AD space. It is then possible to prove that the modal participation factor, the modal equivalent mass and the modal mass participation are related through the following equation:

$$\Gamma_n * m_n^* = e_n^* * M_{dyn} \tag{C.18}$$

where M_{dyn} is the total *dynamic* mass of the MDOF model, and e_n^* is the % of mass participation for mode n. The total dynamic mass is the mass activated by the seismic actions, i.e. in case of an equivalent frame model the mass corresponding to the part of the wall close to the ground is not considered (see Fig. C.2.

The name usually adopted for Γ_n, modal participation factor, however may be misleading, in fact it may give the idea that it is a measure of the degree to which the n-th mode participates in the response. In fact, "Γ_n is not independent of how the mode is normalized, nor a measure of the
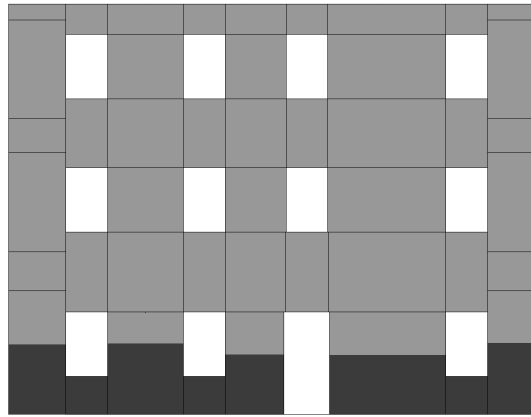
Figure C.2: Example of an URM walls modeled using the EF method. In dark grey the parts of the wall whose mass is not considered activated by the seismic action.

modal contribution to a response quantity" [Cho95]. In the present research all the modes are normalized to their maximum displacement, therefore, in case of rigid diaphragms, Γ coefficient can give information on the modes shape. Some examples are shown in Fig. C.3, where it is possible to observe that "the modal participation factor and the modal participant mass vary according to the relative inter-story displacement over the height of the building" [ATC96].
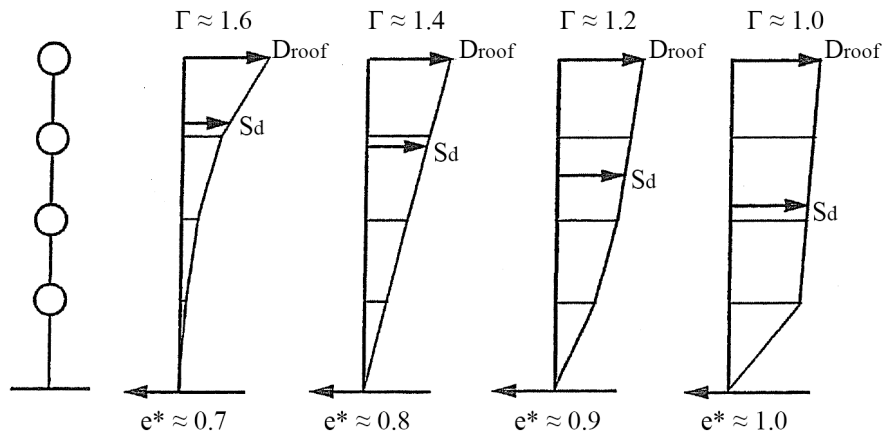
Figure C.3: Example modal participation factors and modal participant masses (adapted from [ATC96])

C.2 Load patterns proportional to natural vibration mode shapes

Due to the dynamic properties of natural vibration modes, if a MDOF system is loaded with a load pattern with shape proportional to a natural vibration mode, the deformed shape will be proportional to a natural vibration mode as well. Therefore, a load pattern proportional to a natural vibration mode may be computed using the equation herein:

$$f_{n,j} = \Gamma_n \phi_{n,j} m_j \tag{C.19}$$

where $f_{n,j}$ is the force applied to node j in a mode shape proportional to mode n, Γ_n is the modal participation factor for the mode n, $\phi_{n,j}$ is the modal displacement of node j in mode n and m_j is the mass of node j of the MDOF system.

List of symbols and acronyms

Symbol	Unit	Description
a	$[L/T^2]$	Acceleration in the AD space ($a=V_b/(\Gamma M^*)$)
$a_{DLk(PLk)}$	$[L/T^2]$	Acceleration at the attainment of DLk (PLk) in the AD space - k=1:4
a_{hyst}	$[-]$	Parameter adopted to evaluate maximum inelastic displacement in [GGPM17]
a_s	$[-]$	Site class factor according to [ASC14]
b_G	$[-]$	Parameter adopted to evaluate maximum inelastic displacement in [GGPM17]
$\tilde{c}$	$[F/L^2]$	*Mann and Müller* equivalent cohesion
c_G	$[-]$	Parameter adopted to evaluate maximum inelastic displacement in [GGPM17]
d	$[L]$	Displacement in the AD space ($d=D/\Gamma$)
$d_{DLk(PLk)}$	$[L]$	Displacement at the attainment of DLk (PLk) in the AD space - k=1:4
$d^*_{e,max}$	$[L]$	Elastic displacement demand for an equivalent SDOF system
d_{max}	$[L]$	Maximum inelastic displacement demand for an equivalent SDOF system
d^*_{max}	$[L]$	Maximum inelastic displacement demand for an equivalent SDOF system (and for the capacity curve transformed into an equivalent bilinear)
d_y	$[L]$	Displacement at yield strength in the AD space
e^*	$[\%]$	% of mass participation computed during the pushover analysis
e^*_n	$[\%]$	% of mass participation for mode n

f_c	$[F/L^2]$	Concrete compressive strength
$f_{CQC,j}$	$[F]$	Force applied to node j of a MDOF system in a LP calculated through CQC rule
f_m	$[F/L^2]$	Masonry compressive strength
$f_{n,j}$	$[F]$	Force applied to node j of a MDOF system in a LP proportional to n-th natural vibration mode
f_s	$[F/L^2]$	Steel compressive strength
$f_{SRSS,j}$	$[F]$	Force applied to node j of a MDOF system in a LP calculated through SRSS rule
$f_{SRSS^+,j}$	$[F]$	Force applied to node j of a MDOF system in a LP calculated through $SRSS^+$ combination
g	$[L/T^2]$	Gravitational acceleration
h_b	$[L]$	Height of a brick
h_l	$[L]$	Height of story l
i	$[-]$	i-th step of a pushover analysis
j	$[-]$	j-th node of a MDOF system
k	$[-]$	k-th DL or PL
l	$[-]$	Level (story of a wall)
m	$[M]$	Mass of a SDOF system
m^*	$[M]$	Mass of an equivalent SDOF
m_n^*	$[M]$	n-th mode equivalent mass
m_j	$[M]$	Mass of node j of a MDOF system
p	$[-]$	Pier
$\underline{p}(t)$	$[F]$	External forces applied to the nodes of a MDOF model
$\underline{q}(t)$	$[-]$	Modal coordinate vector
$q_n(t)$	$[-]$	n-th modal coordinate
s	$[-]$	Spandrel
t	$[T]$	Time variable
t_d	$[L]$	Thickness of the equivalent membrane representative of the diaphragms
$\underline{t}$	$[-]$	Displacement transformation vector
$\underline{u}(t)$	$[L]$	Earthquake acceleration history
$\ddot{u}_g$	$[L/T^2]$	Earthquake acceleration history applied at the structure's supports
w	$[-]$	Wall

$\underset{\sim}{C}$	[-]	Damping matrix of a MDOF model
A_p	$[L^2]$	Cross section area of a pier
C_0	[-]	CM modification factor (see section 4.2.3)
C_1	[-]	CM modification factor (see section 4.2.3)
C_2	[-]	CM modification factor (see section 4.2.3)
C_m	[-]	Effective mass factor to account for higher modal mass participation effects
C_n	[-]	Generalized damping for mode n
D	[L]	Control displacement
D_d	[L]	The lesser of the target displacement, δ_t, or displacement corresponding to the maximum base shear
D_i	[L]	Control displacement at step i of a pushover analysis
$D_{DLk(PLk)}$	[L]	Control displacement at the attainment of DLk (PLk) - k=1:4
$D_{E,DLk}$	[L]	Control displacement at the attainment of DLk within the multiscale approach, local scale
$D_{G,DLk}$	[L]	Control displacement at the attainment of DLk within the multiscale approach, global scale
$D_{M,DLk}$	[L]	Control displacement at the attainment of DLk within the multiscale approach, macroelement scale
D_u	[L]	Ultimate control displacement
$D_{w,l}$	[L]	Displacement of wall w at level l
D_y	[L]	Displacement at yield strength (usually of an equivalent bilinear)
D_Y	[L]	Yield control displacement (N2 method)
E_1	$[F/L^2]$	Diaphragm Young modulus in the principal direction
E_2	$[F/L^2]$	Diaphragm Young modulus in the direction perpendicular to E_1
E_c	$[F/L^2]$	Concrete Young modulus
E_d	[FL]	Energy dissipated by damping
E_m	$[F/L^2]$	Masonry Young modulus
E_s	$[F/L^2]$	Steel Young modulus

$E_{S0\pm}$	[FL]	Maximum strain energy (in + or - direction)
F_e	[F]	Elastic strength
F_y	[F]	Yield strength
G_c	$[F/L^2]$	Concrete shear modulus
G_d	[F/L]	Diaphragm shear stiffness
G_{eq}	$[F/L^2]$	Diaphragm shear modulus
G_m	$[F/L^2]$	Masonry shear modulus
G_s	$[F/L^2]$	Steel shear modulus
H	[-]	Heaviside function
K	[F/L]	Stiffness of a SDOF system
$\underline{K}$	[F/L]	Stiffens matrix of a MDOF model
K^*	[F/L]	Stiffness of an equivalent SDOF system
K_e	[F/L]	Effective lateral stiffness of the building in the direction under consideration
K_i	[F/L]	Elastic lateral stiffness of the building in the direction under consideration
K_n	[F/L]	Generalized stiffness of mode n
L_b	[L]	Length of a brick
$\underline{M}$	[M]	Mass matrix of a MDOF model
M_{dyn}	[M]	Dynamic mass of a model
M_n	[M]	Generalized mass mode n
N_I	[-]	Number of first modes
N_p	[-]	Number of piers in a model
N_s	[-]	Number of spandrels in a model
$P_n(t)$	[-]	Generalized force mode n
R	[-]	Strength reduction factor (elastic over inelastic strength ratio)
R_μ	[-]	Strength reduction factor for a given ductility μ
S_{ae}	$[L/T^2]$	Spectral elastic acceleration
S_a	$[L/T^2]$	Spectral inelastic or overdamped acceleration
S_{de}	$[L/T^2]$	Spectral elastic displacement
S_d	$[L/T^2]$	Spectral inelastic or overdamped displacement
T	[T]	Period of a SDOF model
T^*	[T]	Period of an equivalent SDOF system
T_1	[T]	First of fundamental period of a model

T_C	[T]	Upper limit of the period of the constant spectral acceleration branch
T_d	[T]	Value defining the beginning of the constant displacement range of the response spectrum
T_e	[T]	Effective fundamental period
T_{hyst}	[T]	Parameter adopted to evaluate maximum inelastic displacement in [GGPM17]
T_r	[T]	Return period
T_s	[T]	Equivalent of T_C
V	[F]	Shear in an element
V_b	[F]	Building base shear
V_y	[F]	Effective yield strength
W_c	$[F/L^3]$	Concrete specific weight
W_m	$[F/L^3]$	Masonry specific weight
W_s	$[F/L^3]$	Steel specific weight
α	$[T^{-1}]$	Rayleigh damping coefficient
α_e	[-]	Effective negative post-yield slope ratio
β	[T]	Rayleigh damping coefficient
β_k	[-]	Pier or spandrel strength decay at the attainment of DLk
β_{mn}	[-]	Inverse ratio of the periods of modes m and n
$\delta_D Lk$	[L]	CM target displacement
δ_k	[-]	Drift corresponding to the attainment of DLk in a pier or spandrel
δ_p	[-]	Drift demand in a pier
δ_s	[-]	Drift demand in a spandrel
δ_t	[L]	CM target displacement
$\theta_{w,l}$	[%]	Interstory drift at level l of wall w
κ_G	[-]	Rate of the total base shear over the maximum base shear of the pushover curve
λ	[1/T]	Annual rate of exceedance
$\tilde{\mu}$	[-]	*Mann and Müller* equivalent friction
μ	[-]	Ductility
$\mu_{strength}$	[-]	Elastic strength demand to yield strength coefficient ratio (defined in Eq. 4.40)

ν	[-]	Poisson's ratio of the equivalent membrane representative of the diaphragms
ξ	[%]	Equivalent viscous damping
ξ_0	[%]	Elastic viscous damping
ξ_h	[%]	Hysteretic dissipation
$\xi_{h,max}$	[%]	Asymptote of the hysteretic dampingn
ξ_{PLk}	[%]	Equivalent viscous damping for the PLk (k=1:4)
ρ_{mn}	[-]	Correlation coefficient of modes m and n
ς	[-]	Coefficient that influences the rate of increase of hysteretic damping
τ_0	$[F/L^2]$	Average shear resistance of masonry
$\underline{\phi_n}$	[-]	n-th natural vibration mode of a MDOF system
$\phi_{j,X}$	[-]	Normalized displacement of node j in direction X of a MDOF system due to the application of horizontal loads
$\phi_{n,j}$	[-]	Normalized displacement of node j of a MDOF system for the n-th natural vibration mode
$\varphi_{w,l}$	[-]	Rotation of wall w at level l
ω	$[T^{-1}]$	Natural frequency of a SDOF system
ω_n	$[T^{-1}]$	Natural frequency of mode n of a MDOF system
Γ_n	[-]	Modal participation factor, mode n
Γ_X	[-]	Participation factor direction X (from NSP node displacements)
Γ_{nX}	[-]	Modal participation factor, mode n direction X (in case of 3D MDOF system)
$\Lambda_{P,DLk}$	[-]	Piers cumulative rate of damage
$\Lambda_{S,DLk}$	[-]	Spandrels cumulative rate of damage
Φ	[-]	Modal matrix

Acronyms

AD	Acceleration-Displacement
ADRS	Acceleration-Displacement Response Spectra
CM	Coefficient method
CSM	Capacity spectrum method
DS(s)	Damage state(s)

DL(s)	Damage level(s)
EC*	Eurocode number *
EF	Equivalent frame
EDP	Engineering demand parameter
FEM	Finite element model
IDA	Incremental dynamic analysis
IM	Intensity measure
IM_{PLk}	Intensity measure at performance level k
$IM_{PLk,dyn}$	Intensity measure at performance level k evaluated with a NDP
$IM_{PLk,st}$	Intensity measure at performance level k evaluated with a NSP
ISA	Incremental static analysis
LP	Load pattern
MPA	Modal pushover analysis
MDOF	Multi-degree of freedom
NLTH	Non-Linear Time History analysis
NDP	Non-Linear dynamic procedure
NSP	Non-Linear static procedure
PL(s)	Performance level(s)
PGA	Peak ground acceleration
PP	Performance point
PBEE	Performance-Based Earthquake Engineering
PBSA	Performance-Based Seismic Assessment
PBSD	Performance-Based Seismic Design
RC	Reinforced concrete
SDOF	Single-degree of freedom
TH	Time history
URM	Unreinforced masonry

Terms and definitions

Base shear: shear reaction at the base of a building, corresponds to the sum of the horizontal forces applied to the building (load pattern or inertia forces in case of static and dynamic analysis respectively).

Capacity: general term to express the ability of a structure or a structural element to bear given forces or displacements.

Capacity curve: representation of the pushover curve in the AD space, the required equations to make the transformation are discussed in section 4.1.

Control displacement: displacement of a point (that could be a physical or not) used as representative of the displacement of the MDOF model of a building. In this research the control displacement assumed is the average displacement of all the nodes at top story of weighted by their masses.

Demand: general term to express the forces or displacements expected on a structure or a structural element due to the action of an earthquake.

Diaphragm: A horizontal (or nearly horizontal) structural element, such as a floor or roof system, used to transfer inertial lateral forces to vertical elements of the seismic-force-resisting system. [ASC14]

Ductility: capacity of a structure or a structural element to deform beyond its material elastic limit.

Dynamic mass: is the mass activated by the seismic actions in a MDOF model; in case of an equivalent frame model the mass corresponding to the part of the walls close to the ground is not considered (see Fig. C.2 in Section C).

Effective modal mass: part of the total dynamic mass responding to the earthquake in each mode.

Engineering demand parameter: Variable chosen to be representative of the seismic behavior of the structure and used to evaluate, through the

definition of proper thresholds, the position of DLs. The engineering demand parameters normally comprise global displacements (e.g., roof or other reference point), story drifts, story forces, component distortions, and component forces [FEM05].

Equivalent bilinear: bilinear curve, derived from a pushover curve, representative of the capacity of a structure.

Equivalent mass: computed using Eq. C.13, it may refer to both a mode or the equivalent SDOF system.

Equivalent viscous damping: sum of the initial elastic viscous damping and the hysteretic damping.

First modes: Modes characterized by a constant sign of displacements at different levels in each wall.

Heuristic approach: when the selection depends on a decision system based on probes, evaluations, or approximations to get the solution.

Intensity measure: is a representation of the anticipated seismic ground motion through its severity, various quantities may be adopted as IM, the peak ground acceleration (PGA) is the most frequently adopted.

Load pattern: is an approximate representation of the forces that a building may be subjected during an earthquake.

Macroelement: It refers to portions of an architectonic asset for which, as testified by the earthquake damage survey, it is possible to recognize recurring seismic behaviors. A macroelement may include a set of structural elements (as in the case of a wall, in which piers and spandrels are included) or, in some cases, may coincide with the structure itself [CLD$^+$12].

Master node: Node whose displacements monitored during a nonlinear static analysis. Usually it is located at top level of the least rigid wall of the model for the direction under analysis.

Modal participation factor: coefficient that "depends on the interaction of the mode shape with the spatial distribution of the external load" [CP03].

Participation factor: coefficient with the same meaning of the modal participation factor used in NSPs. In the present research it is computed from the deformed shape obtained by the pushover analysis at the first steps (i.e. in the initial elastic phase.

Performance point: represents "the condition for which the seismic capacity of the structure is equal to the seismic demand imposed on the

structure by the specific ground motion" [ATC96], or equivalently represents a displacement that is associated with a specific performance level.

Pushover curve: Force-displacement curve generally expressed in terms of base shear V versus displacement D of a control point, called control displacement, generally located at top floor level. In the present research the control displacement is assumed as the weighted average displacement of the nodes at top level.

Response spectra (elastic): Are a frequency domain representations of earthquake ground motions. They comprise a relationship of the maximum response (acceleration, velocity and displacement) over the entire response-history record of a SDOF oscillator and the frequency, or more commonly the period, of the oscillator, for a specified level of damping (usually the 5%) [FEM05].

Response spectrum (inelastic): response spectrum derived from the elastic spectrum, the ordinates are reduced to take into account the ductility exploited by the structure during the earthquake.

Response spectrum (overdamped): response spectrum derived from the elastic spectrum, the ordinates are reduced to account for non-linear inelastic behavior of the structural system through effective viscous damping values.

Strength reduction factor: the ratio of the elastic strength demand to inelastic strength demand for a specified ductility ratio.

Target displacement: see *performance point.*

Yield displacement: displacement corresponding to the end of the elastic phase of an equivalent bilinear.

Yield strength: strength of the equivalent bilinear at yield displacement.

List of Figures

List of Tables

Acknowledgments

First of all, I wish to thank my supervisors, prof. Sergio Lagomarsino and prof. Serena Cattari, for giving me the possibility to join their research group almost four years ago. It was unexpected to me to work in one of the leading groups in the field of the seismic analysis of unreinforced masonry buildings. I will never forget their humility, and the capacity to say "I don't know" when they do not know something. Thanks to them I learnt a lot in this period.

Thanks also to prof. Jason Ingham and Dr. Dmytro Dizhur, who gave me the possibility to spend a research period at University of Auckland, in New Zealand, that was an extremely interesting experience from both scientific and human points of view. Indeed, I had the possibility to see a piece of world very different from that I am used to live in.

Then, I wish to thank the external reviewers of the thesis, prof. Andreas Kappos and prof. Stefano Pampanin. Thanks to their very careful reviews and comments, the quality of this thesis improved.

I also wish to thank all the friends that accompanied me in this long period in Genoa: the group of "dottorandi vecchi" that helped me in familiarizing with the city, new to me; all the flatmates I met in the different houses where I lived, among them a special thank to Leonardo, you did a lot for me in these years. There are also numerous more friends I met during the path of last years and that I wish to thank, you are really a lot and it is impossible to thank each of you individually.

Finally, the most important thanks to my family and a special thought to Enzo, to whom this thesis is dedicated. You saw the beginning of my PhD but unfortunately you could not see the end of it, you left us when I was farthermost from you, I miss you.